Magnetic resonance in superconducting junctions

Lars Elster

▶ **To cite this version:**

Lars Elster. Magnetic resonance in superconducting junctions. Condensed Matter [cond-mat]. Université Grenoble Alpes, 2016. English. NNT : 2016GREAY042 . tel-01537244

HAL Id: tel-01537244

https://theses.hal.science/tel-01537244v1

Submitted on 12 Jun 2017

HAL is a multi-disciplinary open access archive for the deposit and dissemination of scientific research documents, whether they are published or not. The documents may come from teaching and research institutions in France or abroad, or from public or private research centers.

L'archive ouverte pluridisciplinaire **HAL**, est destinée au dépôt et à la diffusion de documents scientifiques de niveau recherche, publiés ou non, émanant des établissements d'enseignement et de recherche français ou étrangers, des laboratoires publics ou privés.

UNIVERSITÉ GRENOBLE ALPES

THÈSE

Pour obtenir le grade de

DOCTEUR DE L'UNIVERSITÉ GRENOBLE-ALPES

Spécialité : **Physique théorique**

Arrêté ministériel : 7 août 2006

Présentée par

Lars Elster

Thèse dirigée par **Julia S. Meyer**
et codirigée par **Manuel Houzet**

préparée au sein de **l'INAC/PHELIQS/GT**
et de **l'École Doctorale de Physique**

Magnetic resonance in superconducting junctions

Thèse soutenue publiquement le **28 septembre 2016**,
devant le jury composé de :

M. Marco Aprili
Directeur de Recherche – CNRS, Rapporteur
M. Jerôme Cayssol
Professeur – Université de Bordeaux, Rapporteur
M. Yuli Nazarov
Professeur – TU Delft, Président
M. Clemens Winkelmann
Maître de conférence – Grenoble INP, Examinateur
Mme Julia S. Meyer
Professeur – Université Grenoble-Alpes, Directrice de thèse
M. Manuel Houzet
Chercheur – CEA Grenoble, Co-Directeur de thèse

Contents

1 Introduction

The theoretical description of transport at mesoscopic scales is based on quantum mechanics, since the phase coherence matters at the typical length scales of nanostructures. A conduction electron is thus characterized by its wavefunction, its charge, and a set of quantum numbers, most importantly the spin. Electron transport gives consequently rise to charge and spin currents and a manipulation of the spin properties may modify the charge current. The control of charge currents via a control of the spin properties is especially interesting for nanostructures containing superconductors, since superconductivity provides macroscopic coherence.

Superconductivity was discovered more than a century ago by Kamerlingh Onnes [1] via the vanishing electrical resistivity of mecury below a threshold (critical) temperature. Superconductors are perfect diamagnets [2], expelling magnetic fields from their interior. Early phenomenological explanations [3] could explain these electromagnetic properties of superconductors, but not, e.g., the isotope effect [4, 5], i.e., the dependence of the critical temperature on the isotope. A more rigorous thermodynamical, but still phenomenological, treatment was provided by Ginzburg – Landau theory [6]. The breakthrough in the understanding of superconductivity was BCS theory [7, 8], named after Bardeen, Cooper, and Schrieffer, providing for the first time a microscopic theory. The key idea of BCS theory is that the Fermi surface becomes unstable for a small attractive interaction mediated by phonons, leading to a new groundstate, in which electrons form bosonic Cooper pairs [9]. In a conventional BCS superconductor, such a Cooper pair is a spin singlet state, consisting of two electrons of opposite spins and momenta. A dissipationless current may flow via this ground state. Furthermore, in conventional BCS superconductors, the ground state is separated by a gap from the excitation spectrum. Beyond the gap that was experimentally verified using tunneling spectroscopy [10, 11], a continuum of states exists.

The field of superconductivity has been boosted by the discovery of the high T_c superconductors [12] in two ways. First, applications became easier to realize, since the critical temperature exceeded for the first time the boiling point of liquid nitrogen at ambient pressure, as e.g., for YBCO [13]. Second, high T_c superconductors posses an unconventional (d-wave) pairing mechanism [14, 15]. Even though unconventional

superconductors were already known [16, 17], the technological interest of finding even higher critical temperatures led to intensified investigations of pairing mechanisms. Unconventional superconductors are characterized by a momentum-dependent pair potential and can, in the presence of inversion symmetry, be classified by the angular momentum of the orbital part of their wave function [18]. Particularly interesting are p-wave superconductors that posses an odd orbital part, giving rise to an even spin part, i.e., spin triplet pairing. An example for a recently investigated spin triplet superconductor is $\mathrm{SrRuO_4}$ [19].

Bulk superconductors are interesting for themselves, but new phenomena emerge for superconducting junctions. Josephson predicted that the current between two superconductors in tunnel junctions depends sinusoidally on the superconducting phase difference [20]. This so-called Josephson effect was measured shortly after its prediction [21]. It can be explained via the microscopic properties of the normal metal/superconductor (N/S) interface. An electron impinging towards an N/S interface with an energy below the gap can be reflected as a hole, adding a Cooper pair to the condensate [22]. This mechanism of Andreev reflection is thus crucial for the transport across an N/S interface. Additionally, it leads to the formation of bound states in Josephson junctions. Since these Andreev bound states depend on the macroscopic phase difference, they determine the current-phase relation. Modifying them will thus change the transport properties of superconducting junctions.

Recently Josephson junctions made of topological superconductors [23], materials with a full pairing gap in the bulk and gapless surface states, have attracted most attention, since they display a 4π-periodic Josephson effect [24–27]. It is due to a 4π-periodic bound state spectrum, which, unlike in conventional junctions, is not spin degenerate. However, non-topological junctions containing unconventional superconductors also deserve attention for their peculiar properties. Since the energy-phase relation of their Andreev bound states is modified with respect to conventional junctions, their current-phase relation is different [28–36]. Notably, the periodicity of the current-phase relation may differ from 2π, e.g., for incompatible spin pairing symmetries. Furthermore, Josephson junctions with a non-zero phase difference in the ground state may exist, e.g., ϕ_0-junctions [30, 37–39]. Experiments that measure the current-phase relation might thus be able to clarify the momentum dependence of the pair potential [14, 40]. Most experiments that investigate the momentum dependence use spectroscopic methods, as for example tunneling spectroscopy [41, 42] or microwave spectroscopy [43].

Particularly interesting are unconventional Josephson junctions realized between spin singlet and spin triplet superconductors. Here, the incompatible spin symmetries prohibit the transfer of a single Cooper pair across the junction. As a consequence, at least two pairs have to be transferred, leading to the lowest harmonics in the current-phase relation being $\sin 2\phi$ [36]. Amongst singlet/triplet junctions, a junction realized between a conventional s-wave superconductor and a one-dimensional unconventional $\mathrm{p_x}$-wave superconductor is the simplest. In this $\mathrm{s/p_x}$ junction the transfer of only an even number of Cooper pairs across the junction leads to a π-periodic equilibrium current-phase relation [28, 29, 35, 36, 44]. On the microscopic level, this junction in known to host spin-polarized Andreev bound states [44], in strong contrast to conventional junctions, where the bound states are not spin-polarized. These spin polarized Andreev bound states lead to an equilibrium magnetization [44, 45]. This opens the possibility to change the occupation of the bound states by manipulating the spin.

In order to manipulate the spin, an external control parameter and its coupling to the spin is needed. A natural choice is to use a magnetic field that couples via the Zeeman effect [46] to the spin. The Zeeman effect is the splitting of energy levels of a system subjected to a constant magnetic field. The splitting occurs according to the angular momentum, which in the case of zero orbital momentum is solely given by the spin. Historically, the Zeeman effect led to the proposition of the spin degree of freedom of the electron [47]. If the magnetic field is time-dependent, it may provide a spin-flip mechanism. In a typical magnetic resonance setup, a static field provides the Zeeman splitting and a time-dependent rf-field, perpendicular to the static field, couples the Zeeman levels. This coupling gives rise to coherent Rabi oscillations between the states.

Transitions between Andreev levels have been predicted to appear as resonances in the current-phase relation [48, 49] in the following setup: A single channel (point contact) conventional Josephson junction is subject to an external monochromatic microwave field. The field generates an ac voltage bias acting as an ac phase bias for the junction. Resonances in the zero temperature current-phase relation appear, if the Andreev level spacing matches a multiple of the microwave frequency. Experimentally, these transitions have been used in order to perform spectroscopy on the Andreev levels of superconducting break junctions [50–52]. In these experiments, a voltage-biased Josephson junction was used as a microwave emitter and detector. Remarkably, the coherent manipulation of Andreev bound states of such atomic contacts is possible, plac-

ing the junction into a microwave resonator using a circuit quantum electrodynamics architecture [53]. Resonances may also be expected due to a time-dependent magnetic field in spin-active Josephson junctions, i.e., Josephson junctions containing a local classical magnetization [54]. Rabi resonances appear, if the magnetization direction is resonantly driven, provided the ground state of the junction is magnetic, which was not achieved in a model that considered a Josephson junction through a precessing spin [55].

In part I of this thesis we consider the presented $\mathrm{s}/\mathrm{p_x}$ Josephson junction and show that a time-dependent Zeeman-field indeed induces transitions between the Andreev bound states. The induced Rabi oscillations map to resonances in the current-phase relation. For a circularly polarized magnetic field, Rabi oscillations are only present in a certain range of superconducting phase differences due to a spin selection rule, thus giving a spin detection scheme. The selection rule is lifted for a linearly polarized magnetic field. The magnetic field also induces non-coherent transitions including continuum states. We may distinguish refill and ionization processes, depending on whether a bound state is filled or emptied. These processes are subject to energy and spin constraints, which guarantee that these incoherent field-induced transitions do not provide any decay mechanism for the Rabi oscillations. We provide a detailed discussion of the transition rates due to theses processes and discuss the visibility of the Rabi resonances in the current-phase relation depending on the junction transparency.

Ferromagnets are another class of materials with peculiar spin properties. In a ferromagnet the spins tend to align due to the exchange interaction, discovered by Heisenberg [56] and Dirac [57]. The well-known ferromagets Fe, Co, and Ni are itinerant ferromagnets, where the ferromagnetism arises due to the 3d orbitals. If the orbital part of the wavefunction is antisymmetric, the exchange interaction leads to a larger average distance between the indiscernible electrons, lowering the Coulomb repulsion. Then, the symmetric spin part leads, due to Pauli exclusion, to a higher kinetic energy. In itinerant ferromagnets, the gain due to the exchange interaction overcomes the loss in kinetic energy, giving rise to ferromagnetism. The exchange interaction splits the density of states for the different spin species. A ferromagnet may thus be characterized by its degree of spin polarization, i.e., the number of majority spin carriers divided by the total number. Ferromagnets with perfect spin polarization of the electrons at the Fermi level are called half-metals, as for example $\mathrm{CrO_2}$ [58].

Junctions containing ferromagnets are of both technological and fundamental research interest. For example, they are widely used for data storage. Old hard drives are still based on the giant magnetoresistance effect [59, 60] in ferromagnet/normal metal/ferromagnet junctions. Nowadays, modern hard drives use magnetic tunnel junctions with an insulating layer separating the ferromagnets, and their operation is based on tunnel magnetoresistance [61]. These mechanisms use charge currents and static magnetization directions in the ferromagnetic layers.

Time-dependent magnetization directions can be achieved using ferromagnetic resonance (FMR), i.e., the resonant absorption of external electromagnetic radiation in ferromagnets [62]. FMR has first been acchieved in bulk ferromagnets [63, 64]. It works analogously to nuclear magnetic resonance (NMR), discovered in molecular beams [65, 66], and electron spin resonance [67]. The discovery of NMR has not only revolutionized the spectroscopic methods available to fundamental research, but has also – after its expansion to liquids and solids – opened the possibility of medical imaging by magnetic resonance tomography [68–70]. However, in contrast to NMR and depending on the geometry, no static field is needed for FMR [71].

Concerning dynamical magnetization effects in ferromagnet/normal metal (F/N) junctions under FMR conditions, it has been theoretically [72, 73] and experimentally [74, 75] shown that the precessing magnetization direction looses angular momentum. This spin pumping process injects a spin current into the adjacent normal metal. This is the inverse effect of the spin transfer torque [76–79], where a spin current driven through a ferromagnetic layer exerts a torque onto the magnetization of the ferromagnet. The creation (and detection) of spin currents is hoped to lead to spintronics [80, 81] applications, i.e., using the spin degree of freedom of the electrons (instead of the charge) for information technology devices.

In a ferromagnet the spins tend to align due to the exchange interaction, whereas in a conventional spin singlet superconductor opposite spins are paired. The interplay between these two antagonistic effects, spin singlet superconductivity and ferromagnetism, becomes important in ferromagnet/superconductor (F/S) junctions. It is consequently relevant to study the interplay between ferromagnetism and superconductivity at interfaces, especially because in bulk ferromagnets superconductivity has only been found in some uranium compounds [82–85], in which the Cooper pairs are equal spin pairs, resolving the antagonism. It has been shown that F/S interfaces can be used to analyze

spin-dependent states in magnetic materials [86–88]. The Andreev reflection at an F/S interface is affected by the exchange interaction and the conductance of the interface may be larger or smaller than the conductance of an F/N interface, depending on the degree of spin polarization [89].

Andreev reflections at N/S interfaces induce superconducting correlations into the normal metal. This effect, called proximity effect, is particularly interesting at F/S interfaces. Here, a triplet pairing component, pairing equal spins, can be induced in the ferromagnet. It penetrates over a much longer length scale than the singlet component, since it is not limited by the short pair breaking length due to the exchange field. The first long-range triplet pairing induced at F/S interfaces was found in resistance measurements [90, 91]. Subsequently, long-range triplet pairing was predicted in the presences of local magnetic inhomogenities at F/S interfaces [92]. The corresponding Josephson effect through S/F/S junctions has been predicted for magnetic inhomogenities [93] and layered heterostructures with non-collinear magnetization directions [94–99]. It has been succesfully measured for a single half-metallic layer [100], a ferromagnetic trilayer [101] and multilayers [102, 103]. Singlet pairs may also be converted to triplet pairs in S/F/F layers, so called triplet spin valves [104]. This growing field of research is called superconducting spintronics [105, 106].

The coupling between superconductivity and a time-dependent magnetization direction has already been studied, e.g., the coupling of two conventional superconductors via a single precessing spin [55, 107] has been considered. In this context the manipulation of magnetic moments using the Josephson current has been investigated [108–110], as well as the inverse effect, i.e., a current induced via the manipulation of the magnetization [111]. For an F/S junction it is known that a ferromagnet under FMR conditions tunnel coupled to a superconductor induces a voltage across the junction in an open circuit geometry [112]. In this tunnel regime, the transport is due to excited quasiparticles, since Andreev reflection processes are suppressed. Due to the BCS singularity in the density of states, the induced voltage (compared to the driving frequency) is much larger in F/S tunnel junctions than the voltage predicted for tunnel junctions with a normal metal or a static reference ferromagnet, where charge pumping is adiabatic [113–115]. In ferromagnet/normal metal tunnel junctions, spin accumulation at the interface leads to a voltage across the junction [115]. The spin accumulation strongly depends on spin relaxation. In the F/S junction, no spin accumulation is needed and

the voltage builds up, since the superconductor in the rotating frame behaves effectively as a static ferromagnet [112].

A half-metal/conventional superconductor (HM/S) junction is especially interesting, since the perfect spin polarization forbids Andreev reflection processes. This blockade may be lifted, if the half-metal is subject to FMR conditions, providing a spin-flip mechanism. In part II of this thesis we show that an Andreev current is indeed induced in such a HM/S junction under FMR conditions. This is a purely dynamical effect, since no Andreev current flows for a static magnetization direction. The time-dependent magnetization creates a non-equilibrium situation for the charge carriers, driving the current. If we assume fast spin relaxation, there is no zero-voltage charge current through a point contact geometry in the normal state, even in the presence of a precessing magnetization. We also show that the effect persists for a non-zero minority carrier concentration (i.e., a ferromagnet instead of a half-metal). However, the current is attenuated and vanishes for equal spin polarizations. Furthermore, we consider a more realistic extended interface geometry. Motivated by disorder enhanced currents reported for N/S interfaces [116, 117], we study the influence of disorder. We show that disorder is irrelevant in a point contact geometry. For the extended interface geometry, however, we obtain that disorder is most relevant in the ferromagnet and that the Andreev current in the presence of disorder is much larger than the ballistic current through the same interface geometry.

Outline of the thesis

Chapter 2 introduces the main physical concepts. After an introduction to both conventional and unconventional superconductivity, we turn towards superconducting junctions. The microscopic process of Andreev reflection at a normal metal/superconductor interface is the key to understand the formation of bound states in Josephson junctions. The phase-dependence of these Andreev bound states gives rise to the dissipationless Josephson current. We finish this chapter with an introduction to ferromagnetic resonance in bulk ferromagnets and junctions.

Chapter 3 introduces the theoretical tools used to obtain the results of this thesis. The Bogoliubov – de Gennes formalism is a method to calculate the wave function of a system with a space-dependent pair potential. In order to solve a superconducting transport problem, it is convenient to combine this formalism with the scattering matrix approach. A different way to tackle non-equilibrium transport across a superconducting junction is to use the non-equilibrium Green's functions formalism. Further, we introduce the Markov master equation approach for density matrices that is suitable to deal with open quantum systems. The Andreev bound states of a Josephson junction can be seen as such an open system, coupled to a reservoir, i.e., the continuum of states. Within the master equation approach, the dynamics of the Andreev bound state occupations is accessible.

Part I of this thesis examines the manipulation of the Andreev levels in a singlet/triplet Josephson junction between a conventional s-wave superconductor and an unconventional $\mathrm{p_x}$-wave superconductor using a time-dependent Zeeman field. We focus on the modification of the transport properties, mainly the current-phase relation. In chapter 4 we present the spin-polarized Andreev bound states that form in the junction. Further, using a free energy approach, we determine the equilibrium magnetization and the equilibrium current-phase relation. Chapter 5 discusses the processes induced by a time-dependent Zeeman field. Our main finding is that the Zeeman field leads to coherent Rabi oscillations between different spin states of the junction that appear as resonances in the current-phase relation. For a circularly polarized magnetic field, the current-phase relation is spin sensitive due to a spin selection rule. The field also induces non-coherent processes including continuum states giving rise to refill and

ionization processes of the bound states. We discuss the corresponding transition rates in detail.

In part II of this thesis we consider a half-metal/superconductor junction under ferromagnetic resonance. Chapter 6 sets the stage, providing the non-equilibrium distribution function of the ferromagnet. In Chapter 7 we show that an Andreev current flows through a point-contact junction between a half-metal and a superconductor, if the half-metal is subjected to FMR conditions. No applied bias voltage is needed, due to the non-equilibrium situation created by FMR. If the superconductor is in its normal state, a spin current flows due to the precessing magnetization direction that in the superconducting state is rectified to a charge current. In Chapter 8, we consider two extensions of our model. First, we show that the Andreev current persists for a ferromagnet with non-zero minority carrier concentration, but is attenuated with respect to perfect spin polarization. Second, we consider a more realistic extended interface geometry, in which the Andreev current is enhanced for a disordered ferromagnet. An introduction to the disorder formalism is provided in this chapter.

Chapter 9 summarizes the main results of this thesis and provides a short discussion of possible future research directions.

The appendix provides technical details on calculations that are important to obtain the results presented in the main part, but that provide limited insight into the physics.

2 Concepts

This chapter is an introduction to the concepts that are used in this thesis. The idea is to provide the reader with the basic notions he needs to follow the main part that discusses magnetic resonance in an unconventional $\mathrm{s}/\mathrm{p_x}$ Josephson junction (Part I, Chapters 4 and 5) and the Andreev current through a half-metal/superconductor interface under ferromagnetic resonance conditions (Part II, Chapters 6 – 8). This chapter focuses on the physics, more details on the formalisms and theoretical tools are provided in Chapter 3. In this chapter, Sec. 2.1 introduces conventional superconductivity and its theoretical description, BCS theory, for bulk superconductors. The bulk properties are of importance, since they determine the properties of more complicated junctions of superconductors. Sec. 2.2 introduces unconventional superconductors with momentum-dependent pair potentials. Having introduced bulk superconductors, we consider simple superconducting junctions in Sec. 2.3. Here, we present the microscopic process of Andreev reflection at a normal metal/superconductor interface that is relevant for the formation of bound states in Josephson junctions consisting of two superconductors. We discuss these bound states for conventional junctions of two s-wave superconductors and introduce the notion of the current-phase relation. The last section of this chapter, Sec. 2.4, introduces ferromagnetic resonance both in bulk ferromagnets and in ferromagnet/normal metal junctions. We study the interplay between ferromagnetic resonance and superconductivity in part II of this thesis.

2.1 Conventional superconductivity

The microscopic theory of superconductivity is of importance, since it is a building block for the microscopic description of superconducting junctions. In this section we will show that it predicts an excitation gap in the density of states of a conventional superconductor. The peculiar excitation spectrum governs the transport properties of superconducting junctions.

Historically, superconductivity was discovered by Kamerlingh Onnes (see Ref. [1]). BCS theory [7, 8], named after Bardeen, Cooper, and Schrieffer, was the first microscopic description of the superconducting state for a class of superconductors nowadays called

conventional (or s-wave) superconductors. It followed a work of Cooper [9], who showed that an attractive interaction between two electrons above the Fermi sea leads to the formation of a bound state. The main idea of BCS theory is that electrons form bosonic Cooper pairs, which condense into a macroscopic quantum state. These Cooper pairs consist of two electrons of opposite spins and opposite momenta. BCS proposed to describe the new ground state by the following many-body state

$$|\Psi_{\mathrm{BCS}}\rangle = \prod_{\boldsymbol{k}} (u_{\boldsymbol{k}} + v_{\boldsymbol{k}} c^{\dagger}_{\boldsymbol{k}\uparrow} c^{\dagger}_{-\boldsymbol{k}\downarrow}) \, |0\rangle \, . \tag{2.1}$$

Here, $|0\rangle$ is the vacuum state, $c^{\dagger}_{\boldsymbol{k}\sigma}$ is an operator creating an electron with momentum $\boldsymbol{k}$ and spin σ. The probability to find the spin-singlet pair $(\boldsymbol{k}\uparrow, -\boldsymbol{k}\downarrow)$ occupied is hence $|v_{\boldsymbol{k}}|^2$, whereas it is unoccupied with the probability $|u_{\boldsymbol{k}}|^2 = 1 - |v_{\boldsymbol{k}}|^2$. $u_{\boldsymbol{k}}$ and $v_{\boldsymbol{k}}$ are called BCS coherence factors. This BCS ground state does not have a fixed particle number. However, for large systems the particle number is strongly peaked around the mean particle number (see e.g. Ref. [118]).

The total wave function contains an orbital and a spin part. It has to be antisymmetric, since electrons are fermions. For the BCS ground state the orbital part is symmetric, whereas the spin part is antisymmetric (spin singlet pairing). We discuss superconductors with spin triplet pairing in Sec. 2.2.

BCS originally used a variational method (see also [7, 118, 119]), using their wave function in Eq. (2.1), in order to determine the ground state energy. Here, we choose a different approach (see e.g. Ref. [119]) in order to obtain the excitation spectrum. We start from the pairing Hamiltonian, for which we assume that it contains all important terms for superconductivity, even though we neglect all terms, where electrons are not paired in a state of the form $(\boldsymbol{k}\uparrow, -\boldsymbol{k}\downarrow)$. It reads

$$H = \sum_{\boldsymbol{k},\sigma} \xi_{\boldsymbol{k}} c^{\dagger}_{\boldsymbol{k}\sigma} c_{\boldsymbol{k}\sigma} + \sum_{\boldsymbol{k}\boldsymbol{q}} V_{\boldsymbol{k}\boldsymbol{q}} c^{\dagger}_{\boldsymbol{k}\uparrow} c^{\dagger}_{-\boldsymbol{k}\downarrow} c_{-\boldsymbol{q}\downarrow} c_{\boldsymbol{q}\uparrow}. \tag{2.2}$$

Here, $\xi_{\boldsymbol{k}}$ is the kinetic energy measured with respect to the Fermi level and $\boldsymbol{k}, \boldsymbol{q}$ are momenta. $V_{\boldsymbol{k}\boldsymbol{q}}$ is the interaction that scatters a pair $(\boldsymbol{q}\uparrow, -\boldsymbol{q}\downarrow)$ to $(\boldsymbol{k}\uparrow, -\boldsymbol{k}\downarrow)$. Here, we assumed an interaction that is local in real space. We make a mean-field approximation,

assuming that the deviations of products of operators from their expectation values are small. Introducing the pair potential

$$\Delta_{\boldsymbol{k}} = -\sum_{\boldsymbol{q}} V_{\boldsymbol{kq}} \left\langle c_{-\boldsymbol{q}\downarrow} c_{\boldsymbol{q}\uparrow} \right\rangle , \tag{2.3}$$

where the expression $\langle c_{-\boldsymbol{q}\downarrow} c_{\boldsymbol{q}\uparrow} \rangle$ is called anomalous average, we obtain the mean-field BCS Hamiltonian

$$H_{\mathrm{BCS}} = \sum_{\boldsymbol{k},\sigma} \xi_{\boldsymbol{k}} c^{\dagger}_{\boldsymbol{k}\sigma} c_{\boldsymbol{k}\sigma} - \sum_{\boldsymbol{k}} \left[\Delta_{\boldsymbol{k}} c^{\dagger}_{k\uparrow} c^{\dagger}_{-k\downarrow} + \mathrm{h.c.} \right] . \tag{2.4}$$

Here, we neglected a constant shift of the energy. In BCS theory, the attractive interaction between the electrons is mediated by phonons and assumed to be constant, if the kinetic energy of the electrons is below a cutoff energy, and zero otherwise. This form of the interaction yields a constant absolute value of the pair potential $|\Delta|$, isotropic in momentum space (if the kinetic energy is below the cutoff). We discuss superconductors with momentum-dependent pair potential in Sec. 2.2. The BCS Hamiltonian in Eq. (2.4) is diagonalized using a Bogoliubov transformation [120]. More details on this method are provided in Chapter 3. This procedure allows to obtain the expression for the coherence factors, reading

$$|u_{\boldsymbol{k}}|^2 = \frac{1}{2} \left(1 + \frac{\xi_{\boldsymbol{k}}}{E_{\boldsymbol{k}}} \right) , \tag{2.5}$$

where

$$E_{\boldsymbol{k}} = \sqrt{\xi_{\boldsymbol{k}}^2 + |\Delta|^2} \tag{2.6}$$

is the excitation energy for quasiparticles. Note that the relative phase between $u_{\boldsymbol{k}}$ and $v_{\boldsymbol{k}}$ is the phase of Δ. It is thus possible to choose $u_{\boldsymbol{k}}$ real and give $v_{\boldsymbol{k}}$ a phase factor of $e^{i\phi}$. According to Eq. (2.1), the phase factor is the same for all pairs in the condensate and is therefore called "macroscopic" phase. Note that due to the $U(1)$ symmetry of the Schrödinger equation only phase differences can have physical effects. When dealing with junctions of superconductors, phase differences of this macroscopic phase will become important (see Sec. 2.3.2). According to Eq. (2.6), the excitation spectrum is gapped with a minimum excitation energy of $|\Delta|$ for $\xi_{\boldsymbol{k}} = 0$. Therefore, $|\Delta|$ is also called the (superconducting) gap. The minimum energy required to break a Cooper

pair being in the ground state, separated by $|\Delta|$ from the excitation spectrum, is thus $2|\Delta|$. More precisely, the BCS density of states reads

$$\nu_S = \nu_0 \frac{E}{\sqrt{E^2 - |\Delta|^2}} \Theta(E - |\Delta|), \tag{2.7}$$

where ν_0 denotes the density of states of a normal metal at the Fermi level and E is the excitation energy measured with respect to the Fermi level. The density of states displays a divergence at $E = |\Delta|$. The states that in the normal state are within the gap are moved above the gap, enhancing the density of states in comparison to the normal state. Together with the filling factor, the density of states determines the number of states available for transport. The modifications of the density of states with respect to a normal metal have a crucial influence on the transport properties, especially within heterostructures. Furthermore, we will see that a normal metal/superconductor interface allows for Andreev reflections (see Sec. 2.3.1) within the gap.

BCS theory is able to describe the properties of elemental superconductors, like aluminum or niobium. In the next section, we will discuss superconductors, for which an extension of BCS theory is necessary.

2.2 Unconventional superconductivity

The superconductors that we considered so far are based on a phonon mediated spin singlet pairing mechanism with constant pair potential. However, superconductors can have different, exotic microscopic pairing mechanisms. Following Ref. [121], we may define an unconventional superconductor by the symmetries that are broken during the transition from the normal to the superconducting state. In a conventional superconductor, one macroscopic phase value ϕ of the order parameter is chosen, which can be interpreted as a spontaneous breaking of the $U(1)$ gauge symmetry. If additional symmetries of the symmetry group of the crystal are broken during the transition to a superconducting state, we will speak of unconventional superconductivity.

Since only the total wave function has to be antisymmetric, unconventional superconductors can have spin triplet pairing with an odd momentum dependence. In this section, we provide the theoretical description of superconductors with momentum-

dependent pair potentials with a general spin dependence, containing singlet and triplet parts.

The most prominent example are the high-T_c superconductors [12], even though unconventional superconductors have been discovered earlier [16, 17]. Recently, in the context of topology in condensed matter, topological superconductors (for a review see [23]) with momentum-dependent pair potentials have attracted a lot of attention. These are bulk superconductors with conducting surface states, the superconducting analogue of topological insulators ([122, 123], for a review see [124]). Topological phases may be characterized according to their symmetries [125, 126], i.e., particle-hole symmetry, time-reversal symmetry and chiral symmetry. A chiral superconductor, which is characterized by broken time-reversal symmetry, is the superconducting analogue of the quantum Hall phase, whereas a helical superconductor, which conserves time-reversal symmetry, is the analogue of the quantum spin Hall phase [23]. The edge states of a helical superconductor are a pair of Majorana fermions [127], which in condensed matter systems are fermionic quasiparticles that are its own antiparticles.

Let us give a theoretical description of unconventional superconductivity based on Ref. [121] and consider a bulk superconductor, described by the generalized mean-field Hamiltonian (generalization of Eq. (2.4))

$$H = \sum_{\boldsymbol{k}\sigma} \xi_{\boldsymbol{k}} c^\dagger_{\boldsymbol{k}\sigma} c_{\boldsymbol{k}\sigma} - \sum_{\boldsymbol{k}\alpha\beta} \left[\Delta_{\alpha\beta}(\boldsymbol{k}) c^\dagger_{\boldsymbol{k}\alpha} c^\dagger_{-\boldsymbol{k}\beta} + \text{h.c.} \right]. \tag{2.8}$$

Here, the pair potential is spin dependent (greek indices) and fulfills

$$\Delta_{\alpha\beta}(-\boldsymbol{k}) = -\Delta_{\beta\alpha}(\boldsymbol{k}). \tag{2.9}$$

Let us assume the presence of spatial inversion symmetry. Then, the pair wave function is either symmetric or antisymmetric under inversion symmetry, giving rise to spin singlet, spin triplet pairing, respectively [121]. It is convenient to separate the spin singlet contributions from the spin triplet contributions. Let us therefore introduce the singlet creation operator

$$s^\dagger_{\boldsymbol{k}} = c^\dagger_{\boldsymbol{k}\uparrow} c^\dagger_{-\boldsymbol{k}\downarrow} - c^\dagger_{\boldsymbol{k}\downarrow} c^\dagger_{-\boldsymbol{k}\uparrow} \tag{2.10}$$

and the three triplet creation operators

$$t^\dagger_{\boldsymbol{k}x} = c^\dagger_{\boldsymbol{k}\downarrow} c^\dagger_{-\boldsymbol{k}\downarrow} - c^\dagger_{\boldsymbol{k}\uparrow} c^\dagger_{-\boldsymbol{k}\uparrow}, \tag{2.11}$$

$$t^\dagger_{\boldsymbol{k}y} = i\left[c^\dagger_{\boldsymbol{k}\downarrow} c^\dagger_{-\boldsymbol{k}\downarrow} + c^\dagger_{\boldsymbol{k}\uparrow} c^\dagger_{-\boldsymbol{k}\uparrow}\right], \tag{2.12}$$

$$t^\dagger_{\boldsymbol{k}z} = c^\dagger_{\boldsymbol{k}\downarrow} c^\dagger_{-\boldsymbol{k}\downarrow} + c^\dagger_{\boldsymbol{k}\uparrow} c^\dagger_{-\boldsymbol{k}\uparrow}. \tag{2.13}$$

With help of these definitions, we reexpress the pairing term in Eq. (2.8) as

$$\sum_{\alpha\beta} \Delta_{\alpha\beta}(\boldsymbol{k}) c^\dagger_{\boldsymbol{k}\alpha} c^\dagger_{-\boldsymbol{k}\beta} = d_0(\boldsymbol{k}) s^\dagger_{\boldsymbol{k}} + \boldsymbol{d}(\boldsymbol{k}) \cdot \boldsymbol{t}^\dagger_{\boldsymbol{k}}, \tag{2.14}$$

where the vector of triplet operators is defined as $\boldsymbol{t}^\dagger_{\boldsymbol{k}} = (t^\dagger_{\boldsymbol{k}x}, t^\dagger_{\boldsymbol{k}y}, t^\dagger_{\boldsymbol{k}z})^T$. The spin singlet part of the general pair potential is thus described by d_0, whereas the vector $\boldsymbol{d}$ characterizes the triplet part. The pair potential can be expressed using the $\boldsymbol{d}$-vector and reads

$$\Delta(\boldsymbol{k}) = \left[d_0(\boldsymbol{k}) + \boldsymbol{d}(\boldsymbol{k}) \cdot \boldsymbol{\sigma}\right] i\sigma_y, \tag{2.15}$$

where σ_i denotes the i-th Pauli matrix in spin space. Eq. (2.9) implies the following symmetries:

$$d_0(-\boldsymbol{k}) = d_0(\boldsymbol{k}), \tag{2.16}$$

$$\boldsymbol{d}(-\boldsymbol{k}) = -\boldsymbol{d}(\boldsymbol{k}). \tag{2.17}$$

The singlet part is thus an even function and the triplet part an odd function of the momentum. A BCS superconductor is obviously described by a momentum-independent d_0 and $\boldsymbol{d} = 0$. In the presence of inversion symmetry and in isotropic systems, we may label unconventional superconductors according to their orbital angular momentum. In analogy to the atomic orbitals, we speak of s-wave, p-wave, and d-wave, etc. pairing. A spin triplet p-wave superconductor, for example, is thus characterized by an even spin symmetry and an odd momentum symmetry with an angular momentum equal to one. In general, the details of the momentum dependence of the pair potential depend on the symmetry groups of the crystal. On a generic two-dimensional square lattice, the momentum dependences for s, p, d superconductors can be expressed as const, $\sim \cos\phi$, $\sim \cos(2\phi)$, where $\phi = \arctan \frac{k_y}{k_x}$. A sketch of these generic pair potentials is shown in Fig. 2.1. The p-wave and the d-wave superconductor have gap closing points, at which the sign of the pair potential changes. In Chapter 5, we will deal with a one-dimensional

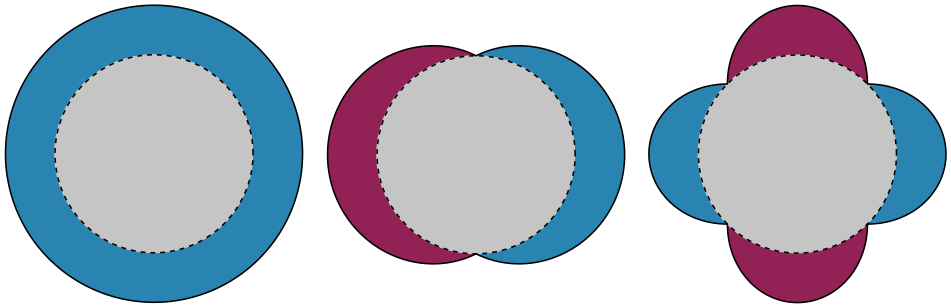

Fig. 2.1: From left to right: s-wave, p-wave, and d-wave pair potentials in a Fermi surface representation for two momentum dimensions. The horizontal direction is k_{x}, whereas the vertical direction is k_{y}. The gray shaded area is the isotropic Fermi surface. The s-wave superconductor in the left panel has a constant gap. The p-wave superconductor in the middle panel has a momentum-dependent gap with two gap closing points, at which the sign of the pair potential changes. Blue (red) color corresponds to a positive (negative) sign. The d-wave pair potential has four gap closing points, at which sign changes occur.

p_x-wave superconductor. Its pair potential corresponds to a cut along the horizontal axis in the middle panel of Fig. 2.1. Consequently, the sign of the pair potential for positive momenta is opposite to the sign for negative momenta. This sign change can also be seen from Eq. (2.17). Note that the one-dimensional p_x-wave superconductor is fully gapped.

Prominent examples for (intrinsic) unconventional superconductors are Sr_2RuO_4 [19], which is possibly a spin triplet p-wave superconductor, and the high-T_c cuprates [15] that are spin singlet d-wave superconductors. More recently, iron pnictides have attracted a lot of attention [128]. They are a class of materials, for which various different superconducting phases have been predicted. Another class of unconventional superconductors are the uranium ferromagnetic superconductors [82], which have spin triplet pairing.

Intrinisic unconventional superconductors are hard to engineer in a controlled way. Therefore, effective setups realizing unconventional superconductors have attracted a lot of attention, especially to realize effective p-wave superconductors. The main idea in common for these setups is to use the proximity effect of a conventional superconductor in order to induce superconductivity. Using a toy-model, it has been shown by Kitaev [24] that a one-dimensional spinless p-wave superconductor has a topological phase, in which it hosts Majorana fermions [127]. Experimental realizations of this toy-model have been proposed [129, 130], e.g., based on spin-orbit coupled nanowires subjected

to a Zeeman field, and realized [131], giving some evidence for Majorana fermions. More recently, the 4π-periodic Josephson effect that is a signature of induced effective p-wave pairing has been reported [27].

2.3 Superconducting heterostructures

Heterostructures are of both technological interest and of interest for fundamental research, since new effects emerge at interfaces. For superconducting heterostructures, we will see that the modifications of the density of states and the macroscopic phase determine the transport properties. This section considers heterostructures containing conventional superconductors in order to introduce the main notions. Unconventional junctions are discussed in Chapter 4. In order to probe the transport properties of a superconductor, it has to be connected to a normal metal, since the current and voltage detection devices are made of normal metals. An understanding of the microscopic processes at such a normal metal/superconductor (N/S) interface is thus necessary. Sec. 2.3.1 introduces the N/S interface and explains the microscopic process of Andreev reflection. In Sec. 2.3.2, we consider a Josphson junction consisting of two superconductors, where Andreev reflection processes lead to the formation of bound states. Further, the macroscopic phase difference across the junction determines the current. In order to calculate the properties of complicated junctions, the Bogoliubov – de Gennes formalism, that we introduce in Sec. 3.1, is needed.

2.3.1 Normal metal/superconductor junctions - Andreev reflection

The normal metal/superconductor (N/S) interface is the building block for Josephson junctions. The microscopic processes at the N/S interface determine the Andreev bound states and therefore the transport through Josephson junctions. In this section we provide a microscopic description of this interface.

Consider an N/S junction, as sketched in Fig. 2.2, with a small insulating barrier separating the normal metal from the superconductor, giving rise to backscattering. Consider an electron in the normal metal impinging towards the superconductor. If its energy is smaller than the gap (#1 in Fig. 2.2), no density of states is available. It can

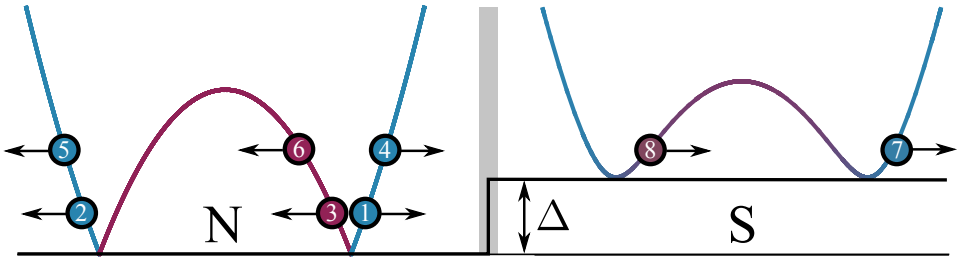

Fig. 2.2: Normal metal (N)/superconductor (S) interface for a step-like pair potential Δ and a barrier (gray), giving rise to backscattering. The band structure is shown for both the normal metal and the superconductor. Red (blue) color corresponds to a hole (electron) branch. The superconductor mixes electrons and holes (linear interpolation of the color, depending on the mixing degree). An impinging electron below the gap (#1) can either be normal reflected (#2) as an electron or Andreev reflected (#3) as a hole. An impinging electron above the gap (#4) can enter the superconductor, forming a quasiparticle (#6 or #7) with electron and hole component. Fig. adapted from [132].

thus not enter the superconductor. There are in principle two possible processes. First, it can be normal reflected as an electron (#2), since the barrier gives rise to backscattering. The corresponding momentum change is large and approximately given by $2k_\mathrm{F}$, where the Fermi momentum is denoted by k_F. Second, the electron can be Andreev reflected [22] as a hole (#3) with a small momentum change of approximately $2\frac{E}{\hbar v_\mathrm{F}}$, where the Fermi velocity is denoted by v_F. Here, we assumed that the excitation energy is much smaller than the Fermi energy, which for the superconducting gap implies $\Delta \ll E_\mathrm{F}$. We can thus linearize the spectrum around k_F and above expression for the momentum change follows. This approximation is called Andreev approximation. The Andreev reflection process consists in transferring two electrons from the normal metal with opposite spin and opposite momenta to the superconductor and adding them as a Cooper pair to the condensate. From the point of view of the normal metal, an incident electron is thus reflected as a hole. If the energy of the impinging electron is larger than the gap of the superconductor (#4), it can, as before, be normal reflected (#5) or Andreev reflected (#6). Note that the probability of Andreev reflection decreases as the energy of the quasiparticle increases until reaching the normal metal limit for large energies. Additionally, the impinging electron can enter the superconductor as a (Bogoliubov [120]) quasiparticle, i.e., a superposition of an electron and a hole. The quasiparticle is either electron-like (#7), i.e., its electron component exceeds its hole component ($|u_{\boldsymbol{k}}|^2 > |v_{\boldsymbol{k}}|^2$), or hole-like (#8).

For a more quantitative description, the Bogoliubov – de Gennes equations [118, 120] have to be solved for the junction (see also Sec. 3.1). Solving them by parts yields the bandstructure sketched in Fig. 2.2. Additionally, this approach allows to obtain the Andreev reflection probability (for details see e.g. [132–136]) that reads

$$r_{\mathrm{A}} = e^{-i\phi} e^{-i\chi}, \tag{2.18}$$

where ϕ denotes the phase of the superconductor. Further,

$$e^{-i\chi} = \frac{E}{\Delta} - \sqrt{\left(\frac{E}{\Delta}\right)^2 - 1}, \tag{2.19}$$

which below the gap ($0 < E < \Delta$) yields $\chi = \arccos \frac{E}{\Delta}$, which is the energy-dependent phase shift an electron acquires in an Andreev reflection process. For the conversion of a hole into an electron, the sign in front of the superconducting phase is inverted. These phase shifts play a crucial role in the formation of bound states in Josephson junctions (see Sec. 2.3.2). Since in an Andreev reflection process the charge of 2e is transferred across the interface, Andreev reflection enhances the current through the N/S interface, whereas normal reflection decreases the current.

Via Andreev reflection electrons and holes in the normal metal have a fixed phase relation. An Andreev reflected hole retraces back the same path as the incident electron, since its velocity is opposite. This means, superconducting correlations are induced in the normal metal. Note that this non-zero anomalous average (see also Eq. (2.3)) does not mean that the pair potential is non-zero, since the pairing interaction is zero in the normal metal. However, at finite energy, the electron and hole dephase, such that the correlations only extend over the finite phase coherence length $\sim \frac{\hbar v_{\mathrm{F}}}{E}$. At finite temperature the length is given by $\sim \frac{\hbar v_{\mathrm{F}}}{kT}$. Note that we considered a ballistic normal metal. This so-called proximity effect also exists for disordered metals.

2.3.2 Josephson junctions - Andreev bound states

We now want to consider Josephson junctions consisting of two superconductors. As we will see, the Andreev reflections at the two N/S interfaces lead to the formation of Andreev bound states. These bound states, whose energy depends on the phase difference across the junction, are responsible for a phase-dependent current across the junction.

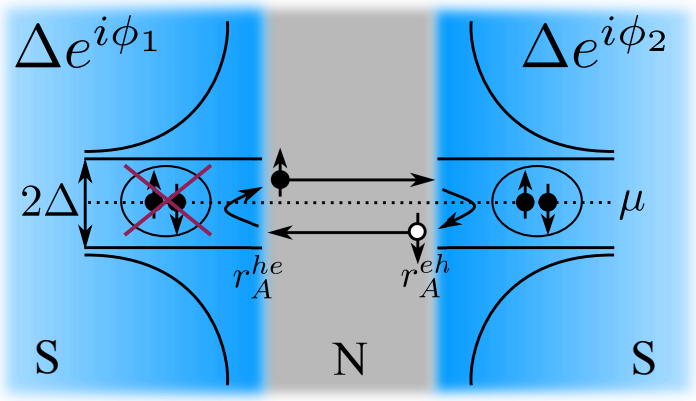

Fig. 2.3: Quasiclassical picture for the formation of Andreev bound states. A spin-up elelectron in the normal region (N) travelling to the right is Andreev reflected as a spin-down hole at the right superconductor (S), adding a Cooper pair to the condensate. The hole travels towards the left superconductor, where it is Andreev reflected as an electron, removing a Cooper pair from the condensate. A bound state forms, if the phases acquired add up to a multiple of 2π (quasiclassical quantization condition).

Let us consider an S/N/S junction, where a second conventional superconductor is attached to the N/S interface discussed in the previous section. For simplicity, we want to consider two superconductors with the same gap. If the length of the normal region is smaller than the phase coherence length, interference effects in the junction play a role. Let us in the following consider short junctions, i.e., the junction length (length of the normal region) fulfilling $L \ll \xi = \frac{\hbar v_\mathrm{F}}{\Delta}$. Here, ξ is the superconducting coherence length for a ballistic junction at zero temperature. We now want to give an intuitive, quasiclassical description of how the microscopic process of Andreev reflection at a ballistic N/S interface leads to the formation of a bound state in the S/N/S junction. Fig. 2.3 shows schematically the following process: Consider an electron in the normal region (N) with an energy smaller than the gap. It travels towards the superconductor and thereby picks up a phase of $k^\mathrm{e}L$, where k^e is the wave vector of the electron. As described in Sec. 2.3.1, it is then Andreev reflected at the right superconductor, adding a Cooper pair to the condensate. According to Eqs. (2.18) and (2.19), the electron picks up a phase of $\phi_2 + \chi$. The hole is now travelling to the left superconductor and picks up a phase of $k^\mathrm{h}L$, where k^h is the hole wave vector. It is then Andreev reflected at the superconductor with a phase shift of $-\phi_1 + \chi$. A Cooper pair is removed from the condensate and the original electron is restored. We can write down a quasiclassical

Bohr-Sommerfeld quanitization condition, requiring that the total phase shift for such a closed path is a multiple of 2π [137, 138]:

$$k^{\mathrm{e}}L + k^{\mathrm{h}}L + \phi + 2\arccos\frac{E}{\Delta} = 2n\pi. \tag{2.20}$$

Here, $n \in \mathbb{Z}$ and we introduced the phase difference across the junction $\phi = \phi_2 - \phi_1$. In the short junction limit, Eq. (2.20) yields two phase-dependent bound state energies given by $E_\pm = \pm\Delta\cos\frac{\phi}{2}$. Note that these Andreev bound states are spin degenerate, since we can reason in the same way starting with an electron with spin down. If we allow for backscattering in the normal region, giving rise to a finite transmission T of the junction, the bound state energies are modified and read [133]

$$E_\pm = \pm\Delta\sqrt{1 - T\sin^2\frac{\phi}{2}}. \tag{2.21}$$

This is the result for a single channel point contact. We generalize this expression in Chapter 4. The dispersion of the bound states is shown in Fig. 2.4(a). The process described above and depicted in Fig. 2.3 transfers a Cooper pair from the left superconductor to the right superconductor. This gives rise to a dissipationless supercurrent across the junction. Since the bound state energies depend on the phase difference, the supercurrent across the junction will also depend on the phase difference. The effect was first theoretically predicted by Josephson [20] for tunnel junctions ($T \ll 1$). In a conventional junction consisting of two s-wave superconductors with equal gaps, the Josephson current is entirely transported via the bound states and can be obtained from the dispersion of the bound states. At zero temperature it reads

$$I = \frac{2e}{\hbar}\sum_{\nu\in\{\pm\}}\frac{dE_\nu}{d\phi}\mathrm{sgn}(E_\nu). \tag{2.22}$$

Note that the last factor is the zero temperature occupation factor. Further, this relation is derived from a more general relation in terms of the free energy that we present in Chapter 4. From Eq. (2.22) it is apparent that modifications of the Andreev bound states will modify the supercurrent across the junction. Note that the expression for the supercurrent is more complicated, if the gaps of the two superconductors are not equal. Fig. 2.4(b) shows the zero temperature Josephson current through the junction.

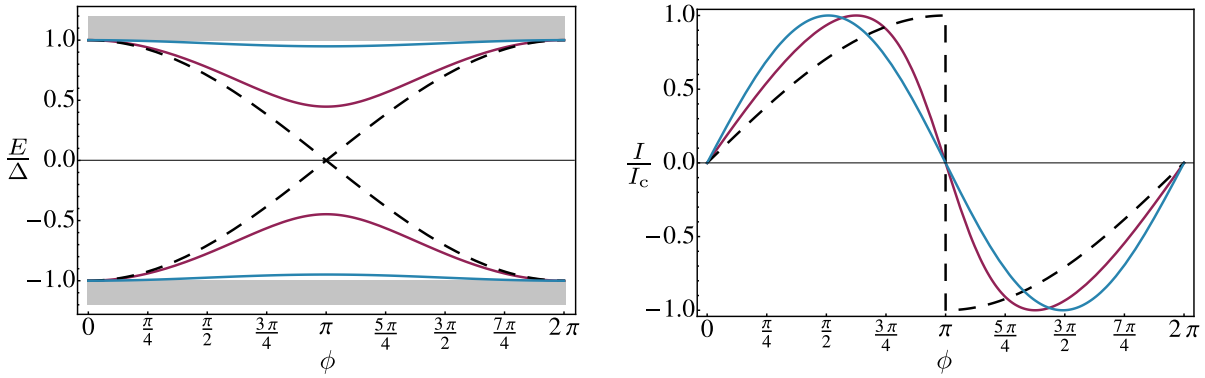

(a) bound states **(b)** Josephson current

Fig. 2.4: (a) Energy of the bound states of an S/N/S junction as a function of the phase difference ϕ across the junction. The bound states are given for three different transmissions: $T = 1$ (black, dashed), $T = 0.8$ (red) and $T = 0.1$ (blue). (b) Corresponding Josephson current at zero temperature, normalized by the critical current, as a function of the phase difference. Note that the current in the tunnel junction case (blue) is sinusoidal, as predicted from the first Josephson relation in Eq. (2.23).

In the tunnel regime, the current expression reduces to the well-known first Josephson relation [20]

$$I = I_c \sin \phi. \tag{2.23}$$

Note that this expression holds true in the tunnel regime for any temperature and for large temperatures at any transparency. The critical current I_c, i.e., the maximum value of the dissipationless supercurrent, scales linearly with T in the tunnel regime. In general, e.g., for a transparent junction for example, the relation between the supercurrent and the phase difference, i.e., the current-phase relation, is more complicated. The Josephson effect without applied bias voltage is called dc Josephson effect, since it gives rise to a time-independent current. If a constant bias voltage V is applied across the junction, the phase difference becomes time dependent and reads according to the second Josephson relation

$$\frac{d\phi}{dt} = \frac{2e}{\hbar} V. \tag{2.24}$$

The supercurrent is thus an ac current and the effect is called ac Josephson effect. A formalism to calculate the current-phase relation at finite temperature is presented in Sec. 4.4 and Appendix B.

Experimentally, the Josephson effect has been measured via $I(V)$ curves shortly after its prediction [139]. The current-phase relation $I(\phi)$ has been measured, e.g., in

superconducting bridges and in superconducting weak links [140–142]. More recently, the current-phase relation has been measured for atomic point contacts and could be compared to theory without adjustable parameters [143]. In this experiment, the atomic point contact was formed by a break junction that was embedded into an assymetric SQUID with a tunnel junction. A similar setup has been used for the spectroscopy of the Andreev levels of a single channel point contact [50, 52] and their coherent manipulation [53]. The experimental observations are in agreement with the theoretical predictions given in this section.

2.4 Ferromagnetic resonance

In part II of this thesis, we want to study an interface between a ferromagnet under ferromagnetic resonance conditions and a superconductor. This section provides an introduction to ferromagnetic resonance in bulk ferromagnets and in ferromagnet/normal metal (F/N) junctions. Ferromagnetic resonance has first been discovered in bulk ferromagnets, where it is well-described by a quasiclassical theory, based on the Landau-Lifshitz-Gilbert equation (Sec. 2.4.1). More recently ferromagnetic resonance has attracted a lot of attention, especially in the spintronics community, since F/N junctions may provide pure spin currents, as we will see in Sec. 2.4.2.

2.4.1 Ferromagnetic resonance in bulk ferromagnets

Since we want to consider junctions under ferromagnetic resonance conditions, we first have to understand ferromagnetic resonance in bulk ferromagnets, where the resonance mechanism is similar. We mainly follow Ref. [62] for this section, where ferromagnetic resonance is defined as the resonant absorption of external electromagnetic radiation in ferromagnets. It was experimentally discovered by [63, 64].

In a ferromagnet, the exchange interaction aligns the electron magnetic moments to yield a macroscopic magnetization $\boldsymbol{M}$. If a magnetic field $\boldsymbol{B_0}$ is applied, a torque acts onto the magnetic moment of the ferromagnet, trying to align it with the field. As a consequence, the magnetization precesses around the magnetic field direction. The magnetization dynamics can be described by the classical equation of motion

$$\frac{d\boldsymbol{M}}{dt} = -\gamma \boldsymbol{M} \times \boldsymbol{B_0}. \tag{2.25}$$

Here, μ_0 is the magnetic constant, γ denotes the gyromagnetic ratio that for the electron takes the form $|\gamma_\mathrm{e}| = g_\mathrm{e}\frac{\mu_\mathrm{B}}{\hbar}$, where μ_B denotes the Bohr magneton. Further, g_e denotes the electron g-factor, which is the proportionality constant between the magnetic moment and the angular momentum of the electron. Under the assumption that the spins only precess in the field $\boldsymbol{B_0}$, the precession frequency is given by the Larmor frequency

$$\omega_0 = \gamma B_0. \tag{2.26}$$

In ferromagnets, there is not only the external field, but there are also demagnetization and crystal anisotropy fields. It is therefore convenient to introduce an effective magnetic field $\boldsymbol{B_\mathrm{eff}}$ that takes into account these fields and replaces $\boldsymbol{B_0}$ in Eq. (2.25). In thermodynamic equilibrium, the effective magnetic field can be obtained from the free energy as

$$B_{\mathrm{eff},j} = -\frac{\partial F}{\partial M_j}. \tag{2.27}$$

Here, j denotes the component of the magnetization/effective magnetic field vector. A ferromagnetic resonance (FMR) experiment consists of applying a static field $\boldsymbol{B_0}$ and a much smaller dynamic field $\boldsymbol{b_\mathrm{rf}}$ (with $b_\mathrm{rf} \ll B_0$) that is perpendicular to the static field. Due to the internal magnetic field in ferromagnets, the resonance frequency deviates from the Larmor frequency. Further, in contrast to a nuclear magnetic resonance experiment, the ferromagnetic resonance frequency may be finite for zero static field. Let us specify the resonance frequency. Following Kittel [71, 144, 145] and considering an ellipsoidal specimen, the resonance frequency obtained from Eq. (2.25) can be written as

$$\omega_0 = \gamma\sqrt{\left(B_0 + \frac{N_y - N_z}{4\pi}\mu_0 M\right)\left(B_0 + \frac{N_x - N_z}{4\pi}\mu_0 M\right)}. \tag{2.28}$$

Here, the static field is $\boldsymbol{B_0} = B_0\hat{\boldsymbol{z}}$ and N_i is the demagnetization factor in direction $\hat{\boldsymbol{i}}$. Let us consider three specific geometries. First, for a sphere, $N_x = N_y = N_z$, giving $\omega_0 = \gamma B_0$, which is the Larmor frequency. Second, for a flat plate, to which the static field is applied perpendicular, $N_x = N_y = 0$ and $N_z = 4\pi$, giving $\omega_0 = \gamma\,|B_0 - \mu_0 M|$. This geometry is an example for a geometry, where no static field is necessary in order to yield a finite resonance frequency. Third, for a flat plate with the static field applied in plane, $N_x = N_z = 0$ and $N_y = 4\pi$, giving $\omega_0 = \gamma\sqrt{B_0(B_0 + \mu_0 M)}$. These expressions are only valid for a uniform magnetic field inside the specimen, corresponding to a single magnetic domain.

So far, we have not taken into account any damping. Damping may be provided by interactions, for example magnetic dipole interaction or phonons. Phenomenologically, a damping term is added to Eq. (2.25), yielding the Landau-Lifshitz-Gilbert equation [146]

$$\frac{d\boldsymbol{M}}{dt} = -\gamma \boldsymbol{M} \times \boldsymbol{B}_{\mathbf{eff}} + \frac{\alpha}{M} \boldsymbol{M} \times \frac{d\boldsymbol{M}}{dt}. \tag{2.29}$$

Here, α is the dimensionless Gilbert damping constant. Eq. (2.29) can be recast into the Landau-Lifshitz equation that has been originally proposed on a phenomenological basis [147] and later been derived from thermodynamics [148]. Therefore, we take the vector product of $\boldsymbol{M}$ and Eq. (2.29) and insert the resulting expression it back into Eq. (2.29). After short algebra, we obtain

$$\frac{d\boldsymbol{M}}{dt} = -\gamma' \boldsymbol{M} \times \boldsymbol{B}_{\mathbf{eff}} - \lambda' \boldsymbol{M} \times (\boldsymbol{M} \times \boldsymbol{B}_{\mathbf{eff}}). \tag{2.30}$$

Here, the effective gyromagnetic ratio is defined as

$$\gamma' = \frac{\gamma}{1+\alpha^2} \tag{2.31}$$

and the effective relaxation frequency is given by

$$\lambda' = \frac{\alpha\gamma}{1+\alpha^2}. \tag{2.32}$$

Note that λ' is given in units of the frequency divided by the magnetic field. The damping gives rise to a finite imaginary part of the susceptibility. Let us consider the susceptibility for a simple example. Assuming Gilbert damping and an external perturbation of the form $\boldsymbol{B_0} \sim \delta(t)\boldsymbol{x}$, the susceptibility as a function of the magnetic field displays a Lorentzian resonance peak [149]. Its half width at half maximum is given as [149]

$$\Delta B = \frac{\alpha\omega}{\gamma}. \tag{2.33}$$

Consequently, the Gilbert damping parameter can be measured from the susceptibility in a resonance experiment.

In the steady-state, the precession of the magnetization direction around the precession axis forms a cone. The cone angle of this precession cone (angle between the magnetization direction and the precession axis) is a function of the resonance width and the

applied fields, as well as the saturation magnetization [150, 151]. At resonance it is determined by [151] (solving the linearized Landau-Lifshitz-Gilbert equation)

$$\theta \sim \frac{b_{\mathrm{rf}}}{\Delta B}. \tag{2.34}$$

The angle is small due to the small applied rf-field. Note that it is in general not possible to revert the magnetization direction (in contrast to nuclear magnetic resonance). For sufficiently large driving powers of the rf-field, spin waves will be excited instead of a further driving of the ferromagnetic resonance.

2.4.2 Ferromagnetic resonance in a ferromagnet/normal metal junction

The ferromagnet/normal metal (F/N) junction corresponds to the ferromagnet/superconductor (F/S) junction, when the superconductor is in its normal state. It is therefore relevant to discuss the properties of the former junction, with the ferromagnet being subjected to ferromagnetic resonance (FMR), before considering the F/S junction. As we will see, the ferromagnet under FMR conditions injects a spin current into the adjacent normal metal. The idea of the injection of a spin polarized current into a non-magnetic material [152] and its realization [153, 154] are quite old. In these realizations, a spin-polarized current is injected from a ferromagnet into an adjacent semiconductor. A spin accumulation is created in the semiconductor over a length scale of the spin diffusion length. One important difference between these realizations and the more recent proposals is that in the latter, which rely on dynamical effects, pure spin currents, i.e., without a net charge current, are possible.

It is well-known that a spin current driven through a ferromagnetic layer may change the magnetization direction of this layer. This effect is called spin transfer torque (theoretical prediction in [76, 77], experimental verification in [78], for an introduction see for example Ref. [79]). The spin current is responsible for a torque onto the magnetization direction, opposing the Gilbert damping. Tserkovnyak and coworkers [72] proposed to consider the inverse effect: A moving magnetization vector looses torque by emitting a spin current. The authors consider a junction of a ferromagnet and a normal metal, where the ferromagnet is subjected to FMR. The precession of the magnetization transfers angular momentum from the ferromagnet to the normal

metal, injecting a spin current into the normal metal. The net spin current flowing gives rise to an additional damping mechanism for the magnetization, enhancing the Gilbert damping. Slonczewski [76] has shown that a spin transfer torque gives rise to extra terms in the Landau-Lifshitz-Gilbert equation (Eq. (2.29)). Ref. [73] identified this torque as being the spin current for the setup under consideration, corresponding to the extra term in Eq. (2.29) being

$$\frac{\gamma}{MV}\boldsymbol{I}_{\mathbf{s}}. \tag{2.35}$$

Here, V denotes the volume of the ferromagnet. The net spin current $\boldsymbol{I}_{\mathbf{s}} = \boldsymbol{I}_{\mathbf{s}}^{\mathbf{pump}} - \boldsymbol{I}_{\mathbf{s}}^{\mathbf{back}}$ vanishes in the absence of spin-flip scattering in the normal metal. Assuming, in contrary, the normal metal being a perfect spin sink, there is no backflow current, yielding maximum spin current. The pump current can be expressed via the complex valued spin pumping conductance. If the ferromaget is thicker than the transverse spin coherence length, the spin pumping conductance equals the mixing conductance, giving [73]

$$\boldsymbol{I}_{\mathbf{s}}^{\mathbf{pump}} = \frac{\hbar}{4\pi}\left(g_{\mathrm{r}}^{\uparrow\downarrow}\boldsymbol{m}\times\frac{d\boldsymbol{m}}{dt} - g_{\mathrm{i}}^{\uparrow\downarrow}\frac{d\boldsymbol{m}}{dt}\right). \tag{2.36}$$

Here, $\boldsymbol{m} = \frac{\boldsymbol{M}}{M}$ is the magnetization direction. The indices r and i label the real and imaginary part of the dimensionless conductance matrix, defined by [155]

$$g^{\sigma\sigma'} = \sum_{mn}\left[\delta_{mn} - r_{mn}^{\sigma}r_{mn}^{\sigma'}\right], \tag{2.37}$$

where σ, σ' are spin indices and m, n are mode indices. For most systems, the imaginary part of the mixing condutance is small [156] and can thus be neglected [157]. In this case, according to Eqs. (2.35) and (2.36), the contribution of the spin pumping to the Gilbert damping is given by

$$\alpha' = \frac{\hbar\gamma}{4\pi MV}g_{\mathrm{r}}^{\uparrow\downarrow}. \tag{2.38}$$

We still consider an F/N interface with the ferromagnet subjected to FMR conditions. Assuming a diffusive normal metal, Ref. [157] has shown by solving a spin diffusion equation that a time-averaged spin accumulation close to the interface builds up. It depends on the ratio between spin injection rate and spin relaxation rate. The spin accumulation is maximal, if the spin injection rate is much larger than the spin-flip rate and is zero in the opposite limit.

Ref. [158] considered the same setup with additional spin-flip scattering in the ferromagnet. The authors found that the spin accumulation is reduced and that a chemical potential difference builds up across the junction. The reason is that a backflowing spin current parallel to the magnetization direction of the ferromagnet builds up that charges the ferromagnet. This opens the possibility of an electrical detection of the spin accumulation that has been realized experimentally both for an F/N interface [74] and an F/I/N junction [113]. In the latter experiment the voltage detected for this tunnel junction was an order of magnitude larger than for ohmic contacts. This was unexpected, since the tunnel barrier decreases significantly the injection rate compared to ohmic contacts, which should suppress the spin pumping effect. The spin pumping theory developed by Ref. [158] would need an unrealistically large spin mixing conductance to explain this large voltage. Therefore, Ref. [115] proposed a different mechanism for the voltage generation. Based on phenomenological Bloch equations, they consider longitudinal and transversal spin relaxation due to disorder. Spin is accumulated along the magnetization direction of the ferromagnet. This nonequilibrium spin accumulation is then transformed into a voltage by the tunnel barrier. In order to obtain a linear scaling with the precession frequency as in the experiment ([113]), Ref. [115] has to assume that a fraction of the disorder follows the magnetization dynamics. If the normal metal is replaced with a ferromagnet with fixed magnetization direction, we obtain an F/I/F junction with one ferromagnet being in FMR and the other one having a fixed, static magnetization direction. In this junction an additional mechanism exists, i.e., the spin bias drives a charge current through the junction. As shown by Ref. [115], the charge current gives rise to a voltage depending on the spin polarizations of the ferromagnets. This charge pumping voltage can be distinguished from the spin accumulation voltage, noting that the former changes sign if the direction of one of the ferromagnets is flipped, whereas the latter does not change sign [115]. The inverse effect, to use a voltage in order to induce ferromagnetic resonance has been proven experimentally in magnetic tunnel junctions [159].

Another experimental detection technique for FMR in F/N junctions is based on the spin Hall effect [160–163]. In a paramagnetical material with spin-orbit interaction a pure spin current is generated transverse to an applied electrical field, even in the absence of a magnetic field. Analogous to the Hall effect, where charge accumulation leads to a transverse voltage, spin will be accumulated at the edges of the sample leading to spin-dependent transverse chemical potentials. The inverse spin Hall effect

[164–166] may be used in the following way: FMR in the ferromagnet generates a spin current in the adjacent normal metal by the previously described spin pumping mechanism. The inverse spin Hall effect transforms the spin current into a transverse charge current. The charge current has been experimentally measured as a dc voltage [150, 164, 167, 168]. As for example in Ref. [150], in experiments the F/N junction is placed into a coplanar waveguide to excite the FMR using a microwave field. We will discuss experiments containing superconductors in Sec. 6.1.

3 Formalisms - theoretical framework

This chapter gives an overview on the different theoretical tools used to achieve the results in the following two parts of this thesis. Note that details concerning the disorder formalism are integrated into Chapter 8, since they are only relevant for a small part of this thesis. In this chapter, Sec. 3.1 introduces the Bogoliubov – de Gennes formalism that is suitable to solve the eigenvalue problem for a Hamiltonian describing a junction of superconductors. We use it in Chapters 4 and 5 and Appendices A, C, and D to obtain the Andreev bound states and the wavefunctions of the $\mathrm{s}/\mathrm{p_x}$ junction. In Sec. 3.2, we present the scattering matrix formalism for the description of quantum transport through a scattering region between two leads that we use in Appendix A and Chapter 4 for the calculation of the bound states. Further we use scattering matrices in Appendices C and D for the calculation of the continuum wave functions that determine the transistion rates in the $\mathrm{s}/\mathrm{p_x}$ junction. In Sec. 3.3, we introduce the non-equilibrium Green's functions formalism in the Keldysh formulation that allows to perform perturbation theory of non-equilibrium systems. We use it in Chapter 7 in order to calculate the current through the half-metal/superconductor interface with the half-metal being at ferromagnetic resonance. Finally, Sec. 3.4 gives details for the master equation approach using density matrices that we use in Chapter 5 in order to calculate the occupations of the Andreev levels of the $\mathrm{s}/\mathrm{p_x}$ junction in the presence of a time-dependent magnetic field.

3.1 Bogoliubov – de Gennes formalism

In order to theoretically describe superconducting junctions, we need the Bogoliubov – de Gennes formalism that can treat space-dependent pair potentials.

The BCS Hamiltonian in Eq. (2.4) describes a bulk s-wave superconductor. Soon after BCS theory was published, Bogoliubov [120] and Valatin [169] proposed independently to use a unitary transformation to diagonalize the Hamiltonian. This so-called Bogoliubov transformation introduces quasiparticles that are a linear combination of electrons and holes. De Gennes [118] generalized this formalism to a real space description that

allows to treat space-dependent pair potentials. The so-called Bogoliubov – de Gennes formalism can consequently treat junctions containing superconductors. In this section, we want to present the formalism generalized to junctions containing unconventional superconductors. Therefore, we need to consider momentum-dependent pair potentials and a general spin dependence of the pair potential, i.e., pair potentials containing spin singlet and spin triplet components. Parts of this derivation and its idea are taken from Refs. [31, 170]. This generalized formalism is used in Chapter 4 to determine the spectrum and the wavefunctions of the $\mathrm{s}/\mathrm{p_x}$ junction.

Let us start from the general interaction Hamiltonian

$$H = H_0 + H_{\mathrm{int}}. \tag{3.1}$$

Here, the single particle part of the Hamiltonian is given by

$$H_0 = \int d\boldsymbol{r} \sum_{\alpha,\beta} \Psi^\dagger_\alpha(\boldsymbol{r}) H_{\alpha\beta}(\boldsymbol{r}) \Psi_\beta(\boldsymbol{r}), \tag{3.2}$$

where α and β are spin indices and $\Psi^\dagger_\alpha(\boldsymbol{r})$ is a field operator that creates an electron with spin α at position $\boldsymbol{r}$. The fields are fermionic, i.e., $\{\Psi^\dagger_\mu(x'), \Psi_\tau(x)\} = \delta_{\mu\tau}\delta(x - x')$. Here, we used the anti-commutator, defined by $\{A, B\} = AB + BA$. The interaction part of the Hamiltonian (Eq. (3.1)) is given by

$$H_{\mathrm{int}} = -\frac{1}{2} \sum_{\alpha\beta\gamma\delta} \iint d\boldsymbol{r} d\boldsymbol{r'} \Psi^\dagger_\alpha(\boldsymbol{r}) \Psi^\dagger_\beta(\boldsymbol{r'}) V_{\alpha\beta\gamma\delta}(\boldsymbol{r}, \boldsymbol{r'}) \Psi_\delta(\boldsymbol{r'}) \Psi_\gamma(\boldsymbol{r}). \tag{3.3}$$

Here, the spin-dependent potential $V_{\alpha\beta\gamma\delta}(\boldsymbol{r}, \boldsymbol{r'})$ mediates the superconducting interaction. We use a mean-field approximation for the interaction (see for example [118, 121]). It consists of assumimg that the difference between the product of two field operators and its expectation value is small.

We introduce the superconducting pair potential as the following matrix in spin space

$$\Delta_{\alpha\beta}(\boldsymbol{r}, \boldsymbol{r'}) = -\sum_{\gamma\delta} V_{\alpha\beta\gamma\delta}(\boldsymbol{r}, \boldsymbol{r'}) \left\langle \Psi_\delta(\boldsymbol{r'}) \Psi_\gamma(\boldsymbol{r}) \right\rangle, \tag{3.4}$$

$$\Delta^\dagger_{\alpha\beta}(\boldsymbol{r}, \boldsymbol{r'}) = -\sum_{\gamma\delta} V_{\gamma\delta\alpha\beta}(\boldsymbol{r}, \boldsymbol{r'}) \left\langle \Psi^\dagger_\gamma(\boldsymbol{r}) \Psi^\dagger_\delta(\boldsymbol{r'}) \right\rangle. \tag{3.5}$$

We obtain (up to a constant shift in energy) for the interaction part of the Hamiltonian

$$H_{\text{int}} = \frac{1}{2}\sum_{\alpha\beta}\iint d\boldsymbol{r}d\boldsymbol{r'}[\Delta_{\alpha\beta}(\boldsymbol{r},\boldsymbol{r'})\Psi^\dagger_\alpha(\boldsymbol{r})\Psi^\dagger_\beta(\boldsymbol{r'}) + \Delta^\dagger_{\alpha\beta}(\boldsymbol{r},\boldsymbol{r'})\Psi_\beta(\boldsymbol{r'})\Psi_\alpha(\boldsymbol{r})]. \tag{3.6}$$

The total Hamiltonian (Eq. (3.1)) can be written (up to a constant shift in energy) as

$$H = \frac{1}{2}\iint d\boldsymbol{r}d\boldsymbol{r'}\boldsymbol{\Psi}^\dagger(\boldsymbol{r})H_{\text{BdG}}(\boldsymbol{r},\boldsymbol{r'})\boldsymbol{\Psi}(\boldsymbol{r'}). \tag{3.7}$$

Here, we introduced a Nambu basis, defining

$$\boldsymbol{\Psi}(\boldsymbol{r}) = \left(\Psi_\uparrow(\boldsymbol{r}), \Psi_\downarrow(\boldsymbol{r}), \Psi^\dagger_\uparrow(\boldsymbol{r}), \Psi^\dagger_\downarrow(\boldsymbol{r})\right)^T. \tag{3.8}$$

Further, the Bogoliubov – de Gennes (BdG) Hamiltonian reads

$$H_{\text{BdG}}(\boldsymbol{r},\boldsymbol{r'}) = \begin{pmatrix} H(\boldsymbol{r})\delta(\boldsymbol{r}-\boldsymbol{r'}) & \Delta(\boldsymbol{r},\boldsymbol{r'}) \\ \Delta^\dagger(\boldsymbol{r'},\boldsymbol{r}) & -H^*(\boldsymbol{r})\delta(\boldsymbol{r}-\boldsymbol{r'}) \end{pmatrix}. \tag{3.9}$$

Here, Δ and $H(\boldsymbol{r})$ are 2×2 matrices in spin space, according to Eqs. (3.2) and (3.4).

We now use a unitary Bogoliubov transformation $U_n(\boldsymbol{r})$, a 4×4 matrix in spin space, defined via

$$\boldsymbol{\Psi}(\boldsymbol{r}) = \sum_n U_n(\boldsymbol{r})\boldsymbol{\gamma_n}. \tag{3.10}$$

Here, the electron field operators are expressed via quasiparticle operators $\gamma_{n\alpha}$ that are fermionic, i.e., $\{\gamma^\dagger_{m\alpha}, \gamma_{n\beta}\} = \delta_{mn}\delta_{\alpha\beta}$. α, β denote spin indices, whereas n labels all remaining quantum numbers. Additionally, we defined the Nambu vector of quasiparticle operators

$$\boldsymbol{\gamma_n} = \left(\gamma_{n\uparrow}, \gamma_{n\downarrow}, \gamma^\dagger_{n\uparrow}, \gamma^\dagger_{n\downarrow}\right)^T. \tag{3.11}$$

The commutation relations ensure the unitarity of the Bogoliubov transformation, i.e.,

$$\int d\boldsymbol{r}U^\dagger_m(\boldsymbol{r})U_n(\boldsymbol{r}) = \delta_{mn}. \tag{3.12}$$

Using this relation, the inverse transformation that relates the electron operators to the quasiparticle operators is just given by

$$\boldsymbol{\gamma_n} = \int d\boldsymbol{r}U^\dagger_n(\boldsymbol{r})\boldsymbol{\Psi}(\boldsymbol{r}). \tag{3.13}$$

With help of the unitarity relation in Eq. (3.12) it is easy to show that the BdG Hamiltonian in Eq. (3.9) can be written as

$$H = \frac{1}{2}\sum_n \boldsymbol{\gamma_n}^\dagger E_n \boldsymbol{\gamma_n}, \tag{3.14}$$

if the following condition holds true:

$$\int d\boldsymbol{r'} H_{\mathrm{BdG}}(\boldsymbol{r}, \boldsymbol{r'}) U_n(\boldsymbol{r'}) = U_n(\boldsymbol{r}) E_n. \tag{3.15}$$

The equations of this matrix equation are called Bogoliubov – de Gennes equations and E_n is a diagonal matrix. We have thus diagonalized the Hamiltonian (see Eq. (3.14)). We now need to solve the BdG equations, in order to obtain the eigenenergies and explicit expressions for the unitary BdG transformation. Therefore, let us further analyze and simplify the BdG equations. We denote a column vector of the matrix U by $\boldsymbol{w}$. Then, for each column, Eq. (3.15) reads

$$\int d\boldsymbol{r'} H_{\mathrm{BdG}}(\boldsymbol{r}, \boldsymbol{r'}) \boldsymbol{w}_n(\boldsymbol{r'}) = \epsilon_n \boldsymbol{w}_n(\boldsymbol{r}), \tag{3.16}$$

where ϵ_n is a scalar. We will now derive approximate equations, suitable for describing junctions. Defining

$$\boldsymbol{w}_n(\boldsymbol{r}) = \begin{pmatrix} \boldsymbol{u}_n(\boldsymbol{r}) \\ \boldsymbol{v}_n(\boldsymbol{r}) \end{pmatrix}, \tag{3.17}$$

we introduce a vector of electron components $\boldsymbol{u}_n(\boldsymbol{r})$ and a vector of hole components $\boldsymbol{v}_n(\boldsymbol{r})$. Far from the junction, the quasiparticle states may be labeled by their wave vector (the label n corresponding to the wave vector) [170]. We can then separate a fast oscillation on the scale of k_{F}^{-1} and introduce new envelope functions, given by

$$\begin{pmatrix} \tilde{\boldsymbol{u}}_n(\boldsymbol{r}) \\ \tilde{\boldsymbol{v}}_n(\boldsymbol{r}) \end{pmatrix} = e^{-i\boldsymbol{k_n}\boldsymbol{r}} \begin{pmatrix} \boldsymbol{u}_n(\boldsymbol{r}) \\ \boldsymbol{v}_n(\boldsymbol{r}) \end{pmatrix}. \tag{3.18}$$

Let us drop the index n for clarity of the notation. Using Eq. (3.17), Eq. (3.16) splits into two equations. Integrating the first equation of Eq. (3.16) over $\boldsymbol{r'}$, we obtain

$$\int d\boldsymbol{r} \int d\boldsymbol{r'} \left[(H(\boldsymbol{r}) - E)\delta(\boldsymbol{r} - \boldsymbol{r'})\tilde{\boldsymbol{u}}(\boldsymbol{r}) + \Delta(\boldsymbol{r}, \boldsymbol{r'})\tilde{\boldsymbol{v}}(\boldsymbol{r'}) e^{i\boldsymbol{k_n}(\boldsymbol{r'}-\boldsymbol{r})} \right] = 0. \tag{3.19}$$

The manipulation of the second equation given by Eq. (3.16) is similar. Therefore, we restrict the presentation to the first one. Changing the integration to a center of mass coordinate $\boldsymbol{R} = \frac{\boldsymbol{r}+\boldsymbol{r}'}{2}$ and a difference coordinate, $\boldsymbol{s} = \boldsymbol{r} - \boldsymbol{r}'$, we obtain an equation for the integrand of $\int d\boldsymbol{R}$:

$$\int d\boldsymbol{s} \left[\left(H\left(\boldsymbol{R} + \frac{\boldsymbol{s}}{2}\right) - E \right) \delta(\boldsymbol{s}) \tilde{\boldsymbol{u}}\left(\boldsymbol{R} - \frac{\boldsymbol{s}}{2}\right) + \Delta(\boldsymbol{R}, \boldsymbol{s}) \tilde{\boldsymbol{v}}\left(\boldsymbol{R} + \frac{\boldsymbol{s}}{2}\right) e^{i\boldsymbol{k}\boldsymbol{s}} \right] = 0. \tag{3.20}$$

We expand the second term in lowest order in k_F (note that $\boldsymbol{v}$ depends also on $\boldsymbol{k}$), see also Ref. [170], i.e.,

$$\int d\boldsymbol{s} \Delta(\boldsymbol{R}, \boldsymbol{s}) \tilde{\boldsymbol{v}}\left(\boldsymbol{R} + \frac{\boldsymbol{s}}{2}\right) e^{i\boldsymbol{k}\boldsymbol{s}} \approx \Delta(\boldsymbol{R}, \boldsymbol{k}) \tilde{\boldsymbol{v}}(\boldsymbol{R}). \tag{3.21}$$

We defined the Fourier transform of the pair potential as

$$\Delta(\boldsymbol{R}, \boldsymbol{k}) = \int d\boldsymbol{s} \Delta(\boldsymbol{R}, \boldsymbol{s}) e^{i\boldsymbol{k}\boldsymbol{s}}. \tag{3.22}$$

We finally obtain (using also the second equation from Eq. (3.16))

$$\begin{pmatrix} H(\boldsymbol{R}) & \Delta(\boldsymbol{R}, \boldsymbol{k}) \\ \Delta^\dagger(\boldsymbol{R}, \boldsymbol{k}) & -H^*(\boldsymbol{R}) \end{pmatrix} \begin{pmatrix} \tilde{\boldsymbol{u}}(\boldsymbol{R}) \\ \tilde{\boldsymbol{v}}(\boldsymbol{R}) \end{pmatrix} = E \begin{pmatrix} \tilde{\boldsymbol{u}}(\boldsymbol{R}) \\ \tilde{\boldsymbol{v}}(\boldsymbol{R}) \end{pmatrix}. \tag{3.23}$$

These Bogoliubov equations can treat space-dependent pair potentials (junctions), where the space dependence is taken into account via the center of mass variable $\boldsymbol{R}$. Further, the pair potential may be momentum-dependent ($\boldsymbol{k}$), which allows to treat unconventional superconductors. We can thus treat junctions of unconventional superconductors. As an example, consider an unconventional superconductor in the right half-space. Then, using a step function model, the pair potential reads $\Delta(\boldsymbol{R}, \boldsymbol{k}) = \Theta(\boldsymbol{R}\hat{\boldsymbol{x}})\Delta(\boldsymbol{k})$, where Θ denotes the Heaviside function and $\hat{\boldsymbol{x}}$ is the unit vector perpendicular to the interface. $\Delta(\boldsymbol{k})$ contains the momentum dependence. For example, a one-dimensional $\mathrm{p_x}$-wave superconductor will have a dependence on $\frac{k_x}{k_\mathrm{F}}$. If these equations are solved in the bulk (far from the junction), it is convenient to Fourier transform the coordinate $\boldsymbol{R}$, giving simply an algebraic eigenvalue problem to solve. Note that $\Delta(\boldsymbol{R}, \boldsymbol{k})$ and $H(\boldsymbol{R})$ are matrices in spin space. We will also refer to the matrix in Eq. (3.23) as the BdG Hamiltonian, since it is an approximation of Eq. (3.9). This set of equations will be used in Chapters 4 and 5. For the simplest case, i.e., if Eq. (3.23) is solved for a bulk s-wave superconductor, the coefficients u and v define

the bulk transformation given by Bogoliubov [120]. In this case, the coefficients are simply the BCS coherence factors, given in Eq. (2.5). Then, u (v) can be interpreted as the electron (hole) amplitude of the Bogoliubov quasiparticle. Note that for an s-wave superconductor the separation of scales is not necessary, since the pair potential does not have a momentum dependence.

Note that we have doubled the number of solutions introducing the particle-hole space. There are two convenient choices to solve this "double counting" problem (double counting is also discussed in Ref. [171], see also Refs. [28, 172]). First, we can restrict ourselves to positive energies only and consider both spins. This choice is called the excitation picture. Second, we can restrict ourselves to one spin species and consider both positive and negative energies. This choice is called the semiconductor picture.

3.2 Scattering matrices for quantum transport

The scattering matrix formalism can be used to solve transport problems through nanostructures. It is suitable to treat junctions of different materials. For superconducting junctions, it can be combined with the Bogoliubov – de Gennes formalism.

The aim of this section is to provide a brief introduction to the concept of scattering matrices that are used in part I of this thesis. For a more detailed introduction, we refer the reader to the books [136, 173]. The idea to describe the transport in a mesoscopic system solving a scattering problem has been developed by Landauer [174, 175] and Büttiker [176–178]. According to the Landauer – Büttiker approach, a nanostructure can be divided into a scattering region (mesoscopic sample) and leads attached to it. The leads shall be macroscopic reservoirs in equilibrium, providing electrons that are scattered in the sample. Confining all scattering to the sample, the wavefunctions for incoming and outgoing electrons in the leads can be expressed as

$$\Psi^{\mathrm{in}} = \sum_{\alpha} c_{\alpha}^{\mathrm{in}} \phi_{\alpha}^{\mathrm{in}}, \tag{3.24}$$

$$\Psi^{\mathrm{out}} = \sum_{\beta} c_{\beta}^{\mathrm{out}} \phi_{\beta}^{\mathrm{out}}, \tag{3.25}$$

where the sets $\{\phi_{\alpha}^{\mathrm{in}}\}$ and $\{\phi_{\beta}^{\mathrm{out}}\}$ form an orthonormal basis. The scattering region being mesoscopic, it has to be treated quantum mechanically. Since the Schrödinger equation

is a linear equation, the outgoing wavefunctions are linearly related to the incoming wavefunctions. The coefficients thus fulfill

$$c_\beta^{\text{out}} = \sum_\alpha S_{\beta\alpha} c_\alpha^{\text{in}}. \tag{3.26}$$

The matrix S, defined by this equation, that relates the incoming coefficient vector to the outgoing coefficient vector, is called the scattering matrix. In general, the scattering matrix can be determined solving the Schrödinger equation in the scattering region and matching the solutions to the wavefunctions in the leads.

Let us discuss some basic properties of the scattering matrix. Particle number conservation in the scattering process can be written as

$$\int d\boldsymbol{r} \left|\Psi^{\text{in}}\right|^2 = \int d\boldsymbol{r} \left|\Psi^{\text{out}}\right|^2, \tag{3.27}$$

imposing for the coefficients to fulfill

$$\sum_\alpha \left|c_\alpha^{\text{in}}\right|^2 = \sum_\alpha \left|c_\alpha^{\text{out}}\right|^2. \tag{3.28}$$

Using Eq. (3.26), we obtain for the scattering matrix

$$S^\dagger S = \mathbb{1}. \tag{3.29}$$

Hence, the scattering matrix is a unitary matrix. Consider a time-reversal invariant system. Then, the time-reversal operation corresponds to complex conjugation of the scattering coefficients and interchanging incoming and outgoing coefficients. It directly follows that the scattering matrix of this system is symmetric, i.e., $S^T = S$.

The current through a nanostructure can be expressed using the scattering matrix. Let us consider the simple case of a two terminal junction. We parametrize the scattering problem in the following way

$$\begin{pmatrix} \hat{c}_{\text{L}}^{\text{out}} \\ \hat{c}_{\text{R}}^{\text{out}} \end{pmatrix} = \begin{pmatrix} r & t' \\ t & r' \end{pmatrix} \begin{pmatrix} \hat{c}_{\text{L}}^{\text{in}} \\ \hat{c}_{\text{R}}^{\text{in}} \end{pmatrix}. \tag{3.30}$$

Here, the superscript distinguishes outgoing from incoming modes and the subscript distinguishes the right hand side from the left hand side of the junction. In general,

the c's in above equation are vectors, containing one entry per mode. Further, the reflection matrix r (r') describes the reflection of waves inciding from the left (right). The transmission matrix t (t') gives the transmission across the nanostructure from left to right (right to left). According to [178], $\hat{c}$ is an electron destruction operator. The current operator on the left hand side of the junction reads

$$\hat{I}_{\mathrm{L}} \propto (\hat{c}_{\mathrm{L}}^{\mathrm{in}})^{\dagger}\hat{c}_{\mathrm{L}}^{\mathrm{in}} - (\hat{c}_{\mathrm{L}}^{\mathrm{out}})^{\dagger}\hat{c}_{\mathrm{L}}^{\mathrm{out}} \tag{3.31}$$

Using the unitarity of the scattering matrix and assuming a Fermi-Dirac distribution $f(E)$ of the electrons on both sides of the junction, we have

$$\langle I_{\mathrm{L}} \rangle = \frac{2e}{h} \int dE \mathrm{Tr}(t^{\dagger}t)[f_{\mathrm{L}}(E) - f_{\mathrm{R}}(E)]. \tag{3.32}$$

$\mathrm{Tr}(t^{\dagger}t)$ can be expressed using the transmission eigenvalues T_p of the nanostructure. If a bias voltage is applied, that is much smaller than the energy dependence of the transmission values, the conductance of the nanostructure (defined via $\langle I_{\mathrm{L}} \rangle = GV$) is given by

$$G = G_0 \sum_p T_p. \tag{3.33}$$

Here, $G_0 = \frac{2e^2}{h}$ is the conductance quantum. This equation is the Landauer formula [174]. For a single channel point contact, that we widely use in the following, the conductance is thus defined by a single parameter, i.e., the transmission value of the channel.

We want to deal with complicated nanostructures that can sometimes be divided into simpler constituents. One might know the scattering matrices for each constituent and want to obtain the combined scattering matrix. We will encouter such a case in Chapter 4 (Appendix A). Consider a system of two scatterers in a row, in a two terminal geometry, where the scatterer i is described by the scattering matrix

$$S_i = \begin{pmatrix} r_i & t_i' \\ t_i & r_i' \end{pmatrix}. \tag{3.34}$$

The total scattering matrix for the combined nanostructure is given by (for a derivation see [179])

$$S^{\mathrm{tot}} = S_{11} + S_{12}(\Sigma_x - S_{22})^{-1}S_{21}, \tag{3.35}$$

where the $N \times N$ matrix Σ_x reads

$$(\Sigma_x)_{\alpha\beta} = \delta_{\alpha,N-\beta}. \tag{3.36}$$

Here, we defined the four matrices

$$S_{11} = \begin{pmatrix} r_1 & 0 \\ 0 & r_2' \end{pmatrix}, \quad S_{12} = \begin{pmatrix} t_1' & 0 \\ 0 & t_2 \end{pmatrix}, \quad S_{21} = \begin{pmatrix} t_1 & 0 \\ 0 & t_2' \end{pmatrix}, \quad S_{22} = \begin{pmatrix} r_1' & 0 \\ 0 & r_2 \end{pmatrix}. \tag{3.37}$$

Scattering matrices are thus not multiplicative, meaning that the total scattering matrix is not the product of the scattering matrices of the subsystem. However, it is possible to define the transfer matrix

$$M_i = \begin{pmatrix} (t_i^\dagger)^{-1} & r_i' t_i'^{-1} \\ -t_i'^{-1} r_i & t_i'^{-1} \end{pmatrix}, \tag{3.38}$$

such that the total transfer matrix $M^{\text{tot}} = M_2 M_1$ is simply the product of the transfer matrices of each scatterer. In contrast to the scattering matrix S that maps the incoming modes to the outgoing modes, the transfer matrix M maps the modes in the right hand region to the modes in the left hand region. Eq. (3.38) gives the mapping between a scattering matrix and the corresponding transfer matrix. The transfer matrix is thus a completely equivalent description.

In this thesis we want to investigate the transport properties of junctions containing superconductors. The scattering matrix formulation of quantum transport has been generalized to superconductors [133–135]. A Josephson junction is described by two superconducting leads that are connected to a normal scattering region that gives rise to the transmission of the junction. The scattering matrix of a single N/S interface takes into account the basic microscopic process of Andreev reflection. The eigenfunctions in the superconducting leads can be obtained solving the Bogoliubov – de Gennes equations (see Sec. 3.1). For details we refer to Refs. [135, 136] and Appendix A.

3.3 Keldysh Green's functions formalism

The aim of this section is to present the non-equilibrium Green's functions formalism that has been developed by Kadanoff and Baym [180] and Keldysh [181]. Here, we use the Keldysh formulation. This formalism is suitable for the calculation of observables of non-equilibrium systems. We use this formalism in Chapter 7, in order to calculate the

current through a half-metal/superconductor interface, when the half-metal is subjected to ferromagnetic resonance. We follow a review article [182] and a book chapter [183] for this presentation.

The Keldysh formalism allows to develop a diagrammatic perturbation theory for non-equilibrium systems. It is assumed that the system has been in equilibrium, described by a statistical average, at some point in the past. Then, a perturbation of the system is "switched on". The aim is to obtain an equation of motion for the single particle Green's function. One finds that this equation of motion involves a hierarchy of correlation functions.

Let us be more precise and consider a system described by the Hamiltonian

$$\mathcal{H}(t) = H + H'(t). \tag{3.39}$$

$H'(t)$ is a perturbation that is "switched on" at $t = t_0$, i.e., $H'(t) = 0$ for $t < t_0$. Before the perturbation is switched on, the system shall be in thermodynamic equilibrium and is then described by the statistical operator $\rho_H = \mathcal{Z}^{-1} e^{-\beta H}$. Here, the temperature is given by $\beta = (kT)^{-1}$ and the partition function reads $\mathcal{Z} = \mathrm{Tr} e^{-\beta H}$. The aim is to calculate the expectation value of an operator O for $t > t_0$, given by

$$\langle O_{\mathcal{H}}(t) \rangle = \mathrm{Tr}(\rho_H O_{\mathcal{H}}(t)), \tag{3.40}$$

where $O_{\mathcal{H}}(t)$ is the operator in the Heisenberg picture (with respect to the Hamiltonian $\mathcal{H}$).

We define the greater ($>$) and lesser ($<$) Green's functions as the following correlation functions

$$G^{<}(1,1') = +i \left\langle \psi^{\dagger}_{\mathcal{H}}(1') \psi_{\mathcal{H}}(1) \right\rangle, \tag{3.41}$$

$$G^{>}(1,1') = -i \left\langle \psi_{\mathcal{H}}(1) \psi^{\dagger}_{\mathcal{H}}(1') \right\rangle, \tag{3.42}$$

where $\psi^{\dagger}_{\mathcal{H}}(1)$ is a fermionic field creation operator in the Heisenberg picture. The dependence on space and time is abbreviated by $1 = (\boldsymbol{x_1}, t_1)$. Let us define the contour Green's function [184]

$$G(1,1') = -i \left\langle T_c \psi_{\mathcal{H}}(1) \psi^{\dagger}_{\mathcal{H}}(1') \right\rangle. \tag{3.43}$$

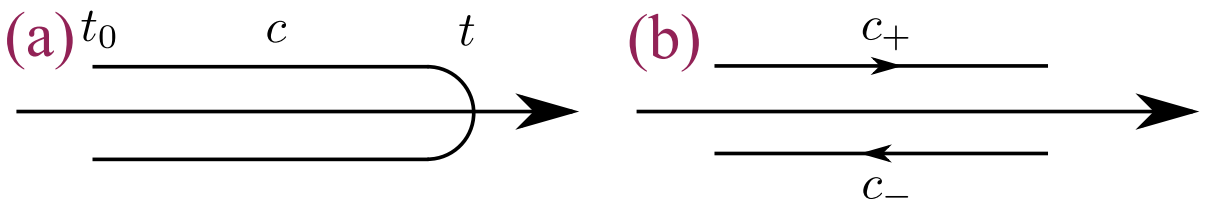

Fig. 3.1: (a) Integration contour for the transformation to the interaction picture, used in Eq. (3.47). (b) Keldysh contour extending from $-\infty$ to $+\infty$, consisting of an upper c_+ and lower c_- integration branch, covered in opposite directions. Fig. adapted from [182].

Here, we introduced the concept of a contour c for time integration, i.e., a path through the complex plane. The contour time-ordering operator T_c orders the operators depending on their time arguments on the contour that we will specify later (see Fig. 3.1), i.e.,

$$T_\mathrm{c} A(t_1)B(t_2) = \begin{cases} A(t_1)B(t_2) & \text{if} \quad t_1 \underset{c}{>} t_2, \\ B(t_2)A(t_1) & \text{if} \quad t_2 \underset{c}{>} t_1. \end{cases} \tag{3.44}$$

The contour Green's function in Eq. (3.43) can thus be expressed via the greater and lesser Green's functions in Eqs. (3.41) and (3.42).

We want to perform perturbation theory on the contour-ordered Green's function. We use an interaction picture representation and express the operator in the Heisenberg picture $O_\mathcal{H}$ via the operator in the interaction picture O_H (with respect to H), using the transformation

$$O_\mathcal{H}(t) = U^\dagger(t,t_0) O_H(t) U(t,t_0), \tag{3.45}$$

where the time-evolution operator is defined as

$$U(t,t_0) = T \exp\left[-\frac{i}{\hbar}\int_{t_0}^{t} dt' H'_H(t')\right]. \tag{3.46}$$

T denotes the usual time-ordering operator (for a time-integration over the real axis) and $H'_H(t)$ is the operator $H'(t)$ in the interaction picture with respect to H.

Using the contour c, shown in Fig. 3.1(a), we can write

$$O_\mathcal{H}(t) = T_\mathrm{c}\left[\exp\left[-\frac{i}{\hbar}\int_c d\tau H'_H(\tau)\right] O_H(t)\right], \tag{3.47}$$

giving for the contour ordered Green's function

$$G_{\mathrm{c}}(1,1') = -i\left\langle T_{\mathrm{c}} \exp\left[-\frac{i}{\hbar}\int_{\mathrm{c}} d\tau H'_H(\tau)\right] \psi_{\mathcal{H}}(1)\psi^{\dagger}_{\mathcal{H}}(1')\right\rangle . \tag{3.48}$$

We want to transform the contour integration back into a regular time integration. We now argue how this can be done using the Keldysh contour c_{K} [181], depicted in Fig. 3.1(b). If we neglect initial correlations, we can put $t_0 \to -\infty$ [185–188]. Using the unitarity of the time-evolution operator, the contour can be extended from the largest time to infinite times. The Keldysh contour c_{K} consists of an upper branch c_+, run through in positive time sense, and a lower branch c_-, run through in negative time sense. The contour ordered Green's function for the Keldysh contour can be written in a matrix representation $\hat{G}$, such that the element $\hat{G}_{ij}$ has the time t_1 on c_i and the time $t_{1'}$ on c_j. The components of $\hat{G}$ explicitly read

$$\hat{G}_{++}(1,1') = -i\left\langle T\psi_{\mathcal{H}}(1)\psi^{\dagger}_{\mathcal{H}}(1')\right\rangle \tag{3.49}$$

$$\hat{G}_{+-}(1,1') = G^{<}(1,1') \tag{3.50}$$

$$\hat{G}_{-+}(1,1') = G^{>}(1,1') \tag{3.51}$$

$$\hat{G}_{--}(1,1') = -i\left\langle \tilde{T}\psi_{\mathcal{H}}(1)\psi^{\dagger}_{\mathcal{H}}(1')\right\rangle \tag{3.52}$$

Here, $\tilde{T}$ is the anti-time-ordering operator that orders in the opposite sense. Larkin and Ovchinnikov [189] introduced a slightly different representation, given by

$$\check{G} = L\tau_3\hat{G}L^{\dagger}. \tag{3.53}$$

Note the difference between the notations $\hat{G}$ and $\check{G}$. Here, τ denotes a Pauli matrix in Keldys space and L is given by

$$L = \frac{1}{\sqrt{2}}(\tau_0 - i\tau_2). \tag{3.54}$$

The time-ordered Green's function reads in this matrix representation

$$\check{G} = \begin{pmatrix} G^{\mathrm{R}} & G^{\mathrm{K}} \\ 0 & G^{\mathrm{A}} \end{pmatrix}. \tag{3.55}$$

Here, we introduced the retarded (R), advanced (A), and Keldysh (K) Green's functions as

$$\begin{aligned} G^{\mathrm{R}}(1,1') &= -i\Theta(t_1 - t_{1'}) \langle \{\Psi_{\mathcal{H}}(1), \Psi_{\mathcal{H}}(1')\} \rangle &&= \Theta(t_1 - t_{1'})[G^{>}(1,1') - G^{<}(1,1')], \\ G^{\mathrm{A}}(1,1') &= +i\Theta(t_{1'} - t_1) \langle \{\Psi_{\mathcal{H}}(1), \Psi_{\mathcal{H}}(1')\} \rangle &&= -\Theta(t_{1'} - t_1)[G^{>}(1,1') - G^{<}(1,1')], \\ G^{\mathrm{K}}(1,1') &= -i \langle [\Psi_{\mathcal{H}}(1), \Psi_{\mathcal{H}}(1')] \rangle &&= G^{>}(1,1') + G^{<}(1,1'). \end{aligned} \tag{3.56}$$

We want to express the total Green's function via the equilibrium Green's function. Therefore, we consider a perturbation expansion. Let us first of all consider the simplest case of a scalar potential. The first order diagram contribution of the contour ordered Green's function given in Eq. (3.48) reads

$$G_{\mathrm{c}}^{(1)}(1,1') = \hbar^{-1} \int dx_2 \int_c d\tau_2 G_{\mathrm{c}}^{(0)}(1,2) V(2) G_{\mathrm{c}}^{(0)}(2,1'). \tag{3.57}$$

Here, $G_{\mathrm{c}}^{(0)}$ is the contour ordered Green's function of the unberturbed system. We have used Wick's theorem, i.e., that the expectation value (quadratically weighted) of a product of contour ordered operators is the sum of all possible products of two operators:

$$\langle \mathcal{T}_{\mathrm{c_K}} c(\tau_n) \cdots c(\tau_1) \rangle = \sum_{\Pi} \prod_{q,q'} \langle \mathcal{T}_{\mathrm{c}} c_q(\tau) c_{q'}(\tau') \rangle \tag{3.58}$$

The sum is taken over all possible products Π of two operators without distinguishing the order. The operators c are either annihilation or creation operators and q, q' label the state that is created/destroyed. We now decompose the contour integration into a forward and backward integration over a real time coordinate. Further introducing the potential in Keldysh space

$$\hat{V}_{ij}(1) = V(1)(\tau_3)_{ij}, \tag{3.59}$$

we obtain

$$\hat{G}_{ij}^{(1)}(1,1') = \hbar^{-1} \sum_{k,l} \int dx_2 \int_{-\infty}^{\infty} dt_2 \hat{G}_{ik}^{(0)}(1,2) \hat{V}_{kl}(2) \hat{G}_{lj}^{(0)}(2,1'). \tag{3.60}$$

The perturbation expansion can be iterated and resummation of terms yields again the full Green's function. Introducing a short notation, we obtain the following Dyson equation

$$\hat{G} = \hat{G}^{(0)} + \hat{G}^{(0)} \otimes \hat{V} \hat{G}, \tag{3.61}$$

where matrix multiplication in Keldysh space is implied for the product of matrices. Further, $\otimes$ denotes matrix multiplication over internal degrees of freedom and integration over all space and time coordinates.

This approach can be generalized, yielding the more general non-equilibrium Dyson equation

$$\check{G} = \check{G}_0 + \check{G}_0 \otimes \check{\Sigma} \otimes \check{G}, \tag{3.62}$$

that contains the self energy Σ. Note that this is an equation for the matrix representation of the time-ordered Green's function, defined in Eq. (3.55). Further, the self-energy in matrix representation is defined as

$$\check{\Sigma} = \begin{pmatrix} \Sigma^{\mathrm{R}} & \Sigma^{\mathrm{K}} \\ 0 & \Sigma^{\mathrm{A}} \end{pmatrix}, \tag{3.63}$$

where

$$\Sigma^{\mathrm{R}}(1,1') = \Theta(t_1 - t_{1'})(\Sigma^{>}(1,1') - \Sigma^{<}(1,1')), \tag{3.64}$$

$$\Sigma^{\mathrm{A}}(1,1') = -\Theta(t_{1'} - t_1)(\Sigma^{>}(1,1') - \Sigma^{<}(1,1')), \tag{3.65}$$

$$\Sigma^{\mathrm{K}}(1,1') = \Sigma^{>}(1,1') + \Sigma^{<}(1,1'). \tag{3.66}$$

Further, we identified $\Sigma_{+-} = \Sigma^{<}$ and $\Sigma_{-+} = \Sigma^{>}$. The self-energy can be calculated in a diagrammatic approach, summing over all single-particle irreducible diagrams without external propagator lines. Knowing the unperturbed matrix Green's function $\check{G}_0$, we are thus able to calculate the full Green's function with help of Eq. (3.62).

The usefulness of this formalism becomes more apparent in Chapter 7. We will see that we can express the expectation value of the current using the Keldysh Green's function. The main task for that kind of problem is thus to determine $\check{G}_0$ and $\check{\Sigma}$.

3.4 Master equation approach - density matrix theory

We start this section by a brief introduction into density matrices. Afterwards, we will show (following Ref. [190]) the main steps for the derivation of a master equation in Markov approximation for the density matrix elements of a system coupled to a

reservoir. Coupling to a reservoir gives rise to relaxation processes for the states of the system. We use this formalism in Chapter 5, where the states of the $\mathrm{s}/\mathrm{p_x}$ Josephson junction are coupled via a Zeeman field to the continuum of states of the junction, which plays the role of a reservoir.

A (quantum) master equation is a first order differential equation that describes the time-evolution of the density matrix elements. It is a generalization of a classical master equation that describes the time-evolution of probabilities (diagonal elements of the density matrix). The general idea is to divide the system into a small observed system S and a large unobserved reservoir R. R and S are weakly coupled by an interaction, which is treated perturbatively. It is assumed that R has many degrees of freedom, such that the interaction with S does not significantly modify R. Further, it is assumed that dissipation processes in R are fast. Finally, the Markov approximation consists of assuming that the system S does not have any memory of its past. Markov master equations are used for the quantum theory of relaxation. The coupling of the system S with the reservoir R gives rise to relaxation, since energy dissipated from S to R may stay in R. Markov master equations are for example relevant in quantum optics, e.g., for the coupling of a two level system with a cavity. They are also used for NMR (Bloch equations).

Before going into more detail concerning the master equation, let us introduce density matrices. The density operator, which is also called statistical operator, describing a mixture of states $|\Psi_n\rangle$, is defined as

$$\rho = \sum_n W_n \left|\Psi_n\right\rangle \left\langle\Psi_n\right| . \tag{3.67}$$

Here, W_n is the probability to find the system in the state $|\Psi_n\rangle$. Let us choose an orthonormal basis given by the set $\{|\phi_n\rangle\}$. The matrix formed of the elements

$$\rho_{ij} = \left\langle\phi_i\right| \left|\rho\right| \left|\phi_j\right\rangle \tag{3.68}$$

is called density matrix. The diagonal elements of the density matrix fulfill $\rho_{ii} \geq 0$ and give the probability of the system to be in the basis state $|\phi_i\rangle$. The expectation value of an operator is given by

$$\langle A\rangle = \frac{\mathrm{Tr}(\rho A)}{\mathrm{Tr}\rho}. \tag{3.69}$$

Normalizing the sum of the probabilities to unity corresponds to imposing $\mathrm{Tr}\rho = 1$. A state is called a pure state, if it fulfills $\mathrm{Tr}(\rho^2) = (\mathrm{Tr}\rho)^2 = 1$ (where the last equality holds for a normalized state). The off-diagonal elements of the density matrix are called coherences, since they are non-zero for a coherent superposition of states. Let us now consider the time evolution of a state that is given by the Schrödinger equation. For the density operator it takes the form

$$i\hbar\frac{\partial\rho(t)}{\partial t} = [H(t), \rho(t)]. \tag{3.70}$$

This equation is called Liouville equation. Assuming that we can write

$$H(t) = H_0 + V(t), \tag{3.71}$$

where H_0 is time independent, we obtain the Liouville equation in the interaction picture

$$i\hbar\frac{\partial\tilde{\rho}(t)}{\partial t} = [\tilde{V}(t), \tilde{\rho}(t)]. \tag{3.72}$$

Here, the operators in the interaction picture are defined via

$$\tilde{A}(t) = e^{\frac{i}{\hbar}H_0 t}A(t)e^{-\frac{i}{\hbar}H_0 t}. \tag{3.73}$$

We now want to give the main steps for the derivation of the master equation. We follow the ideas given in Ref. [190]. We divide our system into a small observed system S, described by the Hamiltonian H_S and an unobserved reservoir R, described by H_R. The total Hamiltonian is given by $H = H_\mathrm{S} + H_\mathrm{R} + V(t)$, where $V(t)$ is the interaction between the system and the reservoir. We assume that the interaction is switched on at $t = 0$. Prior to this point the reservoir and the system are decoupled. The weak interaction between the reservoir and the system is treated perturbatively. Further, we assume that the reservoir is not significantly changed by the perturbation, such that it stays in a thermal state throughout the entire time evolution.

We now define the reduced density matrix of the system as

$$\tilde{\rho}_\mathrm{S} = \mathrm{Tr}_\mathrm{R}\tilde{\rho}, \tag{3.74}$$

where the trace is taken over all reservoir degrees of freedom. At $t = 0$, the system and the reservoir are decoupled and uncorrelated, such that

$$\tilde{\rho}(0) = \tilde{\rho}_{\mathrm{S}}(0)\tilde{\rho}_{\mathrm{R}}(0). \tag{3.75}$$

We now assume that the reservoir has many degrees of freedom, such that the changes in the reservoir due to the interaction with the system can be neglected [191]. This assumption is valid, if the system is much smaller than the reservoir. The density matrix of the reservoir is thus for all times given by the initial ($t = 0$) density matrix of the reservoir. This assumption is also called condition of irreversibility, since it prevents energy dissipated into the reservoir from returning back to the system. Formal integration of the Liouville equation (Eq. (3.72)) gives

$$\tilde{\rho}(t) = -\frac{i}{\hbar}\int_0^t dt'[\tilde{V}(t'), \tilde{\rho}(t')]. \tag{3.76}$$

Inserting this expression into the Liouville equation (Eq. (3.72)) we obtain

$$\dot{\tilde{\rho}}_{\mathrm{S}}(t) = -\frac{i}{\hbar}\mathrm{Tr}_{\mathrm{R}}[\tilde{V}(t), \rho_{\mathrm{S}}(0)\rho_{\mathrm{R}}(0)] - \frac{1}{\hbar^2}\int_0^t dt'\mathrm{Tr}_{\mathrm{R}}[\tilde{V}(t), [\tilde{V}(t'), \tilde{\rho}_{\mathrm{S}}(t')\rho_{\mathrm{R}}(0)]], \tag{3.77}$$

where the dot denotes the time derivative. Eq. (3.77) gives the equation of motion for the density operator up to second order in the interaction $V(t)$. We now make the Markov approximation: We assume that the system has no memory of its past. This corresponds to $\dot{\tilde{\rho}}_{\mathrm{S}}(t)$ only depending on $\tilde{\rho}_{\mathrm{S}}(t)$, i.e., replacing $\tilde{\rho}_{\mathrm{S}}(t') \to \tilde{\rho}_{\mathrm{S}}(t)$ under the integral in Eq. (3.77). If the correlation time τ of the reservoir is much smaller than the decay time, i.e., $\tau \ll \gamma^{-1}$ (where γ is the decay rate), then the Markov approximation holds true. Following Ref. [192], we decompose the interaction

$$\tilde{V}(t) = \sum_i \tilde{R}_i(t)\tilde{S}_i(t), \tag{3.78}$$

where R and S are operators acting only on the reservoir, the system, respectively. Let us analyze the appearing time correlation functions of the form

$$\left\langle \tilde{R}_i(t)\tilde{R}_j(t')\right\rangle = \mathrm{Tr}_{\mathrm{R}}\left(\tilde{R}_i(t)\tilde{R}_j(t')\tilde{\rho}_{\mathrm{R}}(0)\right). \tag{3.79}$$

First note that the correlation function is only a function of $t - t'$. Second, since we assumed quick dissipation in the reservoir, these correlation functions will only be

non-zero for $t - t' < \tau$. Traces over a single reservoir operator are zero and therefore the first term in Eq. (3.77), which is linear in the interaction V, is zero. We now choose a set of basis states $\{|n\rangle\}$ that are eigenstates of H_{S} and obtain from Eq. (3.77)

$$\begin{aligned}\frac{d}{dt}\tilde{\rho}_{mn} = -\frac{1}{\hbar^2}\int_0^\infty dt'' \sum_{ijkl} \Big\{ &\left\langle m\left|\tilde{S}_i(t)\right|k\right\rangle \left\langle k\left|\tilde{S}_j(t-t'')\right|l\right\rangle \tilde{\rho}_{ln} \left\langle \tilde{R}_i(t'')\tilde{R}_j(0)\right\rangle \\ &- \left\langle m\left|\tilde{S}_j(t-t'')\right|k\right\rangle \tilde{\rho}_{kl} \left\langle l\left|\tilde{S}_i(t)\right|n\right\rangle \left\langle \tilde{R}_i(t'')\tilde{R}_j(0)\right\rangle \\ &- \left\langle m\left|\tilde{S}_i(t)\right|k\right\rangle \tilde{\rho}_{kl} \left\langle l\left|\tilde{S}_j(t-t'')\right|n\right\rangle \left\langle \tilde{R}_j(0)\tilde{R}_i(t'')\right\rangle \\ &+ \tilde{\rho}_{mk} \left\langle k\left|\tilde{S}_j(t-t'')\right|l\right\rangle \left\langle l\left|\tilde{S}_i(t)\right|n\right\rangle \left\langle \tilde{R}_j(0)\tilde{R}_i(t'')\right\rangle \Big\}.\end{aligned} \tag{3.80}$$

Here, we could extend the integration to infinity, since contributions from times larger than the correlation time are negligible. Eq. (3.80) is used in Chapter 5. In order to evaluate the remaining matrix elements, the interaction has to be specified. At this point, we will only make two general comments. First, if the reservoir is fermionic and in thermal equilibrium, the correlation functions appearing in Eq. (3.80) are the product of a Fermi-Dirac distribution function and a phase factor $e^{i\omega t''}$ containing the time dependence. In Chapter 5, we will treat the continuum of states of an $\mathrm{s}/\mathrm{p_x}$ Josephson junction as a fermionic thermal reservoir. Second, note that Eq. (3.80) is linear in the elements of the density matrix ρ_{ij}. We can thus rewrite this expression, defining a vector of length N^2 of the entries of the $N \times N$ density matrix, given by

$$\boldsymbol{\rho} = (\rho_{11}, \rho_{12}, ..., \rho_{1N}, \rho_{21}, ...\rho_{2N}, ...\rho_{NN})^T. \tag{3.81}$$

Then, Eq. (3.80) formally reads

$$\dot{\boldsymbol{\rho}}(t) = P(t)\boldsymbol{\rho}(t), \tag{3.82}$$

where $P(t)$ is a (in general time-dependent) $N^2 \times N^2$ matrix. This equation is a master equation, since it is a first order differential equation for the occupations (and coherences). If $P(t)$ is time independent, solving this system of coupled differential equations reduces to an eigenvalue problem. Further, the stationary solution at large time scales is given by $P(t)\boldsymbol{\rho}(t) = 0$. In Chapter 5, we will be interested in the stationary occupations of the $\mathrm{s}/\mathrm{p_x}$ junction that determine the current through the junction.

Part I

Singlet/triplet Josephson junction

4 Equilibrium properties of the singlet/triplet junction

We have seen in Sec. 2.3.2 that the current-phase relation of a conventional Josephson junction contains information about the Andreev levels and their occupations. If we replace one of the conventional superconductors by an unconventional superconductor, we obtain a junction having exotic bound states leading to unusual current-phase relations. Amongst unconventional Josephson junctions, those realized between singlet and triplet superconductors are of special interest, because of their incompatible spin pairing symmetries. Their equilibrium properties have been studied for various types of heterogeneous junctions [28, 31, 35, 193–196]. It has been shown that their current-phase relation is non-sinusoidal, since the incompatible spin properties forbid the transfer of a single Cooper pair across the junction.

In this chapter, we want to focus on the simplest singlet/triplet Josephson junction between a conventional spin singlet, s-wave superconductor and a quasi one-dimensional unconventional spin triplet, $\mathrm{p_x}$-wave superconductor. This junction is presented in Sec. 4.1. All equilibrium properties can be obtained knowing the density of states and the free energy. In order to calculate the density of states, we use a scattering matrix formalism, developed in Appendix A for junctions containing unconventional superconductors that have a constant absolute value of the pair potential. In Sec. 4.2, we will use this formalism to show that the $\mathrm{s/p_x}$ junction hosts two spin-polarized Andreev bound states, which have the same spin [44]. In Sec. 4.3, we determine the free energy of the junction. Based on the density of states obtained from the scattering matrix formalism and the free energy expression, we show in Sec. 4.4 that there is a π-periodic equilibrium supercurrent, which does not probe the exotic spin properties [29, 36, 197]. Sec. 4.5 uses the free energy to show that in equilibrium the peculiar Andreev bound states result in a spontaneous magnetization, which is 2π-periodic in the superconducting phase difference. The spin polarization of the Andreev levels opens the possibility for spin manipulation, using a time-dependent Zeeman field. The resulting non-equilibrium properties are presented in Chapter 5.

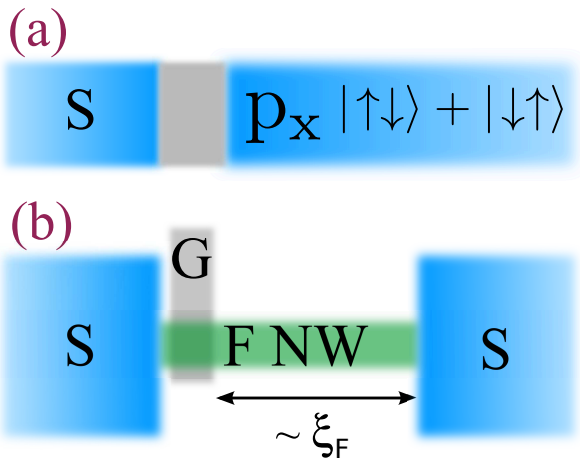

Fig. 4.1: (a) Model of a Josephson junction between an s-wave and a p_x-wave superconductor. (b) Setup of an effective singlet/triplet junction using a semiconducting ferromagnetic nanowire (F NW) contacted with conventional singlet superconductors (S). The gate (G) allows to realize a barrier with tunable transparency. Fig. adapted from Ref. [198].

Parts of this chapter and of the following chapter (Chapter 5) are taken from Ref. [198], the publication to which this part of the thesis has led.

4.1 Setup and Model

Fig. 4.1(a) schematically shows the junction that we want to consider. The left lead is a conventional spin singlet s-wave superconductor, separated by a barrier from the right lead, an unconventional spin triplet p_x-wave superconductor. A possible experimental realization of this junction could be based on the $(TMTSF)_2X$ Bechgaard salts [17], as suggested in Ref. [44]. For $X = PF_6$ significant evidence for quasi one-dimensional triplet pairing has been reported [199, 200]. In this material superconductivity persists for magnetic fields that are much larger than the Pauli paramagnetic limit. However, since the Bechgaard salts are long organic chains, it might be extremely challenging to contact them with metallic superconductors as aluminum. Other intrinsic inorganic quasi one-dimensional compounds with evidence for triplet pairing have been reported [201–204]. In more detail, $Li_{0.9}Mo_6O_{17}$ is a quasi one-dimensional layered superconductor [201], for which the upper critical field of superconductivity is strongly anisotropic and superconductivity persists beyond the paramagnetic limit [205], making a triplet pairing mechanism very probable [202]. Further, superconductivity has been reported in two chromium pnictide compounds, namely $K_2Cr_3As_3$ [203] and $Rb_2Cr_3As_3$ [204]. In both compounds the upper critical field exceeds the Pauli limit. In $Rb_2Cr_3As_3$ the

electronic specific heat coefficient suggests the existence of nodes in the superconducting energy gap [204]. Alternatively, we propose to engineer a junction with effective $\mathrm{p_x}$-wave pairing. As illustrated in Fig. 4.1(b), this junction consists of two conventional superconductors separated by a ferromagnetic semiconducting nanowire that is quasi one-dimensional. The gate acts as a barrier with tunable transparency. The exchange interaction in the ferromagnet spacially modulates the pair amplitude of the Cooper pairs. Both singlet and triplet correlations are induced. They spacially oscillate with the same period, but with a phase shift. At a distance ξ_F from the interface the singlet Cooper pair wave function in the ferromagnet is zero and the triplet correlations are non-zero [206–208]. Consequently, an effective $\mathrm{p_x}$-wave superconductor is realized when the length of the nanowire between the gate and one of the leads matches the coherence length ξ_F for the superconducting correlations induced in the nanowire.

The Hamiltonian describing the Josephson junction between an s-wave superconductor and a one-dimensional time-reversal symmetric $\mathrm{p_x}$-wave superconductor reads

$$H = \int dx\ \Psi^\dagger \mathcal{H} \Psi, \tag{4.1}$$

where we introduced the Nambu spinor $\Psi = (R_\downarrow, L_\uparrow^\dagger, L_\downarrow, R_\uparrow^\dagger)^T$ with $R_\sigma^\dagger$ and $L_\sigma^\dagger$ being creation operators for right-moving and left-moving electrons with spin $\sigma = \uparrow, \downarrow$, respectively. Here, we only considered one spin block, in order to prevent from double counting (see also the discussion in Sec. 3.1). The Bogoliubov – de Gennes Hamiltonian $\mathcal{H}$ is given as

$$\mathcal{H} = v_\mathrm{F} p \eta_z \tau_z + U(x)\eta_x\tau_z - \Delta_\mathrm{s}(x)\tau_x + \Delta_\mathrm{p}(x)\eta_z\tau_x e^{-i\tau_z\phi}\ , \tag{4.2}$$

where $\tau_{x,y,z}$ and $\eta_{x,y,z}$ denote Pauli matrices in particle-hole and R/L spaces, respectively. The first term in Eq. (4.2), with Fermi velocity v_F and momentum operator p, is the kinetic energy. Introducing the the R/L space and working in Andreev approximation, i.e., $\Delta \ll E_\mathrm{F}$ (where E_F denotes the Fermi energy), allowed us to linearize the kinetic energy. The second term describes a scalar potential $U(x)$ in the central region of the junction, $0 < x < L$, where L is the junction length. It gives rise to an electronic transmission probability T, when the junction is in the normal state. Note that the first two terms of Eq. (4.2) correspond to $H(\boldsymbol{R})$ in Eq. (3.23), where we worked in a different basis (particle/hole space and spin space). The third term describes s-wave pairing with gap $\Delta_\mathrm{s}(x) = \Delta_\mathrm{s}\theta(-x)$ in the left lead, where θ is the Heaviside

step function and Δ_s denotes the absolute value of the s-wave pair potential. Using this step function model, we neglect the proximity effect and do not treat the pair potentials self-consistently. As discussed in [134, 209], if the width of the junction W is much smaller than the coherence length ξ, i.e., $W \ll \xi$, the spacial variations of the order parameter extend over a distance W. Since non-uniformities on a scale much smaller than the coherence length do not influence the quasiparticle dynamics, the step function model is valid. The last term in Eq. (4.2) describes time-reversal invariant p_x-wave pairing between electrons having opposite spins in the right lead with gap $\Delta_p(x) = \Delta_p \theta(x - L)$, where Δ_p denotes the absolute value of the pair potential. The spin quantization axis (z-direction) is chosen along the **d**-vector [121] of the triplet pair potential. Note that the momentum dependence of the p_x-wave pairing appears in form of the η_z Pauli matrix. The superconducting phase difference across the junction is denoted ϕ. Using the effective setup presented in Fig. 4.1(b), a SQUID-like geometry can be realized, in which the enclosed magnetic flux fixes the phase difference across the junction. In Chapter 5, we will consider the effect of a small ac magnetic field applied to the junction. This field could be provided by an antenna ending close to the junction.

4.2 Andreev bound states

As in a conventional Josephson junction (see Sec. 2.3.2), phase-dependent Andreev bound states form in the s/p_x junction. Knowledge of their properties is imperative, since they determine the equilibrium and non-equilibrium properties of the junction.

We use the scattering matrix formalism presented in Appendix A in order to determine the Andreev bound state energies. The scattering matrix for Andreev reflection corresponding to the Hamiltonian in Eq. (4.2) reads

$$s_A^\sigma = \begin{pmatrix} 0 & 0 & \sigma\alpha_L & 0 \\ 0 & 0 & 0 & -e^{i\phi}\alpha_R \\ \sigma\alpha_L & 0 & 0 & 0 \\ 0 & e^{-i\phi}\alpha_R & 0 & 0 \end{pmatrix}, \tag{4.3}$$

where we defined

$$\alpha_\beta(E) = \begin{cases} \epsilon_\beta - i\sqrt{1-\epsilon_\beta^2} & \text{for} \quad \epsilon_\beta < 1 \\ \epsilon_\beta - \sqrt{\epsilon_\beta^2 - 1} & \text{for} \quad \epsilon_\beta > 1 \end{cases} \tag{4.4}$$

with $\beta \in \{\mathrm{L}, \mathrm{R}\}$ denoting the side of the junction and $\epsilon_\mathrm{L} = \frac{E}{\Delta_\mathrm{s}}$ and $\epsilon_\mathrm{R} = \frac{E}{\Delta_\mathrm{p}}$. For the bound states we obtain $\alpha_\beta(E) = \exp(i\chi_\beta(E))$. This expression is a phase factor that contains the energy-dependent phase shift $\chi_\beta(E)$ due to Andreev reflection. Let us consider spin-independent time-reversal invariant scattering in the normal region, described by the disorder potential $U(x)$ in Eq. (4.2) and giving rise to the following normal region scattering matrix

$$s_\mathrm{N} = \begin{pmatrix} s_\mathrm{e} & 0 \\ 0 & s_\mathrm{h} \end{pmatrix}, \tag{4.5}$$

where the scattering matrix for electrons reads

$$s_\mathrm{e} = \begin{pmatrix} r(E) & t(E) \\ t(E) & r'(E) \end{pmatrix}. \tag{4.6}$$

Futher, the scattering matrix for holes is related to the scattering matrix for electrons via $s_\mathrm{h}(E) = s_\mathrm{e}^*(-E)$. Assuming the short-junction limit, where the length of the junction L is much shorter than the ballistic coherence length, i.e., $L \ll \hbar v_\mathrm{F}/\Delta$, the entries of the normal region scattering matrix are energy independent. Further, assuming a single conduction channel, the entries r, t, r' are scalars. Using the unitarity of the scattering matrix, the determinant in Eq. (A.12) that determines the bound state energies reads after some algebra

$$\det(1 - s_\mathrm{A}^\sigma(E) s_\mathrm{N}^\sigma(E)) = (2-T)\sqrt{1-\epsilon_\mathrm{L}^2}\epsilon_\mathrm{R} + T\sqrt{1-\epsilon_\mathrm{R}^2}\epsilon_\mathrm{L} + T\sigma\sin\phi. \tag{4.7}$$

Here $T = tt^*$ denotes the transmission of the normal region. The condition

$$\det(1 - s_\mathrm{A}^\sigma(E_n) s_\mathrm{N}^\sigma(E_n)) = 0 \tag{4.8}$$

determines the bound state energies E_n. This equation has a lengthy analytical solution that does not give any insights. We will present the analytical solution in limiting cases and show plots for selected parameter regimes.

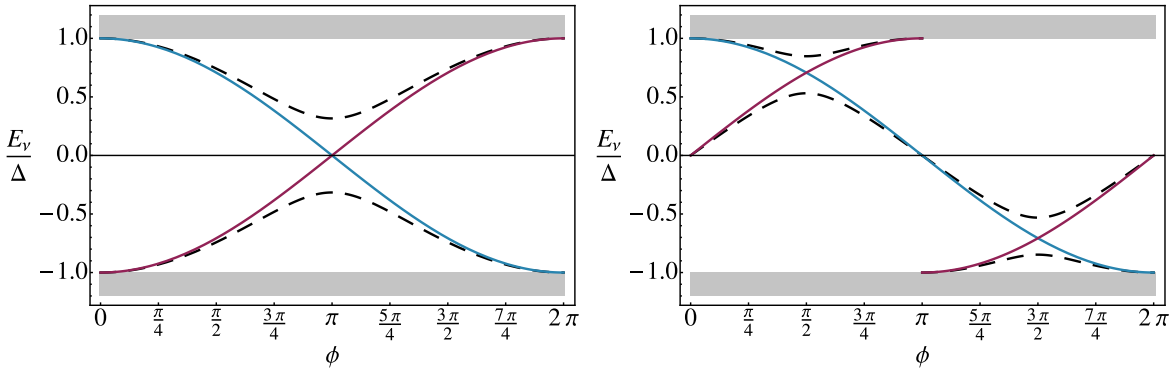

(a) conventional junction **(b)** unconventional $\mathrm{s}/\mathrm{p_x}$ junction

Fig. 4.2: Andreev bound state energy as a function of the phase difference ϕ across the junction. The solid (dashed) lines are given for a transparency of $T = 1$ ($T = 0.8$). The red (blue) lines correspond to solutions from the right (left) moving direction subspace. The red state is π-shifted in the unconventional junction, due to the momentum-dependent pairing.

Let us first of all consider the special case of equal gaps, i.e., $\Delta_\mathrm{s} = \Delta_\mathrm{p} = \Delta$ before discussing the more general properties. Choosing the semiconductor representation with $\sigma = -1$, Eq. (4.8) has the rather simple solution

$$E_\nu = \frac{\mathrm{sgn}(\sin\phi)}{\sqrt{2}}\Delta\sqrt{1+\nu\sqrt{1-T^2\sin^2\phi}}, \tag{4.9}$$

where $\nu \in \pm$ labels the two bound states that have already been reported for this junction in Ref. [28], obtained from a wave-matching approach. It is important to stress that there are two bound states of the same spin for a given phase difference, which both have the same sign of the energy.

There is a more intuitive way of understanding the bound states given by Eq. (4.9). Consider a transparent ($T = 1$) conventional Josephson junction consisting of two s-wave superconductors. The corresponding Andreev bound states in the semiconductor picture (having the same "spin") are shown in Fig. 4.2(a). If we replace one of the superconductors by a $\mathrm{p_x}$-wave superconductor, one of the bound states (the red one in the figure) is phase-shifted by π (see Fig. 4.2(b)). This phase shift is due to the momentum dependence of the pairing. It corresponds to the η_z Pauli matrice in the Hamiltonian in Eq. (4.2). More precisely, an towards the p_x-wave superconductor arriving electron has a positive momentum $k \approx k_\mathrm{F}$, whereas an arriving hole has a negative momentum $k \approx -k_\mathrm{F}$. Hence, the electron "feels" the pair potential $+\Delta$ and

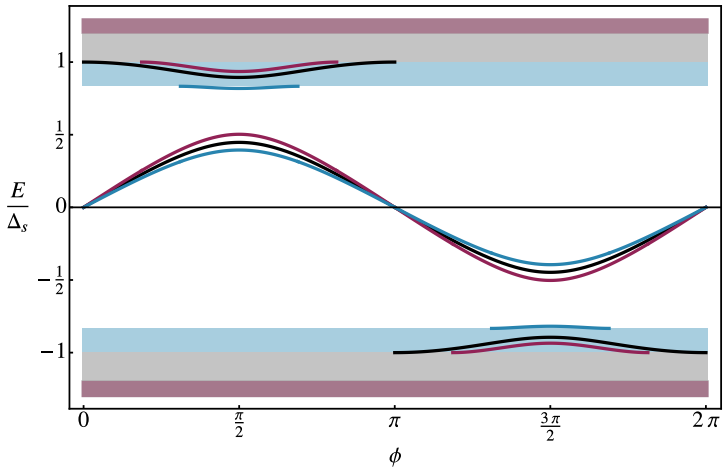

Fig. 4.3: Andreev bound state energy normalized by the gap Δ_s as a function of the phase difference ϕ across the junction for a transparency of $T = 0.8$. The red, black, and blue lines are the Andreev bound states for $\Delta_\mathrm{s} = \frac{5}{6}\Delta_\mathrm{p}$, $\Delta_\mathrm{s} = \Delta_\mathrm{p}$, $\Delta_\mathrm{s} = \frac{6}{5}\Delta_\mathrm{p}$, respectively. The gray box shows the continuum of states in the s-wave superconductor, the blue and red boxes indicate the continuum of the $\mathrm{p_x}$-wave superconductor.

the hole $-\Delta$. One of the bound states is thus π shifted. The bound state energies are consequently given by

$$E_\mathrm{R} = \Delta \sin\frac{\phi}{2}\mathrm{sgn}(\sin\phi), \tag{4.10}$$

$$E_\mathrm{L} = \Delta \cos\frac{\phi}{2}\mathrm{sgn}(\cos\phi). \tag{4.11}$$

Here, R, L stand for the moving direction that we can associate to each state for a transparent junction. If backscattering is introduced, the moving directions are no longer eigenstates, since they are coupled. Thus, a gap opens at the crossings of the states. For the $\mathrm{s/p_x}$ junction the resulting Andreev bound states are given by Eq. (4.9).

At vanishing coupling, $T = 0$ (opaque junction), the two superconductors are decoupled. The spectrum of the s-wave lead is gapped, as in a bulk superconductor. The $\mathrm{p_x}$-wave lead contains a zero-energy edge state, which can be understood as two copies of the Kitaev model [24] (see also [210]) in opposite spin sectors. Note that a finite phase difference across the junction breaks time-reversal symmetry and couples the two Majoranas to one fermionic state. A finite coupling between the two superconductors moves this state to finite energy and yields the bound state $\nu = -$, while the second bound state ($\nu = +$) detaches from the continuum.

Let us now consider what changes if the gaps are different, i.e., $\Delta_\mathrm{s} \neq \Delta_\mathrm{p}$. The bound

state energies are still the solutions of Eq. (4.8). Fig. 4.3 shows examples of the bound state energies for different gap ratios. Again, we chose a semiconductor picture representation with $\sigma = -1$. For a given phase difference ϕ across the junction, we find one or two bound states. The bound state closer to the Fermi level ("lower" bound state) that emerged from the p-wave edge state (at vanishing coupling) is present for all phase values. Its maximum energy is always smaller than both gaps. The other bound state ("upper" bound state) only exists in a certain phase range, or may even be completely absent. A special case is the case of equal gaps, i.e., $\Delta_\mathrm{s} = \Delta_\mathrm{p}$, where the upper state exists for all phases.

In order to investigate the phase range in more detail, let us introduce the ratio of the gaps defined by $\eta = \frac{\Delta_\mathrm{s}}{\Delta_\mathrm{p}}$. Eq. (4.7) gives the following phase boundaries for the upper bound state

$$\phi_0 = \begin{cases} \arccos \eta & \text{for} \quad \eta < 1 \\ \arcsin \frac{2-T}{T} \sqrt{1-\eta^{-2}} & \text{for} \quad \eta > 1 \end{cases} . \tag{4.12}$$

The bound state exists in the phase intervals $[\phi_0, \pi - \phi_0]$ and $[\pi + \phi_0, 2\pi - \phi_0]$. If the s-gap is smaller than the $\mathrm{p_x}$-gap, the phase ϕ_0 is independent of the transparency T. The expression obtained for ϕ_0 in this case is equivalent to the expression for the phase boundary for the bound state of a junction formed of two s-wave superconductors with unequal gaps (see for example Ref. [211]). Note that such a junction only displays bound states for all phase differences, if the gaps are equal. In the opposite case, if the s-gap is bigger than the $\mathrm{p_x}$-gap, ϕ_0 is transmission dependent. We conclude, that the upper bound state detaches only significantly from the continuum, if the gaps of the two superconductors are similar and the junction has a high transparency.

Eq. (4.7) has already been derived in Ref. [44]. However, the expression given in that reference contains a misprint. The authors interchanged the two superconductors. As Fig. 4.3 illustrates, Eq. (4.7) is not symmetric under this operation and it matters, which superconducting gap is bigger. The main results of Ref. [44] are not affected by this mistake. Beside this difference, the plots in Fig. 4.3 have already been presented in Ref. [44].

4.3 Free energy

We want to calculate the free energy, since we can deduce the equilibrium current (Sec. 4.4) and the equilibrium magnetization (Sec. 4.5) from it. First, we diagonalize the Hamiltonian (Eq. (4.2)) using a Bogoliubov transformation

$$\Psi(x) = \sum_{\nu=\pm} \psi_\nu(x)\gamma_\nu + \sum_{E,\mu} \psi_{E\mu}(x)\gamma_{E\mu}, \tag{4.13}$$

where γ_ν and $\gamma_{E\mu}$ are annihilation operators for quasiparticles in the bound state with energy E_ν (given by the solutions of Eq. (4.8)) and for quasiparticles in the continuum with energy E and degeneracy index μ, respectively. $\psi_\pm(x)$ denotes the wavefunction corresponding to the bound state $\pm$. The continuum of (outgoing) propagating states with energies E ($|E| > \Delta$) and wavefunctions $\psi_{E\mu}(x)$ is four-fold degenerate, where μ is a degeneracy index. Explicit expressions for the wavefunctions, that we will need when considering out-of-equilibrium phenomena, are given in Appendix C (for equal gaps). Note that the choice of the spinor Ψ implies that we are considering states with spin down only. The diagonalized Hamiltonian reads

$$H = \sum_{\nu=\pm} E_\nu \gamma_\nu^\dagger \gamma_\nu + \sum_{E,\mu} E \gamma_{E\mu}^\dagger \gamma_{E\mu}. \tag{4.14}$$

Note that we neglected a constant term, that just redefines the energy zero. This form of the Hamiltonian is most suitable for the determination of the bound states dynamics in Chapter 5, since we separated explicitly bound states from continuum states. In order to determine the free energy, however, it is advantageous not to distinguish explicitly between bound and continuum states, but rather write the Hamiltonian as

$$H = E_0 + \sum_{m,\sigma} E_{m\sigma} \left(\gamma_{m\sigma}^\dagger \gamma_{m\sigma} - \frac{1}{2} \right). \tag{4.15}$$

m is a set of quantum numbers. σ denotes the spin that we treat separately from the other quantum numbers. E_0 is a constant that does neither depend on the phase difference nor the magnetic field. The difference between bound states and continuum states is now encoded into the density of states. The free energy is defined as

$$F = -\frac{1}{\beta} \ln Z, \tag{4.16}$$

where $\beta = \frac{1}{kT}$. Here k denotes the Boltzmann constant and T is the temperature. Z is the partition function, defined as

$$Z = \mathrm{Tr}[e^{-\beta H}]. \tag{4.17}$$

The partition function for the Hamiltonian in Eq. (4.15) reads

$$Z = e^{-\beta E_0} \prod_{m,\sigma} \left(e^{\frac{\beta}{2} E_{m\sigma}} + e^{-\frac{\beta}{2} E_{m\sigma}} \right) \tag{4.18}$$

giving for the free energy

$$F = E_0 - \frac{1}{\beta} \sum_{m,\sigma} \ln \left(2 \cosh \frac{\beta E_{m\sigma}}{2} \right). \tag{4.19}$$

We will use this expression in the following two sections in order to calculate the equilibrium current and the equilibrium magnetization of the junction.

4.4 Current-phase relation

The Josephson current through the junction can be obtained from the free energy [212], i.e.,

$$I = \frac{2e}{\hbar} \frac{dF}{d\phi}. \tag{4.20}$$

We follow an approach developed for conventional junctions in Ref. [213] and apply it to our junction. We use the free energy expression in Eq. (4.19) and show in Appendix B that after some manipulations the current reads

$$I = -\frac{4e}{\hbar\beta} \Re \frac{d}{d\phi} \sum_{\sigma \in \{\pm\}} \sum_{n=0}^{\infty} \ln \det(1 - s_{\mathrm{A}}^{\sigma}(i\omega_n) s_{\mathrm{N}}^{\sigma}(i\omega_n)), \tag{4.21}$$

where the sum is evaluated at the fermionic Matsubara frequencies given by

$$\omega_n = (2n+1)\pi\beta^{-1}. \tag{4.22}$$

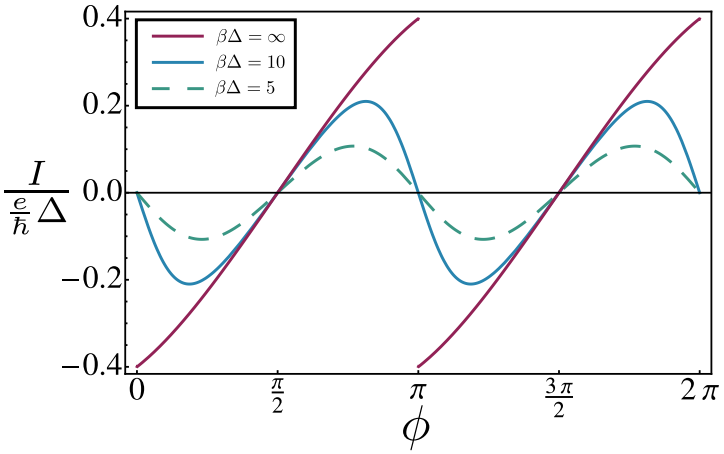

Fig. 4.4: Current-phase relation of the singlet/triplet Josephson junction. Both gaps are taken to be equal and the transmission is $T = 0.8$. The different curves correspond to different temperatures, as given in the legend. The change of sign at $\phi = \pi$ is smoothed at finited temperatures. The curves are obtained from Eq. (4.26).

Let us briefly discuss the current through a short conventional Josephson junction with N conduction channels. Eq. (4.21) yields

$$I = \frac{e\Delta^2}{2\hbar} \sin\phi \sum_{p=1}^{N} \frac{T_p}{E_p} \tanh\left(\frac{\beta E_p}{2}\right), \tag{4.23}$$

where the bound state energies are given by

$$E_p = \Delta\sqrt{1 - T_p \sin^2\frac{\phi}{2}}. \tag{4.24}$$

T_p is the eigenvalue of the matrix $tt^\dagger$, where t is the transmission matrix in Eq. (4.6). This expression for the current has been given in [133] and was originally derived in a different theoretical framework [214].

For the $\mathrm{s/p_x}$ junction, we evaluate Eq. (4.21) using Eq. (4.7). The resulting expression for the current is suitable for numerical evaluation. Obviously, the expression

$$\Re\frac{d}{d\phi} \ln\det(1 - s^\sigma_{\mathrm{A}}(i\omega_n) s^\sigma_{\mathrm{N}}(i\omega_n)) \tag{4.25}$$

is π-periodic in the phase difference ϕ, resulting in a π-periodic current. Thus, the current-phase relation does not probe the peculiar bound state properties. For equal

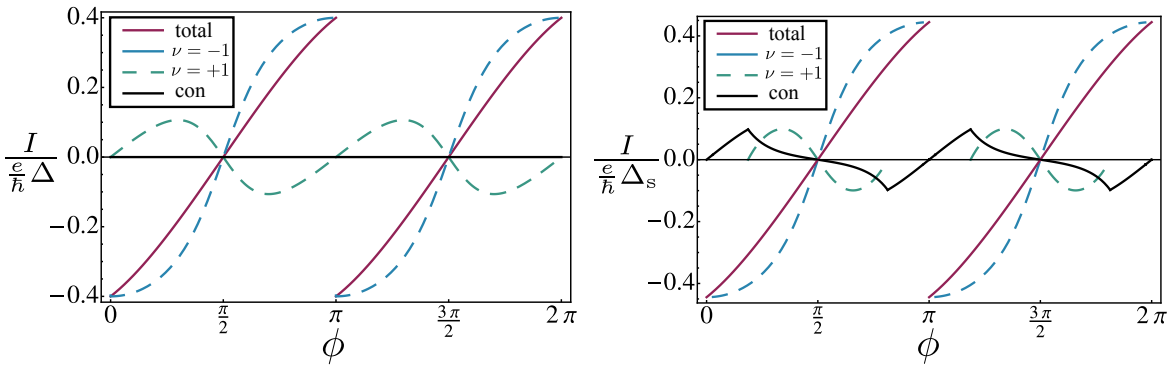

(a) $\Delta_s = \Delta_p$ **(b)** $\Delta_s = \frac{5}{6}\Delta_p$

Fig. 4.5: Contributions of the two bound states and the continuum to the total current at zero temperature. (a) For equal gaps, the current flows entirely via the bound states. (b) If the gaps are not equal, the continuum contributes to the current.

gaps $\Delta_L = \Delta_R = \Delta$, Eq. (4.21) together with Eq. (4.7) yields the simple analytical expression

$$I = \frac{e}{\hbar}\Delta \frac{T^2 \sin^2(2\phi)}{8\sqrt{1 - T^2 \sin^2 \phi}} \left(\frac{\tanh \frac{\beta E_+}{2}}{E_+} - \frac{\tanh \frac{\beta E_-}{2}}{E_-} \right). \tag{4.26}$$

Here, we used the bound state expressions given in Eq. (4.9). For zero temperature, i.e., $\beta \to \infty$, the expression simplifies to

$$I = -\frac{e}{\hbar}\frac{d}{d\phi}(E_+ + E_-) = \frac{e}{\hbar}\frac{T^2 \sin^2(2\phi)}{8\sqrt{1 - T^2 \sin^2 \phi}} \left(E_+^{-1} - E_-^{-1} \right). \tag{4.27}$$

For equal gaps and at zero temperature, the current expression can thus be expressed as the derivative of the energy of the bound states with respect to the phase difference across the junction. The current is consequently entirely transported via the bound states and the continuum does not contribute. At non-zero temperature, temperature weighting factors enters the expression, as evident from Eq. (4.26). Fig. 4.4 shows the current-phase relation of the junction for a transmission of $T = 0.8$ and for equal gaps for different temperatures. At zero temperature it shows a discontinuity at $\phi = \pi$, that is smoothed for finite temperatures. Higher temperature decreases the critical current. The zero-temperature current-phase relation has already been presented in [28, 196]. Note that the first harmonic in the current-phase relation is $\sin(2\phi)$ (and not $\sin \phi$ as in conventional junctions), reflecting the fact that a single Cooper pair cannot be tranferred across the junction due to the incompatible spin pairing symmetries. Fig. 4.5 shows the contributions to the current of the two bound states as well as the

continuum at zero temperature. If both gaps are equal, the contributions of the two bound states add up to the total current. If the gaps are different, the continuum also contributes. For S/N/S junctions consisting of conventional s-wave superconductors this is already well-known [211].

For equal gaps, we can write the Josephson current as

$$I = \frac{2e}{\hbar} \sum_{\nu=\pm} \frac{dE_\nu}{d\phi} \left(n_\nu - \frac{1}{2} \right), \tag{4.28}$$

where the occupation factor is defined via $n_\nu = \left\langle \gamma_\nu^\dagger \gamma_\nu \right\rangle = f(E_\nu)$ and f is the Fermi-Dirac distribution function.

We have seen that the equilibrium current does not probe the peculiar spin properties of the bound states. Thus, in order to probe them, we have to consider out-of-equilibrium effects. These are considered in chapter 5.

4.5 Spontaneous magnetization

A spontaneous equilibrium magnetization of the $\mathrm{s}/\mathrm{p_x}$ Josephson junction has been reported in Ref. [44]. Let us first of all present an intuitive way of grasping this effect before turning towards a mathematical derivation using the free energy. Reconsider Fig. 4.2. Note that one state has been brought from below the Fermi level to above the Fermi level, when going from the conventional junction to the singlet/triplet junction. This state changes consequently its occupation (at zero temperature). Knowing that the conventional junction does not posses any equilibrium magnetization and that the state has spin-$\frac{1}{2}$, we conclude that the $\mathrm{s}/\mathrm{p_x}$ junction has a zero temperature equilibrium magnetization of $\frac{\mu_\mathrm{B}}{2}\mathrm{sgn}(\sin\phi)$.

More quantitatively, the spontaneous equilibrium magnetization can be obtained as the zero magnetic field limit of the magnetization, i.e.,

$$M = -\lim_{B\to 0} \frac{\partial F}{\partial B}. \tag{4.29}$$

Using the expression for the free energy in Eq. (4.19), we obtain after a partial integration

$$M = \frac{\mu_\mathrm{B}}{2} \int_{-\infty}^{0} dE (\rho_\uparrow(E) - \rho_\downarrow(E)) \tanh \frac{\beta E}{2}, \tag{4.30}$$

where $\rho_\sigma(E)$ denotes the density of states for the spin σ and μ_B is the Bohr magneton. We used $\rho_\uparrow(-E) = \rho_\downarrow(E)$. We see that the magnetization at zero temperature is just given by the difference of the density of states for the occupied states below the Fermi level. Eq. (4.30) can be evaluated with the density of states obtained in the scattering matrix formalism.

Eq. (4.30) has the advantage of being intuitive. However, its evaluation might be lengthy. Therefore, we want to express the magnetization using the Matsubara frequencies. Performing the same steps as in Sec. 4.4 and Appendix B, we can express the magnetization as

$$M = -\mu_\mathrm{B} \lim_{h\to 0} \beta^{-1} \sum_{\sigma\in\{\pm 1\}} \sum_{n=0}^{\infty} \Re \frac{\partial}{\partial h} \ln\det(1 - s_\mathrm{A}^\sigma(i\omega_n - \sigma h) s_\mathrm{N}^\sigma(i\omega_n - \sigma h)). \tag{4.31}$$

This expression can be numerically evaluated at arbitrary temperature. Let us now continue the analytical evaluation of this expression at zero temperature, i.e., $\beta = \infty$. Then, the spacing of the Matsubara freqencies goes to zero and the sum over the frequencies becomes an integral.

$$M = -\frac{\mu_\mathrm{B}}{2\pi} \sum_\sigma \int_0^\infty d\omega \Re \lim_{h\to 0} \frac{\partial}{\partial h} \ln\det(1 - s_\mathrm{A}^\sigma(i\omega - \sigma h) s_\mathrm{N}^\sigma(i\omega - \sigma h)) \tag{4.32}$$

We can express the derivative with respect to h as a derivative with respect to ω. Further using $\Im \ln z = \arctan \frac{\Im z}{\Re z}$, we obtain

$$M = \frac{\mu_\mathrm{B}}{2\pi} \sum_\sigma \sigma \int_0^\infty d\omega \frac{\partial}{\partial \omega} \arctan \frac{\Im \det(1 - s_\mathrm{A}^\sigma(i\omega) s_\mathrm{N}^\sigma(i\omega))}{\Re \det(1 - s_\mathrm{A}^\sigma(i\omega) s_\mathrm{N}^\sigma(i\omega))}. \tag{4.33}$$

The integration is trivial and we obtain

$$M = \frac{\mu_\mathrm{B}}{2\pi} \sum_\sigma \sigma \left[\lim_{\omega\to\infty} \arctan \frac{\Im A(i\omega)}{\Re A(i\omega)} - \lim_{\omega\to 0} \arctan \frac{\Im A(i\omega)}{\Re A(i\omega)} \right], \tag{4.34}$$

where we introduced the short notation $A(i\omega) = \det(1 - s_\mathrm{A}^\sigma(i\omega) s_\mathrm{N}^\sigma(i\omega))$. Using the explicit determinant expression given in Eq. (4.7), we have

$$\Re A(i\omega) = T\sigma \sin\phi, \tag{4.35}$$

$$\Im A(i\omega) = (2 - T)\sqrt{1 + \omega_\mathrm{L}^2}\omega_R + T\sqrt{1 + \omega_\mathrm{R}^2}\omega_\mathrm{L}, \tag{4.36}$$

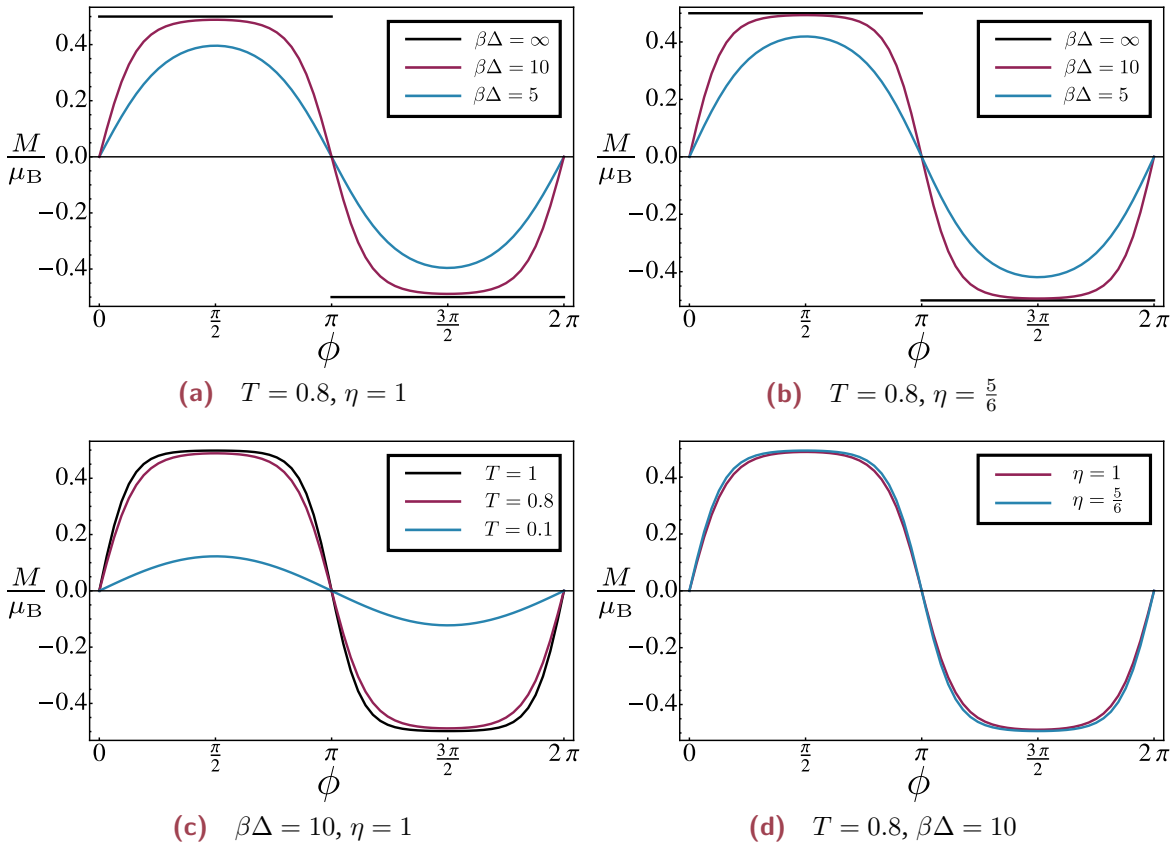

(a) $T = 0.8, \eta = 1$ **(b)** $T = 0.8, \eta = \frac{5}{6}$

(c) $\beta\Delta = 10, \eta = 1$ **(d)** $T = 0.8, \beta\Delta = 10$

Fig. 4.6: Magnetization of the singlet/triplet junction as a function of the phase difference across the junction. (a) and (b) show the evolution with increasing temperature. (c) shows the influence of the transmission and (d) compares different ratios of the gaps.

where $\omega_\beta = \frac{\omega}{\Delta_\beta}$. Using $\lim_{\omega\to\infty} \arctan(a\omega) = \frac{\pi}{2}\mathrm{sgn}(a)$, we finally obtain

$$M = \frac{\mu_B}{2}\mathrm{sgn}(\sin\phi). \tag{4.37}$$

This is the expression that we previously obtained from our intuitive considerations. The junction thus carries a spontaneous magnetization, which is 2π-periodic in the phase difference [44]. Note that this zero temperature magnetization is independent of the ratio of the gaps.

For non-zero temperatures we can numerically evaluate Eq. (4.31), using the determinant expression in Eq. (4.7). Fig. 4.6 shows the curves from numerical evaluation. As evident from Fig. 4.6(a), (b), a finite temperature smoothes the zero temperature magnetization jumps at $\phi = 0, \pi$. Fig. 4.6(c) shows that for a fixed temperature the magnetization decreases when the transmission of the junction decreases. As evident

from Fig. 4.6(d), the gap ratio also influences the magnetization. Similar magnetization curves have first been presented in Ref. [44]. However, the authors only considered the contribution from the $\nu = -$ bound state. Our treatment, in contrary, includes both bound states and the continuum.

We can generalize the magnetization expression for equal gaps in order to treat non-equilibrium situations. Introducing the bound state occupations $n_\nu = \langle \gamma_\nu^\dagger \gamma_\nu \rangle$, we obtain

$$M = -\frac{\mu_\mathrm{B}}{2} \sum_{\nu=\pm} \left(n_\nu - \frac{1}{2} \right). \tag{4.38}$$

In equilibrium $n_\nu = f(E_\nu)$, where f is the Fermi function.

Let us note that Eq. (4.31) indeed gives the result $M = 0$ for a conventional Josephson junction (independently of the gap ratio). This can be easily seen, since the determinant expression is real in that case.

The equilibrium magnetization of the $\mathrm{s}/\mathrm{p_x}$ junction together with the spin polarization of the Andreev bound states opens the possibility of manipulation of the spin properties of the junction using a Zeeman field. The resulting non-equilibrium properties will be analyzed in Chapter 5.

5 Non-equilibrium properties of the singlet/triplet junction

In the previous chapter we have introduced the singlet/triplet Josephson junction consisting of an s-wave and a p_x-wave superconductor. We have shown that the junction has a spin-polarized Andreev spectrum leading to an equilibrium magnetization. The current-phase relation is π periodic and hence not sensitive to the peculiar spin properties. The aim of this chapter is to study non-equilibrium phenomena that probe the spin properties. More precisely, the spin-polarization of the Andreev states opens the possibility of manipulation of the spin state using a time-dependent Zeeman field that creates spin-flip processes. We introduce the Zeeman field in Sec. 5.1 and show that it induces transitions between the states. We will discuss the spin and energy constaints of these transitions. In Sec. 5.2 we focus on the Andreev bound states dynamics induced by the field. We use a master equation approach in order to determine the non-equilibrium occupations of the Andreev levels. Further, we determine the relevant field-induced transition rates for different junction transparencies that enter the expressions for the occupations. The stationary occupations determine the non-equilibrium current-phase relation of the junction that we show in Sec. 5.3 for different polarizations of the magnetic field. The work presented in this chapter has led to a publication and parts of this chapter are taken from this publication (Ref. [198]).

5.1 Processes induced by an ac magnetic field

For simplicity, we will restrict our non-equilibrium analysis to the case $\Delta_s = \Delta_p \equiv \Delta$. When $\Delta_s \neq \Delta_p$, the Rabi oscillations that we find are still possible in the interval of superconducting phase differences with two Andreev bound states.

In order to manipulate the bound state occupations, we apply a weak ac magnetic field, described by the Zeeman Hamiltonian

$$H_Z = \mu_B \sum_{s,s'=\uparrow,\downarrow} \int dx\, \boldsymbol{B} \cdot \left(R_s^\dagger \boldsymbol{\sigma}_{ss'} R_{s'} + L_s^\dagger \boldsymbol{\sigma}_{ss'} L_{s'} \right). \tag{5.1}$$

We consider two different polarizations for the magnetic field $\boldsymbol{B}$. First, let us consider a circularly polarized field $\boldsymbol{B} = B(\cos\Omega t, \sin\Omega t, 0)$, where Ω is the driving frequency. Such a circularly polarized field, perpendicular to the $\boldsymbol{d}$-vector of the triplet pair potential that defines the z-axis leads to spin-flip processes. Second, we investigate a linearly polarized field $\boldsymbol{B} = 2B(\cos\Omega t, 0, 0)$. Such a field is the superposition of two circularly polarized fields with opposite helicities. Therefore, we concentrate our discussion on the case of circular polarization and comment afterwards on the linear polarization.

In order to identify the field-induced processes, we express Eq. (5.1) in terms of quasiparticle operators using the Bogoliubov transformation (4.13). We find

$$H_{\mathrm{Z}} = \mu_{\mathrm{B}} B e^{-i\Omega t}\left(V_{+,-}\gamma_+\gamma_- + \sum_{E;\mu,\nu} V_{\nu,E\mu}\gamma_\nu\gamma_{E\mu} + \frac{1}{2}\sum_{E,E';\mu,\mu'} V_{E\mu,E'\mu'}\gamma_{E\mu}\gamma_{E'\mu'}\right) + \mathrm{h.c.}\,, \tag{5.2}$$

where $V_{\lambda,\lambda'} = \int dx\ \psi_\lambda^T \eta_x(-i\tau_y)\psi_{\lambda'}$ for $\lambda, \lambda' \in \{+, -, E\mu\}$. The field thus couples two quasiparticle states. According to Eq. (5.2), three different types of processes are possible: transitions involving only bound states (first term), transitions involving a bound state and a continuum state (second term), and transitions involving only continuum states (third term). We will now discuss the spin (Sec. 5.1.1) and energy (Sec. 5.1.2) constraints on the different terms.

5.1.1 Spin constraints

In this section we discuss the different processes described by Eq. (5.2) and analyze the spin constraints they are subjected to. We note that the destruction of a quasiparticle with spin down at negative energies corresponds to the creation of a quasiparticle with spin up at positive energies. So far, we used both positive and negative energies for spin $\downarrow$ (semiconductor picture). In the following, we will work with both spin directions, but only positive quasiparticle energies (excitation picture). Furthermore, we assume that the temperature is low, such that the continuum states are empty. The occupation of the continuum states is proportional to $\exp(-\beta\Delta)$, i.e., it is exponentially suppressed for low temperatures.

Depending on the occupation of the Andreev levels, the junction can be in four different states, as sketched in Fig. 5.1(a). If both bound states are empty ($|0\rangle$), the junction is in equilibrium and has the equilibrium magnetization determined in Sec. 4.5. If one

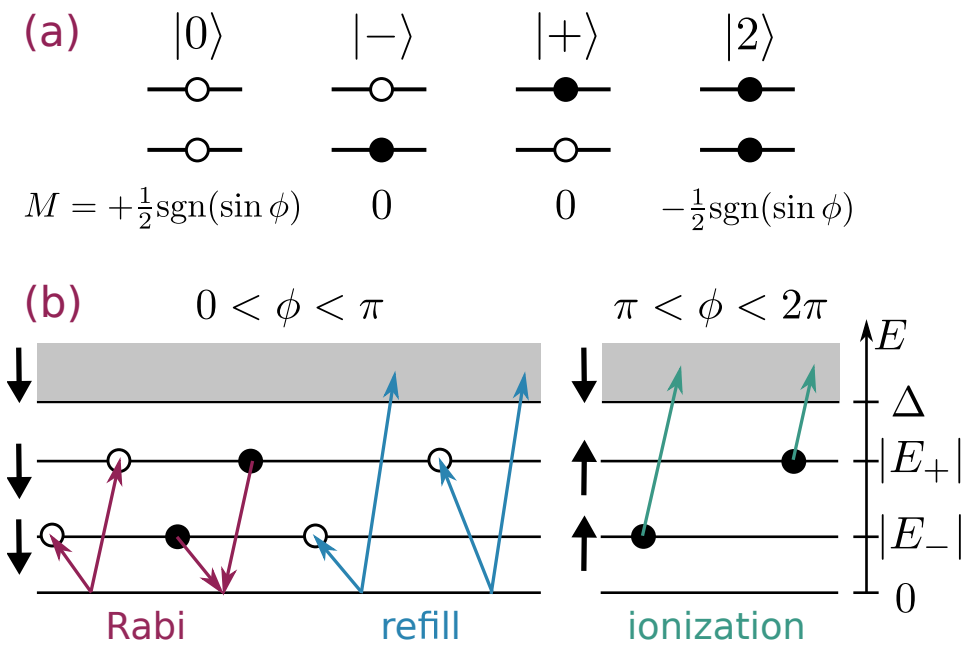

Fig. 5.1: (a) Possible states of the junction and their magnetization M. Full (open) dots represent occupied (empty) states. (b) Transitions induced by a circularly polarized magnetic field with $\Omega < 0$. The shaded region is the continuum of states. The thick black arrows denote the spin of the states. Absorption (emission) of a photon changes the spin by $\Delta S_z = -1$ ($\Delta S_z = +1$). We distinguish Rabi oscillations (red), refill processes (blue) and ionization processes (green). Fig. adapted from [198].

bound state with energy $|E_\nu|$ is occupied and the other bound state is empty, we denote this state of the junction by $|\nu\rangle$. In this case, the magnetization of the junction is zero. If both bound states are occupied ($|2\rangle$), the magnetization has opposite sign with respect to equilibrium.

Let us start the discussion of the field-induced transitions with a circularly polarized magnetic field. The spin of the system changes by $\Delta S_z = \mathrm{sgn}(\Omega)$ when a photon is absorbed, whereas it changes by $\Delta S_z = -\mathrm{sgn}(\Omega)$ when a photon is emitted. For definiteness, we consider the case $\Omega < 0$.

The transitions involving only bound states correspond to Rabi oscillations, i.e., coherent oscillations between the states $|0\rangle$ and $|2\rangle$. The spin selection rule imposes the constraint that Rabi oscillations are only possible if both bound states have spin down, which is the case in the interval $0 < \phi < \pi$.

Transitions involving a bound and a continuum state change the parity of the bound state occupation, connecting the even-parity subspace $\{|0\rangle, |2\rangle\}$ to the odd-parity subspace $\{|-\rangle, |+\rangle\}$. Such a process might represent a decay mechanism for the Rabi

oscillations, since the transfer between the continuum of states and the bound states may not happen in a coherent manner because we assume infinite leads. Whenever a continuum quasiparticle is created, it has zero probability to return to the junction. This corresponds to assuming a Markovian reservoir with short correlation time. We may distinguish two different incoherent processes, sketched in Fig. 5.1(b).

In an *ionization* process, a quasiparticle from a bound state is promoted to a continuum state. The spin selection rule imposes that the bound state has spin up, which is only the case in the interval $\pi < \phi < 2\pi$. Thus, Rabi oscillations and ionization processes occur in different phase intervals.

In a *refill* process, a Cooper pair is broken such that one quasiparticle occupies a bound state, whereas the second quasiparticle is promoted to a continuum state. Here, the spin selection rule imposes that the bound state has spin down, which is the case in the interval $0 < \phi < \pi$.

Let us now consider a linearly polarized magnetic field. As already mentioned, it is the superposition of two circularly polarized fields with opposite helicities. Thus, the spin selection rule is always met by one of the helicities and there is no spin constraint anymore.

5.1.2 Energy constraints

Let us discuss the energy constraints for the different processes due to energy conservation. Fig. 5.2 shows a schematical plot of the energy constraints imposed by energy conservation.

The Rabi oscillations occur when the oscillation frequency of the magnetic field, $|\Omega|$, matches the Rabi frequency, $\Omega_{\mathrm{R}} = \hbar^{-1}|E_+(\phi) + E_-(\phi)|$. Using the energy-phase relation given by Eq. (4.9), the maximum frequency range in which Rabi oscillations may occur is given by $\Delta < \hbar|\Omega| < \sqrt{2}\Delta$. Note that the maximal value of $|E_+(\phi) + E_-(\phi)|$ is transmission dependent. It varies between its minimum Δ at $T = 0$ and its maximum $\sqrt{2}\Delta$ at $T = 1$. Sweeping the phase at fixed frequency, the resonance condition is met (if $\Delta < \hbar\,|\Omega| < \max|E_+(\phi) + E_-(\phi)|$) for four different values of the phase: $\phi_0, \pi - \phi_0, \pi + \phi_0, 2\pi - \phi_0$. These phase values are also indicated in Fig. 5.2. Due to the spin selection rule previously discussed, the circularly polarized field leads to Rabi oscillations only at the two phase values ϕ_0 and $\pi - \phi_0$.

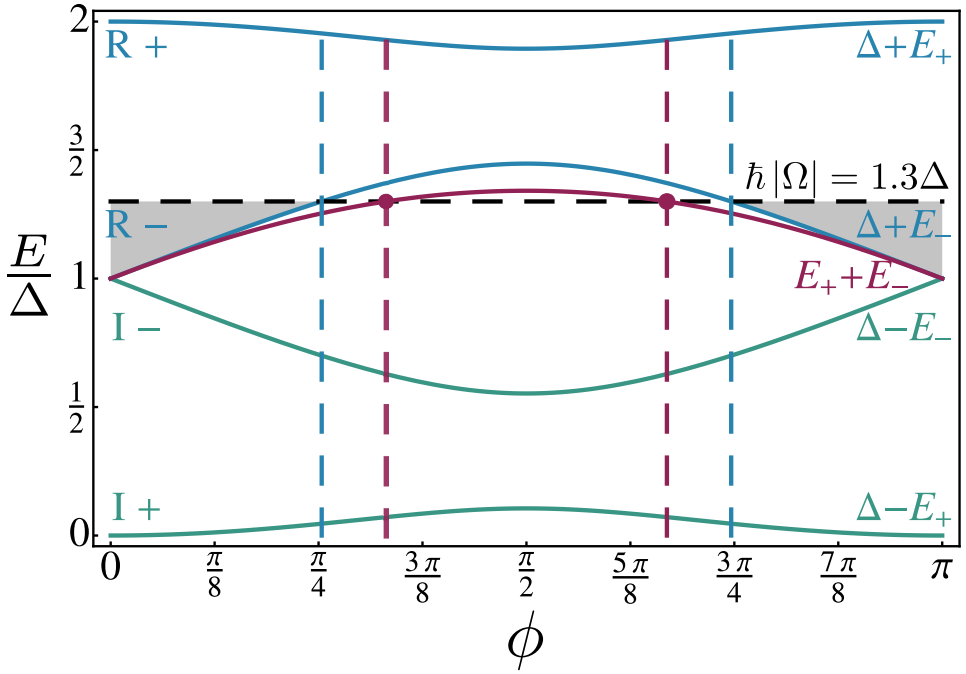

Fig. 5.2: Visualization of the energy constraints as a function of the phase difference ϕ for a junction with a transmission of $T = 0.8$ at a frequency of the magnetic field of $|\Omega| = 1.3\hbar^{-1}\Delta$. The solid red line indicates the condition for Rabi oscillations, that is fulfilled at two phase values indicated by the dots and the vertical dashed lines. The energy thresholds for the refill and ionization processes are shown by the solid blue and green lines. The phase range, for which the frequency is larger than the threshold energy for the refill process of the minus state, is shaded in gray. The critical phase value is indicated by the dashed blue vertical lines. Note that the energy constraints are π periodic and we can thus restrict the plot to the energy interval $[0, \pi]$.

For the refill and ionization processes there is a threshold energy. It is given by a process, where a continuum quasiparticle with an energy equal to Δ is created. Since there is a continuum of states with energies larger than Δ, this threshold energy is only a lower bound. For ionization processes energy conservation imposes $\hbar|\Omega| > \Delta - |E_\nu|$. In the frequency range of interest for Rabi oscillations, this condition is always met, as also illustrated in Fig. 5.2. However, remember that the spin constraints imposed Rabi oscillations and ionization processes to be in different phase intervals. For refill processes energy conservation imposes $\hbar|\Omega| > \Delta + |E_\nu|$. In the frequency range of interest for Rabi oscillations, this condition is never met for the state with energy $|E_+|$. By contrast, for the state with energy $|E_-|$, one obtains a critical phase ϕ_c such that the condition is met in the phase intervals $[-\phi_c, \phi_c]$ and $[\pi - \phi_c, \pi + \phi_c]$. We find $\phi_c < \phi_0$ for all transmissions (see also Fig. 5.2). Thus, Rabi oscillations and refill processes also occur in different phase intervals.

Finally, transitions involving only continuum states are only possible for $\hbar|\Omega| > 2\Delta$. Thus, they do not play a role in the frequency range of interest for Rabi oscillations.

We have seen that Rabi oscillations and both refill and ionization processes occur in different phase intervals. We thus conclude that the field-induced transitions do not provide a decay mechanism for the Rabi oscillations due to energy and spin constraints. However, such a decay may be due to other parity non-conserving processes related to, e.g., quantum phase fluctuations due to the resistive environment of the junction [215, 216]. In that case, the energy to ionize an Andreev level is provided by either an environmental photon or phonon. Assuming that the environment can provide photons or phonons of a large energy range, the energy constraints become irrelevant. Further, the spin selection does not play a role in this case, since environmental photons are unpolarized.

The situation is different for a linearly polarized field. As a consequence of the superposition of both helicities, Rabi oscillations may now occur at the four phases $\phi_0, \pi - \phi_0, \pi + \phi_0$ and $2\pi - \phi_0$. Furthermore, the field-induced ionization rates are non-zero for all superconducting phase differences. Hence, the ionization processes provide a decay mechanism for the Rabi oscillations.

5.2 Andreev bound states dynamics

The modifications of the bound state occupations induced by the different processes discussed in Sec. 5.1 may lead to strong deviations of the Josephson current (Eq. (4.28)) from its equilibrium value. To compute the steady-state Josephson current, we introduce the matrix elements $\rho_{\alpha\beta} = \langle\alpha|\rho|\beta\rangle$ of the reduced density matrix ρ, where $|\alpha\rangle, |\beta\rangle \in \{|0\rangle, |+\rangle, |-\rangle, |2\rangle\}$, such that Eq. (4.28) reads

$$I = (I_+ + I_-)(\rho_{00} - \rho_{22}) + (I_+ - I_-)(\rho_{--} - \rho_{++}) \tag{5.3}$$

with $I_\pm = -\frac{e}{\hbar}\frac{d|E_\pm|}{d\phi}$. Eq. (5.3) neglects a small modification of the current expectation values $I_\pm$ (of order $\mathcal{O}(\mu_B^2 B^2/\Delta^2)$), while it accounts for a large effect (of order $\mathcal{O}(1)$) due to the modified Andreev level occupations. It also neglects charge-imbalance related effects in the presence of an ac drive [216], where more electron-like quasiparticles leave to one lead and more hole-like qasiparticles to the other. The resulting charge

imbalance due to charge accumulation can be safely neglected with the standard assumption of fast inelastic relaxation in the leads.

5.2.1 Master equation approach

To evaluate the current, we use the master equation approach introduced in Sec. 3.4, in order to determine the steady-state occupations $\rho_{\alpha\alpha}$. For the parity-changing processes including a continuum quasiparticle, we make the Born-Markov approximation and treat the continuum of states as a reservoir. The interaction between system and reservoir is given by the Zeeman Hamiltonian in Eq. (5.2). As in Eq. (3.78), we can thus decompose the interaction term for a given continuum energy E and degeneracy index μ (here in the Schrödinger picture): $V = \sum_{\nu\in\{\pm\}} S_\nu R_\nu + \text{h.c.}$ For a circularly polarized field (and in the Schrödinger picture), we find

$$S_\nu = V_{\nu,E\mu} e^{-i\Omega t}\gamma_\nu, \tag{5.4}$$

$$R_\nu = \gamma_{E\mu}. \tag{5.5}$$

We use these definitions to evaluate Eq. (3.80). Further, we assume the continuum to be a thermalized reservoir. Also taking into account the first term in Eq. (5.2) leading to the Rabi oscillations, the master equation describing the time evolution of the density matrix entries for a circularly polarized field is given by

$$\frac{d}{dt}\begin{pmatrix}\rho_{00}\\ \rho_{22}\\ \bar\rho_{02}\\ \bar\rho_{20}\\ \rho_{--}\\ \rho_{++}\end{pmatrix} = \begin{pmatrix} -\Gamma_-^{\mathrm{R}}-\Gamma_+^{\mathrm{R}} & 0 & i\frac{\omega_1^*}{2} & -i\frac{\omega_1}{2} & \Gamma_-^{\mathrm{I}} & \Gamma_+^{\mathrm{I}} \\ 0 & -\Gamma_-^{\mathrm{I}}-\Gamma_+^{\mathrm{I}} & -i\frac{\omega_1^*}{2} & i\frac{\omega_1}{2} & \Gamma_+^{\mathrm{R}} & \Gamma_-^{\mathrm{R}} \\ i\frac{\omega_1}{2} & -i\frac{\omega_1}{2} & i\delta\omega-\frac{\Gamma_\Sigma}{2} & 0 & 0 & 0 \\ -i\frac{\omega_1^*}{2} & i\frac{\omega_1^*}{2} & 0 & -i\delta\omega-\frac{\Gamma_\Sigma}{2} & 0 & 0 \\ \Gamma_-^{\mathrm{R}} & \Gamma_+^{\mathrm{I}} & 0 & 0 & -\Gamma_-^{\mathrm{I}}-\Gamma_+^{\mathrm{R}} & 0 \\ \Gamma_+^{\mathrm{R}} & \Gamma_-^{\mathrm{I}} & 0 & 0 & 0 & -\Gamma_-^{\mathrm{R}}-\Gamma_+^{\mathrm{I}} \end{pmatrix}\begin{pmatrix}\rho_{00}\\ \rho_{22}\\ \bar\rho_{02}\\ \bar\rho_{20}\\ \rho_{--}\\ \rho_{++}\end{pmatrix}. \tag{5.6}$$

Here, $\bar\rho_{02} = e^{i\Omega t}\rho_{02}$ and $\bar\rho_{20} = e^{-i\Omega t}\rho_{20}$ are the coherences in the even sector and we defined

$$\omega_1 = 2\hbar^{-1} V_{+,-}\mu_{\mathrm{B}} B \tag{5.7}$$

with

$$|V_{+,-}|^2 = T^2\,|\sin\phi|\,(1+|\sin\phi|)/(1+T\,|\sin\phi|)^2. \tag{5.8}$$

Additionally, we defined the frequency offset with respect to the resonance frequency as $\delta\omega = \Omega + \mathrm{sgn}(\sin\phi)\Omega_\mathrm{R}$. Further $\Gamma_\nu^{\mathrm{I/R}}$ are the ionization (I) and refill (R) rates of the bound state with energy E_ν, respectively.

Following the master equation approach in Sec. 3.4, we find that the rates are given by Fermi's golden rule expressions (for details see Sec. 5.2.2). We defined $\Gamma_\Sigma = \sum_{\nu=\pm}\Gamma_\nu$, where $\Gamma_\nu = \Gamma_\nu^\mathrm{I} + \Gamma_\nu^\mathrm{R}$. The other 10 elements of the 4×4 density matrix that are not shown in Eq. (5.6) remain zero along the time evolution. For the coherences ρ_{ij}, where i and j are from different subsectors (even vs. odd), this is obvious, since only a process including a continuum state can change between them and we assumed short correlation times in the continuum. Finally, the coherence ρ_{+-} is zero, since the Hamiltonian in Eq. (5.2) can only either create both or destroy both bound states, but not destroy one of them and create the other one.

The stationary occupations are obtained from the master equation, Eq. (5.6), by setting $\dot\rho = 0$. They are most conveniently expressed in the form

$$\rho_{\alpha\alpha}^\mathrm{st} = \rho_{\alpha\alpha}^\infty + \frac{\Gamma^2}{\Gamma^2 + (2\delta\omega)^2}(\rho_{\alpha\alpha}^0 - \rho_{\alpha\alpha}^\infty). \tag{5.9}$$

Here, the width of the resonance is determined by

$$\Gamma = \Gamma_\Sigma\sqrt{1 + \frac{|\omega_1|^2}{\Gamma_+\Gamma_-}}\,. \tag{5.10}$$

The occupations far from resonance ($\rho_{\alpha\alpha}^\infty$), i.e., for a large difference between the resonance frequency and the applied frequency (large $\delta\omega$), corresponding to phase differences across the junction far from ϕ_0, are given as

$$\begin{aligned} \rho_{00}^\infty &= \frac{\Gamma_+^\mathrm{I}\Gamma_-^\mathrm{I}}{\Gamma_+\Gamma_-}, \quad \rho_{--}^\infty = \frac{\Gamma_+^\mathrm{I}\Gamma_-^\mathrm{R}}{\Gamma_+\Gamma_-}, \\ \rho_{++}^\infty &= \frac{\Gamma_-^\mathrm{I}\Gamma_+^\mathrm{R}}{\Gamma_+\Gamma_-}, \quad \rho_{22}^\infty = \frac{\Gamma_+^\mathrm{R}\Gamma_-^\mathrm{R}}{\Gamma_+\Gamma_-}. \end{aligned} \tag{5.11}$$

The occupations at the resonance ($\rho^0_{\alpha\alpha}$) take the form

$$\rho^0_{00} = \rho^\infty_{00}\left\{1+\frac{|\omega_1|^2}{\Gamma^2}\left[\left(1+\frac{\Gamma^{\mathrm{R}}_-}{\Gamma^{\mathrm{I}}_+}\right)\left(1+\frac{\Gamma^{\mathrm{R}}_+}{\Gamma^{\mathrm{I}}_-}\right)-\frac{\Gamma^2_\Sigma}{\Gamma_+\Gamma_-}\right]\right\}, \tag{5.12}$$

$$\rho^0_{--} = \rho^\infty_{--}\left\{1+\frac{|\omega_1|^2}{\Gamma^2}\left[\frac{(\Gamma^{\mathrm{I}}_+ + \Gamma^{\mathrm{R}}_-)^2}{\Gamma^{\mathrm{I}}_+\Gamma^{\mathrm{R}}_-}-\frac{\Gamma^2_\Sigma}{\Gamma_+\Gamma_-}\right]\right\}, \tag{5.13}$$

$$\rho^0_{++} = \rho^\infty_{++}\left\{1+\frac{|\omega_1|^2}{\Gamma^2}\left[\frac{(\Gamma^{\mathrm{I}}_- + \Gamma^{\mathrm{R}}_+)^2}{\Gamma^{\mathrm{I}}_-\Gamma^{\mathrm{R}}_+}-\frac{\Gamma^2_\Sigma}{\Gamma_+\Gamma_-}\right]\right\}, \tag{5.14}$$

$$\rho^0_{22} = \rho^\infty_{22}\left\{1+\frac{|\omega_1|^2}{\Gamma^2}\left[\left(1+\frac{\Gamma^{\mathrm{I}}_+}{\Gamma^{\mathrm{R}}_-}\right)\left(1+\frac{\Gamma^{\mathrm{I}}_-}{\Gamma^{\mathrm{R}}_+}\right)-\frac{\Gamma^2_\Sigma}{\Gamma_+\Gamma_-}\right]\right\}. \tag{5.15}$$

For the linearly polarized magnetic field, we introduce a rotating-wave approximation in order to obtain the occupations. We may apply this approximation under two conditions. First, the level spacing has to be smaller than the energy scale of the interaction, which in our case reads $\mu_{\mathrm{B}}B \ll \Delta$, corresponding to $\Gamma \ll \hbar^{-1}\Delta$. Second, the frequency has to be close to the resonance frequency, i.e., $|\Omega| - \Omega_{\mathrm{R}} \ll |\Omega| + \Omega_{\mathrm{R}}$. This condition is met in the frequency range of interest, i.e., the frequency range, in which Rabi oscillations can occur. Applying this rotating wave approximation, we find that the rates for a linearly polarized field are given by the sum of the rates for a circular field with positive and negative helicity, i.e. $\Gamma^{\mathrm{X}}_\nu = \Gamma^{\mathrm{X}}_\nu(\Omega) + \Gamma^{\mathrm{X}}_\nu(-\Omega)$, where $\mathrm{X} = \mathrm{I}, \mathrm{R}$. With this substitution, the expressions for the occupations given above remain valid for the linearly polarized field.

As pointed out in Sec. 5.1, all field-induced decay rates are zero in the phase interval $[\phi_{\mathrm{c}}, \pi - \phi_{\mathrm{c}}]$ (see also Fig. 5.2). Therefore, we introduce phenomenological rates γ to describe the parity non-conserving processes due to the environment. A refill process requires either an excess quasiparticle above the gap or a spin-flip process. Therefore, refill processes are negligible at low temperatures. Hence, we are left with the two rates γ^{I}_ν for the ionization processes. The total rate for each process is given by the sum of the field-induced and the phenomenological rate.

5.2.2 Transition rates

We will now compute the field-induced transition rates involving continuum states. We assume small magnetic fields $\mu_{\mathrm{B}}B \ll \Delta$, such that we can treat the Zeeman Hamiltonian

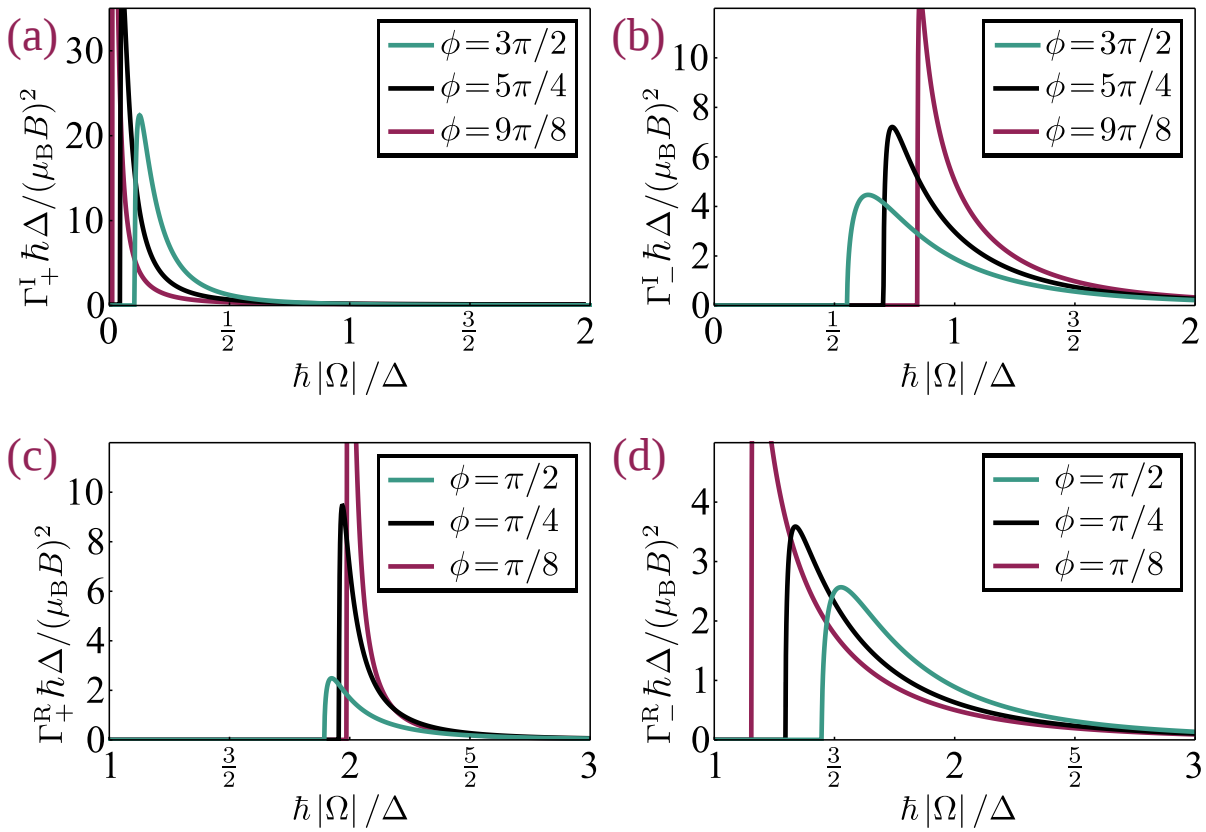

Fig. 5.3: Field-induced ionization (I) and refill (R) rates for $T = 0.8$ as a function of the driving frequency $\Omega < 0$ for several phase differences ϕ. (a) Ionization rate of the bound state $\nu = +$. (b) Ionization rate of the bound state $\nu = -$. (c) Refill rate of the bound state $\nu = +$. (d) Refill rate of the bound state $\nu = -$. Fig. adapted from [198].

in Eq. (5.2) perturbatively. Consequently, the rates for the ionization and refill processes involving the bound state ν can be calculated from Eq. (5.2) using Fermi's golden rule,

$$\Gamma_{\nu}^{\mathrm{I/R}}(\Omega) = 2\pi\hbar^{-1}(\mu_{\mathrm{B}}B)^2 \int_{\Delta}^{\infty} dE\, \rho(E) \sum_{\mu} \left|V_{\nu,\mp E\mathrm{sgn}(\sin\phi)\mu}\right|^2 \delta\left[\hbar\Omega + (|E_{\nu}| \mp E)\mathrm{sgn}(\sin\phi)\right]. \tag{5.16}$$

Here $\rho(E) = (2\pi\hbar v_{\mathrm{F}})^{-1} E/\sqrt{E^2 - \Delta^2}$ is the density of states per mode in the leads (see also Eq. (A.41)). The rates $\Gamma_{\nu}^{\mathrm{I/R}}$, whose typical amplitude is $\sim (\mu_{\mathrm{B}}B)^2/\Delta$, vanish below the threshold frequency $\Omega_{\nu,\mathrm{c}}^{\mathrm{I/R}} = \hbar^{-1}(\Delta \mp |E_{\nu}|)$, as discussed in Sec. 5.1. Furthermore, they are suppressed at large frequencies $|\Omega| \gg \hbar^{-1}\Delta$, while they display a maximum in the vicinity of the threshold frequency. In general, Eq. (5.16) can be evaluated numerically. As an example, Fig. 5.3 shows plots of the different rates as a function of the driving frequency for a transmission of $T = 0.8$. Analytical expressions for Eq. (5.16) can be obtained in the limit of a transparent junction ($T = 1$, see Sec. 5.2.2.1) and

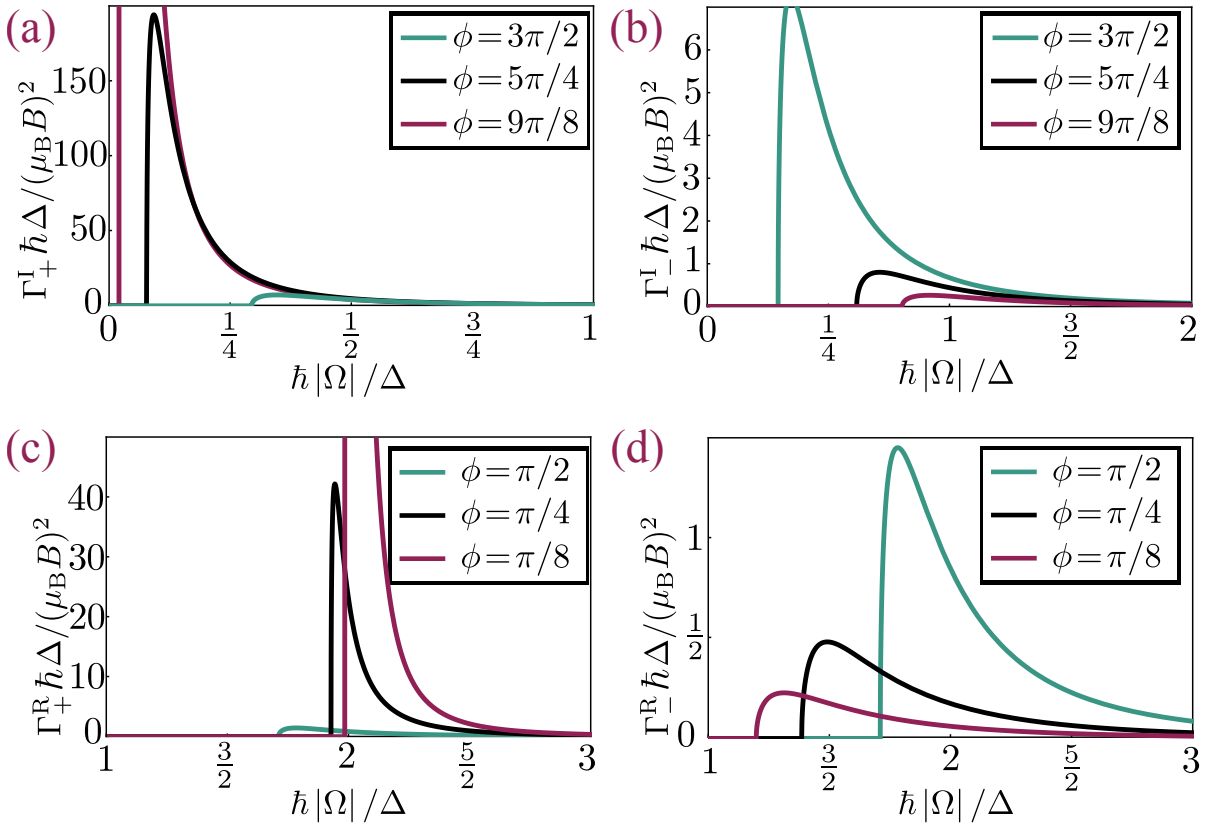

Fig. 5.4: Field-induced ionization (I) and refill (R) rates for $T = 1$ as a function of the driving frequency $\Omega < 0$ for several phase differences ϕ. The corresponding analytical expression is given in Eq. (5.17). (a) Ionization rate of the bound state $\nu = +$. (b) Ionization rate of the bound state $\nu = -$. (c) Refill rate of the bound state $\nu = +$. (d) Refill rate of the bound state $\nu = -$.

for a tunnel junction ($T \ll 1$, see Sec. 5.2.2.2). Appendix D provides details for the calculation of the refill and ionization rates.

5.2.2.1 Transparent junction

Details for the calculation of the rates for a transparent junction ($T = 1$) are provided in Appendix D. We find

$$\Gamma_{\nu}^{\mathrm{I/R}} = \frac{(\mu_{\mathrm{B}}B)^2}{\hbar\Delta}\frac{4\,|\epsilon_{\bar{\nu}}|\,\sqrt{(|\tilde{\Omega}| \pm |\epsilon_\nu|)^2 - 1}[|\tilde{\Omega}| \pm |\epsilon_\nu| + \mathrm{sgn}(\Omega)\,|\epsilon_{\bar{\nu}}|\sin\phi]}{|\tilde{\Omega}|^2(|\tilde{\Omega}| \pm 2\,|\epsilon_\nu|)^2[(|\tilde{\Omega}| \pm |\epsilon_\nu|)^2 - |\epsilon_{\bar{\nu}}|^2]}, \tag{5.17}$$

where we defined $\tilde{\Omega} = \hbar\Omega/\Delta$, $\bar{\nu} = -\nu$, and $\epsilon_\nu = E_\nu/\Delta$, where E_ν is given in Eq. (4.9). Eq. (5.17) is valid above the threshold frequency, $\tilde{\Omega}^{\mathrm{I/R}}_{\nu,\mathrm{c}} = 1 \mp |\epsilon_\nu|$, below which the rates are zero. The rates are shown in Fig. 5.4. Near the threshold frequency the rates $\Gamma_{\nu}^{\mathrm{I/R}}$

grow as $\sqrt{\delta\tilde{\Omega}}$, where $\delta\tilde{\Omega} = |\tilde{\Omega}| - \tilde{\Omega}^{\mathrm{I/R}}_{\nu,\mathrm{c}}$. At large frequencies they decrease as $1/\tilde{\Omega}^4$. In order to describe the rates around their maximum, where the crossover between the two scaling behaviours takes place, we concentrate on the regime $\phi, \delta\tilde{\Omega} \ll 1$ (a similar situation occurs for phases ϕ close to π). We obtain

$$\begin{aligned}\Gamma^{\mathrm{I/R}}_{-} &= \frac{(\mu_{\mathrm{B}}B)^2}{\hbar\Delta}\frac{2\sqrt{2}\sqrt{\delta\tilde{\Omega}}}{\delta\tilde{\Omega}+\frac{\phi^2}{8}},\\ \Gamma^{\mathrm{I/R}}_{+} &= \frac{(\mu_{\mathrm{B}}B)^2}{\hbar\Delta}\frac{\sqrt{\delta\tilde{\Omega}}\,\phi}{\sqrt{2}(\delta\tilde{\Omega}+\frac{\phi^2}{8})^2}.\end{aligned} \tag{5.18}$$

Thus we find that $\Gamma^{\mathrm{I/R}}_{-}$ reaches its maximum, $\Gamma^{\mathrm{I/R}}_{-,\max}/[(\mu_{\mathrm{B}}B)^2(\hbar\Delta)^{-1}] = 4/\phi$, at $\delta\tilde{\Omega}_{-,\max} = \phi^2/8$, while $\Gamma^{\mathrm{I/R}}_{+}$ reaches its maximum, $\Gamma^{\mathrm{I/R}}_{+,\max}/[(\mu_{\mathrm{B}}B)^2(\hbar\Delta)^{-1}] = 6\sqrt{3}/\phi^2$, at $\delta\tilde{\Omega}_{+,\max} = \phi^2/24$.

At larger ϕ, the maximum is less pronounced and further away from the threshold than for small ϕ. Note that for $\phi = \pi/2$, $\Gamma^{\mathrm{I/R}}_{+} = \Gamma^{\mathrm{I/R}}_{-}$, since the bound states are degenerate.

5.2.2.2 Tunnel junction

Let us discuss the rates in the limit of an opaque junction ($T = 0$), before considering the tunnel junction ($T \ll 1$). As discussed in Sec. 4.2, only the bound state with $\nu = -$ exists in the opaque case, and the rates read

$$\Gamma^{\mathrm{I/R}}_{-} = \frac{(\mu_{\mathrm{B}}B)^2}{\hbar\Delta}\frac{16\sqrt{|\tilde{\Omega}|^2-1}}{|\tilde{\Omega}|^5}. \tag{5.19}$$

Since the bound state energy is zero, the rate is identical for refill and ionization processes. Near the threshold frequency, $\tilde{\Omega}_{\mathrm{c}} = 1$, the rate grows as $\sqrt{\delta\tilde{\Omega}}$. It reaches its maximum, $\Gamma_{\max}/[(\mu_{\mathrm{B}}B)^2(\hbar\Delta)^{-1}] = 2^8/(25\sqrt{5})$, at $|\tilde{\Omega}_{\max}| = \sqrt{5}/2$ and decreases as $1/\tilde{\Omega}^4$ at large frequencies. Note that the rate does not depend on the superconducting phase difference, since the bound state energy is independent of the phase.

At small, but finite, transparency (tunnel junction) an additional peak structure develops near the threshold frequency for ionization/refill processes, $\tilde{\Omega}^{\mathrm{I/R}}_{\nu,\mathrm{c}} = 1 \mp |\epsilon_\nu|$. For $\delta\tilde{\Omega} = |\tilde{\Omega}| - \tilde{\Omega}^{\mathrm{I/R}}_{\nu,\mathrm{c}} \ll 1$ the rates for the $\nu = -$ state take the form

$$\Gamma^{\mathrm{I/R}}_{-} = \frac{(\mu_{\mathrm{B}}B)^2}{\hbar\Delta}\left[f^{\mathrm{I/R}}\left(\frac{\delta\tilde{\Omega}}{T^2}\right) + Tg^{\mathrm{I/R}}\left(\frac{\delta\tilde{\Omega}}{T^2}\right)\right], \tag{5.20}$$

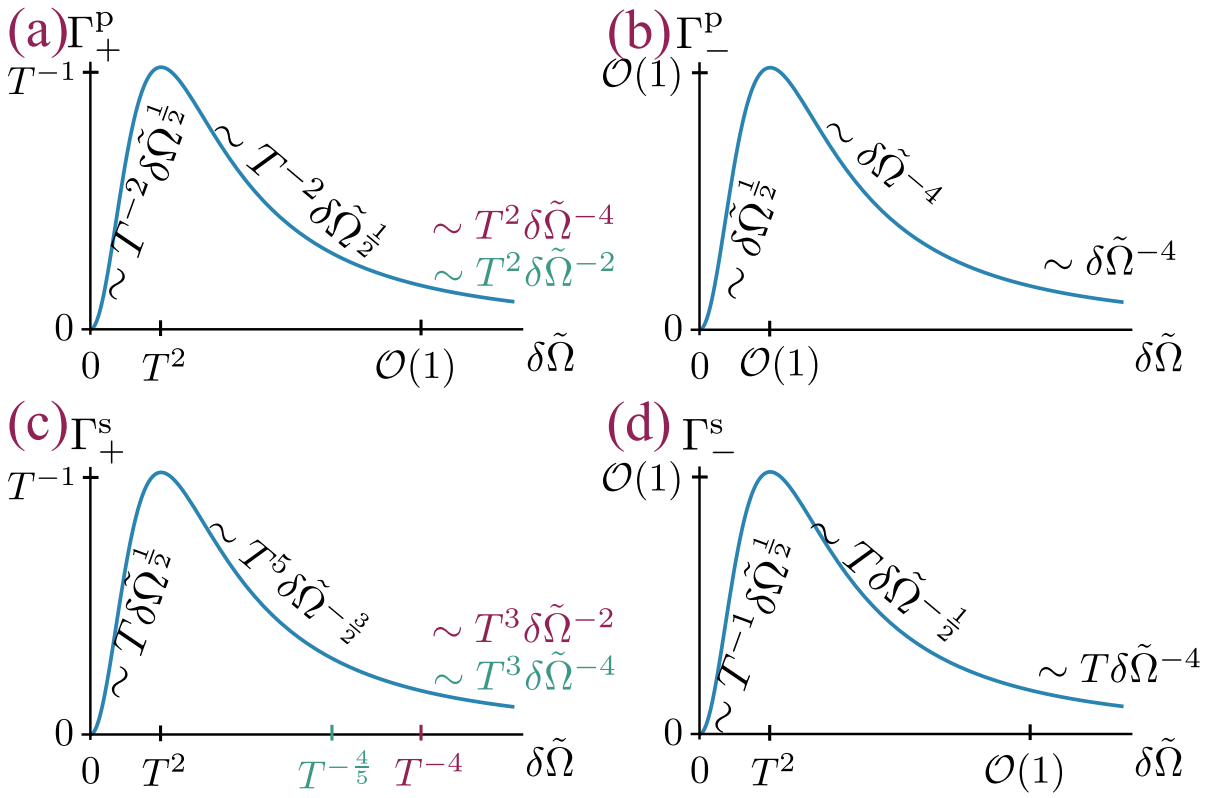

Fig. 5.5: Schematical respresentation of the scaling of the rates for a tunnel junction $T \ll 1$. The rates, which are given in units of $(\mu_{\mathrm{B}}B)^2(\hbar\Delta)^{-1}$, are shown as a function of $\delta\tilde{\Omega}$, i.e., the difference between the frequency and the threshold frequency. The total refill and ionization rates are the sum of the rates for an outgoing quasiparticle in the s lead and an outgoing quasiparticle in the p lead, i.e., $\Gamma^{\mathrm{I/R}}_{\pm} = \Gamma^{\mathrm{p}}_{\pm} + \Gamma^{\mathrm{s}}_{\pm}$. Green color corresponds to the scaling for electron-like quasiparticles, red color corresponds to hole-like quasiparticles. The scaling is given in three different frequency ranges: For frequencies close to the threshold frequency (first range), for frequencies significantly larger than the frequency, at which the maximum of the rate occurs (second range), and for very big frequencies (third range). The ticks on the horizontal axes show the frequency, at which the maximum of the rates occurs and the limiting frequency, that defines the third frequency range. The ticks on the vertical axes indicate the height of the maximum.

where

$$f^{\mathrm{I/R}}(x) = \frac{1}{\sqrt{2x}}\frac{32x(1 \mp |\sin\phi|)}{8x + \sin^2\phi} \approx \begin{cases} 16\sqrt{2x}\frac{1\mp|\sin\phi|}{\sin^2\phi} & \text{for} \quad x \ll 1, \\ 2\sqrt{\frac{2}{x}}(1 \mp |\sin\phi|) & \text{for} \quad x \gg 1, \end{cases} \tag{5.21}$$

$$g^{\mathrm{I/R}}(x) = \frac{1}{\sqrt{2x}}\frac{16x(16x + 1 \pm |\sin\phi|)}{8x + \sin^2\phi} \approx \begin{cases} 8\sqrt{2x}\frac{1\pm|\sin\phi|}{\sin^2\phi} & \text{for} \quad x \ll 1, \\ 16\sqrt{2x} & \text{for} \quad x \gg 1. \end{cases} \tag{5.22}$$

The first term in Eq. (5.20) describes a narrow peak of height $(\mu_B B)^2(\hbar\Delta)^{-1}$ near $\delta\tilde{\Omega} \sim T^2$ and corresponds to an ionization or refill process to the s-wave superconductor lead. Fig. 5.5(d) shows a schematical plot of the corresponding rate, summarizing the scaling behavior in each parameter region. The second term in Eq. (5.20) is dominant for $\delta\tilde{\Omega} > T$, where it matches the result at $T = 0$ (opaque junction), given in Eq. (5.19). This process corresponds to an ionization or refill process to the p_x-wave superconductor lead. The corresponding rate is schematically drawn in Fig. 5.5(b)).

The rates for the $\nu = +$ state read

$$\Gamma_+^{\mathrm{I/R}} = \frac{(\mu_B B)^2}{\Delta T} h\left(\frac{\delta\tilde{\Omega}}{T^2}\right), \tag{5.23}$$

where

$$h(x) = \frac{1}{\sqrt{2x}} \frac{64x\,|\sin\phi|}{(8x + \sin^2\phi)^2} \approx \begin{cases} \frac{64}{\sqrt{2}}\sqrt{x}\frac{1}{|\sin\phi|^3} & \text{for} \quad x \ll 1, \\ \frac{1}{\sqrt{2}} x^{-\frac{3}{2}}\,|\sin\phi| & \text{for} \quad x \gg 1. \end{cases} \tag{5.24}$$

The rates display a narrow peak of height $(\mu_B B)^2(T\hbar\Delta)^{-1}$ near $\delta\tilde{\Omega} \sim T^2$ and correspond to ionization/refill processes to the p_x-wave lead. Fig. 5.5(a) shows a sketch of the corresponding rate. The coupling to the s-wave lead is negligible in the entire frequency range (see also Fig. 5.5(c)). At $x \gg 1$, i.e., in the regime $T^2 \ll \delta\tilde{\Omega} \ll 1$, the rates vanish as $T^2(\delta\tilde{\Omega})^{-\frac{3}{2}}$. Thus, in the frequency range of interest for Rabi oscillations, $\Gamma_+^{\mathrm{I}} \ll \Gamma_-^{\mathrm{I/R}}$.

5.3 Current-phase relation of the singlet/triplet junction

Being equipped with the occupations of the Andreev levels and the expressions for the field-induced transition rates, obtained in Sec. 5.2.2, we calculate the modified current-phase relation in the presence of the magnetic field.

5.3.1 Circular polarization

Let us start with the discussion of the current-phase relation for a circularly polarized magnetic field. Taking into account the considerations in Sec. 5.1, we analyze the behavior of the current given by Eq. (5.3), depending on the phase interval. Recall that we consider $\Omega < 0$. Then, for $\phi \in [\pi, 2\pi]$ only ionization processes are possible. Thus, in

the stationary regime of the Andreev bound state dynamics the bound states are empty and the occupations read $\rho_{00} = 1$ and $\rho_{--} = \rho_{++} = \rho_{22} = 0$. As a consequence, the current equals its equilibrium value, $I^{\mathrm{eq}} = I_+ + I_-$. We have seen in Sec. 5.1.2 that in the intervals $[0, \phi_{\mathrm{c}}]$ and $[\pi - \phi_{\mathrm{c}}, \pi]$ refill processes for the state $\nu = -$ are possible. We assume that the rates for parity non-conserving processes (introduced in Sec. 5.2.1) due to the environment are much smaller than the field-induced rates. Then, the $\nu = -$ bound state is filled in the stationary regime, i.e., $\rho_{--} = 1$ and $\rho_{00} = \rho_{++} = \rho_{22} = 0$. Thus, the current (Eq. (5.3)) is given by $I = I_+ - I_-$.

To evaluate the current in the interval $[\phi_{\mathrm{c}}, \pi - \phi_{\mathrm{c}}]$, which includes the phases ϕ_0 and $\pi - \phi_0$, where Rabi oscillations take place (see Sec. 5.1.2), we insert the stationary occupations, Eqs. (5.12) - (5.15), into the current expression, Eq. (5.3). We find that the non-equilibrium current

$$I = I^{\infty} + \frac{\Gamma^2}{\Gamma^2 + (2\delta\omega)^2}(I^0 - I^{\infty}), \tag{5.25}$$

is the sum of a background term I^{∞} and a resonant term. The background term is given as

$$I^{\infty} = \sum_{\nu\in\{\pm\}} I_\nu \frac{\Gamma_\nu^{\mathrm{I}} - \Gamma_\nu^{\mathrm{R}}}{\Gamma_\nu}. \tag{5.26}$$

The current at resonance reads

$$I^0 = \frac{\Gamma_\Sigma}{\Gamma^2}\left[\Gamma_\Sigma I^{\infty} + \frac{|\omega_1|^2}{\Gamma_+\Gamma_-}(I_+ - I_-)\sum_{\nu=\pm}\nu(\Gamma_\nu^{\mathrm{I}} - \Gamma_\nu^{\mathrm{R}})\right]. \tag{5.27}$$

The symbols used were defined in Sec. 5.2.1, where we also gave the expression for the width of the resonance in Eq. (5.10).

We now assume the two phenomenological rates γ_ν^{I} introduced in Sec. 5.2.1 to be non-zero. They are the only non-zero rates in the phase interval under consideration ($[\phi_{\mathrm{c}}, \pi - \phi_{\mathrm{c}}]$). I^{∞} reduces to the equilibrium current, i.e., $I^{\infty} = I^{\mathrm{eq}}$. Assuming $\gamma_\pm^{\mathrm{I}} \ll |\omega_1|$, the current at resonance is obtained as

$$I^0 \approx (I_+ - I_-)\frac{\gamma_+^{\mathrm{I}} - \gamma_-^{\mathrm{I}}}{\gamma_+^{\mathrm{I}} + \gamma_-^{\mathrm{I}}} \tag{5.28}$$

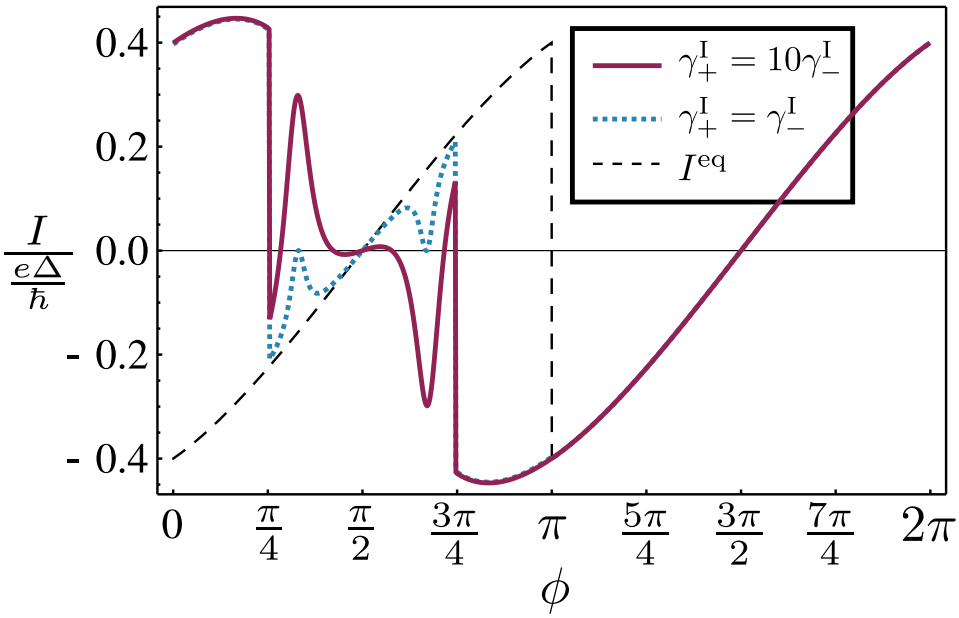

Fig. 5.6: Current-phase relation for an $\mathrm{s}/\mathrm{p_x}$ junction with transmission $T = 0.8$, and a circularly polarized ac magnetic field with amplitude $\mu_{\mathrm{B}}B = 10^{-2}\Delta$ and frequency $\Omega = -1.3\hbar^{-1}\Delta$. The equilibrium current is given for comparison. The current-phase relation is spin-sensitive. The phenomenological ionization rates are chosen as $\gamma_+^{\mathrm{I}} + \gamma_-^{\mathrm{I}} = 10^{-6}\hbar^{-1}\Delta$. Fig. adapted from [198].

and the width of the resonance reads

$$\Gamma \approx |\omega_1| \frac{\gamma_+^{\mathrm{I}} + \gamma_-^{\mathrm{I}}}{\sqrt{\gamma_+^{\mathrm{I}}\gamma_-^{\mathrm{I}}}}. \tag{5.29}$$

As the state $\nu = +$ is closer to the continuum, we expect $\gamma_+^{\mathrm{I}} \geq \gamma_-^{\mathrm{I}}$. We can motivate this assumption noting that ionization processes due to the resistive environment of a conventional Josephson junction have been shown to be more probable, if the Andreev level is closer to the continuum of states [215]. Depending on the relative magnitude of the two phenomenological ionization rates, the current through the $\mathrm{s}/\mathrm{p_x}$ junction may be completely suppressed at resonance, when $\gamma_-^{\mathrm{I}} = \gamma_+^{\mathrm{I}}$, or change its sign as compared to the equilibrium current, reaching the magnitude $I^0 \approx I_+ - I_-$, when $\gamma_-^{\mathrm{I}} \ll \gamma_+^{\mathrm{I}}$.

Fig. 5.6 shows the non-equilibrium current-phase relation for a circularly polarized Zeeman field at $T = 0.8$. The current is given for two different ratios of the phenomenological rates, illustrating the properties discussed above. The 2π-periodicity is due to the spin-sensitive manipulation of the bound state occupations. The spin sensitivity is a consequence of the circular polarization of the field, that pumps one spin direction into the system (fixed by its helicity). If the sign of Ω was reversed, the spin pumped

into the system would be opposite. According to the spin selection rule, the processes would be possible if the spins involved were opposite. The spins of the bound states are opposite, if the phase is shifted by π. Consequently, the current-phase relation is phase-shifted by π, if the sign of Ω is reversed, i.e.,

$$I(\Omega, \phi) = I(-\Omega, \phi + \pi). \tag{5.30}$$

In highly transparent junctions, Rabi oscillations should be visible in a fairly wide range of parameters. The conditions are more restrictive in tunnel junctions that we discuss now.

5.3.1.1 Tunnel junction

At small transparency, the bound state energies are given by $E_+ \simeq \mathrm{sgn}(\sin\phi)\Delta[1 - (T^2/8)\sin^2\phi]$ and $E_- \simeq \Delta(T/2)\sin\phi$, up to quadratic order in T. Thus, the equilibrium current-phase relation takes the form

$$I^{\mathrm{eq}}(\phi) \simeq -\frac{e\Delta}{2\hbar} T \mathrm{sgn}(\sin\phi)\cos\phi. \tag{5.31}$$

Rabi oscillations may be expected in a narrow frequency range $\Delta < \hbar|\Omega| < \hbar\Omega_{\mathrm{max}} \simeq \Delta(1 + T/2 - T^2/8)$. For a given frequency in that range, there is a small separation $\delta\phi \equiv \phi_0 - \phi_{\mathrm{c}}$ between the phase $\phi_0 = \arcsin[((\hbar\Omega)^2/\Delta^2 - 1)/T]$, where a resonance in the current-phase relation can be expected, and the phase $\phi_{\mathrm{c}} \simeq \arcsin[2((\hbar\Omega)/\Delta - 1)/T]$, below which refill processes for the state $\nu = -$ are active. The relation $\hbar\Omega = \Delta + E_-(\phi_{\mathrm{c}}) = E_-(\phi_0) + E_+(\phi_0)$ yields

$$\delta\phi \simeq \begin{cases} (T/4)\sin^2\phi_0/\cos\phi_0 & \text{for} \quad \Omega_{\mathrm{max}} - |\Omega| \gg T^2\hbar^{-1}\Delta, \\ \sqrt{T/2} & \text{for} \quad \Omega_{\mathrm{max}} - |\Omega| \ll T^2\hbar^{-1}\Delta. \end{cases} \tag{5.32}$$

Note that in the first case $\delta\phi \ll \pi/2 - \phi_0$, whereas in the second case $\delta\phi \gg \pi/2 - \phi_0$.

There are two constraints on the visibility of the resonance in the current-phase relation. First, its width must be smaller than $\delta\phi$, because in the intervals $[0, \phi_{\mathrm{c}}]$ and $[\pi - \phi_{\mathrm{c}}, \pi]$, any remnant of Rabi oscillations is completely suppressed, since the hierachy of the field-induced rates $\Gamma^{\mathrm{R}}_+ \ll \Gamma^{\mathrm{I}}_\pm \ll \Gamma^{\mathrm{R}}_-$ (see Sec. 5.1) drives the system into the odd sector. Second, the width of the resonance must be smaller than $\pi/2 - \phi_0$, in order to be distinguishable from the zero of the equilibrium current at $\phi = \pi/2$.

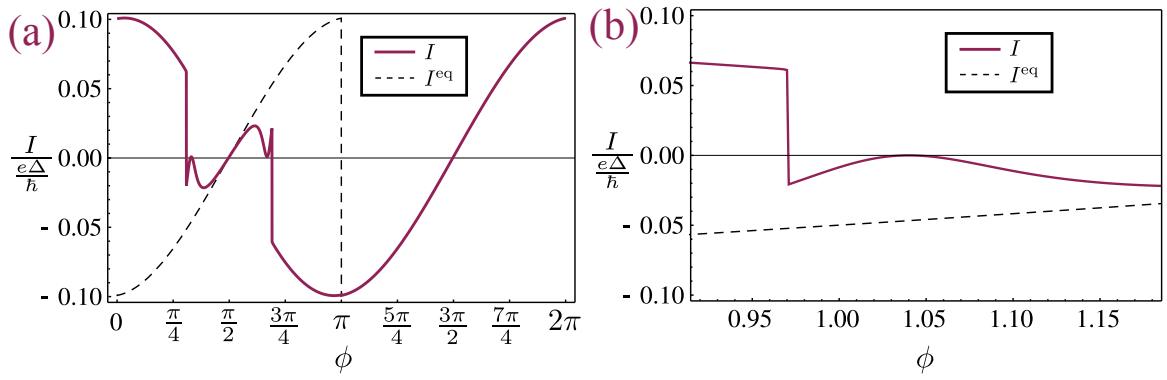

Fig. 5.7: Current-phase relation for an $\mathrm{s/p_x}$ junction with transmission $T = 0.2$, a magnetic field of $\mu_{\mathrm{B}}B = 10^{-2}\Delta$, phenomenological rates $\gamma_+^{\mathrm{I}} + \gamma_-^{\mathrm{I}} = 10^{-6}\hbar^{-1}\Delta$, and a frequency of $\Omega = -1.08\hbar^{-1}\Delta$ corresponding to $\phi_0 \approx 1.04$. The frequency has been choosen such that ϕ_0 is the same as in Fig. 5.6 for $T = 0.8$. Panel (b) shows a zoom of panel (a) around the resonance. Fig. adapted from [198].

According to Eqs. (5.25) and (5.31), the width of the resonances is given by $\delta\phi_{\mathrm{R}} \sim \Gamma/(T\hbar^{-1}\Delta\cos\phi_0)$. Using the assumption of small phenomenological rates γ for a circular polarization, we estimate (using Eqs. (5.7), (5.8), and (5.29)) $\Gamma \propto T\hbar^{-1}\mu_{\mathrm{B}}B$ and, thus, $\delta\phi_{\mathrm{R}} \sim \mu_{\mathrm{B}}B/(\Delta\cos\phi_0)$. When $|\Omega|$ is not too close to Ω_{max}, the condition $\delta\phi_{\mathrm{R}} \ll \delta\phi \ll \pi/2 - \phi_0$ yields $\mu_{\mathrm{B}}B \ll T\Delta$. When $\Omega_{\mathrm{max}} - |\Omega| \ll T^2\hbar^{-1}\Delta$, on the other hand, the condition $\delta\phi_{\mathrm{R}} \ll \pi/2 - \phi_0 \ll \delta\phi$ yields the more restrictive result $\mu_{\mathrm{B}}B \ll (\Omega_{max} - |\Omega|)/T \ll T\Delta$. Fig. 5.7 shows an example for the current-phase relation in the tunnel regime.

5.3.2 Linear polarization

Let us now discuss the case of a linearly polarized field. As discussed in Sec. 5.2.1, we can use a rotating wave approximation for the linearly polarized field. It follows that under the assumption $\Gamma \ll \hbar^{-1}\Delta$ the steady-state current for a linearly polarized field is given by Eqs. (5.25) - (5.27) with $\Gamma_\nu^{\mathrm{X}} = \Gamma_\nu^{\mathrm{X}}(\Omega) + \Gamma_\nu^{\mathrm{X}}(-\Omega)$, where $\mathrm{X} = \mathrm{I}, \mathrm{R}$.

The current-phase relation for a linearly polarized field is shown in Fig. 5.8. As the manipulation of the bound state occcupations is not spin sensitive, the current is π-periodic as in equilibrium. As soon as the ac field carries a finite angular momentum, the out-of-equilibrium current-phase relation is 2π-periodic due to the spin-dependent rates. Consequently, any deviation from linear polarization (elliptic polarization) is sufficient to gain spin sensitivity.

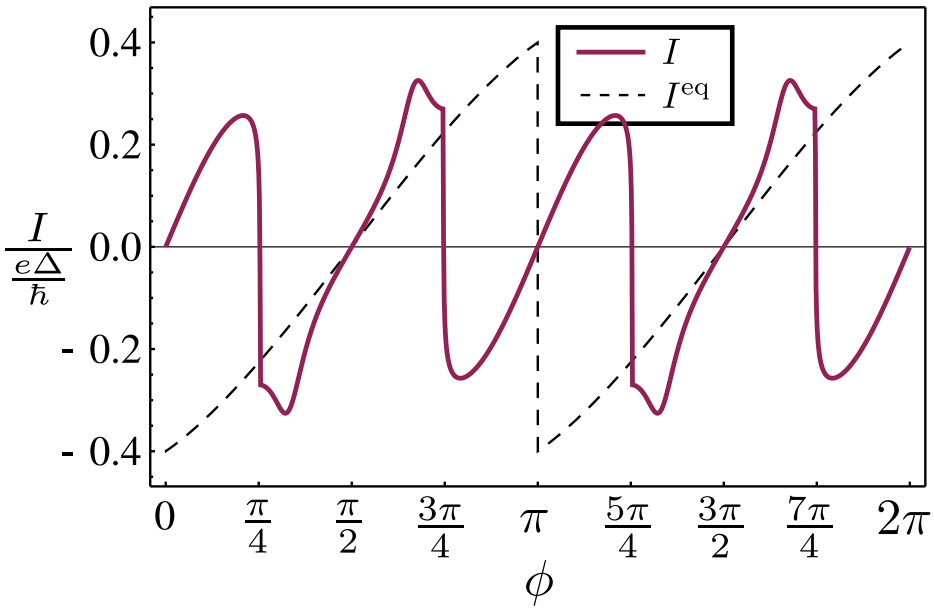

Fig. 5.8: Current-phase relation for a junction with transmission $T = 0.8$, and a linearly polarized ac magnetic field with amplitude $\mu_{\mathrm{B}} B = 10^{-2}\Delta$ and frequency $\Omega = -1.3\hbar^{-1}\Delta$. The equilibrium current is given for comparison. As in equilibrium, the current-phase relation is π-periodic. Note that the sign of the current at the resonances is inverted compared to the curves for circular polarization (shown in Fig. 5.6) because $\Gamma^{\mathrm{I}}_{+} < \Gamma^{\mathrm{I}}_{-}$. Fig. adapted from [198].

For a deeper understanding of the form of the current-phase relation presented in Fig. 5.8, let us discuss the relevant rates in more detail. While the refill process of the state $\nu = +$ is energetically not possible in the frequency range, where Rabi oscillations occur (see Sec. 5.1), the rate Γ^{R}_{-} is non-zero in the phase intervals $[-\phi_{\mathrm{c}}, \phi_{\mathrm{c}}]$ and $[\pi - \phi_{\mathrm{c}}, \pi + \phi_{\mathrm{c}}]$. The current-phase relation displays a kink at the limit of these intervals, see Fig. 5.8. The refill rate competes with both ionization rates that are non-zero for all phase differences, since there is no spin selection rule. The width of the Rabi resonances is determined by the two field-induced ionization rates, since we assume that the phenomenological rates are smaller than the field-induced ones. Recall that the refill processes are energetically impossible in that phase range. The current at the resonances, I_0, is determined by the ratio of the field-induced ionization rates, for which we find $\Gamma^{\mathrm{I}}_{+} \ll \Gamma^{\mathrm{I}}_{-}$ in the frequency range of Rabi oscillations. This finding is also illustrated by Fig. 5.3(a), (b). Since the rates are most important close to the threshold frequency, it is not astonishing that the rate Γ^{I}_{-} is dominant. As can be seen from Fig. 5.2, the frequency of the field is closer to the threshold frequency of Γ^{I}_{-} for the frequencies for which Rabi oscillations occur. Consequently, the current at the

resonances is approximately $I^0 \approx I_- - I_+$ and has opposite sign with respect to the case of circular polarization. In the latter, the phenomenological rates fufilled $\gamma_+^{\mathrm{I}} \geq \gamma_-^{\mathrm{I}}$.

In the case of a tunnel junction, the finding $\Gamma_+^{\mathrm{I}} \ll \Gamma_-^{\mathrm{I}}$ yields a wide and shallow resonance, which might make its observation difficult.

Part II

Ferromagnet/superconductor junction

6 The half-metal/superconductor junction

In the previous part, we have seen how a time-dependent magnetic field modifies the transport properties of a singlet/triplet Josephson junction due to field-induced spin-flip processes. We now want to consider a different heterostructure, in which the charge transport can be strongly modified by manipulating the spin.

More precisely, this heterostructure consists of a superconductor/half-metal junction. A half-metal is a metallic ferromagnet with perfect spin polarization providing only one spin species. The absence of the second spin direction has dramatic consequences for the transport properties. Consider an electron in this heterostructure, located in the half-metal and impinging onto the conventional superconductor. Due to spin-singlet pairing in the superconductor, any transmitted Cooper pair consists of two electrons of opposite spin directions. Therefore, an Andreev reflected hole needs opposite spin compared to the incident electron. Consequently, Andreev reflection is forbidden at the half-metal/superconductor interface. The aim of this chapter is to show how we can restore Andreev reflection by providing a spin-flip mechanism. The spin may be flipped due to magnetic impurities or spin-orbit impurities. However, these mechanisms are not tunable. Here we want to consider an externally tunable mechanism, i.e., a time-dependent magnetic field, that couples to the spin via the Zeeman effect and thus provides a spin-flip mechanism. We show that a half-metal/superconductor junction, where the half-metal is subjected to ferromagnetic resonance (having a time-dependent magnetization direction), allows for Andreev currents.

This part of the thesis is organized in three chapters. This chapter introduces the junction and the main notions of the model that is used in the two following chapters. Chapter 7 presents the Andreev current through a ballistic junction for a point contact geometry, obtained in the framework of the Keldysh Green's functions formalism. Chapter 8 discusses the Andreev current through a ferromagnet/superconductor tunnel junction in an extended interface geometry, where the current expression is obtained from a Fermi's golden rule calculation. Additionally, we investigate the influence of non-magnetic impurities (disorder) in the leads.

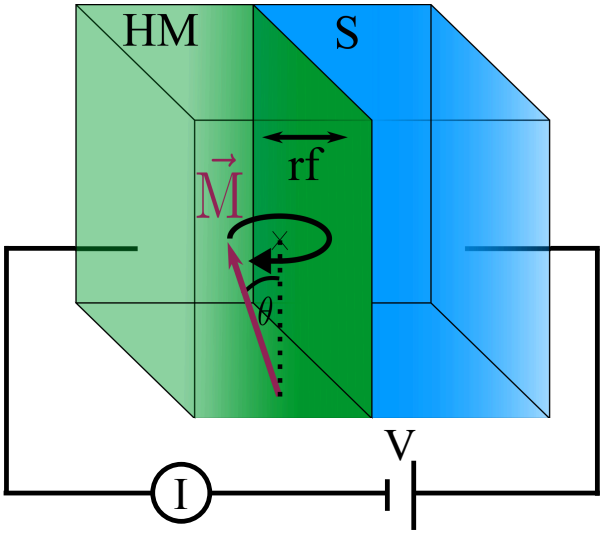

Fig. 6.1: Setup of the junction: A 3D half-metal (HM, green, left part) is in contact with a 3D superconductor (S, blue, right part). The half-metal is brought into ferromagnetic resonance condition applying an rf field, that provokes a time-dependent magnetization direction (indicated by the arrows). In an open circuit geometry a voltage V can be detected.

This chapter is organized in the following way. In Sec. 6.1 we present the setup of the half-metal/superconductor junction. Sec. 6.2 gives details about the tunnel Hamiltonian used to evaluate the current. In Sec. 6.3 we determine the non-equilibrium distribution function of the ferromagnetic lead that determines the occupation of the energy levels.

6.1 Setup of the half-metal/superconductor junction

Fig. 6.1 schematically shows the setup that we want to consider: A half-metal is brought into ferromagnetic resonance (FMR) condition using an rf-field. The magnetization direction precesses around the precession axis with a cone angle θ. The half-metal forms a junction with a conventional superconductor. In an open circuit geometry charge accumulation leads to a voltage buildup.

It is well-known that without breaking of the spin rotation symmetry no subgap current flows across the half-metal/superconductor (HM/S) junction, since Andreev reflection is blocked due to the perfect spin polarization. We will explicitly verify this fact within our formalism in Sec. 7.4.4. Various possibilities to introduce spin-flip processes have

already been proposed. One possibility is a spin-active interface, containing magnetic impurities or spin-orbit impurities [217–223]. A spacially non-uniform magnetization direction has been first proposed for a ferromagnet/superconductor (F/S) junction in the context of long-range spin triplet pairing [92, 93, 224, 225]. Layered heterostructures with non-collinear magnetization directions [94–97, 99, 109, 226] have been studied afterwards. The idea of a non-uniform magnetization has also been applied to a half-metal [227]. Instead of using a space-dependent magnetization, our proposal relies on using a time-dependent magnetization direction. Ferromagnetic Josephson junctions [228–230] and half-metallic junctions [231] subjected to time-dependent magnetizations have been investigated, where the idea of a time-dependent manipulation of the spin properties was first studied in conventional Josephson junctions with embedded spins [232, 233]. Further, magnon-assisted Andreev reflection has been considered in F/S tunnel junctions [234, 235].

Andreev reflections due to spacially non-uniform magnetization directions have been experimentally proven, both for half-metallic and ferromagnetic junctions. For half-metallic junctions, the long-range Josephson effect has been measured in CrO_2 junctions [100, 236]. Further evidence was found in point contact junctions with LCMO, a half-metallic compound, using a superconducting tip [237, 238]. Another important experiment was performed on interfaces containing holmium (Ho), a ferromagnet with an intrinsic non-uniform magnetization direction [239]. Other experiments on ferromagnet/superconductor layers, that have measured a long-range Josephson effect, involve Co [102, 103].

It is particularly interesting to study the case of a large spin polarization. It has been shown for a ballistic F/S interface that the Andreev reflections are incomplete for large spin polarizations [89]. For an S/F/S junction this effect provoques the critical current to oscillate as a function of the exchange energy and of the length of the ferromagnet [240].

If the superconductor is in its normal phase, the effects discussed in Sec. 2.4.2 for ferromagnetic resonance in a ferromagnet/normal metal (F/N) junction are important. In this context, Ref. [72] has shown that a precessing magnetization direction in a thin ferromagnetic layer between two normal metal leads injects a spin current into one of the adjacent normal metals. The pumped spin current slows down the precession. This corresponds to an enhanced Gilbert damping constant with respect to a bulk

ferromagnet. A slightly different setup, a ferromagnet at ferromagnetic resonance in ohmic contact with a normal metal, has been shown to act as a "spin battery" [157]. A dc spin current is injected into the normal metal without a charge current flowing. The pumped spin current may lead to a spin accumulation effect next to the interface, depending on the ratio of the spin injection rate and the spin relaxation rate. In this chapter, we investigate what happens if we replace the normal metal by a singlet superconductor, which does not allow for a subgap spin current. For a ferromagnetic superconductor under FMR, it has been predicted, that it injects a spin current and a charge current into an adjacent normal metal [241].

The experiments [74, 113] that have measured spin injection into a normal metal from a ferromagnet under FMR have used aluminum in its normal phase, at room temperature. Cooling down the devices should make them superconducting. Further, recent progress for the growth of the half-metal CrO_2 [242] makes HM/S junctions with high transparencies available.

An F/S bilayer with the ferromagnet under FMR has experimentally been studied [243]. The ferromagnet $Ni_{80}Fe_{20}$ (permalloy) has been used, deposited onto the superconductor Nb. A sharpening of the resonance width of the ferromagnetic resonance below T_c has been observed, which was attributed to a lowering of the Gilbert damping (see also Eq. (2.33)). The authors interpreted their results within the spin-pumping model. In the normal state, the spins can relax in the Nb layer, whereas in the superconducting state, electrons cannot enter the superconductor below the gap and no relaxation takes place in the adjacent layer. Since Andreev reflection processes do not relax the magnetization, the Gilbert damping due to the spin-pumping is less efficient in the superconducting state. Note that spin relaxation may still take place close to the interface, where the superconducting gap is suppressed.

F/S interfaces with static magnetization directions have also been used to study spin injection and spin relaxation in superconductors. Spin can be injected via the quasiparticles above the gap. Non-local measurements in F/S tunnel junctions allow to measure the spin relaxation length [244]. Using a non-local spin valve geometry, pure spin currents could be injected into a superconductor [245]. For a lateral F/I/S/I/F spin valve geometry, it has been shown that almost chargeless spin imbalance can be created [246]. In such a geometry the created spin imbalance depends on the polarization of

the injector electrode and the Zeeman splitting of the superconducting density of states due to an applied in-plane magnetic field.

In a nutshull, F/S junctions have attracted much attention, since they are hoped to be suitable for spintronics applications [105]. Especially, junctions with large spin polarization are of interest. Our HM/S junction presented in Fig. 6.1 is the building block for more complicated junctions. Its properties have to be understood in depth before considering more complicated layered structures.

6.2 Tunnel Hamiltonian

In order to model the junction in Fig. 6.1, we use a tunnel Hamiltonian approach. We use two leads, a half-metallic lead under FMR conditions and a superconducting lead. The leads are tunnel coupled. In Chapter 7 we will assume a simple point contact geometry, whereas in Chapter 8, we consider a more realistic extended interface geometry. The tunnel amplitude depends on the interface geometry. Therefore, the interface geometry defines how the leads are coupled. We apply a bias voltage V to the junction and calculate the current $I(V)$. In an open circuit geometry, the situation is inverted and a voltage can be measured. It builds up due to charge accumulation as a consequence of the current flow. The results from our model can be easily converted to an open geometry, solving $I(V) = 0$ for the voltage V.

The rf-field forces the magnetization direction to precess around the precession axis, which we choose as z-axis. The time-dependent magnetization reads

$$\boldsymbol{m}(t) = m(\sin\theta\cos(\Omega t), \sin\theta\sin(\Omega t), \cos\theta)^T, \tag{6.1}$$

where θ is the angle between the magnetization direction and the precession axis. m is the constant absolute value of $\boldsymbol{m}(t)$. Further, Ω denotes the angular precession frequency, which is the angular frequency of the rf-field. The total Hamiltonian of the junction is given by

$$H = H_{\mathrm{S}} + H_{\mathrm{F}} + H_{\mathrm{T}}. \tag{6.2}$$

Here, the s-wave superconductor is modeled by the standard BCS Hamiltonian

$$H_{\mathrm{S}} = \sum_{q\sigma} \zeta_q a^\dagger_{q\sigma} a_{q\sigma} + \Delta \sum_q a^\dagger_{q\uparrow} a^\dagger_{-q\downarrow} + \mathrm{h.c.}, \tag{6.3}$$

where $a^\dagger_{q\sigma}$ creates an electron with spin σ and momentum q in the superconductor. The first term ζ_q measures the kinetic energy in the normal state with respect to the Fermi level for a state with momentum q, and Δ is the gap. The half-metal is described by the Hamiltonian

$$H_\mathrm{F} = \sum_{k\sigma\sigma'} b^\dagger_{k\sigma}(\xi_{k\sigma}\delta_{\sigma\sigma'} + \boldsymbol{h}_\mathrm{F}(t)\cdot\boldsymbol{\sigma}_{\sigma\sigma'})b_{k\sigma'}, \tag{6.4}$$

where $b^\dagger_{k\sigma}$ creates an electron with spin σ and momentum k in the half-metal. The first term is the kinetic energy and the second term is the coupling between the time-dependent exchange field $\boldsymbol{h}_\mathrm{F}$ and the spin of the electrons. We assume the exchange field to be momentum independent, which is a valid approximation for energies close to the Fermi level. The direction of the exchange field, $\hat{\boldsymbol{h}}_\mathrm{F}(t)$, is given by the direction of the magnetization, $\hat{\boldsymbol{m}}(t)$. At this point, Eq. (6.4) can describe a ferromagnet, that contains both spin species with respect to the exchange field direction. In a generic ferromagnet one spin species is more abundant (majority spin) than the other (minority spin). The polarization of the ferromagnet is the difference between the majority and the minority carrier concentration (normalized by the total carrier concentration). Eq. (6.4) can also describe a half-metal with perfect spin polarization (if the minority carrier concentration is zero). The tunnel Hamiltonian allows for the transfer of electrons between the two reservoirs and reads

$$H_\mathrm{T} = \sum_{\sigma,\eta}\sum_{kq} a^\dagger_{q\sigma} t^{\sigma\eta}_{qk} b_{k\eta} + \mathrm{h.c.} \tag{6.5}$$

In the following, we want to consider spin conserving tunneling. Then, the interface does not provide any spin-flip mechanism and the time-dependent magnetic field is the only source of spin-flip mechanisms in our model. Consequently, the hopping element can be written as $t^{\sigma\eta}_{qk} = t^{\sigma}_{qk}\delta_{\sigma\eta}$, where

$$t^{\sigma}_{qk} = \int d\boldsymbol{r} \int d\boldsymbol{r'} t(\boldsymbol{r},\boldsymbol{r'})\phi^{\mathrm{S}*}_{q\sigma}(\boldsymbol{r'})\phi^{\mathrm{F}}_{k\sigma}(\boldsymbol{r}). \tag{6.6}$$

$t(\boldsymbol{r},\boldsymbol{r'})$ is the tunnel amplitude for a tunnel event from position $\boldsymbol{r}$ in the ferromagnet to position $\boldsymbol{r'}$ in the superconductor. Choosing an interface geometry consists of defining this tunnel amplitude. It will consequently be specified in the following chapters. The spin index σ refers to the spin along the magnetization direction, i.e., the direction that defines majority and minority carriers in the ferromagnet. $\phi^{\mathrm{S}}_{q\sigma}$ ($\phi^{\mathrm{F}}_{k\sigma}$) denotes the wave function of an eigenstate of the superconductor (half-metal/ferromagnet) with momentum q (k) and spin σ.

The time-dependent Hamiltonian can be brought into a time-independent form, at the cost of working in a rotating frame of reference. The transformation between the laboratory frame and the rotating frame is given by the unitary transformation

$$U = e^{-i\frac{\Omega}{2}\sigma_3 t}. \tag{6.7}$$

The Pauli matrice σ_3 acts in spin space. The Hamiltonian in the rotating frame of reference is given by $H' = U^\dagger H U - i\hbar U^\dagger \dot{U}$, where $i\hbar U^\dagger \dot{U} = \frac{\hbar\Omega}{2}\sigma_3$. Further, note that $U^\dagger \boldsymbol{m}(t)\boldsymbol{\sigma} U = \boldsymbol{m}(0)\boldsymbol{\sigma}$.

The spin quantization axis in the ferromagnet is given by the magnetization direction, which is static in the rotating frame. Majority and minority carriers are defined with respect to this axis, which is inclined by an angle α with respect to the z-axis, where α is given by

$$\tan\alpha = \frac{\sin\theta}{\tilde{\Omega} + \cos\theta}. \tag{6.8}$$

Here, we introduced the dimensionless frequency $\tilde{\Omega} = \frac{\hbar\Omega}{2|\boldsymbol{h}_\mathrm{F}(0)|}$. We use the unitary spin rotation, $W = e^{-i\frac{\alpha}{2}\sigma^y}$ in order to map the direction of the effective exchange field onto the z-axis. This unitary transformation diagonalizes H_F at the cost of working with a more complicated structure of the tunnel Hamiltonian. We denote the Hamiltonian after spin rotation and in the rotating frame by $H'' = W^\dagger H' W$ and introduce creation and annihilation operators for the half-metal in the new basis:

$$\begin{pmatrix} B_{k\uparrow} \\ B_{k\downarrow} \end{pmatrix} = W \begin{pmatrix} b_{k\uparrow} \\ b_{k\downarrow} \end{pmatrix} \tag{6.9}$$

The diagonalized Hamiltonian of the ferromagnet reads

$$H''_\mathrm{F} = \sum_{k,\eta} (\xi_k - \eta J) B^\dagger_{k\eta} B_{k\eta}, \tag{6.10}$$

where the effective exchange field J is given by

$$J = |\boldsymbol{h}_\mathrm{F}(0)| \sqrt{\tilde{\Omega}^2 + 2\tilde{\Omega}\cos\theta + 1}. \tag{6.11}$$

Here, J determines the splitting between the two spin bands. Fig. 6.2 schematically shows the density of states of a ferromagnet as a function of the energy. Consider a chemical potential that lies within the lower band and that is well separated from the

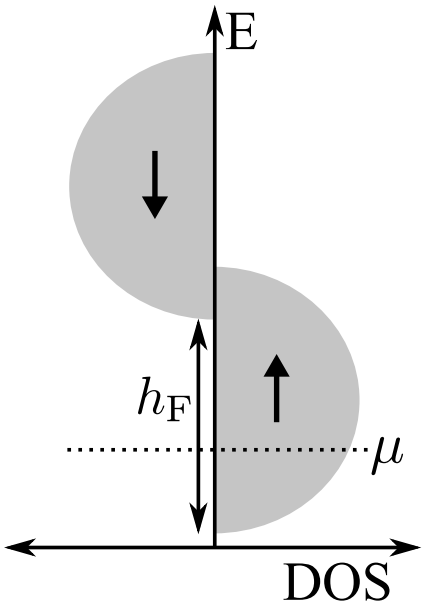

Fig. 6.2: Schematic plot of the spin-dependent density of states (DOS) for a ferromagnet. The bands for the two different spin species are offset by the exchange coupling h_F. Consider a chemical potential μ lying in the $\uparrow$-band and $h_\mathrm{F} \gg \Delta, k_\mathrm{B}T, \hbar\Omega$, such that excitations can only take place within the band, but the excitation energy is not sufficient for excitations into the $\downarrow$-band. Then, the ferromagnet has effectively perfect spin polarization at the Fermi level and is a half-metal.

upper band with opposite spin. If additionally the effective exchange coupling J is the largest energy scale, i.e., $J \gg \Delta, \hbar\Omega, k_\mathrm{B}T$, such that the energy for the occupation of the upper band may not be provided by excitations, the ferromagnet is perfectly spin polarized, i.e., a half-metal. In the following, we consider both ferromagnets and half-metals with large exchange splittings $|\boldsymbol{h}_\mathrm{F}(0)| \gg \hbar\Omega$, giving $J \approx |\boldsymbol{h}_\mathrm{F}(0)|$ and $\alpha \approx \theta$.

6.3 Distribution functions of the leads

In order to evaluate the current, knowledge about the occupation of the states of the leads is needed. Therefore, we need to determine the distribution function of the leads in the absence of tunneling. The precessing magnetization, described in the rotating frame of reference, acts as a spin-dependent chemical potential

$$\boldsymbol{\mu}_\mathrm{S} = \frac{\hbar\Omega}{2}\hat{\boldsymbol{z}}, \tag{6.12}$$

$$\boldsymbol{\mu}_\mathrm{F} = \frac{\hbar\Omega}{2}\cos\theta\hat{\boldsymbol{m}}, \tag{6.13}$$

where "ˆ" denotes the unit vector and we used $\hat{\boldsymbol{m}}\hat{\boldsymbol{z}} = \cos\theta$ for the projection of the magnetization direction onto the z-axis. Since the effective exchange splitting is much larger than the rotation frequency, i.e., $J \gg \hbar\Omega$, the chemical potential of the ferromagnet does not have a significant component perpendicular to the magnetization direction.

Since the BCS density of states of the superconductor is energy dependent, knowledge of only the chemical potentials is not sufficient to obtain the current and the distribution functions are needed.

For the superconducting lead the distribution function is only modified due to the change of the frame of reference, and reads

$$f_{\mathrm{S}}^{\sigma}(E) = f\left(E + \sigma\frac{\hbar\Omega}{2}\right), \tag{6.14}$$

where $f(E)$ denotes the Fermi-Dirac distribution function. Changing the frame of reference shifts the energy variable according to the spin-dependent chemical potential given in Eq. (6.12).

The situation is more complicated in the ferromagnet, where the precessing magnetization leads to a non-equilibrium situation for the conduction electrons. The distribution function now depends on the microscopic relaxation processes. In the following, we want to discuss two different relaxation models. First, we assume a relaxation model that has been used in [228, 247, 248]. It consists of modeling the ferromagnet attached to a normal metal region, in which the relaxation can take place. The normal region is assumed to be in equilibrium and both spin species relax separately to their equilibrium distributions. This model captures quite well the experimental reality, where the ferromagnet is likely to be connected to a normal metal. In order to determine the non-equilibrium distribution function f, we use a Boltzmann equation approach and make the relaxation time approximation, yielding

$$\frac{i}{\hbar}[H_k', f] = -\frac{f - f_{\mathrm{N}}}{\tau}. \tag{6.15}$$

Here, τ denotes the relaxation time, $f_{\mathrm{N}} = f_+ + f_-\sigma_3$ is the normal metal distribution function in the rotating frame with $f_\pm = \frac{1}{2}[f(E + \frac{\hbar\Omega}{2}) \pm f(E - \frac{\hbar\Omega}{2})]$. Further, $H_k' =$

$\xi_k + J\hat{\boldsymbol{m}}\boldsymbol{\sigma} - \frac{\hbar\Omega}{2}\sigma_3$ is the Hamiltonian of the ferromagnet in the rotating frame. We solve Eq. (6.15) using the ansatz

$$f = f_0 + f_1\hat{\boldsymbol{m}}\boldsymbol{\sigma} + \delta f, \tag{6.16}$$

where f_0, f_1 are scalar variables and δf is a matrix. We obtain $f_0 = f_+$, $f_1 = f_- \cos\theta$ and an equation for the determination of δf. Supposing $J \gg \hbar\tau^{-1}$, which is assuming that the relaxation rate is much smaller than the effective exchange coupling, we obtain $\delta f = 0$. Thus, the strong effective exchange coupling J forces the alignment with the magnetization direction. The off-diagonal elements of the distribution function will consequently vanish in the eigenbasis. Indeed, applying the unitary transformation that rotates the quantization axis to the distribution function we finally obtain

$$f_{\mathrm{F}}(E) = WfW^{\dagger} = f_+ + f_- \cos\theta\sigma_3. \tag{6.17}$$

Using the definition of $f_\pm$, this expression can be rewritten using the Fermi-Dirac distribution function:

$$f_{\mathrm{F}}^{\sigma}(E) = \cos^2\frac{\theta}{2} f\left(E + \sigma\frac{\hbar\Omega}{2}\right) + \sin^2\frac{\theta}{2} f\left(E - \sigma\frac{\hbar\Omega}{2}\right) \tag{6.18}$$

The distribution function is thus a linear combination of shifted Fermi-Dirac distribution functions.

A different distribution function has been proposed in [112]. In this publication, the authors calculate the current through an F/I/S tunnel junction, under the assumption of a precessing magnetization direction in the ferromagnet. The authors argue that the injection currents are weak due to the tunnel barrier. As a consequence, they assume the spin relaxation rate in the ferromagnet to be much larger than the tunnel rate (see also [115]). Further, they assume that at each instant in time the electrons are in equilibrium and thus the distribution function becomes a Fermi Dirac distribution with the spin-dependent chemical potentials given by Eqs. (6.12) and (6.13), i.e.,

$$f_{\mathrm{F}}^{\sigma} = \left(1 + \exp\left[\frac{E + \sigma\frac{\hbar\Omega}{2}\cos\theta}{k_{\mathrm{B}}T}\right]\right)^{-1} \tag{6.19}$$

$$f_{\mathrm{S}}^{\sigma} = \left(1 + \exp\left[\frac{E + \sigma\frac{\hbar\Omega}{2}}{k_{\mathrm{B}}T}\right]\right)^{-1} \tag{6.20}$$

The idea is to consider the adiabatic response of the carriers to the magnetization that is driven by external fields and to work in the adiabatic approximation [249]. The latter is valid, if the frequency Ω is much smaller than the exchange coupling J.

We can show that this choice of distribution function corresponds to the following underlying relaxation model. We assume that both spin species interact via electron/phonon interaction with a common bath of phonons at a fixed temperature. Consequently, the distribution function is a shifted Fermi-Dirac distribution function, as can be shown in a Boltzmann equation approach in relaxation time approximation. Further, we assume spin-orbit interactions in the ferromagnet, giving a spin-flip mechanism. The spin-orbit interaction fixes the spin-dependent chemical potential to be given by Eq. (6.13). It follows the distribution function in Eq. (6.19).

7 Andreev current through the point contact half-metal/superconductor junction

In the previous chapter we have shown the setup for the junction and given the tunnel Hamiltonian that we will now use for the evaluation of the current. In this chapter we use a point contact geometry, assuming that tunneling between the two leads may take place at one point in real space. Even though this model may seem to be oversimplified, it captures the basic physics. Further, a point contact geometry has even experimental relevance: In a scanning tunneling microscope setup, electrons tunnel from the sample to an atom size tip. We will consider an extended interface geometry in Chapter 8.

This chapter is organized in the following way. Sec. 7.1 explains the point contact model used for the computation of the current. Sec. 7.2 gives the non-equilibrium Green's functions of the leads, needed for the calculation of the current. Sec. 7.3 shows how the current operator can be written in terms of the Keldysh Green's function and how the latter can be calculated from the Green's functions of the leads using a Dyson equation. Sec. 7.4 gives the current expressions for different junctions. The normal metal/normal metal (N/N) junction allows us to determine the transmission of the junction as a function of other model parameters. The current through the normal metal/superconductor (N/S) junction contains a quasiparticle contribution and an Andreev current. We show that the latter is reduced in a ferromagnet/superconductor (F/S) junction with a static magnetization direction, when the concentrations of majority and minority spins are not equal. For a precessing magnetization direction, we first determine the charge current and the spin current through a ferromagnet/normal (F/N) metal junction that allows to understand the properties of the half-metal/superconductor (HM/S) junction, when the superconductor is in its normal state. Afterwards, we "switch on" superconductivity in Sec. 7.5. We present the main result of this part of the thesis: A precessing magnetization direction in the half-metal drives an Andreev current at zero voltage through the HM/S interface.

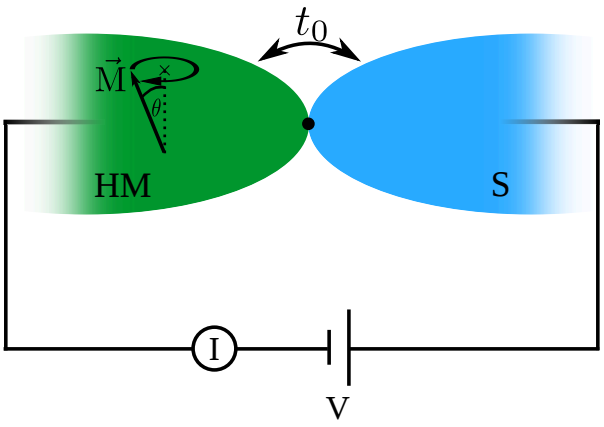

Fig. 7.1: Effective setup of the junction presented in Fig. 6.1 in a point contact geometry. The half-metallic lead on the left hand side is subjected to ferromagnetic resonance conditions. The superconducting lead on the right hand side is coupled to the half-metal in one point in real space with a constant tunnel amplitude t_0. An applied bias voltage V drives a current I through the junction.

7.1 Model and Formalisms

The aim of this section is to present the mathematical framework that we use to calculate the current through the HM/S junction introduced in Chapter 6. We use the non-equilibrium Green's functions technique in the Keldysh formalism, introduced in Chapter 3, to calculate the current. The main idea is to perform a perturbation expansion in the tunnel coupling that connects the two leads [250, 251]. As we will see, the expansion can be calculated up to infinite order yielding algebraic expressions, which are exact.

In order to model the junction in Fig. 6.1, we use the simple effective setup shown in Fig. 7.1. We model the junction using two leads, a half-metallic lead under ferromagnetic resonance conditions and a superconducting lead. We assume a point contact geometry, meaning that the leads are tunnel coupled at one point of real space. The corresponding tunnel amplitude entering Eq. (6.6) reads

$$t(\boldsymbol{r_1}, \boldsymbol{r_2}) = t_0 \delta(\boldsymbol{r_1}) \delta(\boldsymbol{r_2}). \tag{7.1}$$

The corresponding tunnel Hamiltonian given by Eq. (6.5) reads in real space

$$H_{\mathrm{T}} = t_0 b^{\dagger}(\boldsymbol{r}=0) a(\boldsymbol{r}=0) + \mathrm{h.c.} \tag{7.2}$$

We can absorb the wave functions at $\boldsymbol{r} = 0$ into the definition of the hopping element, reading

$$t_{qk}^{\sigma} = t_0 \phi_{q\sigma}^{\mathrm{S}*}(0) \phi_{k\sigma}^{\mathrm{F}}(0) \equiv t. \tag{7.3}$$

We assume that the tunnel element is constant in the energy range of interest, i.e., for energies around the Fermi level. We want to consider applied voltages V that are small compared to the Fermi energy E_{F}, i.e., $eV \ll E_{\mathrm{F}}$.

In order to calculate the current $I(V)$, it is convenient to write the Hamiltonian (Eq. (6.2)) in a Nambu basis. We introduce the Nambu vector of creation and annihilation operators given by

$$\Psi_{aq}^{\dagger} = (a_{q\uparrow}^{\dagger}, a_{q\downarrow}^{\dagger}, a_{-q\downarrow}, -a_{-q\uparrow}). \tag{7.4}$$

This choice of the basis corresponds to particle-hole space $\otimes$ spin space. This representation allows us to write the Hamiltonian as $\tilde{H}'' = \tilde{H}_{\mathrm{S}}'' + \tilde{H}_{\mathrm{F}}'' + \tilde{H}_{\mathrm{T}}''$. Here, we work in the rotating frame and we have rotated the spin quantization axis in the ferromagnet. Further, we defined

$$\tilde{H}_{\mathrm{S}}'' = \frac{1}{2} \sum_{q} \Psi_{aq}^{\dagger} H_q \Psi_{aq}, \tag{7.5}$$

$$\tilde{H}_{\mathrm{F}}'' = \frac{1}{2} \sum_{k} \Psi_{Bk}^{\dagger} H_k \Psi_{Bk}, \tag{7.6}$$

$$\tilde{H}_{\mathrm{T}}'' = \frac{1}{2} \sum_{q,k} \Psi_{aq}^{\dagger} H_\theta \Psi_{Bk}. \tag{7.7}$$

Here the factor $\frac{1}{2}$ compensates the doubling of the space due to the Nambu basis. Additionally, we defined

$$H_q = \zeta_q \tau_3 - \frac{\hbar\Omega}{2} \sigma_3 + \Delta \tau_1, \tag{7.8}$$

$$H_k = \xi_k \tau_3 - J \sigma_3, \tag{7.9}$$

$$H_\theta = t e^{i\frac{\theta}{2}\sigma_2} \tau_3, \tag{7.10}$$

where τ_i and σ_i are the i-th Pauli matrix in particle hole space, spin space, respectively. The tunnel elements in the Hamiltonian in Eq. (7.10) have now acquired an angle dependence due to the rotation of the spin quantization axis.

7.2 Non-equilibrium Green's functions of the leads

We need the non-equilibrium Green's functions of the leads in order to calculate the Keldysh Green's function of the junction that enters the current expression. First of all, we determine the retarded and advanced Green's functions to then determine the matrix Green's functions. We put the shift of the chemical potential due to the voltage bias into the Green's functions of the ferromagnet. Let us start with the superconducting lead. The retarded/advanced Green's function in Nambu space is defined by

$$g_{\mathrm{SS}}^{\mathrm{R/A}} = \sum_q (E \pm i0^+ - H_q)^{-1}, \tag{7.11}$$

where H_q is given by Eq. (7.8). We now replace the sum over the momenta by an integral over energies. Using the density of states given by $\nu_{\mathrm{S}}(\zeta) = \sum_q \delta(\zeta - \zeta_q)$ and assuming a constant density of states in the normal state (which is a good approximation for energies around the Fermi level), we obtain

$$\begin{aligned} g_{\mathrm{SS}}^{\mathrm{R/A}} &= -\nu_{\mathrm{S}} \int_{-\infty}^{\infty} \frac{d\zeta}{(\zeta + \sqrt{\Delta^2 - (\epsilon_\sigma \pm i0^+)^2})(\zeta - \sqrt{\Delta^2 - (\epsilon_\sigma \pm i0^+)^2})} \\ &= -\pi\nu_{\mathrm{S}} \frac{E_\sigma \pm i0^+ + \Delta\tau^1}{\sqrt{\Delta^2 - (E_\sigma \pm i0^+)^2}}. \end{aligned} \tag{7.12}$$

We introduced the shifted energy variable $E_\sigma = E + \frac{\hbar\Omega}{2}\sigma$ and obtain for the matrix Green's functions (see also Sec. 3.3)

$$\check{g}_{\mathrm{SS}} = \begin{cases} -\pi\nu_{\mathrm{S}} \frac{E_\sigma + \Delta\tau^1}{\sqrt{\Delta^2 - E_\sigma^2}} \begin{pmatrix} 1 & 0 \\ 0 & 1 \end{pmatrix} & \text{for} \quad |E_\sigma| < \Delta, \\ -i\pi \mathrm{sgn}(E_\sigma)\nu_{\mathrm{S}} \frac{E_\sigma + \Delta\tau^1}{\sqrt{E_\sigma^2 - \Delta^2}} \begin{pmatrix} 1 & 2F_{\mathrm{S}} \\ 0 & -1 \end{pmatrix} & \text{for} \quad |E_\sigma| > \Delta. \end{cases} \tag{7.13}$$

The explicitly written matrix is in Keldysh space. Recall that τ and σ denote particle/hole space, spin space, respectively. We use the thermal equilibrium relation

$$G^{\mathrm{K}} = (G^{\mathrm{R}} - G^{\mathrm{A}}) \tanh \frac{E}{2kT} \tag{7.14}$$

for the uncoupled leads. Further using $1 - 2f(E) = \tanh \frac{E}{2kT}$ (where f denotes the Fermi-Dirac distribution) for the distribution function of the superconductor given in Eq. (6.14), we find

$$F_{\mathrm{S}} = \tanh\left(\frac{E + \frac{\hbar\Omega}{2}\sigma_3}{2kT}\right). \tag{7.15}$$

Let us now consider the ferromagnetic lead. The calculation is similar, where the Hamiltonian in Eq. (7.9) determines the advanced/retarded Green's function of the ferromagnet. We obtain for the matrix Green's function in triagonal representation

$$\check{g}_{\mathrm{FF}} = -i\pi\nu_{\mathrm{F}} \begin{pmatrix} 1 & 2F_{\mathrm{F}} \\ 0 & -1 \end{pmatrix}. \tag{7.16}$$

Again, the explicitly written matrix is in Keldysh space. Let us assume a constant density of states for a given spin species, since we are interested into energies around the Fermi level. Then, the diagonal matrix ν_{F} reads

$$\nu_{\mathrm{F}} = \sum_{\eta\in\{\uparrow,\downarrow\}} P_\eta \nu_\eta, \tag{7.17}$$

where $\nu_\uparrow$ ($\nu_\downarrow$) denotes the majority (minority) density of states and

$$P_{\uparrow/\downarrow} = \frac{1}{2}(1 \pm \sigma_3\tau_3) \tag{7.18}$$

is the projector in Nambu space onto the majority spin ($\uparrow$), minority spin ($\downarrow$), respectively. The function F_{F} in Eq. (7.16) that determines the occupations depends on the model of relaxation chosen. For the first model presented in Sec. 6.3, corresponding to relaxation in an adjacent normal metal, the function is given by

$$F_{\mathrm{F}} = 1 - 2WfW^\dagger = \cos^2\frac{\theta}{2}\tanh\frac{E + \frac{\hbar\Omega}{2}\sigma_3 + eV\tau_3}{2kT} + \sin^2\frac{\theta}{2}\tanh\frac{E - \frac{\hbar\Omega}{2}\sigma_3 + eV\tau_3}{2kT}, \tag{7.19}$$

where we used the previously calculated distribution function given in Eq. (6.18). For the relaxation model including electron/phonon interaction and spin-orbit interaction, the function F_{F} corresponding to the distribution function given in Eq. (6.19) is given by

$$F_{\mathrm{F}} = \tanh\frac{E + \frac{\hbar\Omega}{2}\cos\theta\sigma_3 + eV\tau_3}{2kT}. \tag{7.20}$$

7.3 General current expression

In order to calculate the current through the junction, we follow the idea given in Refs. [250, 251]. We formally treat the tunnel Hamiltonian as a perturbation of the uncoupled electrodes. Our model consists of a single-channel atomic contact, where the outer atoms of each lead are coupled via the tunnel element. In the following, we will show how the current through the junction can be expressed using the Keldysh Green's function of the junction. Afterwards, we will show how the Keldysh Green's function of the junction can be obtained from the Green's functions of the leads using a Dyson equation for the perturbation expansion.

7.3.1 Current in terms of the Keldysh Green's function

Since the charge current is a conserved quantity, we can calculate it at any point of our junction. It is however advantageous to calculate it on the half-metal (ferromagnet) side using the electron number operator on that side. The current operator is given by

$$I = e\dot{N}_{\mathrm{F}} = \frac{ie}{\hbar}[H, N_{\mathrm{F}}], \tag{7.21}$$

where $N_{\mathrm{F}} = \sum_{k,\sigma} b^{\dagger}_{k\sigma} b_{k\sigma}$ is the electron number operator for the ferromagnet. We use the sign convention $e > 0$ implying that the current is positive, if electrons flow into the half-metal. We work in the laboratory frame for the derivation of the current expression. Obviously, N_{F} commutes with H_{S} (Eq. (6.3)) and H_{F} (Eq. (6.4)). Assuming a momentum-independent tunnel element and using Eq. (6.5) for a spin-dependent, momentum-independent tunnel element, we obtain

$$I = \frac{ie}{\hbar} \sum_{\sigma\eta} [a^{\dagger}_{\sigma} t_{\sigma\eta} b_{\eta} - \mathrm{h.c.}]. \tag{7.22}$$

Here, we dropped the momentum indices of the operators for clarity of the notation. We express the expectation value of the current in a symmetric way.

$$\langle I(\tau) \rangle = \frac{ie}{2\hbar} \sum_{\sigma\eta} [t_{\sigma\eta} \left\langle a^{\dagger}_{\sigma}(\tau) b_{\eta}(\tau) \right\rangle - t_{\sigma\eta} \left\langle b_{\eta}(\tau) a^{\dagger}_{\sigma}(\tau) \right\rangle - t^{\dagger}_{\sigma\eta} \left\langle b^{\dagger}_{\eta}(\tau) a_{\sigma}(\tau) \right\rangle + t^{\dagger}_{\sigma\eta} \left\langle a_{\sigma}(\tau) b^{\dagger}_{\eta}(\tau) \right\rangle], \tag{7.23}$$

where τ is the time argument. Let us define the following Green's functions

$$(G_{\mathrm{FS}}^{+-})_{11}^{\sigma\eta}(\tau,\tau') = i\left\langle a_\sigma^\dagger(\tau')b_\eta(\tau)\right\rangle, \tag{7.24}$$

$$(G_{\mathrm{FS}}^{+-})_{22}^{\sigma\eta}(\tau,\tau') = i\left\langle a_\sigma(\tau')b_\eta^\dagger(\tau)\right\rangle, \tag{7.25}$$

$$(G_{\mathrm{FS}}^{-+})_{11}^{\sigma\eta}(\tau,\tau') = -i\left\langle b_\eta(\tau')a_\sigma^\dagger(\tau)\right\rangle, \tag{7.26}$$

$$(G_{\mathrm{FS}}^{-+})_{22}^{\sigma\eta}(\tau,\tau') = -i\left\langle b_\eta^\dagger(\tau')a_\sigma(\tau)\right\rangle. \tag{7.27}$$

Here G^{+-} is a greater Green's function, whereas G^{-+} is a lesser Green's function. F and S label the ferromagnet, the superconductor, respectively. The indices σ and η are spin indices and the lower indices are Nambu indices. τ and τ' are time arguments. These Green's functions are standard definitions, that have been used for example in [252–255]. With help of the definitions in Eqs. (7.24) - (7.27), the expectation value of the current in Eq. (7.23) reads

$$\begin{aligned}\langle I\rangle = \frac{e}{4\hbar}\sum_{\sigma\eta}\{&t_{\sigma\eta}[(G_{\mathrm{FS}}^{+-})_{11}^{\sigma\eta} - (G_{\mathrm{SF}}^{-+})_{22}^{\eta\sigma} + (G_{\mathrm{FS}}^{-+})_{11}^{\sigma\eta} - (G_{\mathrm{SF}}^{+-})_{22}^{\eta\sigma}\\ &+ t_{\sigma\eta}^\dagger[(G_{\mathrm{FS}}^{-+})_{22}^{\sigma\eta} - (G_{\mathrm{SF}}^{+-})_{11}^{\eta\sigma} + (G_{\mathrm{FS}}^{+-})_{22}^{\sigma\eta} - (G_{\mathrm{SF}}^{-+})_{11}^{\eta\sigma}]\}.\end{aligned} \tag{7.28}$$

We dropped the time arguments for clarity of the notation. We introduce the hopping matrix in Nambu space

$$T = \begin{pmatrix} t & 0 \\ 0 & -t^\dagger \end{pmatrix}, \tag{7.29}$$

where t is a 2×2 matrix in spin space. Further, we use the definition of the Keldysh Green's function

$$G_{ij}^{\mathrm{K}} = G_{ij}^{+-} + G_{ij}^{-+}. \tag{7.30}$$

After Fourier transformation to energy space (and dropping the energy dependence of the Keldysh Green's function for clarity of the notation), we obtain

$$\langle I\rangle = \frac{e}{4\hbar}\int\frac{dE}{2\pi}\sum_{\sigma\eta}[T_{11}^{\sigma\eta}(G_{\mathrm{FS}}^{\mathrm{K}})_{11}^{\sigma\eta} + T_{22}^{\sigma\eta\dagger}(G_{\mathrm{SF}}^{\mathrm{K}})_{22}^{\eta\sigma} - T_{11}^{\sigma\eta\dagger}(G_{\mathrm{SF}}^{\mathrm{K}})_{11}^{\eta\sigma} - T_{22}^{\sigma\eta}(G_{\mathrm{FS}}^{\mathrm{K}})_{22}^{\sigma\eta}], \tag{7.31}$$

where the upper indices of T are spin indices and the lower indices are Nambu indices. Using the relation

$$((G_{\mathrm{FS}}^{\mathrm{K}})_{ii}^{\sigma\eta})^\dagger = -(G_{\mathrm{SF}}^{\mathrm{K}})_{ii}^{\eta\sigma}, \tag{7.32}$$

where η and σ are spin indices and i is a Nambu indix, we finally obtain

$$\langle I \rangle = \frac{e}{2\hbar} \int_{-\infty}^{\infty} \frac{dE}{2\pi} \Re \left[\mathrm{Tr}_{\sigma\tau} (\mathcal{T} G^{\mathrm{K}}_{\mathrm{FS}} \tau_3) \right], \tag{7.33}$$

where the trace is over the spin (σ) and Nambu (τ) space, τ_3 is a Pauli matrix in Nambu space and we defined $\mathcal{T} = T^T$. This expression is a generalization of the expressions given in Refs. [250, 252, 254]. We can now evaluate Eq. (7.33) in any basis, since the trace is independent of the basis. Eq. (7.33) relates the Keldysh Green's function of the junction to the current flowing through the junction. In order to obtain the current, we are left with the determination of the Keldysh Green's function.

7.3.2 Dyson equation for the Keldysh Green's function

In order to evaluate Eq. (7.33), we need to calculate the Keldysh Green's function. We have already calculated the Green's functions of the leads in the absence of tunneling in Sec. 7.2. We now switch on the tunnel coupling. The perturbation expansion up to infinite order can be written as a Dyson equation for the matrix Green's function (see Sec. 3.3 and e.g., Ref. [253]) that reads in triangular representation

$$\check{G} = \check{g} + \check{g}\check{\Sigma}\check{G}. \tag{7.34}$$

Written in the basis of the leads, Eq. (7.34) reads

$$\check{G}_{\mathrm{FS}} = \check{g}_{\mathrm{FF}}\check{\Sigma}_{\mathrm{FS}}\check{G}_{\mathrm{SS}}, \tag{7.35}$$

$$\check{G}_{\mathrm{SS}} = \check{g}_{\mathrm{SS}} + \check{g}_{\mathrm{SS}}\check{\Sigma}_{\mathrm{SF}}\check{G}_{\mathrm{FS}}. \tag{7.36}$$

We combine both equations and obtain the matrix Green's function of the junction.

$$\check{G}_{\mathrm{FS}} = (1 - \check{g}_{\mathrm{FF}}\check{\Sigma}_{\mathrm{FS}}\check{g}_{\mathrm{SS}}\check{\Sigma}_{\mathrm{SF}})^{-1}\check{g}_{\mathrm{FF}}\check{\Sigma}_{\mathrm{FS}}\check{g}_{\mathrm{SS}} \tag{7.37}$$

The Keldysh component of this expression enters the current. Since the tunneling is elastic, the components Σ^{+-} and Σ^{-+} of the self energy vanish [253]. Further $\Sigma^{++} = -\Sigma^{--}$, from which we get in triagonal representation

$$\check{\Sigma}_{\mathrm{SF}} = \begin{pmatrix} \mathcal{T} & 0 \\ 0 & \mathcal{T} \end{pmatrix}, \tag{7.38}$$

where $\mathcal{T}$ for the tunnel Hamiltonian in Eq. (7.10) reads

$$\mathcal{T} = te^{i\frac{\theta}{2}\sigma_2}\tau_3. \tag{7.39}$$

Further, the self energy with interchanged lead indices reads

$$\check{\Sigma}_{\mathrm{FS}} = \check{\Sigma}^{\dagger}_{\mathrm{SF}}. \tag{7.40}$$

We have now all ingredients to evaluate the Keldysh Green's function of the junction and therefore the current through our ferromagnet/superconductor junction given in Eq. (7.33).

In order to model a half-metal with perfect spin polarization, we put the minority carrier density of states to zero. The calculation can be simplified applying the following mathematical trick: We put the tunnel elements including the minority spin to zero, such that only the majority spin contributes to the current. Defining the projector onto the majority spin $P = \frac{1}{2}(1 + \sigma_3\tau_3)$, we obtain for the tunnel coupling $\mathcal{T}^{\mathrm{HM}} = \mathcal{T}P$. The result is identical to calculating with the original tunnel expression and afterwards putting the minority carrier density of states to zero. For definiteness we use $\uparrow$ for the majority spin and $\downarrow$ for the minority spin.

7.4 Current expressions for various heterostructures

We give the current expressions for heterostructures containing different combinations of normal metals, superconductors or ferromagnets in this section. We focus on junctions, that are important for the understanding of the physics of the half-metal/superconductor junction (HM/S). The normal metal/normal metal (N/N) junction in Sec. 7.4.1 allows us to define the transparency in the normal state. The normal metal/superconductor (N/S) junction in Sec. 7.4.2 is used to introduce the Andreev current through a junction without spin polarization. Sec. 7.4.3 shows the current and spin transport properties of a ferromagnet/normal metal junction (F/N) under ferromagnetic resonance (FMR) conditions, which corresponds to a ferromagnet/superconductor (F/S) junction in the normal state. Finally, we discuss the properties of the F/S junction for a static magnetization in Sec. 7.4.4 and show that no Andreev current

flows through an HM/S interface with fixed magnetization direction. The expressions for the current are obtained within the formalism presented in the preceding sections. More precisely, we evaluate Eq. (7.33) using the Green's function of the junction given in Eq. (7.37) that is obtained using Eqs. (7.38) - (7.40) and the Green's functions of the leads given in Eqs. (7.13) and (7.16).

7.4.1 Normal metal/normal metal junction

Let us start with the simplest case of an N/N junction containing two normal metals. It corresponds to an N/S junction, where the superconductor is in its normal phase above the critical temperature. The aim is to obtain an expression for the normal state transparency of the junction, expressed as a function of the microscopic model parameters. Without an applied voltage, the junction is in equilibrium and no current flows. Let us calculate the current for an applied voltage. For a normal metal in a static frame ($\Omega = 0$, $\theta = 0$), the matrix Green's function in triagonal representation reads

$$\check{g}_{\mathrm{jj}} = -i\pi\nu_{\mathrm{j}} \begin{pmatrix} 1 & 2F_j \\ 0 & -1 \end{pmatrix}, \tag{7.41}$$

where $j \in \{\mathrm{L}, \mathrm{R}\}$ labels the side of the junction. Further, we assume a constant density of states ν_j in both leads. The occupation factor reads

$$F_j = \tanh \frac{E + eV_j\tau_3}{2kT}, \tag{7.42}$$

where we put the voltages to $V_L = 0$ and $V_R = V$. Note that this expression is obtained from the Green's functions of the superconductor (Eq. (7.13)) and the ferromagnet (Eq. (7.16)) in the limit of a normal metal. The evaluation of Eq. (7.33) involves matrix inversions and taking the trace. For the latter operation, a useful decomposition (presented for example in [256]) of the occupation factor is given by

$$\tanh \frac{E + eV\tau_3}{2kT} = f_{\mathrm{L}} + f_{\mathrm{T}}\tau_3 \tag{7.43}$$

with the definitions

$$f_{\mathrm{L/T}} = \frac{1}{2}\left(\tanh \frac{E + eV}{2kT} \pm \tanh \frac{E - eV}{2kT}\right). \tag{7.44}$$

Deviations from equilibrium in the longitudinal component (f_{L}) stem from a change in the effective temperature, whereas deviations in the transverse component (f_{T}) stem from an effective chemical potential shift [256, 257]. It is consequently not surprising that the remaining term for the N/N junction is f_{T}, since the applied voltage shifts the chemical potential. Using the relation $\tanh \frac{E}{2kT} = 1 - 2f(E)$, where $f(E)$ denotes the Fermi-Dirac distribution function, the current can be expressed as

$$\langle I_{\mathrm{NN}} \rangle = \frac{2e}{h} \int_{-\infty}^{\infty} dE\, T[f(E - eV) - f(E)], \tag{7.45}$$

where $f(E)$ denotes the Fermi-Dirac distribution function and we introduced the transmission

$$T = \frac{4\alpha}{(1+\alpha)^2}, \tag{7.46}$$

that takes values between 0 and 1. The transmission is energy independent, since we assumed a flat density of states. $\alpha = \pi^2 \nu_{\mathrm{R}} \nu_{\mathrm{L}} |t|^2$ is the product of the two reduced (unitless) hopping elements $t_j = \pi \nu_j |t|$ (with $j \in \{\mathrm{L}, \mathrm{R}\}$), where the hopping amplitude $|t|$ (energy units) is divided by the bandwidth $W = (\pi \nu_j)^{-1}$. A similar expression for the transmission has been found by Refs. [252, 258, 259]. Further, note that a given product of hopping elements α and its inverse α^{-1} have the same transmission value $T(\alpha) = T(\alpha^{-1})$. For a given transmission $0 < T < 1$, there are consequently two values of α. Consider for example a small transmission, which might be on the one hand realized by a small hopping amplitude. In this tunnel limit the transfer of an electron is unlikely. On the other hand, it might also be realized by a large hopping amplitude, when (higher order) interference effects are important.

Let us comment on the expression for a tunnel junction, when the hopping elements are small, i.e., $t_{\mathrm{R}}, t_{\mathrm{L}} \ll 1$. Then, the transmission (Eq. (7.46)) is approximatively given by $T \approx 4\alpha$. This result is also obtained in a Fermi's golden rule calculation of the current (for more details see Sec. 8.2.1), treating the hopping element as a perturbation and calculating up to second order in the tunnel coupling. If the coupling strength is increased, Fermi's golden rule breaks down, since higher order contributions become important. The non-equilibrium Green's functions formalism is capable of capturing this regime, since the perturbation expansion is taken to infinite order.

A microscopic theory for N/N junctions and N/S junctions is given in Ref. [260]. Within this so-called Blonder-Tinkham-Klapwijk (BTK) formalism the current through

an interface is obtained from a simple microscopic model: The Bogoliubov – de Gennes equations are solved by parts and their solutions are matched at the interface that is modeled by a Dirac-δ potential barrier, which is characterized by its barrier height Z, giving rise to a transmission $T = (1 + Z^2)^{-1}$. This wave matching gives the coefficients for normal electron reflection and Andreev reflection, that enter the current expression. Our current expression given in Eq. (7.45) coincides with the BTK result.

Let us calculate the conductance of the interface G_{NN}, defined via $\langle I_{\mathrm{NN}} \rangle = G_{\mathrm{NN}} V$. The integral over the distribution functions in Eq. (7.45) yields

$$\int_{-\infty}^{\infty} dE[f(E - eV) - f(E)] = eV, \tag{7.47}$$

where we used the explicit expression for the Fermi-Dirac distribution function. This result is valid at any temperature. The conductance reads

$$G_{\mathrm{NN}} = G_0 T, \tag{7.48}$$

where the conductance quantum is given by $G_0 = \frac{2e^2}{h}$. Note that we have only one conduction channel, since we assumed a point contact. We expressed the conductance of the interface as a product of the conductance quantum and the transmission of the conduction channel, which is a well-known result from the Landauer-Büttiker formalism [174].

7.4.2 Normal metal/superconductor junction

The N/S junction is of interest, since Andreev reflection modifies the conductance for subgap energies. A deeper understanding of its properties is therefore necessary before considering the F/S junction. The N/N junction, studied in the previous subsection, corresponds to an N/S junction with the superconductor being in its normal phase. Let us now "switch on" superconductivity. The current can be written as the sum of two terms,

$$\langle I_{\mathrm{NS}} \rangle = \langle I^{<} \rangle + \langle I^{>} \rangle , \tag{7.49}$$

where the first term $\langle I^{<} \rangle$ is due to Andreev reflections at an energy inferior to the gap Δ. The second term $\langle I^{>} \rangle$ is due to quasiparticles with an energy above the gap, when Andreev reflection competes with normal reflection and direct transmission. The Green's function for the normal metal is given in Eq. (7.41). We take the Green's

function for the superconductor (Eq. (7.13)) in the laboratory frame ($\Omega = 0$). After lengthy algebraic manipulations, the current contribution from quasiparticles above the gap can be expressed as

$$\langle I^{>} \rangle = \frac{2e}{h} \int_{|E|>\Delta} dE\, T_{\mathrm{NS}}^{>}(E)[f(E - eV) - f(E)]. \tag{7.50}$$

Here we introduced the energy-dependent transmission

$$T_{\mathrm{NS}}^{>}(E) = \frac{4\alpha \frac{|E|}{\sqrt{E^2-\Delta^2}}}{1 + 2\alpha \frac{|E|}{\sqrt{E^2-\Delta^2}} + \alpha^2}, \tag{7.51}$$

where $\alpha = \pi^2 \nu_{\mathrm{N}} \nu_{\mathrm{S}} t^2$ contains the normal state density of states of the superconductor ν_{S}, that we assume to be constant. The current contribution from quasiparticles below the gap can be expressed as

$$\langle I^{<} \rangle = \frac{2e}{h} \int_{|E|<\Delta} dE\, T_{\mathrm{NS}}^{<}(E)[f(E - eV) - f(E)], \tag{7.52}$$

where we introduced the energy dependent-transmission

$$T_{\mathrm{NS}}^{<}(E) = 2\frac{\Delta^2}{\Delta^2 - E^2} \frac{4\alpha^2}{(1+\alpha^2)^2 + 4\alpha^2 \frac{E^2}{\Delta^2 - E^2}}. \tag{7.53}$$

Let us first of all establish the connection to Subsection 7.4.1. If the junction is in the normal state, i.e., $\Delta = 0$, the current contribution from pure Andreev reflection vanishes, i.e., $\langle I^{<} \rangle = 0$. Further, the transmission in Eq. (7.51) becomes the normal state transmission, i.e., $T_{\mathrm{NS}}^{>}(E) = T$ and the current is given by the expression obtained for an N/N junction.

We express the energy-dependent transmissions using the normal state transmission given in Eq. (7.46) and obtain

$$T_{\mathrm{NS}}^{>} = \frac{2}{1 + \frac{\sqrt{E^2-\Delta^2}}{|E|} \frac{2-T}{T}}, \tag{7.54}$$

$$T_{\mathrm{NS}}^{<} = \frac{2\frac{\Delta^2}{E^2}}{1 + \frac{\Delta^2 - E^2}{E^2} \left(\frac{2-T}{T}\right)^2}. \tag{7.55}$$

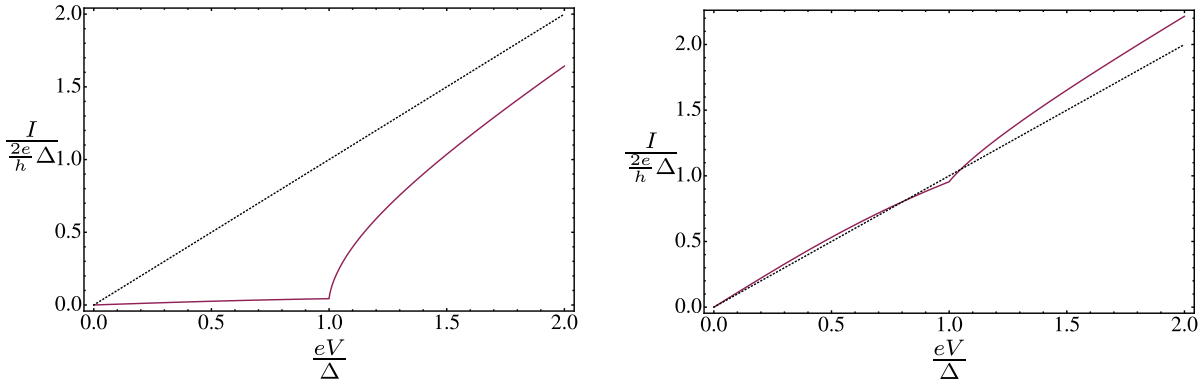

(a) tunnel junction, transmission $T = 0.1$ **(b)** transmission $T = 0.8$

Fig. 7.2: Current I through the N/S interface as a function of the bias voltage V (red curve). The black curve gives the current for an N/N junction (superconductor in the normal state) for comparison. (a) Current for a tunnel junction. (b) Current for an interface with a high transmission. Note that there is an excess current, i.e., the current through the N/S junction exceeds the current through the N/N junction.

Let us now discuss the zero temperature properties of the current. The Fermi-Dirac distribution function becomes a step function and the integrals in Eqs. (7.50) and (7.52) are trivial. Further using Eqs. (7.54) and (7.55), it is straightforward to show that

$$\langle I^{<}\rangle = \frac{2e}{h}\Delta\frac{T^2}{(2-T)\sqrt{1-T}}\begin{cases}\arctan\left(\frac{eV}{\Delta}\frac{2\sqrt{1-T}}{2-T}\right) & \text{for} \quad eV<\Delta,\\ \arctan\left(\frac{2\sqrt{1-T}}{2-T}\right) & \text{for} \quad eV\geq\Delta,\end{cases} \tag{7.56}$$

and

$$\langle I^{>}\rangle = \begin{cases}0 & \text{for} \quad eV<\Delta,\\ \frac{4e}{h}\Delta\int_1^{\frac{eV}{\Delta}}\frac{d\epsilon}{\frac{2-T}{T}\frac{\sqrt{\epsilon^2-1}}{\epsilon}+1} & \text{for} \quad eV\geq\Delta.\end{cases} \tag{7.57}$$

The integral in the last line has a cumbersome analytical solution that does not give much insight. Fig. 7.2 shows the current as a function of the bias voltage for different transparencies. For a tunnel junction, the subgap contribution due to Andreev reflection is small. For a junction with higher transparency, there is a so-called excess current, defined ([260]) by

$$I_{\text{exc}} = \lim_{V\to\infty}\left[I_{\text{NS}}(V) - I_{\text{NN}}(V)\right]. \tag{7.58}$$

For certain bias voltages, the current through the N/S junction exceeds the N/N junction value. The effect is due to Andreev reflections that are more probable for transparent interfaces and give a larger contribution to the current in that case.

If the voltage is small compared to the gap, i.e., $eV \ll \Delta$, the conductance of the junction obtained from Eq. (7.56) reads

$$G_{\mathrm{NS}} = 2G_0 T_{\mathrm{A}}. \tag{7.59}$$

As first shown by BTK [260], $T_{\mathrm{A}} = \frac{T^2}{(2-T)^2}$ is the Andreev reflection probability. For a transparent junction ($T = 1$), the conduction is twice the conduction quantum, since in an Andreev reflection process the charge of 2e is transferred. For a tunnel junction ($T \ll 1$), the conductance is proportional to the square of the transparency, i.e., $G_{\mathrm{NS}} \sim T^2 = \left(\frac{G_{\mathrm{NN}}}{G_0}\right)^2$. Hence, the conductance is proportional to the square of the normal state conductance, reflecting the fact that in an Andreev reflection process two electrons are transferred in order to form a Cooper pair. This process is of order two in the transparency (order four in the tunnel element).

More general, the expression for the subgap current contribution (Eqs. (7.52) and (7.53)) contains only even powers of $\alpha \sim t^2$, showing that only an even number of electrons can tunnel. Above the gap, also single electrons can tunnel and the current expression (Eqs. (7.50) and (7.51)) contains also odd powers of α.

An important experimentally accessible quantity is the differential conductance $\frac{dI}{dV}$. Let us without loss of generality assume $V > 0$. At zero temperature, we use that the derivative of the Fermi-Dirac distribution function becomes a Dirac-δ distribution and obtain from Eqs. (7.50) - (7.53)

$$\frac{d\langle I_{\mathrm{NS}}\rangle}{dV} = \begin{cases} \frac{2G_0}{\frac{(2-T)^2}{T^2} - \frac{4(1-T)}{T^2}(\frac{eV}{\Delta})^2} & \text{for} \quad eV < \Delta, \\ \frac{2G_0}{\frac{2-T}{T}\sqrt{1-(\frac{\Delta}{eV})^2}+1} & \text{for} \quad eV > \Delta. \end{cases} \tag{7.60}$$

For small voltages $eV \ll \Delta$, the differential conductance equals the previously established Andreev conductance, given in Eq. (7.59). Consequently, there is a linear relation between the current and the voltage in this parameter regime. For large voltages $eV \gg \Delta$, the differential conductance equals the conductance of a junction in the normal state (Eq. (7.48)). The reason is that at large energies well above the superconducting gap the superconducting properties do not play a role for the charge transport across the junction.

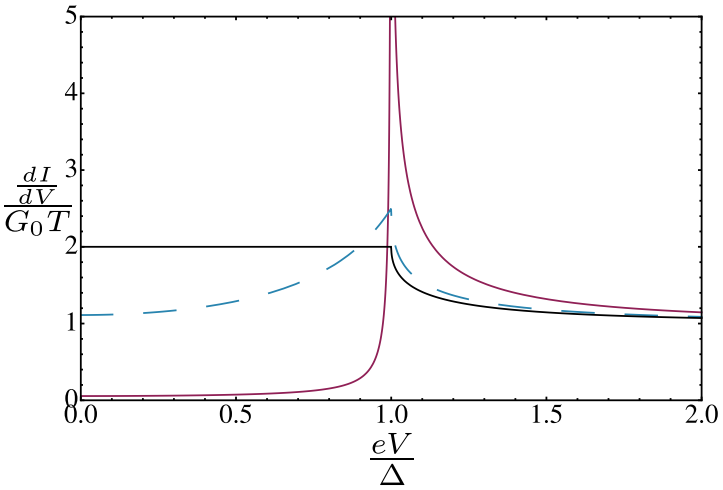

Fig. 7.3: Differential conductance (in units of the normal state conductance) as a function of the applied voltage of an N/S junction. The solid red, dotted blue, and solid black lines are for transparencies of $T = 0.1$, $T = 0.8$, and $T = 1$, respectively.

Fig. 7.3 shows a plot of the differential conductance normalized by the normal state conductance as a function of the bias voltage. For large voltages, the differential conductance equals the normal state conductance, as discussed above. For a low interface transparency $T = 0.1$, there is nearly no subgap differential conductance and a very pronounced coherence peak at $eV = \Delta$. The differential conductance is known to map the density of states in the tunnel limit $T \ll 1$. For a junction with high transparency ($T = 0.8$), the subgap contribution is important and the coherence peak is less pronounced. For an entirely transparent junction ($T = 1$), the subgap conductance equals twice the conductance quantum. In this parameter regime only Andreev reflection is possible. Each Andreev reflection process transfers two electron charges across the junction, giving twice the normal state conductance.

The differential conductance curves presented in Fig. 7.3 can be found in Ref. [260]. Our results can be mapped to the BTK results and both formalism give the same results for the current through the N/S junction. The non-equilibrium Green's functions formalism has the advantage that ferromagnets can be easily included (see the following subsections).

Let us finally comment on small transparencies, $T \ll 1$, i.e., a tunnel junction. Expanding in lowest order in $\alpha \ll 1$, the energy-dependent transmission above the gap, defined in Eq. (7.51), reads

$$T_{\mathrm{NS}}^{>}(E) = 4\alpha \frac{|E|}{\sqrt{E^2 - \Delta^2}}, \tag{7.61}$$

and the energy-dependent transmission below the gap, defined in Eq. (7.53), reads

$$T_{\mathrm{NS}}^{<}(E) = 8\alpha^2 \frac{\Delta^2}{\Delta^2 - E^2}. \tag{7.62}$$

Note that the transmission above the gap is in second order in the tunnel element t, whereas the transmission below the gap is in forth order in t. There is no subgap current (pure Andreev current) in second order in t, since Andreev reflection needs the transfer of two electrons. These current expressions equal the expressions from a Fermi's golden rule calculation.

7.4.3 Ferromagnet/normal metal junction

Let us have a look at the properties of an F/N junction, that corresponds to an F/S junction with the superconductor being in its normal phase. The HM/N junction is obtained as a special case of the F/N junction. We will also study the spin properties of the junction, that will change when the normal metal is replaced by a superconductor. Consider a precessing magnetization, as described in Sec. 7.1. The current is obtained from Eq. (7.33) using the Green's functions of the leads given in Eqs. (7.16) and (7.41) (with the distribution functions in the rotating frame given in Eqs. (7.15) and (7.19)/(7.20)). After some algebra, the trace in Eq. (7.33) can be written as the product of an energy-independent factor and a factor containing the distribution functions. We can shift the integration variable, such that it absorbs the frequency dependence. The resulting current expression is frequency independent and given by

$$\langle I_{\mathrm{FN}} \rangle = \frac{2e}{h} \int_{-\infty}^{\infty} dE\, T_{\mathrm{FN}} [f(E - eV) - f(E)], \tag{7.63}$$

where we defined the energy-independent transmission

$$T_{\mathrm{FN}} = \frac{T_\uparrow + T_\downarrow}{2} \tag{7.64}$$

with

$$T_\sigma = \frac{4\alpha_\sigma}{(1+\alpha_\sigma)^2}. \tag{7.65}$$

Thus, the current through the F/N junction does not depend on the magnetization properties. It is independent both of the precession frequency Ω and of the tilt angle θ. Further, both majority and minority spin species give independent contributions to the current. Note that there is no charge current across the junction at zero voltage. Using Eq. (7.47), we can write the conductance as $G_{\rm FN} = G_0 T_{\rm FN}$, which is a similar form as obtained for the N/N junction.

The charge current through the F/N interface is independent of the choice of the distribution function. It depends only on the spin-dependent chemical potentials (and not on the precise form of the distribution function), since the density of states of both the ferromagnet and the normal metal are energy independent.

Let us emphasize that in the limit of a normal metal with equal density of states for both spin species, i.e., $\alpha_\uparrow = \alpha_\downarrow = \alpha$, both spin species have the same transmission values $T_\uparrow = T_\downarrow = T$. We obtain the current expression for the N/N junction, discussed in Sec. 7.4.1.

Let us consider an HM/N metal junction as a special case of the more general F/N junction. Then, due to perfect spin polarization, the density of states of the minority carriers is zero, giving $\alpha_\downarrow = 0$. The current is then given by Eq. (7.63) with $T_\downarrow = 0$ (Eq. (7.65)).

There is not only charge transport across the junction, but there is also a net spin current injected into the adjacent normal metal. Instead of evaluating the charge current operator $I^{\rm C} = e\dot{N}_{\rm F}$, we will now evaluate the spin current operator. We are interested into the z-component of the spin current, for which the operator reads $I_z^{\rm S} = \frac{\hbar}{2}(\dot{N}_\uparrow - \dot{N}_\downarrow)$. Spin is pumped into the system due to the precessing magnetization, that creates spin-flip processes. Hence, the ferromagnet acts as a source for the spin current and the spin current is not a conserved quantity. We evaluate the spin current in the adjacent normal metal. We can show that

$$\left\langle I^{\rm S}_{z,{\rm FN}} \right\rangle = \frac{1}{8\pi}\int_{-\infty}^{\infty} dE \Re\left[{\rm Tr}_{\sigma\tau}(\mathcal{T} G^{\rm K}_{\rm FN}\sigma_3)\right]. \tag{7.66}$$

The procedure of evaluation of this expression is similar to the charge current and we obtain

$$\left\langle I^{\mathrm{S}}_{z,\mathrm{FN}} \right\rangle = \frac{\hbar}{2e} G_p V \cos\theta - \hbar\Omega \sin^2\theta \frac{G^{\uparrow\downarrow}}{2\pi G_0}, \tag{7.67}$$

where we defined the conductance due to spin polarization as

$$G_p = G_0 \frac{T_\uparrow - T_\downarrow}{2}. \tag{7.68}$$

Further, we introduced the mixing conductance

$$G^{\uparrow\downarrow} = G_0 \frac{\alpha_\uparrow + \alpha_\downarrow}{(1+\alpha_\uparrow)(1+\alpha_\downarrow)}. \tag{7.69}$$

The first term of Eq. (7.67) is a spin current driven by the voltage difference. It is proportional to the difference of transmissions of the two spin species. Within our model, a difference in the density of states for the two spin components is needed, as evident from Eq. (7.68). The $\cos\theta$ factor is the projection of the magnetization direction on the z-axis. This contribution to the spin current vanishes for a normal metal and is maximal for a half-metal.

Let us now discuss the spin current in the absence of a bias voltage. The second term of Eq. (7.67) is proportional to the frequency and the mixing conductance. The concept of the mixing conductance for an F/N interface has been introduced in Ref. [155], where the general definition

$$G^{\uparrow\downarrow} = \frac{e^2}{h}\left[M - \sum_{n,m} r^{nm}_\uparrow (r^{nm}_\downarrow)^*\right] \tag{7.70}$$

was given. Here M is the number of channels and r^{nm}_σ is the reflection of an electron in mode m to an electron in mode n on the normal side of the junction. Assuming one conduction channel ($M = 1$, point contact) and time-reversal invariant scattering in the barrier, we can parametrize $r_\sigma = \sqrt{1 - T_\sigma}$, where T_σ is the transmission of the barrier. Using the previously established result for the transmission given in Eq. (7.65), the mixing conductance indeed yields Eq. (7.69). As in Ref. [155], the mixing conductance for our junction yields in the tunnel limit

$$G^{\uparrow\downarrow} = \frac{G_\uparrow + G_\downarrow}{2}, \tag{7.71}$$

where $G_\sigma = 2\alpha_\sigma G_0$. For a transparent (ballistic) junction, it reads $G^{\uparrow\downarrow} = \frac{G_0}{2}$, since the conductance is $\frac{e^2}{h}$ per channel. Note that in general the mixing conductance in

Eq. (7.70) cannot be expressed using only the spin-dependent transmissions T_σ in Eq. (7.65), but is rather a function of the α_σ. We will see in Sec. 7.5, that the Andreev current through the HM/S interface under ferromagnetic resonance conditions also explicitly depends on the α_σ, not on the T_σ.

The term proportional to the frequency in Eq. (7.67) is consistent with the spin-pumping expression

$$I^{\mathrm{S}} = \frac{\hbar}{4\pi} g^{\uparrow\downarrow} \hat{\boldsymbol{m}} \times \frac{d\hat{\boldsymbol{m}}}{dt} \tag{7.72}$$

given in Refs. [72] and [157] (see also Sec. 2.4.2) and valid for a negligible imaginary part of the (unitless) mixing conductance $g^{\uparrow\downarrow} = \frac{h}{e^2} G^{\uparrow\downarrow} = \frac{2}{G_0} G^{\uparrow\downarrow}$. It describes the spin current emitted into a normal metal, coupled via an interface to an adjacent ferromagnet under ferromagnetic resonance conditions. Note that Eq. (7.72) is given in units of the mechanical torque. Using the explicit expression of the magnetization given in Eq. (6.1), we obtain for the projection on the z-axis

$$\hat{\boldsymbol{z}} (\hat{\boldsymbol{m}} \times \frac{d\hat{\boldsymbol{m}}}{dt}) = \Omega \sin^2 \theta, \tag{7.73}$$

yielding the same dependence as in Eq. (7.67).

We can interprete the zero voltage spin current in a slightly different way. Therefore, we follow a consideration given in Ref. [115] in the context of an F/I/F spin valve. Consider the difference in chemical potentials created by the time-dependent magnetization across the junction. Using the expressions of the chemical potentials given in Eqs. (6.12) and (6.13) and evaluating them in the z-basis, we obtain

$$\Delta\mu = \boldsymbol{\mu}_{\mathrm{F}} \boldsymbol{z} - \boldsymbol{\mu}_{\mathrm{N}} \boldsymbol{z} = -\frac{\hbar\Omega}{2} \sin^2 \theta. \tag{7.74}$$

The authors of Ref. [115] call this expression a “spin bias”. We can express the zero voltage spin current as

$$\left\langle I^{\mathrm{S}}_{z,\mathrm{FN}} \right\rangle \propto G^{\uparrow\downarrow} \Delta\mu. \tag{7.75}$$

Consequently, the precessing magnetization creates a difference of chemical potentials, that drives the spin current.

Ref. [157] reported a spin accumulation effect on the normal metal side of the F/N interface. We do not obtain any spin accumulation on the normal side within our model,

since we assume that our reservoirs are in equilibrium. This corresponds to assuming a much higher spin-flip rate than spin injection rate. The latter is of the order of Ω.

Note that from Eqs. (7.63) and (7.67) follows that there is a non-zero spin current, but a zero charge current for a half-metallic junction at zero voltage bias. The finding of a zero charge current is consistent with other models (in the absence of spin accumulation) [115].

7.4.4 Ferromagnet/superconductor junction - static magnetization

If we replace the normal metal by a superconductor, the transport properties change. The superconductor does not allow for spin currents below the gap, since the supercurrent below the gap is due to spin singlet Cooper pairs, formed of electrons with opposite spins. We will show that the spin current (obtained for an F/N interface) is rectified to a charge current through the interface. The resulting Andreev current for a dynamic magnetization direction is calculated and discussed in Sec. 7.5.

Before having a look at the dynamic case, let us consider an F/S junction with a fixed, static magnetization direction $\hat{\boldsymbol{m}}(t) = \hat{\boldsymbol{m}}(0)$. The current is obtained as previously described, using $\Omega = 0$. As for the N/S junction, it is useful to decompose the current into the two contributions from quasiparticles above and below the superconducting gap, i.e., $\langle I_{\mathrm{FS}}\rangle = \langle I_{\mathrm{FS}}^{<}\rangle + \langle I_{\mathrm{FS}}^{>}\rangle$. Below the gap, the current is a pure Andreev current and can be written as

$$\langle I_{\mathrm{FS}}^{<}\rangle = \frac{2e}{h}\int_{|E|<\Delta} dE\, T_{\mathrm{FS}}^{<}(E)[f(E-eV)-f(E)] \tag{7.76}$$

with

$$T_{\mathrm{FS}}^{<}(E) = 2\frac{\Delta^2}{\Delta^2-E^2}\frac{4\alpha_\uparrow\alpha_\downarrow}{1+\alpha_\uparrow^2\alpha_\downarrow^2+(\alpha_\uparrow^2+\alpha_\downarrow^2)\frac{E^2}{\Delta^2-E^2}+2\alpha_\uparrow\alpha_\downarrow\frac{\Delta^2}{\Delta^2-E^2}}. \tag{7.77}$$

Note that as for the subgap current through the N/S junction, only even powers of α are present, indicating that only an even number of electrons can be transferred across the junction. The contribution from quasiparticles above the gap reads

$$\langle I_{\mathrm{FS}}^{>}\rangle = \frac{2e}{h}\int_{|E|>\Delta} dE\, T_{\mathrm{FS}}^{>}(E)[f(E-eV)-f(E)] \tag{7.78}$$

with

$$T_{\rm FS}^{>}(E) = 2\frac{\left(\alpha_\uparrow(1+\alpha_\downarrow^2)+\alpha_\downarrow(1+\alpha_\uparrow^2)\right)\frac{|E|}{\sqrt{E^2-\Delta^2}} + 4\alpha_\uparrow\alpha_\downarrow\frac{E^2}{E^2-\Delta^2}}{\left[1+\alpha_\uparrow\alpha_\downarrow+(\alpha_\uparrow+\alpha_\downarrow)\frac{|E|}{\sqrt{E^2-\Delta^2}}\right]^2}. \tag{7.79}$$

The current is independent of the orientation of the magnetization direction in the ferromagnet, since the superconductor is isotropic (spin rotation invariant). In the limit of the superconductor becoming a normal metal ($\Delta = 0$), the pure Andreev current vanishes and we get the expressions given in Eqs. (7.63) and (7.65) for an F/N junction. In the limit of the ferromagnet becoming a normal metal ($\alpha_\uparrow = \alpha_\downarrow = \alpha$), Eqs. (7.77) and (7.79) yield the N/S junction result given in Eqs. (7.51) and (7.53).

Let us consider a ballistic junction with $\alpha_\uparrow = \alpha_\downarrow = 1$. Then, the subgap conductance given by Eqs. (7.76) and (7.77) yields

$$G_{\rm FS}^{<} = 2G_0. \tag{7.80}$$

Here, we only have one conduction channel. Ref. [89] pointed out that for a ballistic point contact with many conduction channels, the subgap conductance at an F/S interface may be either larger or smaller as the normal state conductance, depending on the ratio of the conduction channels for the different spin species.

Let us discuss the current for small voltages, i.e., $eV \ll \Delta$. Then, only the subgap current is non-zero. The current is entirely due to Andreev reflections and the corresponding conductance yields

$$G_{\rm FS}^{<} \approx G_0 T_{\rm FS}^{<}(eV). \tag{7.81}$$

We can approximate $T_{\rm FS}^{<}(eV) \approx T_{\rm FS}^{<}(0)$ and obtain using Eq. (7.77)

$$G_{\rm FS}^{<} = G_0\frac{8\alpha_\uparrow\alpha_\downarrow}{(1+\alpha_\uparrow\alpha_\downarrow)^2}. \tag{7.82}$$

The conductance thus vanishes for perfect spin polarization. For a ballistic junction, we recover Eq. (7.80).

Let us now consider a half-metal instead of the ferromagnet. The perfect spin polarization ($\alpha_\downarrow = 0$) gives for the current (using Eqs. (7.76) - (7.79))

$$\langle I_{\rm HMS}(\Omega=0)\rangle = \frac{2e}{h}\int_{|E|>\Delta} dE \frac{2\alpha_\uparrow\frac{|E|}{\sqrt{E^2-\Delta^2}}}{(1+\alpha_\uparrow\frac{|E|}{\sqrt{E^2-\Delta^2}})^2}[f(E-eV)-f(E)]. \tag{7.83}$$

In the normal state, this result becomes the result of the HM/N junction (see Sec. 7.4.3), which is half the current through an N/N interface, since only one spin species is available. The difference between the HM/S and HM/N junction is only the density of states of the superconductor, that is energy dependent in the HM/S case, whereas it is energy independent in the HM/N case. Contrary to the N/S junction, no other terms containing the pair potential appear. The reason is that the tunneling electrons cannot form a spin singlet Cooper pair, since the half-metal can only provide one spin species. As a result, any Andreev reflection process is forbidden. For zero temperature, there is consequently no subgap current for $eV < \Delta$, as evident from Eq. (7.83).

7.5 Andreev current through the half-metal/superconductor junction

In the previous sections we have developed the formalism and we have studied the normal state properties as well as the static properties of the HM/S junction. Let us now "turn on" superconductivity and the precession of the magnetization direction, i.e., consider the situation presented in Sec. 6.1 with the model given in Sec. 7.1.

We want to evaluate Eq. (7.33). This task can be divided into two steps: First, we have to evaluate the trace and afterwards the integral. In order to evaluate the former, we use the expressions for the Green's functions of the leads (Eqs. (7.13) - (7.16), (7.19)) and the Dyson equation (Eqs. (7.37) - (7.40)) to compute the Keldysh Green's function. Depending on whether $E_\sigma = E + \sigma\frac{\hbar\Omega}{2}$ is smaller or bigger than the gap of the superconductor Δ, the Green's function of the superconductor takes a different form (see Eq. (7.13)). This condition defines four energy intervals with the following current contributions

$$I_i = \frac{e}{2h}\int_{-\infty}^{\infty} dE\Theta_i(E)S_i, \tag{7.84}$$

where S_i denotes $\Re\left[\mathrm{Tr}(\mathcal{T}G^{\mathrm{K}}_{\mathrm{FS}}\tau^3)\right]$, evaluated for the interval i. The definitions of the intervals and the corresponding integral boundaries $\Theta_i(E)$ (that can be expressed in terms of Heaviside functions) are given in Tab. 7.1.

In the first interval, the absolute values of the energies for both spin species are smaller than the superconducting gap, such that pure Andreev reflection occurs for both spin species. In the second and third interval, only the absolute value of the energy for one

i	$E_\uparrow$	$E_\downarrow$	$\Theta_i(E)$
1	$\lvert E_\uparrow\rvert < \Delta$	$\lvert E_\downarrow\rvert < \Delta$	$\Theta(-\lvert E_\uparrow\rvert + \Delta)\Theta(-\lvert E_\downarrow\rvert + \Delta)$
2	$\lvert E_\uparrow\rvert > \Delta$	$\lvert E_\downarrow\rvert < \Delta$	$\Theta(+\lvert E_\uparrow\rvert - \Delta)\Theta(-\lvert E_\downarrow\rvert + \Delta)$
3	$\lvert E_\uparrow\rvert < \Delta$	$\lvert E_\downarrow\rvert > \Delta$	$\Theta(-\lvert E_\uparrow\rvert + \Delta)\Theta(+\lvert E_\downarrow\rvert - \Delta)$
4	$\lvert E_\uparrow\rvert > \Delta$	$\lvert E_\downarrow\rvert > \Delta$	$\Theta(+\lvert E_\uparrow\rvert - \Delta)\Theta(+\lvert E_\downarrow\rvert - \Delta)$

Tab. 7.1: Definition of the energy intervals for the evaluation of the current.

of the spin species is smaller than the gap, whereas the other one is larger. In the forth interval, the absolute values of the energies for both spin species are larger than the gap. The total current is given by the sum of the four current contributions:

$$\langle I_{\mathrm{HMS}}\rangle = \sum_{i=1}^{4} I_i \tag{7.85}$$

So far this decomposition is of purely mathematical nature. The evaluation of the trace involves matrix inversions, that are readily done, since the matrices to be inverted are triagonal matrices of the form $M = \begin{pmatrix} A & B \\ 0 & D \end{pmatrix}$ with inverse $M^{-1} = \begin{pmatrix} A^{-1} & -A^{-1}BD^{-1} \\ 0 & D^{-1} \end{pmatrix}$. After lengthy and cumbersome, but straightforward algebra, we obtain lengthy analytical expressions for the trace in each of the four intervals. These expressions can be found in Appendix E for the distribution function of the ferromagnet corresponding to relaxation in an adjacent normal metal layer. In this section we restrict the discussion to the distribution function given in Eq. (7.19). We give expressions for the other distribution function, corresponding to the relaxation model with phonons and spin-orbit interaction in Chapter 8, when discussing tunnel junctions.

The interesting physics will appear in the parameter regime of pure Andreev reflection, when then energy of the quasiparticles is smaller than the gap. Since the half-metal provides only one spin species, no current flows in this regime for a static magnetization, as we have seen in Sec. 7.4.4. Let us in the following consider this parameter regime. In order to simplify the discussion, we consider zero temperature $k_{\mathrm{B}}T = 0$. Then, the total current is due to Andreev reflections ($\langle I_{\mathrm{HMS}}\rangle = I_1$), if

$$\hbar\Omega + eV < \Delta. \tag{7.86}$$

The explicit expression for the trace in this parameter regime, obtained in the previously described manner, reads

$$S_1 = \sin^2\theta \frac{N_1}{D_1}(F_{\uparrow\uparrow} - F_{\downarrow\downarrow}), \tag{7.87}$$

where we defined

$$N_1 = \left(\epsilon_\uparrow^{-1}\tilde{\alpha}_\uparrow - \epsilon_\downarrow^{-1}\tilde{\alpha}_\downarrow\right)^2, \tag{7.88}$$

$$\begin{aligned} D_1 = \Bigg[1 - \left(\tilde{\alpha}_\uparrow \cos^2\frac{\theta}{2} + \tilde{\alpha}_\downarrow \sin^2\frac{\theta}{2}\right)\left(\tilde{\alpha}_\uparrow \sin^2\frac{\theta}{2} + \tilde{\alpha}_\downarrow \cos^2\frac{\theta}{2}\right) \\ + \cos^2\frac{\theta}{2}\sin^2\frac{\theta}{2}\left(\epsilon_\uparrow^{-1}\tilde{\alpha}_\uparrow - \epsilon_\downarrow^{-1}\tilde{\alpha}_\downarrow\right)^2\Bigg]^2 + \left(\tilde{\alpha}_\uparrow + \tilde{\alpha}_\downarrow\right)^2. \end{aligned} \tag{7.89}$$

Further we introduced the dimensionless quantities $\epsilon = \frac{E}{\Delta}$, $\omega = \frac{\hbar\Omega}{\Delta}$ and defined $\tilde{\alpha}_\sigma = \alpha\frac{\epsilon_\sigma}{\sqrt{1-\epsilon_\sigma^2}}$ and $\epsilon_\sigma = \epsilon + \sigma\frac{\omega}{2}$. Recall the definition of $\alpha_\uparrow = \pi^2\nu_\uparrow\nu_S\left|t\right|^2$ and note that $F_{\tau\sigma}$ is defined in Eq. (7.19). We note the following symmetries

$$I_1(-\Omega,\theta) = -I_1(\Omega,\pi-\theta), \tag{7.90}$$

$$I_1(-V,\theta) = -I_1(V,\pi-\theta), \tag{7.91}$$

that allow us without loss of generality to assume $V > 0$ and $\Omega > 0$. Let us now further evaluate the distribution functions that are step functions at zero temperature and thus modify the integral boundaries in Eq. (7.84). The relevant expression in Eq. (7.87) can be written as

$$\begin{aligned} F_{\uparrow\uparrow} - F_{\downarrow\downarrow} =& 2\cos^2\frac{\theta}{2}[f(E - \frac{\hbar\Omega}{2} - eV) - f(E + \frac{\hbar\Omega}{2} + eV)] \\ &+ 2\sin^2\frac{\theta}{2}[f(E + \frac{\hbar\Omega}{2} - eV) - f(E - \frac{\hbar\Omega}{2} + eV)]. \end{aligned} \tag{7.92}$$

The current can thus be expressed as

$$\langle I_{\mathrm{HMS}}\rangle = \frac{e\Delta}{h}\sin^2\theta\left[\cos^2\frac{\theta}{2}\int_{-\omega-U}^{\omega+U}\frac{N_1}{D_1}d\epsilon + \sin^2\frac{\theta}{2}\int_{\omega-U}^{-\omega+U}\frac{N_1}{D_1}d\epsilon\right]. \tag{7.93}$$

Here we simplified the integral boundaries with help of the relation

$$\int_{-\infty}^{\infty} d\epsilon\,\Theta(-\epsilon + \sigma\frac{w}{2} + \mu U)\theta_1 - \int_{-\infty}^{\infty} d\epsilon\,\Theta(-\epsilon + \sigma'\frac{\omega}{2} + \mu' U)\theta_1 = \int_{\sigma'\frac{\omega}{2}+\mu' U}^{\sigma\frac{\omega}{2}+\mu U} d\epsilon, \tag{7.94}$$

where we defined $\theta_1 = \Theta(-|\epsilon_\uparrow| + 1)\Theta(-|\epsilon_\downarrow| + 1)$. Further, we introduced the dimensionless voltage $U = \frac{eV}{\Delta}$.

Let us consider the scaling for frequencies and voltages much smaller than the gap Δ, i.e., $\omega \ll 1$ and $U \ll 1$. We expand the integrand in Eq. (7.93) in powers of ω:

$$\frac{N_1}{D_1} \approx \alpha^2 \frac{\epsilon^2}{(1-\epsilon^2)^3}\omega^2 + \mathcal{O}\left(\omega^3\right) \tag{7.95}$$

The approximation is valid for $\alpha \ll \omega^{-1}$. Since the integral boundaries also depend on ω, we keep only the lowest order term in ϵ for a consistent approximation. Then, integration yields the result

$$\begin{aligned}\langle I_{\mathrm{HMS}} \rangle = \frac{8}{3}\frac{e\Delta}{h}\sin^2\theta\,\alpha^2 \left(\frac{\hbar\Omega}{2\Delta}\right)^2 \Bigg[&\frac{eV}{\Delta}\left(\left(\frac{eV}{\Delta}\right)^2 + 3\left(\frac{\hbar\Omega}{2\Delta}\right)^2\right) \\ &+ \frac{\hbar\Omega}{2\Delta}\left(\left(\frac{\hbar\Omega}{2\Delta}\right)^2 + 3\left(\frac{eV}{\Delta}\right)^2\right)\cos\theta\Bigg].\end{aligned} \tag{7.96}$$

The current is due to the non-equilibrium situation created by the time-dependent magnetization. The rf-field that drives the magnetization dynamics pumps spin into the system. The spins cannot relax in the ferromagnet to reestablish equilibrium since we do not assume any spin-flip mechanism in the ferromagnet. Further, the spin-singlet pairing of the superconductor forbids a net spin current below the gap. It only allows for a charge current to flow. Seen from a slightly different perspective, the situation is as follows: The half-metal provides only one spin species. Therefore Andreev reflection is impossible (see Sec. 7.4.4), since the Andreev reflected hole has opposite spin compared to the impinging electron. The time-dependent magnetization provides a spin-flip mechanism and makes Andreev reflection possible. Indeed, Eq. (7.96) gives zero charge current if the magnetization is static, i.e., $\omega = 0$ (or $\theta = 0$).

Remarkably, there is a current at zero voltage ($V = 0$). If the superconductor was in its normal state, zero charge current would flow, as we have seen in Sec. 7.4.3. However, we have also seen that there is a spin current at $V = 0$ through the F/N junction, which is now forbidden, since the spin singlet pairing in the superconductor does not allow for a net spin current. First of all, we want to emphasize that the charge current given by Eq. (7.96) is indeed zero in the limit $\Delta \to 0$ (normal state). More precisely, the zero voltage current scales with Ω^5. This high suppression factor indicates that it

is impossible to transfer two electrons at the same instant in time. Indeed, the two electrons can only have opposite spins, if they are transferred with a delay with respect to each other, since for a given instant in time the magnetization direction fixes the spin polarization of the half-metal.

In the tunnel limit, i.e., for small transparencies, the zero voltage current through the HM/S interface reads

$$\langle I_{\mathrm{HMS}} \rangle \, (\alpha \ll 1) = \frac{e\Delta}{h} \frac{\sin^2\theta \cos\theta}{6} \frac{G^2}{G_0^2} \left(\frac{\hbar\Omega}{2\Delta} \right)^5 . \tag{7.97}$$

The conductance in the tunnel limit reads $G = 4\alpha$. Let us compare Eq. (7.97) for the Andreev current to the Andreev current induced by ferromagnetic resonance in a slightly different, but related system. The latter consists of a quantum dot, tunnel coupled to a ferromagnetic and a superconducting lead and is discussed in Ref. [247]. If the quantum dot is strongly coupled to the superconducting reservoir, the dot becomes superconducting and we can identify the Thouless energy with the superconducting gap. We are left with a system consisting of a ferromagnet and a superconductor coupled via a tunnel barrier. The Andreev current given in Ref. [247] scales with the fifth power of the precession frequency and has an angle dependence of $\cos\theta \sin^2\theta$. Remarkably, this is the same scaling behavior as obtained within our model, given by Eq. (7.97). Further, assuming perfect spin polarization, i.e., a half-metal, the current scales with the square of the conductance between the half-metal and the dot, as within our model. However, let us emphasize that the setup we use should be simpler to realize experimentally, since no quantum dot is needed.

At non-zero voltages applied across the junction, the angular dependence of the current is strongly modified. In general, the voltage competes with the frequency. In the limit of $U \gg \omega \gg 1$, the current scales with the third power of the voltage. However, note that this is only true, if the spin polarization is perfect.

Note that the general current expression (at arbitrary ω and U) in the pure Andreev regime is not invariant under $\alpha \to \alpha^{-1}$, as can be seen from Eqs. (7.87) - (7.89). Since the normal state transparency is invariant under this operation (see Eq. (7.46)), the general current expression is not a function of only the normal state transparency, but rather a function of α.

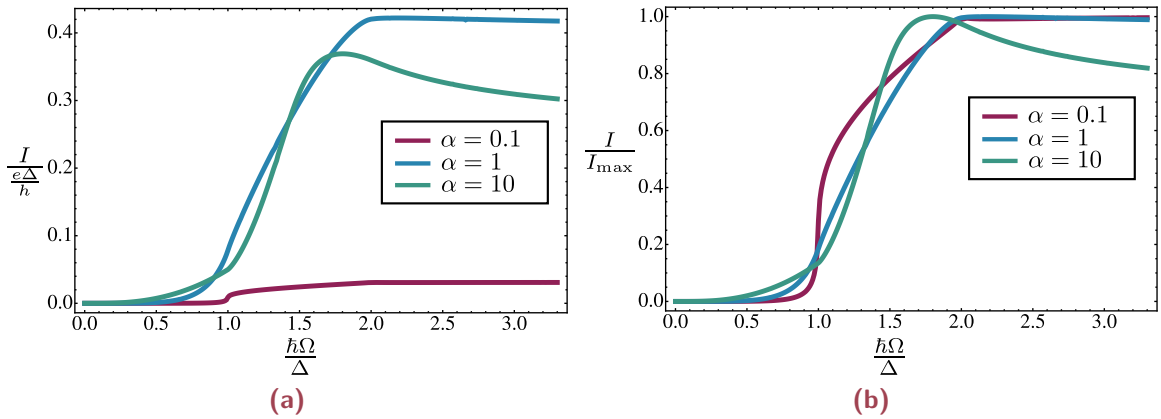

Fig. 7.4: Current through the half-metal/superconductor interface as a function of the precession frequency Ω at zero voltage and zero temperature. In (b) the curves are normalized to their maximum values. The red and green curves show the current for a tunnel junction with the same transparency, but different values for α. The blue curve is a transparent junction. The precession angle for all curves is $\theta = \arctan\sqrt{2}$, which is the angle that yields the highest current in the tunnel limit (see Eq. (7.97)).

Let us now consider the Andreev current through the junction beyond the restrictive limit of $\omega \ll 1$, but let us keep zero temperature and consider no voltage bias. In the absence of a voltage bias the lowest order contribution to the current is in t^4 for the relaxation model considering an adjacent normal metal. Hence, the dominant contribution to the current are Andreev processes. Note that in the subgap regime ($\hbar\Omega < \Delta$), the current is a pure Andreev current, since only even powers of α contribute. The current can be evaluated numerically. Fig. 7.4 shows the current as a function of the precession frequency for a tunnel junction ($\alpha = 0.1$ and $\alpha = 10$, that both give rise to the same transmission $T \approx 0.33$) and for a transparent junction ($\alpha = 1$ with $T = 1$). The cone angle of the magnetization $\theta = \arctan\sqrt{2}$ is chosen, such that it maximizes the tunnel junction angular dependence function $\sin^2\theta\cos\theta$ (see Eq. (7.97)).

For small frequencies $\hbar\Omega \ll \Delta$, the curves follow the Ω^5 scaling as evident from Eq. (7.96). Beyond this interval, the current increases until its maximum at around $\hbar\Omega \approx 2\Delta$. Depending on α, the saturation value for large frequencies, discussed in Appendix F, may be significantly smaller than the maximum. Note that the maximum value of the current is not determined by the transmission T, but rather by the reduced hopping element α, as evident from Fig. 7.4(a).

For large frequencies far beyond the gap, we find a finite zero voltage current driven by the magnetization dynamics. This current is an excess current, since there is no current

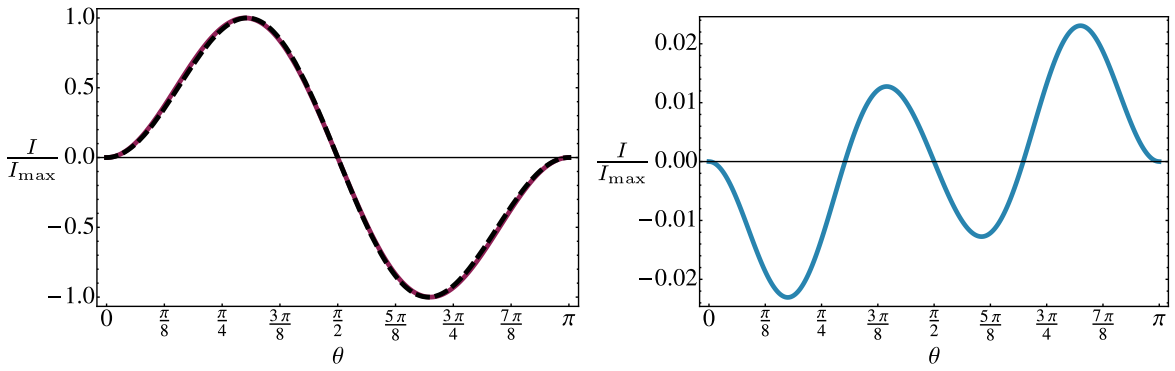

(a) angular dependence of the current **(b)** deviation from $\sin^2\theta\cos\theta$

Fig. 7.5: (a) Current through the half-metal/superconductor interface as a function of the precession angle θ at zero voltage and zero temperature. The current is normalized to its maximum value. The red curve is given for a transparent junction $\alpha = 1$ and a frequency of $\hbar\Omega = 3\Delta$. The dashed black curve is the function $\sin^2\theta\cos\theta$ (normalized to its maximum value) for comparison. (b) The difference of the two curves in (a).

in the normal state (see Sec. 7.4.3). This excess current is similar to the (voltage driven) excess current in N/S junctions.

Appendix F discusses in more detail the current at high frequencies, i.e., $\omega \gg 1$, for zero voltage bias and zero temperature. The main result is that the angular dependence follows the $\sin^2\theta\cos\theta$ behavior in the tunnel limit. The angle dependence is changed for a transparent junction. However, these changes are small, such that in a very good approximation the angular dependence is still given by $\sin^2\theta\cos\theta$. Fig. 7.5(a) shows the angular dependence of the current for a transparent junction at zero voltage bias and zero temperature. The curve is given for a frequency of $\hbar\Omega = 3\Delta$. Fig. 7.5(b) gives the deviations of the angular dependence of the current from the tunnel junction behavior. For smaller frequencies the dependence matches even better the $\sin^2\theta\cos\theta$ dependence.

Let us comment on the feasibility of an experimental detection of an Andreev current through the HM/S junction. The zero voltage current scales with the fifth power of the frequency (see Eq. (7.96)), which results in small currents. However, the frequency can be chosen of the order of the gap, $\hbar\Omega \sim \Delta$, giving a reasonable current amplitude. Further, an interface with a high transparency should be favored. Since there is no normal state current at zero voltage bias (see Sec. 7.4.3), the Andreev current can be easily distinguished from a normal current by measuring once in the superconducting

state, once in the normal state. Additionally, as we will show in Chapter 8, a more realistic interface geometry and disorder in the ferromagnet both enhance the current.

So far, we have considered an HM/S junction, but we have formulated the formalism generally enough to treat an F/S junction. However, since the general expressions were already complicated for the half-metal, we will focus on F/S tunnel junctions, where the problem can be treated in a Fermi's golden rule calculation. The results are given in Chapter 8.

We will also show in Chapter 8 that the other distribution function (given in Eq. (6.19)), corresponding to a relaxation model with phonons and spin-orbit interaction, yields the same result for tunnel junctions for small precession angles θ. The subgap Andreev current is thus independent of the specific relaxation model chosen. However, there is a region of intermediate frequencies for the distribution function given in Eq. (6.19), for which a quasiparticle current in order $|t|^2$ is dominant (see also Ref. [112]). For large frequencies, there is again an excess current due to Andreev reflections. The crossover takes place at $\omega \sim (\alpha \ln \alpha)^{-1}$.

8 Andreev current through the extended ferromagnet/superconductor tunnel junction

In the previous chapter we established the current expression through an HM/S junction in the point contact geometry. This geometry allowed us to capture the basic physics of the system. In this chapter we want to focus on the experimentally more relevant extended interface geometry. We restrict our considerations to tunnel junctions with small transparency. In Sec. 8.1 we derive a general current expression from a golden rule calculation and derive an expression for the tunnel conductance of the interface. In Sec. 8.2 we evaluate the current for a ballistic F/S junction. In Sec. 8.3 we treat disorder in the leads. We give a brief introduction to the disorder formalism and show that disorder enhances the current through the interface.

8.1 Current expression from Fermi's golden rule

We consider the setup presented in Sec. 6.1 with two modifications: First, throughout the entire chapter we consider tunnel junctions with a small transparency. Second, we consider a more general hopping element that allows us to treat different interface geometries. Additionally, we are only interested in the subgap Andreev current. The tunnel regime allows us to calculate this current using lowest order perturbation theory, i.e., within a Fermi's golden rule expression.

The following presentation of the general formalism is based on the calculation of the Andreev current through a disordered N/S interface used in [117, 261] and given in detail in [262]. This section gives the generalization of this formalism to an F/S interface using the same steps as in the previously cited references. F/S interfaces have been investigated within this formalism in the context of non-local processes in multi-terminal structures [263] and for ferromagnets with domain walls [264].

It is convenient to express the tunnel Hamiltonian using the eigenbasis of both leads. In Sec. 6.2 we have seen that for the ferromagnet this corresponds to working in a rotating frame of reference (Eq. (6.7)) and applying a spin rotation (Eq. (6.9)). So far (see Chapter 7), we have used a description in terms of electrons for the superconductor, since the Green's functions had easy definitions in this basis. Now, we diagonalize the BCS Hamiltonian using the following Bogoliubov transformation

$$a_{q\sigma} = e^{i\frac{\phi}{2}}[u_q \gamma_{q\sigma} - \sigma v_q \gamma^\dagger_{-(q\sigma)}], \tag{8.1}$$

where the BCS coherence factors read $u_q = \frac{1}{\sqrt{2}}\sqrt{1+\frac{\zeta_q}{E_q}}$ and $v_q = \frac{1}{\sqrt{2}}\sqrt{1-\frac{\zeta_q}{E_q}}$ and the energy is given by $E_q = \sqrt{\zeta_q^2 + \Delta^2}$. Further, we introduced the quasiparticle operator $\gamma^\dagger_{q\sigma}$ that creates a Bogoliubov quasiparticle, which is a superposition of an electron and a hole. The diagonalized superconductor Hamiltonian in the rotating frame reads

$$\tilde{H}_\mathrm{S} = \sum_{q,\sigma} \underbrace{\left(\sqrt{{\zeta_q}^2 + \Delta^2} - \sigma\frac{\hbar\Omega}{2}\right)}_{E_{q\sigma}} \gamma^\dagger_{q\sigma}\gamma_{q\sigma}. \tag{8.2}$$

The excitations are fermionic with a Fermi-Dirac distribution function. Using the Bogoliubov transformation in Eq. (8.1), we can write the tunnel Hamiltonian Eq. (6.5) as

$$\tilde{H}_\mathrm{T} = \sum_{qk\sigma} e^{-i\frac{\phi}{2}}[u^*_q \gamma^\dagger_{q\sigma} - \sigma v^*_q \gamma_{-(q\sigma)}](\tilde{u}_\sigma t^\uparrow_{qk}\beta_{k\uparrow} - \sigma\tilde{v}_\sigma t^\downarrow_{qk}\beta_{k\downarrow}) + \mathrm{h.c.}, \tag{8.3}$$

where the hopping elements were previously defined in Eq. (6.6). We assume a spin conserving hopping, giving a tunnel amplitude that does not have spin indices. The rotation of the spin quantization axis given in Eq. (6.9) gives the factors $\tilde{u}_\uparrow = \tilde{v}_\downarrow = \cos\frac{\theta}{2}$ and $\tilde{v}_\uparrow = \tilde{u}_\downarrow = \sin\frac{\theta}{2}$.

8.1.1 Tunnel conductance

The purpose of this subsection is to show how the tunnel conductance can be obtained within this formalism. We derive a general expression that can be further evaluated depending on the interface geometry. For a disordered junction, the disorder average over the conductance has to be taken. The necessity of knowing the tunnel conductance becomes more apparent, when using a diagrammatic approach for the current evaluation in the presence of disorder.

We determine the tunnel conductance for the junction in the normal state with a static magnetization. Fermi's golden rule applied to the tunnel Hamiltonian given in Eq. (8.3) yields for the current

$$I = \frac{2\pi e}{\hbar} \sum_{k,q,\sigma} \left| t_{qk}^{\sigma} \right|^2 \delta(\xi_k + eV - \zeta_q)[f(\xi_k) - f(\zeta_q)]. \tag{8.4}$$

At zero temperature and in the limit of zero voltage the conductance reads

$$G_{\mathrm{T}} = 2\pi^2 G_0 \sum_{k,q,\sigma} \left| t_{qk}^{\sigma} \right|^2 \delta(\xi_k)\delta(\zeta_q), \tag{8.5}$$

where we introduced the conductance quantum $G_0 = \frac{2e^2}{h}$. Let us introduce the non-local density of states, which is also called spectral function,

$$K_{\xi}^{X\sigma}(\boldsymbol{r_1}, \boldsymbol{r_2}) = \sum_{k} \delta(\xi - \xi_{k\sigma}) \phi_{k\sigma}^{X}(\boldsymbol{r_1}) \phi_{k\sigma}^{X*}(\boldsymbol{r_2}), \tag{8.6}$$

where the superscript $X \in \{\mathrm{N}, \mathrm{S}, \mathrm{F}\}$ denotes the lead. Further using the expressions for the hopping element in Eq. (6.6), the tunnel conductance can be expressed as

$$G_{\mathrm{T}} = 2\pi^2 G_0 \sum_{\sigma} \int d\boldsymbol{r_1} \int d\boldsymbol{r_2} \int d\boldsymbol{r_1'} \int d\boldsymbol{r_2'} t(\boldsymbol{r_1}, \boldsymbol{r_1'}) t^*(\boldsymbol{r_2}, \boldsymbol{r_2'}) K_0^{\mathrm{N}\sigma}(\boldsymbol{r_2'}, \boldsymbol{r_1'}) K_0^{\mathrm{F}\sigma}(\boldsymbol{r_1}, \boldsymbol{r_2}). \tag{8.7}$$

We will evaluate this expression depending on the geometry and depending on whether we consider a ballistic or a disordered junction.

8.1.2 Andreev current

In order to calculate the Andreev current perturbatively from Eq. (8.3), we consider the following microscopic process. Two electrons from the ferromagnet are transferred to the superconductor and form a Cooper pair, i.e., they are added to the condensate. The intial ($|i\rangle$) and final ($|f\rangle$) states corresponding to this process, written in an excitation basis, are given by

$$|i\rangle = |0\rangle_{\mathrm{S}} \, |k\sigma, k'\sigma'\rangle_{\mathrm{F}} \,, \tag{8.8}$$

$$|f\rangle = |0\rangle_{\mathrm{S}} \, |0\rangle_{\mathrm{F}} \,. \tag{8.9}$$

Here the subscript S refers to quasiparticle states in the superconductor, whereas the subscript F refers to the ferromagnet. The probability of a direct transfer of two electrons is proportional to $\left|\langle i|\tilde{H}_{\mathrm{T}}|f\rangle\right|^2$ and, therefore, vanishes. A direct transfer corresponds to a process in second order in the tunnel element. As we have already seen in Sec. 7.4.2, the lowest non-zero contribution to the Andreev current is in forth order in the tunnel amplitude. The matrix element from the next order term in the perturbation expansion is well-known and can be written as [265]

$$A = \sum_m \frac{\left\langle f \left| \tilde{H}_{\mathrm{T}} \right| m \right\rangle \left\langle m \left| \tilde{H}_{\mathrm{T}} \right| i \right\rangle}{E_m - E_i}, \tag{8.10}$$

where the sum runs over all virtuel intermediate states $|m\rangle$ and E_m (E_i) denotes the energy of the intermediate state (initial state). The Andreev current can be written as

$$I = \frac{2\pi e}{\hbar} \sum_{\sigma,\sigma'} \sum_{k,k'} \left| A^{\sigma\sigma'}_{kk'} \right|^2 \delta(\xi_{k\sigma} + \xi_{k'\sigma'} + 2eV)(1 - f_\sigma(\xi_k) - f_{\sigma'}(\xi_{k'})). \tag{8.11}$$

Here $A^{\sigma\sigma'}_{kk'}$ denotes the matrix element A (Eq. (8.10)) evaluated for the initial and final states given in Eqs. (8.8) and (8.9). Recall that $\xi_{k\sigma}$ denotes the kinetic energy in the ferromagnetic lead. We use the previously derived distribution function of the ferromagnet (for the relaxation model assuming relaxation in an adjacent normal metal), given by Eq. (6.18) that reads

$$f^{\mathrm{F}}_\sigma(E) = \cos^2\frac{\theta}{2} f\left(E + \sigma\frac{\hbar\Omega}{2}\right) + \sin^2\frac{\theta}{2} f\left(E - \sigma\frac{\hbar\Omega}{2}\right), \tag{8.12}$$

where $f(E)$ is the Fermi-Dirac distribution function. We will afterwards compare the result to the current that we obtain with the distribution function defined in Eq. (6.19), proposed by Ref. [112] (corresponding to a relaxation model with phonons and spin-orbit coupling). We rewrite the energies in the current expression (given in Eq. (8.11)) using

$$\int d\xi \delta(\xi - \xi_{k\sigma}) \int d\xi' \delta(\xi' - \xi_{k'\sigma'}) = 1. \tag{8.13}$$

Further, we change the newly defined continuous energy variables ξ, ξ' to a center of mass variable ξ_0 and a difference variable ϵ, defined via

$$\xi = \xi_0 + \frac{\epsilon}{2}, \tag{8.14}$$

$$\xi' = \xi_0 - \frac{\epsilon}{2}. \tag{8.15}$$

After integration over the center of mass energy variable ξ_0 the current expression yields

$$I = \frac{\pi e}{\hbar} \int d\epsilon \sum_{\sigma,\sigma'} A_{\sigma,\sigma'}(\epsilon, eV) \left[1 - f_\sigma\left(\frac{\epsilon}{2} - eV\right) - f_{\sigma'}\left(-\frac{\epsilon}{2} - eV\right)\right], \tag{8.16}$$

where we defined the dimensionless quantity

$$A_{\sigma\sigma'}(\epsilon, eV) = \sum_{k,k'} \delta\left(\frac{\epsilon}{2} - eV - \xi_{k\sigma}\right) \delta\left(-\frac{\epsilon}{2} - eV - \xi_{k'\sigma'}\right) \left|A^{\sigma\sigma'}_{kk'}\right|^2. \tag{8.17}$$

We will now evaluate this expression. Therefore, we need to evaluate the matrix element $A^{\sigma\sigma'}_{kk'}$. It is straightforward to evaluate Eq. (8.10) with the states given in Eqs. (8.8) and (8.9). Note that the virtual intermediate state can be written as $|m\rangle = |q\sigma_1\rangle_{\mathrm{S}} |k_1\eta_1\rangle_{\mathrm{F}}$. In the following we give the explicit expressions for all four different combinations of the spin indices. We start the evaluation with the expression for $A^{\uparrow\uparrow}_{kk'}$, which is the only matrix element in the case of a half-metal. As in the previous chapter, we denote the majority spin by $\uparrow$. We obtain

$$\begin{aligned} A^{\uparrow\uparrow}_{kk'} = e^{-i\phi} \cos\frac{\theta}{2} \sin\frac{\theta}{2} \sum_q u_q v_q \Big[& t^{\uparrow}_{-qk'} t^{\uparrow}_{qk} \left((E_{q\uparrow} - E_{k\uparrow})^{-1} - (E_{q\downarrow} - E_{k\uparrow})^{-1}\right) \\ & - t^{\uparrow}_{-qk} t^{\uparrow}_{qk'} \left((E_{q\uparrow} - E_{k'\uparrow})^{-1} - (E_{q\downarrow} - E_{k'\uparrow})^{-1}\right)\Big], \end{aligned} \tag{8.18}$$

where the energy of the superconductor is given by $E_{q\sigma} = \sqrt{{\zeta_q}^2 + \Delta^2} - \sigma\frac{\hbar\Omega}{2}$ (see Eq. (8.2)) and the energy of the ferromagnet is given by $E_{k\eta} = \xi_{k\eta} + eV$, incorporating the chemical potential shift due to the applied voltage to the ferromagnet side. As

shown in Eq. (8.13), we change to continuous integration variables. Additionally manipulating the summation indices ($p \to -p$ and $q \to -q$), we obtain

$$\begin{aligned} A_{\uparrow\uparrow}(\epsilon, eV) = \frac{\sin^2\theta}{4} \sum_{kk'qp} \int d\xi \int d\xi' \int d\zeta \int d\zeta' \delta(\xi - \xi_{k\uparrow})\delta(\xi' - \xi'_{k'\uparrow})\delta\left(\zeta - \zeta_q\right)\delta\left(\zeta' - \zeta_p\right) \\ \cdot \delta(\frac{\epsilon}{2} - eV - \xi)\delta(-\frac{\epsilon}{2} - eV - \xi')t^{\uparrow}_{-qk'}t^{\uparrow}_{qk}t^{\uparrow *}_{-pk'}t^{\uparrow *}_{pk} \\ \cdot [G_\uparrow(\zeta,\xi) - G_\downarrow(\zeta,\xi) - G_\uparrow(\zeta,\xi') + G_\downarrow(\zeta,\xi')] \\ \cdot [G_\uparrow(\zeta',\xi) - G_\downarrow(\zeta',\xi) - G_\uparrow(\zeta',\xi') + G_\downarrow(\zeta',\xi')], \end{aligned} \tag{8.19}$$

where we defined

$$G_\sigma(\zeta,\xi) = u(\zeta)v(\zeta)\left(E(\zeta) - \sigma\frac{\hbar\Omega}{2} - \xi + eV\right)^{-1}. \tag{8.20}$$

We defined $E(\zeta) = \sqrt{\zeta^2 + \Delta^2}$. Using the expression for the hopping element in Eq. (6.6), we obtain

$$\begin{aligned} A_{\uparrow\uparrow}(\epsilon, eV) = \frac{\sin^2\theta}{4} \int d\xi \int d\xi' \int d\zeta \int d\zeta' \delta\left(\frac{\epsilon}{2} - eV - \xi\right)\delta\left(-\frac{\epsilon}{2} - eV - \xi'\right) \\ \cdot \Xi^{\uparrow\uparrow}(\zeta,\zeta',\xi,\xi')[G_\uparrow(\zeta,\xi) - G_\downarrow(\zeta,\xi) - G_\uparrow(\zeta,\xi') + G_\downarrow(\zeta,\xi')] \\ \cdot [G_\uparrow(\zeta',\xi) - G_\downarrow(\zeta',\xi) - G_\uparrow(\zeta',\xi') + G_\downarrow(\zeta',\xi')], \end{aligned} \tag{8.21}$$

where we defined the dimensionless quantity

$$\begin{aligned} \Xi^{\sigma\sigma'}(\zeta,\zeta',\xi,\xi') = \int d\boldsymbol{r_1} \int d\boldsymbol{r_2} \int d\boldsymbol{r_3} \int d\boldsymbol{r_4} \int d\boldsymbol{r'_1} \int d\boldsymbol{r'_2} \int d\boldsymbol{r'_3} \int d\boldsymbol{r'_4} t(\boldsymbol{r_1},\boldsymbol{r'_1})t(\boldsymbol{r_2},\boldsymbol{r'_2}) \\ \cdot t(\boldsymbol{r_3},\boldsymbol{r'_3})^* t(\boldsymbol{r_4},\boldsymbol{r'_4})^* K^{\mathrm{S}}_{\zeta}(\boldsymbol{r'_1},\boldsymbol{r'_2})K^{\mathrm{S}}_{\zeta'}(\boldsymbol{r'_4},\boldsymbol{r'_3})K^{\mathrm{F}\sigma}_{\xi}(\boldsymbol{r_2},\boldsymbol{r_4})K^{\mathrm{F}\sigma'}_{\xi'}(\boldsymbol{r_1},\boldsymbol{r_3}). \end{aligned} \tag{8.22}$$

Further, we used the non-local density of states, introduced in Eq. (8.6). Eq. (8.22) depends on the interface geometry via the hopping amplitudes. Hence, the geometry has to be specified for a further evaluation of Eqs. (8.16) and (8.21). The presented formalism allows us to treat disorder. In the case of disordered leads, presented in Sec. 8.3, we have to perform the disorder average over Eq. (8.22).

For a ferromagnet with both spin polarizations we have to evaluate Eq. (8.17) for the remaining three spin combinations. For $\sigma = \sigma' = \downarrow$ the calculation is analogous to above

calculation. $A_{\downarrow\downarrow}(\epsilon, eV)$ is given by the right hand side of Eq. (8.21) with $\Xi^{\uparrow\uparrow}$ replaced by $\Xi^{\downarrow\downarrow}$.

Now consider nonequal spins $\sigma = \uparrow$ and $\sigma' = \downarrow$. Evaluation of the matrix element from Fermi's golden rule (Eqs. (8.8) - (8.10)) yields:

$$\begin{aligned} A_{\uparrow\downarrow}(\epsilon, eV) = \sum_{k,k'} \delta\left(\frac{\epsilon}{2} - eV - \xi_{k\uparrow}\right) \delta\left(-\frac{\epsilon}{2} - eV - \xi_{k'\downarrow}\right) \sum_{pq} u_q v_q u_p v_p \\ \cdot \Bigg[\sin^2\frac{\theta}{2} (t^{\uparrow}_{-qk} t^{\downarrow}_{qk'} (E_{q\uparrow} - E_{k'\downarrow})^{-1} + t^{\downarrow}_{-qk'} t^{\uparrow}_{qk} (E_{q\downarrow} - E_{k\uparrow})^{-1}) \\ + \cos^2\frac{\theta}{2} (t^{\uparrow}_{-qk} t^{\downarrow}_{qk'} (E_{q\uparrow} - E_{k'\downarrow})^{-1} + t^{\downarrow}_{-qk'} t^{\uparrow}_{qk} (E_{q\uparrow} - E_{k\uparrow})^{-1} \Bigg] \\ \cdot \Bigg[\sin^2\frac{\theta}{2} (t^{\uparrow *}_{-pk} t^{\downarrow *}_{pk'} (E_{p\uparrow} - E_{k'\downarrow})^{-1} + t^{\downarrow *}_{-pk'} t^{\uparrow *}_{pk} (E_{p\downarrow} - E_{k\uparrow})^{-1}) \\ + \cos^2\frac{\theta}{2} (t^{\uparrow *}_{-pk} t^{\downarrow *}_{pk'} (E_{p\uparrow} - E_{k'\downarrow})^{-1} + t^{\downarrow *}_{-pk'} t^{\uparrow *}_{pk} (E_{p\uparrow} - E_{k\uparrow})^{-1} \Bigg] \end{aligned} \tag{8.23}$$

The energies for the superconductor $E_{q\sigma}$ and the ferromagnet $E_{k\eta}$ are defined as before. The indices p, q refer to the superconductor, whereas the indices k, k' refer to the ferromagnet. Introducing continuous integration variables, the expression reads

$$\begin{aligned} A_{\uparrow\downarrow}(\epsilon, eV) = \int d\xi \int d\xi' \int d\zeta \int d\zeta' \delta\left(\frac{\epsilon}{2} - eV - \xi\right) \delta\left(-\frac{\epsilon}{2} - eV - \xi'\right) \Xi^{\downarrow\uparrow}(\zeta, \zeta', \xi', \xi) \\ \cdot \left[\sin^2\frac{\theta}{2} \left(G_{\uparrow}(\zeta, \xi') + G_{\downarrow}(\zeta, \xi)\right) + \cos^2\frac{\theta}{2} \left(G_{\downarrow}(\zeta, \xi') + G_{\uparrow}(\zeta, \xi)\right) \right] \\ \cdot \left[\sin^2\frac{\theta}{2} \left(G_{\uparrow}(\zeta', \xi') + G_{\downarrow}(\zeta', \xi)\right) + \cos^2\frac{\theta}{2} \left(G_{\downarrow}(\zeta', \xi') + G_{\uparrow}(\zeta', \xi)\right) \right]. \end{aligned} \tag{8.24}$$

Note that the arguments ξ and ξ' in $\Xi^{\downarrow\uparrow}(\zeta, \zeta', \xi', \xi)$ are interchanged with respect to the definition given in Eq. (8.22). $A_{\uparrow\downarrow}(\epsilon, eV)$ can analogously be expressed by the right hand side of Eq. (8.24) with $\cos\frac{\theta}{2} \leftrightarrow \sin\frac{\theta}{2}$ and $\Xi^{\downarrow\uparrow}(\zeta, \zeta', \xi', \xi) \to \Xi^{\downarrow\uparrow}(\zeta, \zeta', \xi, \xi')$. Note that we expressed both terms $A_{\uparrow\downarrow}$ and $A_{\downarrow\uparrow}$ using the same function $\Xi^{\downarrow\uparrow}$.

In order to further evaluate the expressions, we have to specify the geometry of the junction. In the Sec. 8.2 we will evaluate the current for a ballistic junction in a point contact geometry and in an extended interface geometry.

8.2 Andreev current for a ballistic ferromagnet/superconductor junction

In this section we want to evaluate the current given by Eq. (8.16) for ballistic junctions, where the leads do not contain any disorder. We will use the ballistic results for comparison with disordered junctions. In the following we consider a point contact geometry, as in Chapter 7. The difference with respect to the previous chapter is that we include a finite minority carrier concentration, i.e., we consider an F/S junction, whereas previously we considered an HM/S junction with perfect spin polarization. However, we are now restricted to the tunnel regime. We show that the point contact results obtained in Sec. 8.2.1 can be easily generalized to the extended interface (Sec. 8.2.2). In both cases, the main task is to evaluate Eq. (8.22) with the appropriate hopping amplitudes corresponding to the interface geometries.

8.2.1 Point contact geometry

We now want to calculate the current for an F/S tunnel junction with ballistic leads in a point contact geometry. The current through the HM/S junction can be obtained from the F/S junction as a special case for a zero minority carrier concentration.

Using the tunnel amplitude for a point contact geometry introduced in Eq. (7.1) and using $K_0^{\mathrm{S}\sigma}(0,0) = \nu_{\mathrm{S}}$ and $K_0^{\mathrm{F}\sigma}(0,0) = \nu_\sigma$, valid for ballistic leads, the tunnel conductance for a point contact defined in Eq. (8.7) reads

$$G_{\mathrm{T}}^{\mathrm{BPC}} = 2G_0 \sum_\sigma \alpha_\sigma \tag{8.25}$$

As in Chapter 7, we assumed a constant (normal state) density of states. Recall the definition $\alpha_\sigma = \pi^2 \nu_{\mathrm{S}} \nu_\sigma t^2$. The tunnel conductance agrees with the lowest order expression for the conductance from the NEGF formalism, obtained expanding Eqs. (7.65) and (7.64) in lowest order in t.

Let us now calculate the Andreev current. First, we evaluate Eq. (8.22) for the point contact hopping element in Eq. (7.1):

$$\Xi_{\mathrm{BPC}}^{\sigma\sigma'}(\zeta, \zeta', \xi, \xi') = \pi^{-4} \alpha_\sigma \alpha_{\sigma'} \tag{8.26}$$

$\Xi_{\mathrm{BPC}}^{\sigma\sigma'}$ does not depend on the energy variables and can thus be taken out of the integrals in Eqs. (8.21) and (8.24). The integration over the ferromagnet variables ξ and ξ' is then trivial (Dirac-δ distributions). Further, the two integrals over the superconductor variables ζ and ζ' separate. The remaining integrals can be solved using the following relation that follows from Eq. (G.5) (for $a < 1$, see Appendix G):

$$\int d\zeta u(\zeta)v(\zeta)\left((E(\zeta)-a\Delta)^{-1}+(E(\zeta)+a\Delta)^{-1}\right)=\frac{\pi}{\sqrt{1-a^2}} \tag{8.27}$$

Finally, the ballistic current in a point contact geometry reads

$$\begin{aligned} I_{\mathrm{FS}}^{\mathrm{BPC}} = 4\frac{e\Delta}{h}\int_{-\infty}^{\infty} d\epsilon \Theta(-|\epsilon_\uparrow|+1)\Theta(-|\epsilon_\downarrow|+1) \\ \cdot\Bigg\{ \alpha_\uparrow^2 \frac{\sin^2\theta}{4}\left|\frac{1}{\sqrt{1-\epsilon_\uparrow^2}}-\frac{1}{\sqrt{1-\epsilon_\downarrow^2}}\right|^2 [f_\downarrow^{\mathrm{F}}(\epsilon+U)-f_\uparrow^{\mathrm{F}}(\epsilon-U)] \\ +\alpha_\uparrow\alpha_\downarrow\left|\frac{\cos^2\frac{\theta}{2}}{\sqrt{1-\epsilon_\uparrow^2}}+\frac{\sin^2\frac{\theta}{2}}{\sqrt{1-\epsilon_\downarrow^2}}\right|^2 [f_\uparrow^{\mathrm{F}}(\epsilon+U)-f_\uparrow^{\mathrm{F}}(\epsilon-U)] \\ +\alpha_\uparrow\alpha_\downarrow\left|\frac{\sin^2\frac{\theta}{2}}{\sqrt{1-\epsilon_\uparrow^2}}+\frac{\cos^2\frac{\theta}{2}}{\sqrt{1-\epsilon_\downarrow^2}}\right|^2 [f_\downarrow^{\mathrm{F}}(\epsilon+U)-f_\downarrow^{\mathrm{F}}(\epsilon-U)] \\ +\alpha_\downarrow^2\left|\frac{1}{\sqrt{1-\epsilon_\uparrow^2}}-\frac{1}{\sqrt{1-\epsilon_\downarrow^2}}\right|^2 [f_\uparrow^{\mathrm{F}}(\epsilon+U)-f_\downarrow^{\mathrm{F}}(\epsilon-U)]\Bigg\}, \end{aligned} \tag{8.28}$$

where we defined the dimensionless quantities $U=\frac{eV}{\Delta}$, $\epsilon_\sigma=\frac{E+\sigma\frac{\hbar\Omega}{2}}{\Delta}$ and $\omega=\frac{\hbar\Omega}{\Delta}$. We used that the distribution function given in Eq. (8.12) fulfills $f_\uparrow^{\mathrm{F}}(-E)=f_\downarrow^{\mathrm{F}}(E)$. For further evaluation we assume zero temperature. Additionally, we consider the small voltages and small frequencies scaling for $eV, \hbar\Omega \ll \Delta$. We can thus evaluate the distribution functions using Eq. (7.94). Additionally we develop the integrand and keep only the lowest order terms in Ω and ϵ. We obtain after integration and after some algebra keeping only the lowest order terms

$$\begin{aligned} I_{\mathrm{FS}}^{\mathrm{BPC}} =& \frac{e\Delta}{h}\frac{8}{3}\left(\frac{\omega}{2}\right)^2\sin^2\theta\left[(\alpha_\uparrow^2+\alpha_\downarrow^2)U\left(U^2+3\left(\frac{\omega}{2}\right)^2\right)\right. \\ &\left.+(\alpha_\uparrow^2-\alpha_\downarrow^2)\frac{\omega}{2}\left(\left(\frac{\omega}{2}\right)^2+3U^2\right)\cos\theta\right]+\frac{e\Delta}{h}2^4\alpha_\uparrow\alpha_\downarrow U. \end{aligned} \tag{8.29}$$

First of all, note that for a half-metal with zero minority carrier concentration ($\alpha_\downarrow = 0$), the expression coincides with the previously obtained (more general, since for any transparency) expression given in Eq. (7.96).

Let us discuss the current in the absence of a bias voltage, i.e., $U = 0$. The zero bias current is proportional to the difference of the squares of the reduced hopping elements and therefore proportional to the difference of the squares of the spin-dependent density of states. Expressing the reduced hopping elements α_σ via the transmission using the tunnel junction relation $T_\sigma \approx 4\alpha_\sigma$, the current is proportional to the difference of the squares of the transmissions, i.e., $I \propto (T_\uparrow^2 - T_\downarrow^2)$. The two spin species give thus independent contributions with opposite signs to the current. For equal transmissions (as in a normal metal) the current vanishes. As for the HM/S junction, the current scales with the fifth power of the driving frequency. Further, the angular dependence is not changed including a finite minority carrier concentration.

Let us now focus on $U \neq 0$. The term in the second line of Eq. (8.29) containing the product of the reduced hopping elements $\alpha_\uparrow \alpha_\downarrow$ is absent in the half-metal case. This term is due to Andreev processes that involve electrons with opposite spins. A voltage is needed for this contribution. Further, it is independent of the magnetization dynamics. Indeed, expanding our result for the current through an F/S junction with a static magnetization from Sec. 7.4.4, i.e., Eqs. (7.76) and (7.77), in lowest order in the tunnel amplitude t at zero temperature and using $U \ll 1$, we reproduce this term.

Let us consider a finite bias voltage ($U \neq 0$) and a non-zero $\alpha_\downarrow$. In this case Eq. (8.29) simplifies to

$$I_{\mathrm{FS}}^{\mathrm{BPC}} = \frac{e\Delta}{h}\left[\frac{8}{3}\sin^2\theta\cos\theta\left(\frac{\omega}{2}\right)^5(\alpha_\uparrow^2 - \alpha_\downarrow^2) + 2^4\alpha_\uparrow\alpha_\downarrow U\right]. \tag{8.30}$$

The first term is only relevant if $U \sim \omega^5$, i.e., at very low voltages $U \ll \omega \ll 1$. At voltages that are comparable to the frequency, the effect of the precessing magnetization is negligible and we get a linear relation between current and voltage with a conductance given by

$$G = G_0 \frac{T_\uparrow T_\downarrow}{2}. \tag{8.31}$$

These results predict which parameter regime is most suitable for an experimental detection. In order to detect the peculiar Andreev reflection properties, a zero voltage measurement is preferrable. First, as we have seen in Sec. 7.4.3, no normal state effect

exists. Second, the term involving Andreev reflections from electrons with opposite spins is also absent. Even though any difference in the transparency for minority and majority carriers gives rise to a non-zero current, a ferromagnet with strong spin polarization is advantageous in order to maximize the effect. Ideally, a half-metal at zero voltage bias is chosen.

In order to check in how far the result depends on the chosen relaxation machanism, let us now use the other distribution function given in Eq. (6.19) and corresponding to the relaxation model with phonons and spin-orbit coupling (see also Sec. 6.3). We evaluate the current expression in Eq. (8.28) with this distribution function in the same limits as before, i.e., at zero temperature and for small voltages and small frequencies ($\omega, U \ll 1$). Performing the previously explained steps, the current yields after a lengthy calculation

$$\tilde{I}_{\mathrm{FS}}^{\mathrm{BPC}} = \frac{e\Delta}{h}\frac{8}{3}\left(\frac{\omega}{2}\right)^2 \sin^2\theta \left[(\alpha_\uparrow^2+\alpha_\downarrow^2)U\left(U^2+3\left(\frac{\omega}{2}\right)^2 \cos^2\theta\right)\right.$$
$$\left.+(\alpha_\uparrow^2-\alpha_\downarrow^2)\frac{\omega}{2}\left(\left(\frac{\omega}{2}\right)^2 \cos^2\theta+3U^2\right)\cos\theta\right] + \frac{e\Delta}{h}2^4\alpha_\uparrow\alpha_\downarrow U. \tag{8.32}$$

Here, we kept only the lowest order in ω, U contributions to the current. The difference with respect to the previous result given in Eq. (8.29) is indicated in red. The additional $\cos^2\theta$ factor becomes important for large angles. However, in general, the precession angle θ is small, since $\hbar\Omega \ll J$. For small angles, both models give identical expressions.

8.2.2 Extended interface

After having established the results for a point contact geometry, we can now consider a more realistic geometry, i.e., an extended interface, as shown schematically in Fig. 6.1. This geometry is easier to realize in a possible experiment. Further, it allows us to study disorder effects in the leads. However, before considering disorder, let us understand the basic properties, when the leads are ballistic and make the connection to the previously established point contact results.

We assume three dimensional leads. Let the tunnel barrier, separating the leads, be located at $z = 0$. The corresponding tunnel amplitude is given by [266]

$$t(\boldsymbol{r_1}, \boldsymbol{r_2}) = \delta'(z_1)\delta'(z_2)\delta(\boldsymbol{\rho_1} - \boldsymbol{\rho_2})t(\boldsymbol{\rho_1}), \tag{8.33}$$

where $'$ denotes the derivative with respect to the argument. Further, we introduced polar coordinates $\boldsymbol{r} = (\boldsymbol{\rho}, z)$, where $\boldsymbol{\rho}$ lies in the plane of the junction.

In order to compute the current, we evaluate Eq. (8.22) using the tunnel amplitude in Eq. (8.33). We are left with the evaluation of the non-local density of states, defined in Eq. (8.6). Without disorder the non-local density of states reads

$$K_\xi^X(\boldsymbol{r_1}, \boldsymbol{r_2}) = \nu_X g_0(\boldsymbol{r_1} - \boldsymbol{r_2}), \tag{8.34}$$

where $X \in \{\mathrm{S}, \mathrm{F}\}$ and we defined

$$g_0(\boldsymbol{r}) = \frac{\sin k_\mathrm{F} r}{k_\mathrm{F} r}. \tag{8.35}$$

This expression can be obtained from Eq. (H.13) (expression in the presence of disorder given in Appendix H) in the limit of $r \ll l_\mathrm{e}$, where $r = |\boldsymbol{r}|$ and l_e denotes the mean free path. Using the expression for the density of states (Eq. (8.34)) and the tunnel amplitude (Eq. (8.33)), Eq. (8.22) yields after partial integration over the z-coordinates and evaluation of the Dirac-δ distribution functions

$$\begin{aligned}\Xi_{\mathrm{Bext}}^{\sigma\sigma'}(\zeta, \zeta', \xi, \xi') = \Xi_{\mathrm{Bext}}^{\sigma\sigma'} = \nu_\mathrm{S}^2 \nu_\sigma \nu_{\sigma'} \int d\boldsymbol{\rho_1} \int d\boldsymbol{\rho_2} \int d\boldsymbol{\rho_3} \int d\boldsymbol{\rho_4}\, t(\boldsymbol{\rho_1}) t(\boldsymbol{\rho_2}) t(\boldsymbol{\rho_3}) t(\boldsymbol{\rho_4}) \\ \tilde{g}_0(\boldsymbol{\rho_1} - \boldsymbol{\rho_2}) \tilde{g}_0(\boldsymbol{\rho_4} - \boldsymbol{\rho_3}) \tilde{g}_0(\boldsymbol{\rho_2} - \boldsymbol{\rho_4}) \tilde{g}_0(\boldsymbol{\rho_1} - \boldsymbol{\rho_3}).\end{aligned} \tag{8.36}$$

We defined $\tilde{g}_0(\boldsymbol{r}) = \frac{g_0'(r)}{|\boldsymbol{r}|}$. We change the integration coordinates to a center of mass system with center of mass coordinate $\boldsymbol{R}$ and difference coordinates defined as $\boldsymbol{r_1} = \boldsymbol{\rho_1} - \boldsymbol{\rho_2}$, $\boldsymbol{r_2} = \boldsymbol{\rho_3} - \boldsymbol{\rho_4}$, and $\boldsymbol{r_3} = \boldsymbol{\rho_2} - \boldsymbol{\rho_3}$. Further, we assume that t depends only on the center of mass coordinate and obtain

$$\Xi_{\mathrm{Bext}}^{\sigma\sigma'} = \nu_\mathrm{S}^2 \nu_\sigma \nu_{\sigma'} X \int d\boldsymbol{R}\, t^4(\boldsymbol{R}), \tag{8.37}$$

where we defined

$$X = \int d\boldsymbol{r_1} \int d\boldsymbol{r_2} \int d\boldsymbol{r_3}\, \tilde{g}_0(\boldsymbol{r_1})\tilde{g}_0(-\boldsymbol{r_2})\tilde{g}_0(\boldsymbol{r_2}+\boldsymbol{r_3})\tilde{g}_0(\boldsymbol{r_1}+\boldsymbol{r_3}) = \frac{(2\pi)^3}{6}k_{\mathrm{F}}^2 \tag{8.38}$$

We present the steps for the solution of the integrals in Appendix I. Here, we introduced dimensionless variables $\boldsymbol{x_i} = k_{\mathrm{F}}\boldsymbol{r_i}$. If we assume a homogeneous interface, where t is space independent, we obtain

$$\Xi_{\mathrm{Bext}}^{\sigma\sigma'} = \nu_{\mathrm{S}}^2 \nu_\sigma \nu_{\sigma'} t^4 \frac{(2\pi)^3}{6} k_{\mathrm{F}}^2 S, \tag{8.39}$$

where S denotes the area of the interface between the superconductor and the ferromagnet. This expression can be expressed in terms of the point contact result given in Eq. (8.26), yielding

$$\Xi_{\mathrm{Bext}}^{\sigma\sigma'} = (2\pi)^3 \frac{k_{\mathrm{F}}^2}{6} S \Xi_{\mathrm{BPC}}^{\sigma\sigma'}. \tag{8.40}$$

Note that the number of open transport channels, as obtained from the Sharvin conductance [267], is given by

$$N_{\mathrm{ch}} = \frac{S k_{\mathrm{F}}^2}{4\pi} \tag{8.41}$$

The point contact has one conduction channel, whereas for the extended interface each transverse mode is a conduction channel. We can think of the extended interface as being a lot of point contacts in parallel. The transfer of electrons across the junction is local. Thus, the main modification of the extended interface with respect to the point contact is the larger number of transport channels. Using that above expression in Eq. (8.40) is energy independent, we obtain

$$I_{\mathrm{FS}}^{\mathrm{Bext}} = \frac{(2\pi)^4}{3} N_{\mathrm{ch}} I_{\mathrm{FS}}^{\mathrm{BPC}}. \tag{8.42}$$

The current through the extended ballistic interface $I_{\mathrm{FS}}^{\mathrm{Bext}}$ is thus proportional to the current through the ballistic point contact $I_{\mathrm{FS}}^{\mathrm{BPC}}$. The proportionality factor is a number times the large number of open transport channels, giving $I_{\mathrm{FS}}^{\mathrm{Bext}} \gg I_{\mathrm{FS}}^{\mathrm{BPC}}$. The entire discussion of the physics of the ballistic tunnel junction in the point contact geometry is thus also valid for the extended interface.

8.3 Disorder formalism

So far, we considered ballistic leads. Let us now consider a junction containing disorder. We focus on a low concentration of non-magnetic impurities in the leads. These impurities induce spin conserving backscattering and may thus change the current through the junction. Disordered junctions are experimentally relevant, since no sample is a perfect crystal and thus any junction contains impurities.

It has been shown for an N/S junction in Ref. [117] that disorder has a strong influence on the subgap current. The authors have shown that interference effects in the presence of disorder lead to a current that largely exceeds the current for clean junctions. We will show that this is also true for the subgap current through our F/S junction, subjected to ferromagnetic resonance.

In the following we show that a point contact geometry is not sensitive to disorder in the leads. We demonstrate that, in contrary, disorder affects the current flowing through the extended interface. We want to evaluate the disorder averaged current, i.e., the disorder average of Eq. (8.16). Therefore we need to compute the disorder average of Eq. (8.22), for which we need to know the disorder average of products of the non-local density of states, defined in Eq. (8.6).

8.3.1 General disorder formalism

A presentation of the disorder formalism can be found in [268]. Here, we present the main underlying assumptions and the main concepts. For the presentation of the general formalism we mainly follow Ref. [268].

We consider a Gaussian disorder model, where the disorder is described by a random potential $V(\boldsymbol{r})$ that has zero average $\langle V(\boldsymbol{r})\rangle = 0$, but a non-zero second cumulant

$$\langle V(\boldsymbol{r})V(\boldsymbol{r'})\rangle = B(\boldsymbol{r}-\boldsymbol{r'}). \tag{8.43}$$

All further cumulants shall be zero. The disorder potential scatters electrons. In the following we assume weak disorder, where the momentum vector k and the mean free path l_e fulfill $kl_\mathrm{e} \gg 1$.

We treat the disorder potential perturbatively. We express the non-local density of states in terms of advanced and retarded Green's functions, for which we can write down a perturbation expansion in form of a Dyson series. The Dyson series can be represented as an infinite sum over different diagrams. It is convenient to separate the contribution from connected diagrams from the contribution from disconnected diagrams.

Denoting the disorder average by $\langle \cdots \rangle$, we can write the disorder average over the product of two non-local density of states as a sum of two terms:

$$\left\langle K_\epsilon(\boldsymbol{r_1}, \boldsymbol{r_1'}) K_{\epsilon-\omega}(\boldsymbol{r_2'}, \boldsymbol{r_2}) \right\rangle = \left\langle K_\epsilon(\boldsymbol{r_1}, \boldsymbol{r_1'}) K_{\epsilon-\omega}(\boldsymbol{r_2'}, \boldsymbol{r_2}) \right\rangle^{\mathrm{c}} + \left\langle K_\epsilon(\boldsymbol{r_1}, \boldsymbol{r_1'}) \right\rangle \left\langle K_{\epsilon-\omega}(\boldsymbol{r_2'}, \boldsymbol{r_2}) \right\rangle, \tag{8.44}$$

where the superscript c stands for connected diagrams. The disorder average over a single non-local density of states is relatively easy to obtain. The explicit calculation (see Ref. [268]) can be found in Appendix H. Here, we review the steps that need to be done: The total Green's function can be obtained from a perturbation expansion in the potential V and the unperturbed Green's function. The self-energy is taken until first order and its imaginary part is expressed using the elastic mean collision time τ_e. In the weak disorder limit, we obtain (see Eq. (H.13))

$$\langle K_\epsilon(\boldsymbol{r_1}, \boldsymbol{r_2}) \rangle = \nu_0 g(\boldsymbol{r_1} - \boldsymbol{r_2}), \tag{8.45}$$

where ν_0 denotes the local density of states, assumed to be constant. Further, we defined

$$g(\boldsymbol{R}) = \frac{\sin kR}{kR} e^{-\frac{R}{2l_\mathrm{e}}}. \tag{8.46}$$

In order to evaluate the contribution from connected diagrams in Eq. (8.44), we make the "Diffuson" (or ladder) approximation (not to be confused with the diffusion approximation). We assume that for weak disorder the typical length between two scattering centers, i.e., the mean free path l_e, is much bigger than the length scale of the Gaussian disorder potential. Then, the main contribution to the average is due to trajectories that have the same scattering centers. For weak disorder, the scattering events are independent. This has a second consequence: If the order of the scattering centers for two trajectories is different, the paths taken differ at least by l_e, which is much larger than the wave length λ. Consequently, the dephasing between two such processes is large and we can neglect such a contribution. We are thus left with two different coherent processes that give the main contribution: A diagram called

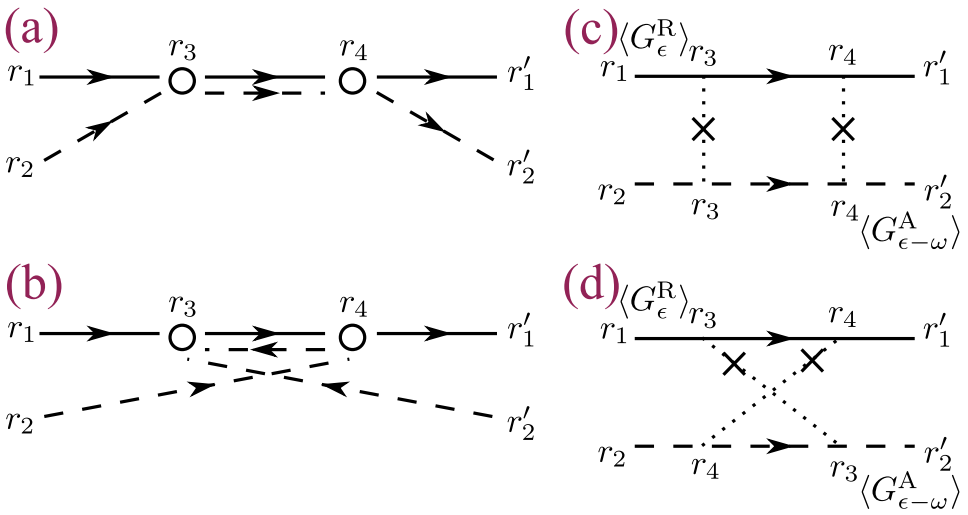

Fig. 8.1: (a), (b): Real space representation of two different coherent processes. The arrows indicate the paths taken by two electrons, the circles represent diffusion centers. For a Diffuson (a) (Cooperon (b)) the path between the diffusion centers is covered in the same (opposite) order. (c), (d): Diagrammatic representation of the relevant Green's functions. The retarded (advanced) Green's function is drawn as a solid (dashed) line. The interaction due to the disorder potential is indicated by a dotted line with an X. The diagrams are shown for two scattering centers involved. In general, there are many scattering centers involved.

"Diffuson" describes a coherent process between two trajectories having all scattering centers in common and covering them in the same order. A diagram called "Cooperon" describes a coherent process between two trajectories having all scattering centers in common and covering them in opposite order. The processes are schematically depicted in Figs. 8.1(a), (b).

We now calculate the contributions of the Cooperon and Diffuson diagrams to the connected average in Eq. (8.44). We express the non-local density of states in terms of Green's functions:

$$K_{\epsilon}(\boldsymbol{r},\boldsymbol{r}') = \frac{i}{2\pi}\left(G^{\mathrm{R}}(\boldsymbol{r},\boldsymbol{r}',\epsilon) - G^{\mathrm{A}}(\boldsymbol{r},\boldsymbol{r}',\epsilon)\right), \tag{8.47}$$

where G^{R} (G^{A}) denotes the retarded (advanced) Green's function. In the weak disorder limit, we approximate the average of the product of the retarded Green's functions by the product of the averages of the retarded Green's functions, i.e., $\left\langle G_1^{\mathrm{R}} G_2^{\mathrm{R}}\right\rangle = \left\langle G_1^{\mathrm{R}}\right\rangle\left\langle G_2^{\mathrm{R}}\right\rangle$, giving

$$\left\langle K_{\epsilon}(\boldsymbol{r_1},\boldsymbol{r_1'}) K_{\epsilon-\omega}(\boldsymbol{r_2'},\boldsymbol{r_2})\right\rangle^{\mathrm{c}} \approx \frac{1}{2\pi^2}\Re\left\langle G^{\mathrm{R}}_{\epsilon}(\boldsymbol{r_1},\boldsymbol{r_1'}) G^{\mathrm{A}}_{\epsilon-\omega}(\boldsymbol{r_2},\boldsymbol{r_2'})\right\rangle^{\mathrm{c}}. \tag{8.48}$$

The Cooperon and Diffuson diagrams for the Green's functions, that give the main contribution to the average are depicted in Fig. 8.1(c), (d). Following Ref. [268], we introduce the structure factor $\Gamma_\omega(\boldsymbol{r_3}, \boldsymbol{r_4})$ that accounts for all scattering processes between coordinates $\boldsymbol{r_3}$ and $\boldsymbol{r_4}$ in Fig. 8.1(c). The contribution for the Diffuson can then be written as

$$\int d\boldsymbol{r_3} \int d\boldsymbol{r_4}\, \Gamma_\omega(\boldsymbol{r_3}, \boldsymbol{r_4}) \left\langle G^{\mathrm{R}}_\epsilon(\boldsymbol{r_1}, \boldsymbol{r_3}) \right\rangle \left\langle G^{\mathrm{R}}_\epsilon(\boldsymbol{r_4}, \boldsymbol{r_1'}) \right\rangle \left\langle G^{\mathrm{A}}_{\epsilon-\omega}(\boldsymbol{r_3}, \boldsymbol{r_2}) \right\rangle \left\langle G^{\mathrm{A}}_{\epsilon-\omega}(\boldsymbol{r_2'}, \boldsymbol{r_4}) \right\rangle . \tag{8.49}$$

Before evaluating this expression, let us comment on the structure factor. It can be written as a recursive integral equation, where the structure factor is decomposed into a sum of two parts: One scattering event is taken out of the structure factor and the remaining structure factor is computed, taking into account the free propagation between the scattering event taken out of the structure factor and the remaining structure factor. Further, it is proportional to the diffusion probability and one can show that the structure factor (and therefore the diffusion probability P_{d}) fulfill a diffusion equation given by

$$(-i\omega - D\Delta_{\boldsymbol{r_2}}) P_{\mathrm{d}}(\boldsymbol{r_1}, \boldsymbol{r_2}, \omega) = \delta(\boldsymbol{r_1} - \boldsymbol{r_2}), \tag{8.50}$$

where the diffusion constant reads $D = \frac{v_{\mathrm{F}}^2 \tau_{\mathrm{e}}}{d}$ with d being the dimension. $\Delta_{\boldsymbol{r_2}}$ denotes the Laplace operator with respect to the coordinate $\boldsymbol{r_2}$. We will thus express our results in terms of the diffusion probability that we obtain for a given model solving above diffusion equation. For our model, we solve this diffusion equation in Sec. 8.3.2.

We now turn back to the evaluation of the Diffuson contribution in Eq. (8.49). We make the so called "diffusion approxmation" (not to be confused with the already made Diffuson approximation). The approximation consists of neglecting the spacial variations of the structure factor with respect to the spacial variations of the Green's functions. We can thus take Γ out of the integrals and the integral expression separates into a product of two independent integrals. These are of the form

$$\int d\boldsymbol{r_3} \left\langle G^{\mathrm{R}}_\epsilon(\boldsymbol{r_1}, \boldsymbol{r_3}) \right\rangle \left\langle G^{\mathrm{A}}_\epsilon(\boldsymbol{r_3}, \boldsymbol{r_2}) \right\rangle = 2\pi\nu_0\tau_{\mathrm{e}} g(\boldsymbol{r_1} - \boldsymbol{r_2}). \tag{8.51}$$

Here, we neglected the frequency dependence of the advanced Green's function. A similar calculation can be done for the Cooperon contribution, where we denote P_c the Cooperon diffusion probability. Finally, Eq. (8.44) yields

$$\begin{aligned}\left\langle K_\epsilon^\sigma(\boldsymbol{r_1},\boldsymbol{r_1'})K_{\epsilon-\omega}^{\sigma'}(\boldsymbol{r_2'},\boldsymbol{r_2})\right\rangle =&\nu_\sigma\nu_{\sigma'}g(\boldsymbol{r_1}-\boldsymbol{r_1'})g(\boldsymbol{r_2'}-\boldsymbol{r_2})\\ &+\frac{\nu_\sigma}{\pi}\delta_{\sigma\sigma'}\Re\left[P_\mathrm{d}(\boldsymbol{r_1},\boldsymbol{r_1'},\omega)g(\boldsymbol{r_1}-\boldsymbol{r_2})g(\boldsymbol{r_1'}-\boldsymbol{r_2'})\right.\\ &\left.+P_\mathrm{c}(\boldsymbol{r_1},\boldsymbol{r_1'},\omega)g(\boldsymbol{r_1}-\boldsymbol{r_2'})g(\boldsymbol{r_1'}-\boldsymbol{r_2})\right],\end{aligned} \tag{8.52}$$

where the first line is due to the non-connected terms. The second (third) line is the contribution from a Diffuson (Cooperon). We neglected diffusion terms that are due to electrons of opposite spins, since their energy difference is big in the ferromagnet, due to the large effective exchange splitting.

Contrary to a magnetic field, the exchange field does not couple to the momentum of the electrons. Therefore, if we assume the driving ac field to be small, the Cooperon and Diffuson will be described by the same diffusion equation.

8.3.2 Solution of the diffusion equation

For a further evaluation of the current, we need the diffusion probabilities that are solutions of the diffusion equation given in Eq. (8.50) and that enter the expression for the average of the non-local density of states in Eq. (8.52).

We assume 3D leads that occupy the half-space bounded by the interface. Let us first of all present how the boundary condition can be enforced. There are two different types of boundary conditions. First, the Neumann boundary condition ensures zero probability current across the boundary. Consequently, as discussed for example in Ref. [268], particles may not leave the diffusion region. This corresponds to an isolated system. Second, Dirichlet boundary conditions ensure zero probability at the boundary. This corresponds to the system being coupled to reservoirs, from which an injected particle never returns. We want to consider Neumann boundary conditions for the diffusion, since electrons should not leave their half-space by means of diffusion. The only process that should allow for a transfer across the interface is the tunneling, described by the tunnel Hamiltonian. We can enforce the boundary condition with the

so-called “image method”. It consists in combining the diffusion probability with its mirror image, such that the probability current vanishes:

$$P_{\mathrm{N}}(\boldsymbol{\rho}, z \geq 0, \boldsymbol{\rho'}, z' \geq 0, t) = P(\boldsymbol{\rho}, z, \boldsymbol{\rho'}, z', t) + P(\boldsymbol{\rho}, -z, \boldsymbol{\rho'}, -z', t), \tag{8.53}$$

where P_{N} denotes the probability with Neumann boundary conditions and P the probability obtained in a free 3D space. We used the previously defined polar coordinates $\boldsymbol{r} = (\boldsymbol{\rho}, z)$.

After a Fourier transform in both the frequency and the real space coordinates, the diffusion equation in Eq. (8.50) reads (for an isotropic space)

$$(\partial_t + Dk^2)P(\boldsymbol{k}, t) = \delta(t) \tag{8.54}$$

and has the solution $P(\boldsymbol{k}, t) = \Theta(t)e^{-Dk^2t}$. After a Fourier transform back from reciprocal space to real space, we have

$$P(\boldsymbol{R}, t) = \Theta(t)(4\pi Dt)^{-\frac{d}{2}}e^{-\frac{R^2}{4Dt}}, \tag{8.55}$$

where this result is valid for any integer dimension d. In $d = 3$, a Fourier transform back to energy space yields

$$P(\boldsymbol{R}, \omega) = \frac{1}{4\pi DR}e^{-(1-i)R\sqrt{\frac{\omega}{2D}}}. \tag{8.56}$$

We give the explicit calculation for the last Fourier transform, using complex integration methods, in Appendix J. Due to the interface geometry, we need the diffusion probability for two in plane coordinates, given by

$$P_{\xi-\xi'}(\boldsymbol{\rho_1}, \boldsymbol{\rho_2}) = \frac{1}{2\pi\hbar D\left|\boldsymbol{\rho_1} - \boldsymbol{\rho_2}\right|}e^{-(1-i)|\boldsymbol{\rho_1}-\boldsymbol{\rho_2}|\sqrt{\frac{\xi-\xi'}{2\hbar D}}}. \tag{8.57}$$

8.3.3 Point contact geometry

We want to show that disorder does not significantly change the results in the point contact geometry. The disorder averaged current depends on the disorder average of

the quantity Ξ, defined in Eq. (8.22). Using the hopping amplitude defined in Eq. (7.1), we obtain for a point contact

$$\left\langle \Xi_{DPC}^{\sigma\sigma'} \right\rangle = t^4 \left\langle K_{\zeta}^{\mathrm{S}}(0,0) K_{\zeta'}^{\mathrm{S}}(0,0) \right\rangle \left\langle K_{\xi}^{\mathrm{F}\sigma}(0,0) K_{\xi'}^{\mathrm{F}\sigma'}(0,0) \right\rangle . \tag{8.58}$$

Let us further evaluate the disorder averages. Using Eq. (8.52), we obtain

$$\left\langle K_{\epsilon}^{\sigma}(0,0) K_{\epsilon-\omega}^{\sigma'}(0,0) \right\rangle = \nu_\sigma \nu_{\sigma'} + \frac{\nu_\sigma}{\pi} \delta_{\sigma\sigma'} \Re \left[P_{\omega}^{\mathrm{d}}(0,0) + P_{\omega}^{\mathrm{c}}(0,0) \right] . \tag{8.59}$$

We will now show that the second term is negligible with respect to the first term and we thus recover the result for the ballistic junction. Using Eq. (8.55) the probability for a Diffuson reads

$$P_{\omega}^{\mathrm{d}}(0,0) = \int \frac{dt}{\sqrt{2\pi}} (4\pi D t)^{-\frac{3}{2}}. \tag{8.60}$$

Hence,

$$\Re P_{\omega}^{\mathrm{d}}(0,0) \sim \sqrt{\frac{|\omega|}{\hbar^2 D^3}}, \tag{8.61}$$

where the diffusion constant is given by $D = \frac{v_{\mathrm{F}}^2 \tau_{\mathrm{e}}}{3}$ and the frequency is the frequency of the magnetization precession, i.e., $\omega = \Omega$. We use the expression for the density of states in three dimensions $\nu = \frac{k_{\mathrm{F}}^3}{(2\pi)^2 E_{\mathrm{F}}}$, where k_{F} is the Fermi wave vector and E_{F} is the Fermi energy and obtain

$$\frac{P_{\omega}^{\mathrm{d}}(0,0)}{\nu} \sim \sqrt{\frac{\hbar\Omega}{E_{\mathrm{F}}} \left(\frac{\hbar \tau_{\mathrm{e}}^{-1}}{E_{\mathrm{F}}} \right)^3}. \tag{8.62}$$

We consider the diffusive regime of weak disorder, where $\hbar\tau_{\mathrm{e}}^{-1} \ll E_{\mathrm{F}}$ and we maintain the assumption of a small rotation frequency $\hbar\Omega \ll E_{\mathrm{F}}$, giving $P_{\omega}^{\mathrm{d}}(0,0) \ll \nu$. Thus, the second term in Eq. (8.59) is negligible with respect to the first one, giving

$$\left\langle \Xi_{\mathrm{DPC}}^{\sigma\sigma'} \right\rangle \approx \nu_\sigma \nu_{\sigma'} t^4. \tag{8.63}$$

Comparing this expression to Eq. (8.26), we see that it is equivalent to the ballistic expression. Thus, disorder is not relevant in a point contact geometry. As we will see in the following subsection, long-range diffusion processes give rise to modifications of the current. However, these processes are absent in a point contact geometry, since all trajectories are confined to one point.

8.3.4 Extended interface

In Sec. 8.3.4.1 we show that the tunnel conductance through the extended disordered interface is up to numerical factors given by the point contact tunnel conductance times the number of open transport channels. In Sec. 8.3.4.2 and Sec. 8.3.4.3 we show that the subgap current through the HM/S and the F/S interface is strongly enhanced in the presence of disorder compared to the clean extended interface.

8.3.4.1 Tunnel conductance

Let us determine the tunnel conductance given in Eq. (8.7) for the disordered extended interface geometry.

We evaluate the expression for the tunnel conductance in Eq. (8.7) using the tunnel amplitude for the extended interface given in Eq. (8.33). Splitting the integrations into an in-plane and a perpendicular part, partial integration over the perpendicular coordinate and evaluation of the Dirac-δ distributions yields

$$\left\langle G_{\mathrm{T}}^{\mathrm{Dext}} \right\rangle = 4\pi^2 G_0 \nu_\uparrow \nu_{\mathrm{S}} \int d\boldsymbol{\rho_1} \int d\boldsymbol{\rho_2} t(\boldsymbol{\rho_1}) t(\boldsymbol{\rho_2}) \tilde{g}(\boldsymbol{r_1} - \boldsymbol{r_2}) \tilde{g}(\boldsymbol{r_2} - \boldsymbol{r_1}), \tag{8.64}$$

where

$$\tilde{g}(\boldsymbol{r}) = \frac{g'(\boldsymbol{r})}{|\boldsymbol{r}|}. \tag{8.65}$$

We transform to a center of mass coordinate $\boldsymbol{\rho}$ and the difference coordinate $\boldsymbol{\rho_{12}}$, giving

$$\left\langle G_{\mathrm{T}}^{\mathrm{Dext}} \right\rangle = \int d\boldsymbol{\rho} g_{\mathrm{T}}(\boldsymbol{\rho}), \tag{8.66}$$

where the conductance per unit surface area is defined as

$$g_{\mathrm{T}}(\boldsymbol{\rho}) = 4\pi^2 G_0 \nu_{\mathrm{S}} \nu_\uparrow t^2(\boldsymbol{\rho}) \int d\boldsymbol{\rho}_{12} \tilde{g}^2(\boldsymbol{\rho}_{12}). \tag{8.67}$$

Assuming a homogeneous interface, the integration over the center of mass coordinate yields the interface area S. Using the explicit expression of $g(\boldsymbol{r})$ in the presence of disorder, given in Eq. (8.46), we can write the remaining integral as

$$\int d\boldsymbol{r}\, \tilde{g}^2(\boldsymbol{r}) \approx 2\pi k_{\mathrm{F}}^2 \int_0^\infty dx \frac{(x\cos x - \sin x)^2}{x^5} + \mathcal{O}\left((k_{\mathrm{F}} l_{\mathrm{e}})^{-1}\right) = \frac{\pi}{2} k_{\mathrm{F}}^2 + \mathcal{O}\left((k_{\mathrm{F}} l_{\mathrm{e}})^{-1}\right). \tag{8.68}$$

We used the assumption of weak disorder $k_{\mathrm{F}} l_{\mathrm{e}} \gg 1$ and kept only the lowest order term in $(k_{\mathrm{F}} l_{\mathrm{e}})^{-1}$. Finally, the conductance yields

$$\left\langle G_{\mathrm{T}}^{\mathrm{Dext}} \right\rangle = 2\pi^3 G_0 \nu_{\mathrm{S}} \nu_{\uparrow} t^2 S k_{\mathrm{F}}^2 = G_{\mathrm{T}}^{\mathrm{BPC}} \frac{S k_{\mathrm{F}}^2 \pi}{2} = 2\pi^2 N_{\mathrm{ch}} G_{\mathrm{T}}^{\mathrm{BPC}}. \tag{8.69}$$

Hence, the conductance of the extended interface is proportional to the point contact conductance and the number of open conduction channels. The effect of disorder on the tunnel conductance is negligible (see Eq. (8.68)), since no long-range diffusion process is possible (see als Sec. 8.3.4.2).

8.3.4.2 Disordered extended half-metal/superconductor junction

Let us now evaluate the current in the presence of disorder through the HM/S junction in the extended interface geometry. We evaluate Eq. (8.22) using the tunnel amplitude in Eq. (8.33) and the disorder average over the non-local density of states in Eq. (8.52). After partial integration and evaluation of the Dirac-δ distributions we have for a homogeneous interface

$$\begin{aligned}
&\left\langle \Xi_{\mathrm{Dext}}^{\sigma\sigma'}(\zeta, \zeta', \xi, \xi') \right\rangle = t^4 \int d\boldsymbol{\rho_1} \int d\boldsymbol{\rho_2} \int d\boldsymbol{\rho_3} \int d\boldsymbol{\rho_4} \Big[\nu_{\mathrm{S}}^2 \tilde{g}(\boldsymbol{\rho_1} - \boldsymbol{\rho_2}) \tilde{g}(\boldsymbol{\rho_4} - \boldsymbol{\rho_3}) \\
&+ \frac{\nu_{\mathrm{S}}}{\pi} \Re P_{\zeta - \zeta'}^{d}(\boldsymbol{\rho_1}, \boldsymbol{\rho_2}) \tilde{g}(\boldsymbol{\rho_1} - \boldsymbol{\rho_3}) \tilde{g}(\boldsymbol{\rho_2} - \boldsymbol{\rho_4}) + \frac{\nu_{\mathrm{S}}}{\pi} \Re P_{\zeta - \zeta'}^{\mathrm{c}}(\boldsymbol{\rho_1}, \boldsymbol{\rho_2}) \tilde{g}(\boldsymbol{\rho_1} - \boldsymbol{\rho_4}) \tilde{g}(\boldsymbol{\rho_2} - \boldsymbol{\rho_3}) \Big] \\
&\cdot \Big[\nu_\sigma \nu_{\sigma'} \tilde{g}(\boldsymbol{\rho_2} - \boldsymbol{\rho_4}) \tilde{g}(\boldsymbol{\rho_1} - \boldsymbol{\rho_3}) + \frac{\nu_\sigma}{\pi} \delta_{\sigma\sigma'} \Re P_{\xi - \xi'}^{d}(\boldsymbol{\rho_2}, \boldsymbol{\rho_4}) \tilde{g}(\boldsymbol{\rho_2} - \boldsymbol{\rho_3}) \tilde{g}(\boldsymbol{\rho_4} - \boldsymbol{\rho_1}) \\
&+ \frac{\nu_\sigma}{\pi} \delta_{\sigma\sigma'} \Re P_{\xi - \xi'}^{\mathrm{c}}(\boldsymbol{\rho_2}, \boldsymbol{\rho_4}) \tilde{g}(\boldsymbol{\rho_2} - \boldsymbol{\rho_1}) \tilde{g}(\boldsymbol{\rho_4} - \boldsymbol{\rho_3}) \Big].
\end{aligned} \tag{8.70}$$

This expression is the sum of nine terms. In order to identify the leading terms, let us consider the decay lengths of the different expressions. The function $\tilde{g}$ decays on the length l_{e} as evident from Eq. (8.46). The diffusion probability in the ferromagnet decays on the scale $x \sim \sqrt{\frac{\hbar D}{|\xi - \xi'|}}$ as evident from Eq. (8.57). Using $l_{\mathrm{e}} = v_{\mathrm{F}} \tau_{\mathrm{e}}$, the ratio of the decay lengths for the ferromagnet reads

$$\frac{x}{l_{\mathrm{e}}} \sim \sqrt{\frac{\hbar \tau_{\mathrm{e}}^{-1}}{\hbar \Omega}} \gg 1, \tag{8.71}$$

where we used the hierarchy of energy scales $\hbar\Omega \ll \hbar\tau_e^{-1} \ll E_F$. The main contribution is thus given by terms, where the functions $\tilde{g}$ do not impose all four interface coordinates to be close to each other, but where in contrary a long-range diffusion is possible.

For the superconductor the analogous range is given by $x \sim \sqrt{\frac{\hbar D}{|\zeta-\zeta'|}}$. We will now argue why $\zeta - \zeta' > 2\Delta$. Consider the propagator of the diffusion equation Eq. (8.50) given by

$$P(k) \sim \frac{1}{\hbar D k^2 + i(\zeta - \zeta')} \sim \Xi(\zeta - \zeta'). \tag{8.72}$$

The integrals that have to be solved in order to obtain the current (see Eq. (8.21)) will be of the form

$$\int d\zeta \int d\zeta' \frac{\Delta}{\Delta^2 + \zeta^2} \frac{\Delta}{\Delta^2 + \zeta'^2} \frac{1}{\hbar D k^2 + i(\zeta - \zeta')} \geq \frac{1}{2\Delta}, \tag{8.73}$$

where the last identity can be proven using the residue theorem. Thus, $\zeta - \zeta' > 2\Delta$. In the ferromagnet we had $\xi - \xi' = \hbar\Omega$. For small frequencies $\hbar\Omega \ll \Delta$, the diffusion range is consequently much shorter in the superconductor than it is in the ferromagnet. Note that this is already well-known for an N/S junction [117]. For frequencies $\hbar\Omega \ll \Delta$, we can thus neglect the diffusion terms with diffusion in the superconductor with respect to the terms in the ferromagnet.

So far the expressions are valid both for the HM/S and F/S junction. Let us now consider the HM/S junction with perfect spin polarization ($\nu_\downarrow = 0$). Neglecting the diffusion terms in the superconductor and imposing long-range diffusion in the ferromagnet, the number of terms in Eq. (8.70) reduces to two, where one of the terms is the ballistic term. Here, we neglect the ballistic term. We will show for the resulting current that it is indeed much larger than the ballistic result and hence this approximation is valid. Eq. (8.70) reads

$$\begin{aligned}\left\langle \Xi^{\sigma\sigma'}_{\mathrm{Dext}}(\zeta,\zeta',\xi,\xi') \right\rangle \approx t^4 \int d\boldsymbol{\rho_1} \int d\boldsymbol{\rho_2} \int d\boldsymbol{\rho_3} \int d\boldsymbol{\rho_4} \frac{\nu_\uparrow \nu_S^2}{\pi} \Re P^c_{\xi-\xi'}(\boldsymbol{\rho_2},\boldsymbol{\rho_4}) \cdot \\ \cdot \tilde{g}^2(\boldsymbol{\rho_1}-\boldsymbol{\rho_2}) \tilde{g}^2(\boldsymbol{\rho_3}-\boldsymbol{\rho_4})\end{aligned} \tag{8.74}$$

The remaining process corresponds to a Cooperon in the ferromagnet and is depicted in Fig. 8.2(a). Introducing center of mass and difference coordinates, we obtain

$$\left\langle \Xi^{\uparrow\uparrow}_{\mathrm{Dext}}(\xi - \xi') \right\rangle = \pi^{-1} \nu_S^2 \nu_\uparrow t^4 \left[\int d\boldsymbol{r} \tilde{g}^2(\boldsymbol{r}) \right]^2 \int d\boldsymbol{R_1} \int d\boldsymbol{R_2} \Re P^c_{\xi-\xi'}(\boldsymbol{R_1},\boldsymbol{R_2}), \tag{8.75}$$

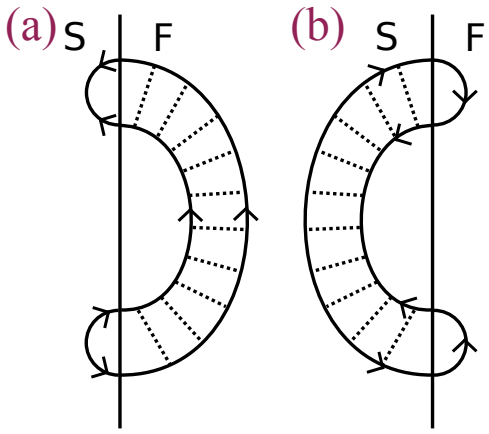

Fig. 8.2: Contributions to the subgap conductivity. (a) Cooperon in the ferromagnet. (b) Diffuson in the superconductor. Solid lines represent retarded Green's functions, dotted lines diffusion processes. Note that in the subgap regime the Green's functions in the superconductor are anomalous Green's functions.

where we neglected the dependence of $P^{\mathrm{c}}_{\xi-\xi'}$ on the difference coordinate. We assume a homogeneous interface, use the expression for the integral in Eq. (8.68) and the solution of the diffusion equation given by Eq. (8.57) to obtain after integration

$$\left\langle \Xi^{\uparrow\uparrow}_{\mathrm{Dext}}(\xi-\xi')\right\rangle = \Xi^{\uparrow\uparrow}_{\mathrm{BPC}}\sqrt{2}\frac{(2\pi)^3 S k_{\mathrm{F}}^2}{32}\frac{\xi^{\mathrm{F}}_{\mathrm{B}}}{\xi^{\mathrm{F}}_{D}} = \Xi^{\uparrow\uparrow}_{\mathrm{Bext}}\frac{3\sqrt{2}}{16}\frac{\xi^{\mathrm{F}}_{\mathrm{B}}}{\xi^{\mathrm{F}}_{D}}, \tag{8.76}$$

where $\Xi^{\uparrow\uparrow}_{\mathrm{BPC}}$ is given in Eq. (8.26), and $\Xi^{\uparrow\uparrow}_{\mathrm{Bext}}$ is given in Eq. (8.40). Further, we introduced the ballistic coherence length $\xi^{\mathrm{F}}_{\mathrm{B}} = \frac{v_{\mathrm{F}}}{\Omega}$ and the diffusive coherence length $\xi^{\mathrm{F}}_{\mathrm{D}} = \sqrt{\frac{D}{\Omega}}$ for the ferromagnet. We have thus expressed the quantity Ξ for the extended diffusive interface using the point contact result, the ballistic extended result, respectively. We use this expression to evaluate Eq. (8.21), where the remaining integral can be solved as described in Sec. 8.3.3. For the calculation of the current in Eq. (8.16) we consider the zero temperature expression at small frequencies and zero voltage. After evaluating the distribution functions as described in Sec. 8.3.3 and using the expression for the ballistic current in the same geometry in Eq. (8.42), we obtain after some algebra

$$\frac{I^{\mathrm{Dext}}}{I^{\mathrm{Bext}}} = \frac{9}{20\sqrt{2}}\frac{\xi^{\mathrm{F}}_{\mathrm{B}}}{\xi^{\mathrm{F}}_{\mathrm{D}}} \sim \sqrt{\frac{\hbar\tau_{\mathrm{e}}^{-1}}{\hbar\Omega}} \gg 1 \tag{8.77}$$

Thus, the current in the presence of disorder is much larger than the ballistic current through the same interface geometry. A similar effect has been reported for N/S interfaces [117].

So far, we have neglected any orbital effect due to the magnetization of the ferromagnet. Depending on the geometry, the orbital effect of the magnetization might be important and lead to sufficient dephasing between the trajectories, such that no coherent process is possible in the ferromagnet. In this case, the Diffuson in the superconductor is the dominant term contributing. We evaluate this contribution in Sec. 8.3.4.3 and will show that the corresponding current is also enhanced compared to the ballistic result.

8.3.4.3 Disordered extended ferromagnet/superconductor junction

Let us now consider the F/S junction. $\Xi^{\downarrow\downarrow}$ can be obtained from Eq. (8.76) replacing $\uparrow\rightarrow\downarrow$. We now describe how to evaluate $\left\langle \Xi^{\downarrow\uparrow}_{\mathrm{Dext}} \right\rangle$. First, note that there is no contribution due to diffusion in the ferromagnet, since the spins are opposite. We have assumed that the Zeeman splitting is sufficiently big, such that electrons with opposite spins to not diffuse coherently. Using, as previously, that the main contribution is given for long-range diffusion processes, we are left with two terms, i.e., the ballistic result and a contribution due to a Diffuson in the superconductor. The latter diagram is depicted in Fig. 8.2(b). The expression is analoguous to Eq. (8.75), where we have a dependence of the diffusion probability on $\zeta - \zeta'$ instead of $\xi - \xi'$. We have already established the relation $\zeta - \zeta' > 2\Delta$. We now approximate $\zeta - \zeta' \approx 2\Delta$ and obtain

$$\left\langle \Xi^{\downarrow\uparrow}_{\mathrm{Dext}} \right\rangle = \left\langle \Xi^{\downarrow\uparrow}_{\mathrm{BPC}} \right\rangle \frac{(2\pi)^3 k_{\mathrm{F}}^2 S}{32} \frac{\xi^{\mathrm{S}}_{\mathrm{B}}}{\xi^{\mathrm{S}}_{\mathrm{D}}} = \left\langle \Xi^{\downarrow\uparrow}_{\mathrm{Bext}} \right\rangle \frac{3}{16} \frac{\xi^{\mathrm{S}}_{\mathrm{B}}}{\xi^{\mathrm{S}}_{\mathrm{D}}}, \tag{8.78}$$

where the ballistic extended expression is defined in Eq. (8.40) and the point contact result is given in Eq. (8.26). This expression is analoguous to Eq. (8.76), with the difference that the coherence lengths are replaced by the corresponding coherence lengths in the superconductor. We defined the ballistic coherence length $\xi^{\mathrm{S}}_{\mathrm{B}} = \frac{\hbar v_{\mathrm{F}}}{\Delta}$ and the diffusive coherence length $\xi^{\mathrm{S}}_{\mathrm{D}} = \sqrt{\frac{\hbar D}{\Delta}}$ of the superconductor. Note that Eq. (8.78) is formally obtained from Eq. (8.76) replacing $\hbar\Omega \rightarrow 2\Delta$, which reflects the different energy scale of the Diffuson in the superconductor with respect to the ferromagnet. The ratio of the current contributions is given by the ratio of the Ξ, since they are energy independent, giving

$$\frac{I^{\downarrow\uparrow}_{\mathrm{Dext}}}{I^{\downarrow\uparrow}_{\mathrm{Bext}}} = \frac{\Xi^{\downarrow\uparrow}_{\mathrm{Dext}}}{\Xi^{\downarrow\uparrow}_{\mathrm{Bext}}} = \frac{3}{16} \frac{\xi^{\mathrm{S}}_{\mathrm{B}}}{\xi^{\mathrm{S}}_{\mathrm{D}}}. \tag{8.79}$$

The ratio of the coherence lengths is given by

$$\frac{\xi_{\mathrm{B}}^{\mathrm{S}}}{\xi_{\mathrm{D}}^{\mathrm{S}}} \sim \sqrt{\frac{\hbar\tau_{\mathrm{e}}^{-1}}{\Delta}} \gg 1, \tag{8.80}$$

where we used $\Delta \ll \hbar\tau_{\mathrm{e}}^{-1}$ (corresponding to $\xi_{\mathrm{D}}^{\mathrm{S}} \gg l_{\mathrm{e}}$). Thus, we find that the disordered current is much larger than the ballistic current through the same interface geometry. The current contribution for both spins inverted fulfills analogous expressions.

Depending on the geometry, the dephasing due to the orbital effect of the magnetization will destroy the Cooperon contribution, in which case this Diffuson contribution is dominant.

The ratio of the coherence lengths can be written as

$$\frac{\xi_{\mathrm{B}}^{\mathrm{S}}}{\xi_{\mathrm{D}}^{\mathrm{S}}} \sim \frac{\xi_{\mathrm{D}}^{\mathrm{S}}}{l_{\mathrm{e}}} \sim \frac{N}{g} \tag{8.81}$$

where $g \sim k_{\mathrm{F}}^2 l_{\mathrm{e}} \xi_{\mathrm{D}}^{\mathrm{S}}$ [268] is the dimensionless conductance and $N \sim (\xi_{\mathrm{D}}^{\mathrm{S}})^2 k_{\mathrm{F}}^2$ is the number of channels (diffusive junction).

Summing up the four contributions from $\left\langle \Xi_{\mathrm{Dext}}^{\sigma\sigma'} \right\rangle$ (for $\sigma, \sigma' \in \{\uparrow, \downarrow\}$) and extending to non-zero voltages, we finally obtain

$$\begin{aligned} \left\langle I_{\mathrm{FS}}^{\mathrm{Dext}} \right\rangle = \frac{4\omega^2}{5} I_0^{\mathrm{D}} \sin^2\theta \Bigg[& \mathrm{sgn}\left(\frac{\omega}{2}+U\right)\left|\frac{\omega}{2}+U\right|^{\frac{5}{2}} \left(\alpha_\uparrow^2 \cos^2\frac{\theta}{2} + \alpha_\downarrow^2 \sin^2\frac{\theta}{2}\right) \\ & + \mathrm{sgn}\left(-\frac{\omega}{2}+U\right)\left|\frac{\omega}{2}-U\right|^{\frac{5}{2}} \left(\alpha_\uparrow^2 \sin^2\frac{\theta}{2} + \alpha_\downarrow^2 \cos^2\frac{\theta}{2}\right)\Bigg] + 2^4 I_0^{\mathrm{D}} \alpha_\uparrow \alpha_\downarrow U \end{aligned} \tag{8.82}$$

with

$$I_0^{\mathrm{D}} = \frac{e\Delta}{h}\frac{\xi_{\mathrm{B}}^{\mathrm{S}}}{\xi_{\mathrm{D}}^{\mathrm{S}}}\frac{(2\pi)^3}{32} S k_{\mathrm{F}}^2 = \frac{e\Delta}{h}\frac{\xi_{\mathrm{B}}^{\mathrm{S}}}{\xi_{\mathrm{D}}^{\mathrm{S}}}\pi^4 N_{\mathrm{ch}}. \tag{8.83}$$

Here, the factor N_{ch} reflects the increased number of transport channel with respect to the point contact geometry. Further, the ratio of the coherence lengths appears due to the disorder, giving a much larger disorder current than the ballistic current through the same interface geometry. Note that the disorder changes the frequency dependence of the current via the Cooperon that is frequency dependent. We conclude that for a possible experiment it is thus advantageous to have some impurities. However, the impurity concentration might be difficult to control in the growth process. Additionally, the extended interface has to be favored over the point contact, due to the larger

number of conduction channels. Even taking into account disorder, a half-metal at zero voltage bias is still the ideal setup to detect the subgap current induced by ferromagnetic resonance.

9 Conclusions

In this thesis we investigated the possibility to change the charge current in superconducting junctions manipulating the spin properties using magnetic resonance.

In part I of this thesis we considered an unconventional Josephson junction between a conventional s-wave superconductor and an unconventional $\mathrm{p_x}$-wave superconductor. This junction hosts two spin-polarized Andreev bound states that are 2π-periodic, giving rise to a spontaneous magnetization in equilibrium. The current-phase relation is π-periodic and does hence not probe the peculiar bound state properties. We have shown that a time-dependent magnetic field, that couples to the spin via the Zeeman effect, may change the occupations of the bound states. The field induces coherent Rabi oscillations between different spin states of the junction that due to energy constraints are possible at four phase values. These oscillations appear as resonances in the current-phase relation. For a circularly polarized magnetic field, a spin selection rule only allows Rabi oscillations in a certain range of superconducting phase differences, giving a spin detection scheme.

The field also induces non-coherent transitions including continuum states that act as refill or ionization processes for the Andreev levels, depending on whether a bound state is filled or emptied. For a circularly polarized field, these field-induced processes do not provide a decay mechanism for the Rabi oscillations, due to spin and energy constraints. In this case, the width of the resonances in the current-phase relation is thus determined by other processes, such as, e.g., phase fluctuations. For a linear polarization, there is no spin selection rule and Rabi oscillations appear at the four energetically possible phase values. The resulting current-phase relation is thus spin insensitive, as long as the field is purely linearly polarized. Further, the width of the resonances is determined by the field-induced ionization processes. For both polarizations, the resonances are clearly visible in transparent junctions, but their visibility is more challenging in tunnel junctions.

Future research on this $\mathrm{s}/\mathrm{p_x}$ junction could be focussed on a more detailed study of the decay mechanisms that are not field-induced. In this thesis they were only treated in a phenomenological manner. A resistive environment can induce transitions, as known from conventional Josephson junctions [215]. Since these processes determine

the width of the resonance in the current-phase relation for a circularly polarized field, further investigation needs to be done. Further, it might be interesting to study the combination of a bias voltage and an ac magnetic field that should give rise to Shapiro steps in the current-voltage characteristics [269]. Due to the spin-polarization of the bound states, a spin-dependent effect might be possible. So far, we have studied ballistic leads. In experiments however, there is always disorder. Impurity scattering due to disorder acts as a pair breaker in the $\mathrm{p_x}$-wave superconductor, suppressing superconductivity, whereas the s-wave superconductor is not sensitive to time-reversal invariant scattering [270, 271]. Therefore, adressing the effect of disorder in the superconducting leads is interesting. Last but not least, it is worth to consider the proposed experimental setup using a ferromagnetic nanowire to engineer an effective $\mathrm{p_x}$-wave superconductor in more detail. We have only considered the idealized junction. A more thorough investigation of all the elements in the SQUID-like geometry might be necessary with the aim to understand possible modifications of our results.

In part II of this thesis we considered a half-metal/conventional superconductor (HM/S) interface. No Andreev current may flow through this junction in the case of a static magnetization direction, since the perfect spin polarization of the half-metal forbids Andreev reflection processes at the interface. We have shown that if the half-metal is subjected to ferromagnetic resonance (FMR) an Andreev current flows. The precessing magnetization direction in the half-metal provides the necessary spin-flip mechanism. If the superconductor was in its normal phase, a spin current would be injected due to spin-pumping. In the superconducting state however, spin singlet pairing inhibits any spin current, leading to a charge current. This Andreev current scales with the fifth power of the precession frequency for small frequencies, showing that the transfer of two electrons at the same time is strongly suppressed. The current does not require any voltage bias across the junction, since a non-equilibrium situation is created for the charge carriers in the ferromagnet due to the precession of the magnetization direction.

We have also shown that for a point contact junction, a non-zero minority carrier concentration reduces the current that vanishes at equal carrier concentrations. Additionally, we considered a more realistic extended interface geometry. For a ballistic junction, the current is enhanced compared to a point contact geometry due to the larger number of transport channels. This extended interface geometry allows to treat disordered junctions. We have shown that disorder is more important in the ferromagnet than in

the superconductor. Further, the current through the disordered junction is much larger than the current through a ballistic junction in the same geometry.

Future research could investigate in more detail the effect of spin-orbit interaction (SOI). SOI in the ferromagnet under FMR provides a spin-relaxation mechanism and thus modifies the transport properties. There will thus be a competition between spin-pumping due to the precession and spin-relaxation due to the spin-orbit coupling. It has been shown that in a ferrmagnet/normal metal (F/N) junction, spin-orbit coupling induces a backflow spin current, creating a voltage across the junction if spin may be accumulated in the ferromagnet [158]. It is interesting to investigate how this effect is modified, if the normal metal is replaced by a superconductor that does not allow for subgap spin currents. Recently, spin-orbit coupling in a ferromagnet has been used to electrically induce a non-equilibrium spin-polarization [272–275]. In this setup, an oscillating electrical current is driven through a uniformely magnetized sample, creating a non-equilibrium time-dependent spin polarization. The polarization is responsable for a transverse component of the exchange field, exerting a torque onto the magnetization and thereby driving the precession. It might be interesting to investigate this effect, when the ferromagnet is coupled to a superconductor. Spin-orbit coupling is not only relevant in the ferromagnet, but also in the superconductor. An HM/S interface, in a lateral contact geometry and with spin-orbit coupling in the superconductor, has been shown to lead to triplet Andreev reflections [276]. This finding motivates further investigation of spin-orbit coupling in the superconductor. SOI can also be relevant at the interface, where it leads to a spin-dependent transmission probability of the barrier, therby influencing the charge transport across the barrier. Recently, spin-orbit coupling at the interface between a ferromagnet under FMR and a normal metal has been considered [277], as well as interfacial spin-orbit coupling for a static ferromagnet/superconductor (F/S) interface [278].

Further, it is interesting to combine the HM/S interface with a second superconductor, in order to create a Josephson junction. Such a S/HM/S junction under ferromagnetic resonance (for a recent review on S/F/S junctions see [279]) has already been considered [231], but only for tunnel barriers between the superconductors and the half-metal. Since Andreev reflection is most relevant for transparent interfaces, the study of such a transparent junction might lead to an interesting interplay of superconducting phase coherence and ferromagnetic resonance.

In this thesis we have investigated magnetic resonance in superconducting junctions, which is of interest for fundamental research. Nevertheless, it might be possible that the advances in the understanding of dynamical effects in superconducting heterostructures lead to the conception of new devices for applications at some point in the future.

Résumé français

Contrôler le courant de charge par un contrôle des propriétés de spin est intéressant pour des nanostructures qui contiennent des supraconducteurs, parce que le transport de charge dans l'état fondamental d'un supraconducteur est cohérent. Dans cette thèse, on analyse la possibilité de modifier le courant de charge dans des jonction supraconductrices par une manipulation des propriétés de spin en utilisant la résonance magnétique.

Le Chapitre 2 introduit les concepts physiques principaux. Dans un supraconducteur conventionel qui est décrit par la théorie BCS, la surface de Fermi devient instable en raison d'une interaction attractive médiée par des phonons. Le nouvel état fondamental, dans lequel des électrons forment des paires de Cooper, est séparé du spectre d'excitation par un gap. Cet état supporte un supracourant sans dissipation. Les supraconducteurs non-conventionels sont caracterisés par une dépendence en impulsion des potentiels de pair. En présence d'une symétrie d'inversion, ils peuvent être classifiés par le moment angulaire de la partie orbitale de leur fonction d'onde. Les supraconducteurs de type p sont particulairement intéressants, parce que leur fonction d'onde possède une partie orbitale impaire, ce que donne lieu à une partie de spin paire, i.e., un appariement triplet. La physique des jonctions supraconductrices est déterminée par la physique de l'interface entre un métal normal et un supraconducteur (interface N/S). Une telle interface N/S réfléchit un électron arrivant avec une énergie sous le gap comme un trou. Un tel processus de réflexion d'Andreev ajoute une paire de Cooper dans le condensat. Ce mécanisme mène, dans des jonctions conventionels, à la formation de deux états liés dégénérés en spin. Ces états dépendent de la différence de phase à travers la jonction et déterminent ainsi la relation courant-phase.

Dans cette thèse, on étudie également l'interaction entre la supraconductivité et le ferromagnétisme qui est particulairement intéressante dans des jonctions avec une

direction d'aimentation qui dépend du temps. Dans ce but, on commence par introduire la résonance ferromagnétique (RFM) dans le Chapitre 2. Contrairement à la résonance magnétique nucléaire et en fonction de la géométrie, aucun champ statique n'est nécessaire pour la RFM. Les jonctions entre un matériau ferromagnétique et un métal normal (jonctions F/N) sont intéressantes pour leurs effets quand elles sont soumises à une aimentation dynamique. Le matériau ferromagnétique, étant soumis aux conditions de la RFM, injecte un courant de spin dans le métal normal adjacent. L'aimantation précessante perd du moment cinétique lors de ce processus de pompage de spin.

Le Chapitre 3 introduit des outils théoriques utilisés pour obtenir les résultats de cette thèse. Le formalisme de Bogoliubov – de Gennes est une méthode pour calculer la fonction d'onde d'un système avec un potentiel de paire dépendant de l'espace. Afin de résoudre un problème de transport supraconducteur, il est approprié de combiner ce formalisme à l'approche des matrices de diffusion. Une autre façon d'approcher le transport hors équilibre à travers une jonction supraconductrice est d'utiliser le formalisme des fonctions de Green hors équilibre, que l'on présente dans sa formulation Keldysh. Dans ce formalisme, le couplage tunnel entre les deux côtés de la jonction peut être traité comme une perturbation. En outre, on présente l'approche de l'équation maîtresse de Markov pour les matrices de densité, adaptée pour faire face à des systèmes quantiques ouverts. Les états liés d'une jonction Josephson peuvent être traités comme un système couplé à un réservoir, i.e., le continuum d'états. Ce continuum joue le rôle d'un réservoir thermique et possède un temps de relaxation court. L'approche de l'équation maîtresse permet alors d'obtenir l'évolution temporelle des occupations des états.

La Partie I de cette thèse examine la manipulation des niveaux d'Andreev dans une jonction Josephson singulet/triplet entre un supraconducteur conventionel de type s et un supraconducteur non-conventionel de type $\mathrm{p_x}$ en utilisant un champ Zeeman dépendant du temps.

Dans le Chapitre 4, on montre que cette jonction $\mathrm{s/p_x}$ possède deux états liés d'Andreev polarisés en spin, qui sont 2π-periodiques. Selon le rapport des gaps des supraconducteurs, un de ces états liés peut exister seulement dans un certain intervalle de différences de phases supraconductrices. La polarisation en spin des états liés donne lieu à une aimantation spontanée en équilibre, que l'on détermine en utilisant une approche d'énergie libre. La relation courant-phase de la jonction $\mathrm{s/p_x}$ est π-periodique

et ne sonde donc pas les propriétés particulières des états liés. En outre, les symétries de spin incompatibles interdisent le transfert d'une seule paire de Cooper à travers la jonction. En conséquence, au moins deux paires doivent être transférées, entraînant une valeur de $\sin 2\phi$ pour l'harmonique la plus basse dans la relation courant-phase. On calcule également la relation courant-phase et l'aimantation pour des températures finies.

La polarisation en spin de la jonction ouvre la possibilité de changer l'occupation des états liés en manipulant le spin. Afin de manipuler le spin, un choix naturel est d'utiliser un champ magnétique, qui se couple au spin par l'effet Zeeman. Dans le Chapitre 5, on montre qu'un champ magnétique dépendant du temps peut changer les occupations des états liés. Pour simplifier le problème, on considère une jonction avec des gaps égaux et à température zéro. Le champ induit des oscillations de Rabi cohérentes entre les différents états de spin de la jonction, qui se manifestent comme des résonances dans la relation courant-phase. Pour un champ magnétique polarisé circulairement, une règle de sélection de spin autorise des oscillations de Rabi seulement dans un certain intervalle de différences de phases supraconducteurs ce qui peut permettre de détecter le spin. En raison de la conservation de l'énergie, des résonances apparaissent à deux valeurs de phase.

Le champ induit aussi des transitions non-cohérentes comprenant des quasiparticules dans le continuum. Ces transitions peuvent remplir ou vider les niveaux d'Andreev. On appèlle une telle transition processus de recharge ou d'ionisation. Ces processus changent la parité des occupations des états liés. Pour un champ polarisé circulairement, ces processus induits par le champ ne fournissent pas de mécanisme de relaxation pour les oscillations de Rabi, en raison des contraintes en spin et en énergie. Dans ce cas, la largeur des résonances dans la relation courant-phase est donc déterminée par d'autres processus, tels que, par exemple, des fluctuations de phase. Pour une polarisation linéaire, il n'y a pas de règle de sélection de spin et les oscillations de Rabi apparaissent à quatre valeurs de phase. Leur largeur est déterminée par les processus d'ionisation induits par le champ. Les résonances sont clairement visibles dans des jonctions transparentes, mais leur visibilité est plus difficile dans des jonctions tunnels.

Dans la partie II de cette thèse, on considère une interface entre un supraconducteur conventionel et un demi-métal. Dans le cas d'une direction d'aimantation statique, aucun courant d'Andreev ne peut circuler à travers cette jonction, que l'on présente

dans le Chapitre 6. La raison est que la polarisation parfaite de spin du demi-métal interdit les processus de réflexion d'Andreev à l'interface. On montre dans le Chapitre 7 pour une jonction de point contact, que si le demi-métal est soumis à la résonance ferromagnétique, un courant d'Andreev s'écoule. La précession de la direction d'aimantation dans le demi-métal fournit le mécanisme de spin-flip nécessaire. Si le supraconducteur était dans sa phase normale, un courant de spin serait injecté en raison du pompage de spin. Dans l'état supraconducteur, cependant, l'appariement spin singulet inhibe tout courant de spin, menant à un courant de charge. Le courant d'Andreev ne nécessite aucun biais de tension à travers la jonction, étant donné qu'une situation hors équilibre est créée pour les porteurs de charge dans le matériau ferromagnétique en raison de la précession de la direction d'aimantation.

On montre aussi dans le Chapitre 8, que, pour une jonction de point contact, une densité non-nulle de porteurs minoritaires (i.e., un matériau ferromagnétique) réduit le courant, qui disparaît pour une proportion égale de porteurs majoritaires et minoritaires. De plus, on considère une géométrie d'interface étendue, plus réaliste. Pour une jonction balistique, le courant est augmenté par rapport à une géométrie de point contact en raison du plus grand nombre de canaux de transport. Cette géométrie d'interface étendue permet de traiter des jonctions désordonnées. Après une introduction au formalisme de désordre, on montre que le désordre est le plus important dans le matériau ferromagnétique. Le résultat principal est que le courant à travers la jonction désordonnée est beaucoup plus grand que le courant traversant une jonction balistique dans la même géométrie.

Le Chapitre 9 résume les principaux résultats de cette thèse et fournit une brève discussion de futures pistes de recherche possibles. L'annexe fournit des détails techniques sur les calculs, qui sont importants pour obtenir les résultats présentés dans la partie principale, mais qui fournissent des informations limitées sur la physique.

Abstract

In this thesis we investigate the possibility to change the charge current in superconducting junctions by manipulating the spin properties using magnetic resonance. We consider two different junctions: First, an unconventional Josephson junction between a conventional s-wave superconductor and an unconventional $\mathrm{p_x}$-wave superconductor and second a half-metal/conventional superconductor junction.

The $\mathrm{s}/\mathrm{p_x}$ junctions hosts two spin-polarized Andreev bound states, which are 2π periodic, giving rise to a spontaneous magnetization in equilibrium. This opens the possibility to manipulate the occupations of the Andreev levels using a time-dependent magnetic field. We show that the field induces coherent Rabi oscillations between different spin states of the junction that appear as resonances in the current-phase relation. For a cicularly polarized magnetic field, we find a spin selection rule, giving Rabi oscillations only in a certain range of superconducting phase differences, which provides a spin detection scheme. In contrary, for a linear polarization, there is no spin constraint on the Rabi oscillations. The field also induces non-coherent transitions including continuum states that act as refill and ionization processes for the Andreev levels. For a circularly polarized field, these field-induced processes do not provide a decay mechanism for the Rabi oscillations, due to spin and energy constraints. For a linear polarization, the width of the Rabi resonances in the current-phase relation is determined by the field-induced ionization processes.

No Andreev current may flow across the half-metal/conventional superconductor junction for a static magnetization direction, since the perfect spin polarization of the half-metal forbids Andreev reflection processes at the interface. We show that an Andreev current flows, if the half-metal is subjected to ferromagnetic resonance. The precessing magnetization direction in the half-metal provides the necessary spin-flip mechanism. The current is driven by the precession of the magnetization direction that

creates a non-equilibrium situation for the charge carriers. We also show for a point contact geometry that in a ferromagnet with non-zero minority carrier concentration the current is reduced and vanishes at equal minority and majority carrier concentrations. Additionally, we consider a more realistic, extended interface geometry. For a ballistic junction, the current is enhanced compared to a point contact geometry due to the larger number of transport channels. Furthermore, we show that disorder is most important in the ferromagnet. The Andreev current through the disordered junction is much larger than the current through a ballistic junction in the same geometry.

Abstract français

Dans cette thèse, on analyse la possibilité de changer un courant de charge dans des jonctions supraconductrices par une manipulation des propriétés de spin en utilisant la résonance magnétique. On considère deux jonctions différentes : Premièrement, une jonction Josephson non-conventionnelle entre un supraconducteur conventionel de type s et un supraconducteur non-conventionel de type $\mathrm{p_x}$. Deuxièmement, une jonction entre un demi-métal et un supraconducteur conventionel.

La jonction $\mathrm{s/p_x}$ contient deux états liés d'Andreev qui sont 2π-periodiques. Ils donnent lieu à une aimentation spontanée à l'équilibre. Ceci ouvre la possibilité de manipuler l'occupation des niveaux d'Andreev en utilisant un champ magnétique dépendant du temps. On demontre que ce champ induit des oscillations de Rabi cohérentes entre différents états de spin de la jonction. Ces oscillations se manifestent comme des résonances dans la relation courant-phase de la jonction. Pour un champ polarisé circulairement, on trouve une règle de sélection de spin qui autorise des oscillations de Rabi seulement dans un certain intervalle de phases dans la relation courant-phase permettant une éventuelle détection du spin. De plus, le champ induit des transitions non-cohérentes qui nécessitent la présence d'une quasiparticule dans le continuum d'états. Ces transitions agissent comme processus de recharge et d'ionization pour les niveaux d'Andreev. Pour un champ polarisé circulairement, ces processus induits par le champ ne donnent pas lieu à un mécanisme de relaxation pour les oscillations de Rabi à cause des contraintes en spin et en énergie. Pour un champ polarisé linéairement, il n'y a pas de contraintes en spin et la largeur des résonances de Rabi dans la relation courant-phase est déterminée par les processus d'ionization induits par le champs.

Dans la jonction entre le demi-métal et le supraconducteur conventionel, il n'y a pas de courant d'Andreev pour une aimentation statique, puisque la polarization parfaite en spin du demi-métal interdit les processus de réflexion d'Andreev à l'interface. On

demontre que pour une géométrie de point contact, un courant d'Andreev passe, si le demi-métal est soumis à la résonance ferromagnétique. La précession de la direction de l'aimentation dans le demi-métal donne lieu au mécanisme de spin-flip nécessaire. Le courant est forcé par la précession de la direction de l'aimentation qui crée une situation hors équilibre pour les porteurs de charge. De plus, dans un matériau ferromagnétique avec une densité de porteurs minoritaires non-nulle, le courant est réduit et disparaît si les densités majoritaires et minoritaires sont égales. On considère, par ailleurs, une géométrie d'interface étendue, plus réaliste. Pour une jonction ballistique, le courant est augmenté par rapport à la géometrie de point contact, en raison du nombre plus élevé de canaux. De plus, on demontre que le désordre est le plus important dans le matériau ferromagnétique. Le courant d'Andreev à travers la jonction désordonnée est beaucoup plus grand que le courant à travers la jonction ballistique dans la même géométrie.

Appendix

A Density of states of unconventional Josephson junctions

The aim of this appendix is to express the density of states of an unconventional Josephson junction using the scattering matrix of the junction that can be obtained solving the Bogoliubov – de Gennes equations by parts and matching them at the interfaces. The equilibrium properties, as equilibrium current and magnetization, can be determined knowing the density of states. Ref. [133] was the first to develop a scattering matrix formalism for a conventional Josephson junction (see also the review [135]). A generalization for conventional s-wave superconductors with different gaps also exists [280]. Here we present and generalize the formalism to pair potentials that are momentum dependent. However, let us only consider fully gapped pair potentials with a momentum-independent absolute value, i.e., s, p_x and p+ip pairing. For these pair potentials the momentum dependence can be written as a phase factor. The formalism should be generalizable to pair potentials with momentum-dependent absolute value.

The density of states can be obtained from the scattering matrix S of the junction via [280, 281]

$$\rho(E) = \frac{1}{2\pi i}\mathrm{Tr}\left[S^\dagger \frac{\partial S}{\partial E}\right] = \frac{1}{2\pi i}\frac{\partial}{\partial E}\ln\det S, \tag{A.1}$$

where $\rho(E)$ gives the density of states up to an energy-independent constant. The expression is derived from the Wigner time-delay [282–284]. In more detail, following Ref. [285], we may express the elements of the scattering matrix as $S_{ij} = \sqrt{g}e^{i\theta}$. The corresponding Wigner time-delay is then given by $\tau_{\mathrm{delay}} = \hbar\frac{d\theta}{dE}$. The density of states

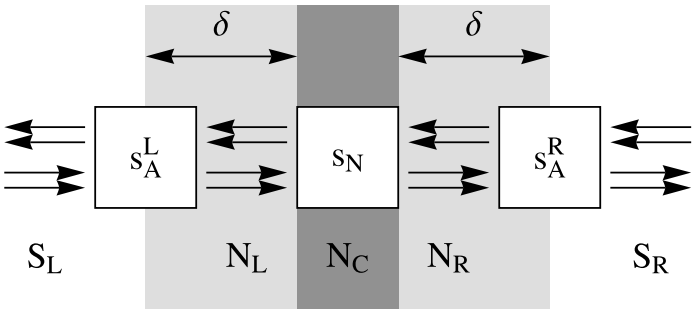

Fig. A.1: Schematical representation of the modes and the scattering matrices. The total scattering matrix of the system relates the modes in the two superconductors $\mathrm{S_R}$ and $\mathrm{S_L}$ with each other. In order to define the modes in the normal region, we split it into two small regions $\mathrm{N_L}$ and $\mathrm{N_R}$ containing no disorder and a central region $\mathrm{N_C}$, described by the scattering matrix $\mathrm{s_N}$, containing the disorder. Solving the scattering problem, we can determine the Andreev reflection matrices of the left (s_A^L) and right (s_A^R) interface.

is proportional to the time-delay: $\rho(E) = \frac{1}{2\pi}\sum_i \frac{d\theta_i}{dE}$, where the sum is over all modes. Using the unitarity of the scattering matrix, this expression yields Eq. (A.1).

In order to evaluate the total scattering matrix S of the junction, we will calculate the modes in the left and the right superconductor. We use a central normal region that allows for backscattering due to disorder, giving rise to a finite transmission of the junction. For calculation purpose we follow the idea of [134] and split this region into a region N_C containing the disorder and two adjacent small regions N_R and N_L that are disorder free and allow for the definition of the modes in the normal region. A schematical plot of the junction is drawn in Fig. A.1.

Let us start to evaluate the modes in the superconductors. The most general form of the pair potential with constant absolute value is given by

$$\Delta_{\beta\sigma\delta} = \Delta_\beta e^{i\psi^\beta_{\sigma\delta}} e^{i\phi_\beta}. \tag{A.2}$$

The index $\beta \in \{\mathrm{L},\mathrm{R}\}$ labels the left (right) superconductor. $\Delta_\beta \in \mathbb{R}$ is the absolute value of the pair potential for the side β. ϕ_β labels the superconducting phase value for side β. σ is the spin index. The phase $\Psi^\beta_{\sigma\delta} \in \mathbb{R}$ is due to the momentum-dependent pairing. It may depend on δ, that is the sign of the real part of the momentum vector.

Solving the linearized Bogoliubov-de Gennes equations (in Andreev approximation, where $\Delta_\beta \ll E_\mathrm{F}$) for a bulk superconductor (side β), we obtain the four eigenfunctions

$$
\begin{aligned}
\chi_{\mathrm{e}+} &= \begin{pmatrix} e^{i\frac{\phi_\beta}{2}}(\alpha_\sigma^\beta)^{-\frac{1}{2}} e^{i\frac{\psi^\beta_{\sigma+}}{2}} \\ e^{-i\frac{\phi_\beta}{2}}(\alpha_\sigma^\beta)^{+\frac{1}{2}} e^{-i\frac{\psi^\beta_{\sigma+}}{2}} \\ 0 \\ 0 \end{pmatrix} e^{ik_\beta x}, \\
\chi_{\mathrm{h}+} &= \begin{pmatrix} e^{i\frac{\phi_\beta}{2}}(\alpha_\sigma^\beta)^{+\frac{1}{2}} e^{i\frac{\psi^\beta_{\sigma+}}{2}} \\ e^{-i\frac{\phi_\beta}{2}}(\alpha_\sigma^\beta)^{-\frac{1}{2}} e^{-i\frac{\psi^\beta_{\sigma+}}{2}} \\ 0 \\ 0 \end{pmatrix} e^{-ik_\beta x}, \\
\chi_{\mathrm{e}-} &= \begin{pmatrix} 0 \\ 0 \\ e^{i\frac{\phi_\beta}{2}}(\alpha_\sigma^\beta)^{-\frac{1}{2}} e^{i\frac{\psi^\beta_{\sigma-}}{2}} \\ e^{-i\frac{\phi_\beta}{2}}(\alpha_\sigma^\beta)^{+\frac{1}{2}} e^{-i\frac{\psi^\beta_{\sigma-}}{2}} \end{pmatrix} e^{-ik_\beta x}, \\
\chi_{\mathrm{h}-} &= \begin{pmatrix} 0 \\ 0 \\ e^{i\frac{\phi_\beta}{2}}(\alpha_\sigma^\beta)^{+\frac{1}{2}} e^{i\frac{\psi^\beta_{\sigma-}}{2}} \\ e^{-i\frac{\phi_\beta}{2}}(\alpha_\sigma^\beta)^{-\frac{1}{2}} e^{-i\frac{\psi^\beta_{\sigma-}}{2}} \end{pmatrix} e^{+ik_\beta x},
\end{aligned}
\tag{A.3}
$$

where $k_\beta = \frac{\sqrt{E^2-\Delta_\beta^2}}{v_\mathrm{F}}$. The eigenfunctions are given in the basis $\eta \otimes \tau$, where η is the index, that gives the sign of k_F ("valley") and τ is the particle-hole space. These four modes will be the basis for the wave function represented by the coefficent vector $(c_e^+(S_\beta), c_h^+(S_\beta), c_e^-(S_\beta), c_h^-(S_\beta))$. The coefficient $c_t^\nu(X_\beta)$ describes a particle of type t (electron e or hole h) in valley $\nu \in \{\pm\}$ on side $\beta \in \{\mathrm{L}, \mathrm{R}\}$ of the junction. $X \in \{\mathrm{S}, \mathrm{N}\}$ denotes either the normal metal or the superconductor. The scattering matrix relates the coefficient vector of incoming modes to the coefficient vector of outgoing modes.

We define the following four coefficient vectors for the junction (as drawn schematically in Fig. A.1)

$$\begin{aligned} c_{\mathrm{N}}^{\mathrm{out}} &= \left(c_{\mathrm{e}}^{-}(N_{\mathrm{L}}), c_{\mathrm{e}}^{+}(N_{\mathrm{R}}), c_{\mathrm{h}}^{+}(N_{\mathrm{L}}), c_{\mathrm{h}}^{-}(N_{\mathrm{R}})\right), \\ c_{\mathrm{S}}^{\mathrm{out}} &= \left(c_{\mathrm{e}}^{-}(S_{\mathrm{L}}), c_{\mathrm{e}}^{+}(S_{\mathrm{R}}), c_{\mathrm{h}}^{+}(S_{\mathrm{L}}), c_{\mathrm{h}}^{-}(S_{\mathrm{R}})\right), \\ c_{\mathrm{S}}^{\mathrm{in}} &= \left(c_{\mathrm{e}}^{+}(S_{\mathrm{L}}), c_{\mathrm{e}}^{-}(S_{\mathrm{R}}), c_{\mathrm{h}}^{-}(S_{\mathrm{L}}), c_{\mathrm{h}}^{+}(S_{\mathrm{R}})\right), \\ c_{\mathrm{N}}^{\mathrm{in}} &= \left(c_{\mathrm{e}}^{+}(N_{\mathrm{L}}), c_{\mathrm{e}}^{-}(N_{\mathrm{R}}), c_{\mathrm{h}}^{-}(N_{\mathrm{L}}), c_{\mathrm{h}}^{+}(N_{\mathrm{R}})\right), \end{aligned} \tag{A.4}$$

where the scattering matrix of the junction S relates the outgoing modes (in the superconducting leads) to the incoming modes (in the superconducting leads), such that

$$c_{\mathrm{S}}^{\mathrm{out}} = S c_{\mathrm{S}}^{\mathrm{in}}. \tag{A.5}$$

Further, the normal region is described by a scattering matrix s_{N} that fulfills

$$c_{\mathrm{N}}^{\mathrm{out}} = s_{\mathrm{N}} c_{\mathrm{N}}^{\mathrm{in}}. \tag{A.6}$$

The scattering in the normal region gives rise to a transmission T. There are now three distinct parameter regimes. First, if the energy is larger than both absolute values of the pair potentials, the modes in both superconductors are propagating. We will refer to this parameter regime as the continuum. Second, if the energy is larger than one gap, but smaller than the other, we only obtain propagating modes in one of the superconductors. We call this parameter regime the intermediate regime. Third, if the energy is smaller than both gaps, there are no propagating solutions in the leads and we call this regime the bound state regime. In the following subsections we calculate the density of states separately for each regime.

A.1 Continuum

In the continuum, we have propagating modes in both superconductors. We match the wave functions at the left interface (between S_{L} and N_{L}) and the right interface (between N_{R} and S_{R}). We treat s_{N} as an input parameter to our theory and obtain after some algebraic manipulations and using Eq. (A.1)

$$\rho(E) = -\frac{1}{\pi}\frac{\partial}{\partial E}\Im \ln\det(1 - s_{\mathrm{A}} s_{\mathrm{N}}) + \frac{1}{2\pi i}\frac{\partial}{\partial E}\ln\det s_{\mathrm{N}}. \tag{A.7}$$

We defined the Andreev reflection matrix as

$$s_{\mathrm{A}} = \begin{pmatrix} 0 & 0 & e^{i\phi_{\mathrm{L}}} e^{i\psi^{\mathrm{L}}_{\sigma+}} \alpha^{\mathrm{L}}_{\sigma} & 0 \\ 0 & 0 & 0 & e^{i\phi_{\mathrm{R}}} e^{i\psi^{\mathrm{R}}_{\sigma-}} \alpha^{\mathrm{R}}_{\sigma} \\ e^{-i\phi_{\mathrm{L}}} e^{-i\psi^{\mathrm{L}}_{\sigma-}} \alpha^{\mathrm{L}}_{\sigma} & 0 & 0 & 0 \\ 0 & e^{-i\phi_{\mathrm{R}}} e^{-i\psi^{\mathrm{R}}_{\sigma+}} \alpha^{\mathrm{R}}_{\sigma} & 0 & 0 \end{pmatrix} \tag{A.8}$$

with the definition

$$\alpha^{\beta}_{\sigma}(E) = \begin{cases} \epsilon^{\beta}_{\sigma} - i\sqrt{1 - \left(\epsilon^{\beta}_{\sigma}\right)^2} & \epsilon^{\beta}_{\sigma} < 1 \\ \epsilon^{\beta}_{\sigma} - \sqrt{\left(\epsilon^{\beta}_{\sigma}\right)^2 - 1} & \epsilon^{\beta}_{\sigma} > 1 \end{cases}, \tag{A.9}$$

where $\epsilon^{\beta}_{\sigma} = \frac{E_{\sigma}}{\Delta_{\beta}}$. For a conventional junction the expression for s_{A} reduces to the expression given in [133]. For the $\mathrm{s/p_x}$ junction, the density of states of the continuum given in Eq. (A.7) reads after some lengthy algebra

$$\rho_{\mathrm{con}}(E) = -\frac{\sigma}{\pi}\frac{\partial}{\partial E} \arctan \frac{T \sin\phi}{(2-T)\sqrt{\epsilon^2_{\mathrm{L}} - 1}\epsilon_{\mathrm{R}} + T\sqrt{\epsilon^2_{\mathrm{R}} - 1}\epsilon_{\mathrm{L}}}. \tag{A.10}$$

A.2 Bound state regime

There are no propagating modes in the superconductors, i.e., $c^{\mathrm{in}}_{\mathrm{S}} = 0$, yielding the relation

$$c^{\mathrm{in}}_{\mathrm{N}} = s_{\mathrm{A}} c^{\mathrm{out}}_{\mathrm{N}}. \tag{A.11}$$

s_{A} has been defined in Eq. (A.8). Using the definition of s_{N} (in Eq. (A.6)), we obtain the relation

$$\det(1 - s_{\mathrm{A}}(E_n) s_{\mathrm{N}}(E_n)) = 0. \tag{A.12}$$

The solutions E_n of this determinant equation are the bound state energies of the bound states formed in the normal region sandwiched between the superconductors. Knowledge of the Andreev reflection matrix s_{A} and the normal region scattering matrix s_{N} is thus sufficient to determine the bound state energies (given in Sec. 4.2). We obtain the following density of states

$$\rho_{\mathrm{abs}}(E) = \sum_n \delta(E - E_n) = -\frac{1}{\pi}\frac{\partial}{\partial E} \Im \ln \frac{\det\left[1 - s_{\mathrm{A}}(E + i0^+) s_{\mathrm{N}}(E + i0^+)\right]}{\sqrt{-\det s_{\mathrm{A}}(E)}}. \tag{A.13}$$

Note, that $\det s_{\mathrm{A}}(E)$ is phase independent.

A.3 Intermediate regime

Let us assume without loss of generality that the right superconductor has the larger gap, such that $\Delta_{\mathrm{L}} < E < \Delta_{\mathrm{R}}$. Then, there are no propagating solutions in the right superconductor. We divide the problem into two tasks: First, we derive a scattering matrix for the disordered NS interface with perfect Andreev reflection at the right superconductor. Afterwards, we add the left superconductor and calculate the scattering matrix of the total system that relates the incoming and outgoing modes with each other. This formalism has first been proposed for an N/S junction consisting of a conventional superconductor [135, 286]. We will then show how the determinant expression can be expressed in terms of quantities that we already defined for the continuum case.

We define the incoming and outgoing coefficient vectors for the N/S interface consisting of the regions $\mathrm{N_L}, \mathrm{N_R}, \mathrm{S_R}$ (see also Fig. A.1):

$$\tilde{c}_{\mathrm{N}}^{\mathrm{in}} = \begin{pmatrix} c_{e^-}(\mathrm{N_L}) \\ c_{h^+}(\mathrm{N_L}) \end{pmatrix}, \tag{A.14}$$

$$\tilde{c}_{\mathrm{N}}^{\mathrm{out}} = \begin{pmatrix} c_{e^+}(\mathrm{N_L}) \\ c_{h^-}(\mathrm{N_L}) \end{pmatrix}. \tag{A.15}$$

These coefficient vectors are connected via the scattering matrix of the N/S interface $\tilde{S}$ by

$$\tilde{c}_{\mathrm{N}}^{\mathrm{out}} = \tilde{S}\tilde{c}_{\mathrm{N}}^{\mathrm{in}}. \tag{A.16}$$

The scattering matrix can be obtained by matching the wave functions at the interface between $\mathrm{N_R}$ and $\mathrm{S_R}$ and using the normal region scattering matrix. After some algebra, the scattering matrix can be parametrized as

$$\tilde{S} = \begin{pmatrix} s_{\mathrm{ee}} & s_{\mathrm{eh}} \\ s_{\mathrm{he}} & s_{\mathrm{hh}} \end{pmatrix} \tag{A.17}$$

with

$$s_{\mathrm{ee}} = r_{11} + t_{12}(1 - (\alpha_\sigma^{\mathrm{R}})^2 e^{i(\psi_{\sigma-}^{\mathrm{R}} - \psi_{\sigma+}^{\mathrm{R}})} r_{22}^* r_{22})^{-1} (\alpha_\sigma^{\mathrm{R}})^2 e^{i(\psi_{\sigma-}^{\mathrm{R}} - \psi_{\sigma+}^{\mathrm{R}})} r_{22}^* t_{21}, \tag{A.18}$$

$$s_{\mathrm{eh}} = t_{12}(1 - (\alpha_\sigma^{\mathrm{R}})^2 e^{i(\psi_{\sigma-}^{\mathrm{R}} - \psi_{\sigma+}^{\mathrm{R}})} r_{22}^* r_{22})^{-1} \alpha_\sigma^{\mathrm{R}} e^{i\psi_{\sigma-}^{R}} e^{i\phi} t_{21}^*, \tag{A.19}$$

$$s_{\mathrm{he}} = t_{12}^*(1 - (\alpha_\sigma^{\mathrm{R}})^2 e^{i(\psi_{\sigma-}^{\mathrm{R}} - \psi_{\sigma+}^{\mathrm{R}})} r_{22} r_{22}^*)^{-1} \alpha_\sigma^{\mathrm{R}} e^{-i\psi_{\sigma+}^{\mathrm{R}}} e^{-i\phi} t_{21}, \tag{A.20}$$

$$s_{\mathrm{hh}} = r_{11}^* + t_{12}^*(1 - (\alpha_\sigma^{\mathrm{R}})^2 e^{i(\psi_{\sigma-}^{\mathrm{R}} - \psi_{\sigma+}^{\mathrm{R}})} r_{22} r_{22}^*)^{-1} (\alpha_\sigma^{\mathrm{R}})^2 e^{i(\psi_{\sigma-}^{\mathrm{R}} - \psi_{\sigma+}^{\mathrm{R}})} r_{22} t_{21}^*. \tag{A.21}$$

Here we parametrized the normal region scattering matrix as

$$s_{\mathrm{N}} = \begin{pmatrix} s_0(E) & 0 \\ 0 & s_0^*(-E) \end{pmatrix} \tag{A.22}$$

with

$$s_0 = \begin{pmatrix} r_{11} & t_{12} \\ t_{21} & r_{22} \end{pmatrix}, \tag{A.23}$$

where we dropped the energy argument for clarity of the notation. Now, we define the scattering matrix of the junction in the intermediate regime S^{int} via

$$c_{\mathrm{S}}^{\mathrm{out}} = S^{\mathrm{int}} c_{\mathrm{S}}^{\mathrm{in}} \tag{A.24}$$

with the coefficient vectors defined as

$$c_{\mathrm{S}}^{\mathrm{in}} = \begin{pmatrix} c_{e^+}(S_{\mathrm{L}}) \\ c_{h^-}(S_{\mathrm{L}}) \end{pmatrix}, \tag{A.25}$$

$$c_{\mathrm{S}}^{\mathrm{out}} = \begin{pmatrix} c_{e^-}(S_{\mathrm{L}}) \\ c_{h^+}(S_{\mathrm{L}}) \end{pmatrix}. \tag{A.26}$$

Solving the matching problem at the interface between $\mathrm{S_L}$ and $\mathrm{N_L}$, we obtain

$$\det S^{\mathrm{int}} = \det(1 - \tilde{S} s_{\mathrm{R}}^+)^{-1} \det(1 - s_{\mathrm{R}}^- \tilde{S}^{-1}) \det \tilde{S} \cdot (e^{-i(\psi_{\sigma+}^{\mathrm{R}} - \psi_{\sigma-}^{\mathrm{R}})}), \tag{A.27}$$

where we defined the Andreev reflection matrix of the right interface

$$s_{\mathrm{R}}^{\pm} = \begin{pmatrix} 0 & e^{i\phi_{\mathrm{R}}} e^{i\psi_{\sigma\mp}^{\mathrm{R}}} \alpha_\sigma^{\mathrm{R}} \\ e^{-i\phi_{\mathrm{R}}} e^{-i\psi_{\sigma\pm}^{\mathrm{R}}} \alpha_\sigma^{\mathrm{R}} & 0 \end{pmatrix}. \tag{A.28}$$

We can relate the determinant expression in Eq. (A.27) to determinants of the 4×4 matrices defined for the continuum using

$$\det(1 - \tilde{S} s_{\mathrm{R}}^{+}) = \det(1 - s_{\mathrm{N}} s_{\mathrm{A}}) \det M. \tag{A.29}$$

Here, M is a matrix that will drop out again, since we can write after some algebra

$$\det \tilde{S} = \det M \det s_{\mathrm{L}} \det s_{\mathrm{N}} \det(M^{-1})^{\dagger}, \tag{A.30}$$

where we introduced the Andreev reflection matrix of the left interface

$$s_{\mathrm{L}} = \begin{pmatrix} 0 & e^{i\phi_{\mathrm{L}}} e^{i\psi_{\sigma+}^{\mathrm{L}}} \alpha_{\sigma}^{\mathrm{L}} \\ e^{-i\phi_{\mathrm{L}}} e^{-i\psi_{\sigma-}^{\mathrm{L}}} \alpha_{\sigma}^{\mathrm{L}} & 0 \end{pmatrix}. \tag{A.31}$$

Finally, we obtain for the density of states expression in the intermediate regime

$$\rho_{\mathrm{int}}(E) = -\frac{1}{\pi} \frac{\partial}{\partial E} \Im(\ln \det(1 - s_{\mathrm{N}} s_{\mathrm{A}})) + \frac{1}{2\pi i} \frac{\partial}{\partial E} \ln \det s_{\mathrm{N}} + \frac{1}{2\pi i} \frac{\partial}{\partial E} \ln \det s_{\mathrm{L}}. \tag{A.32}$$

For an explicit evaluation, the following relation is useful: $\ln \det s_{\mathrm{L}} = -2i\chi_{\mathrm{L}}$ with $\chi_{\mathrm{L}} = \arccos \frac{E}{|\Delta_{\mathrm{L}}|}$. We can easily generalize the problem to more than one conduction channel. In this case, the parameters defined in Eq. (A.23) are matrices.

The density of states of the $\mathrm{s/p_x}$ junction in the intermediate regime depends on which superconductor has the larger gap. For $\Delta_{\mathrm{p}} > \Delta_{\mathrm{s}}$, we obtain using Eq. (A.32) and after some algebra

$$\rho_{\mathrm{int}} = -\frac{1}{\pi} \frac{\partial}{\partial E} \arctan \frac{T\sqrt{1 - \epsilon_{\mathrm{R}}^2}\epsilon_{\mathrm{L}} + T\sigma \sin\phi}{(2 - T)\sqrt{\epsilon_{\mathrm{L}}^2 - 1}\epsilon_{\mathrm{R}}}. \tag{A.33}$$

In the opposite regime, $\Delta_{\mathrm{p}} < \Delta_{\mathrm{s}}$, Eq. (A.32) yields

$$\rho_{\mathrm{int}} = -\frac{1}{\pi} \frac{\partial}{\partial E} \arctan \frac{(2 - T)\sqrt{1 - \epsilon_{\mathrm{L}}^2}\epsilon_{\mathrm{R}} + T\sigma \sin\phi}{T\sqrt{\epsilon_{\mathrm{R}}^2 - 1}\epsilon_{\mathrm{L}}}. \tag{A.34}$$

A.4 Contribution of the leads

So far, we have obtained the modification of the density of states due to the presence of the junction. The contribution of the leads to the total density of states is however missing. In order to obtain this contribution, we have to include the phase of the wave

function acquired during a translation process. Let us consider a bulk superconductor of a given length l. We define the modes on the right and left termination of this superconductor (indices L, R). Choosing the following coefficient vectors

$$c^{\mathrm{in}} = (c_{\mathrm{e}^+}(\mathrm{L}), c_{\mathrm{h}^-}(\mathrm{L}), c_{\mathrm{e}^-}(\mathrm{R}), c_{\mathrm{h}^+}(\mathrm{R}))\,, \tag{A.35}$$

$$c^{\mathrm{out}} = (c_{\mathrm{e}^-}(\mathrm{L}), c_{\mathrm{h}^+}(\mathrm{L}), c_{\mathrm{e}^+}(\mathrm{R}), c_{\mathrm{h}^-}(\mathrm{R}))\,, \tag{A.36}$$

we can write the scattering matrix due to a translation in the superconductor as

$$S_{\mathrm{T}} = \begin{pmatrix} 0 & T_\beta(l) \\ T_\beta(l) & 0 \end{pmatrix}, \tag{A.37}$$

where

$$T_\beta(l) = e^{i\frac{\sqrt{E^2-\Delta_\beta^2}}{\hbar v_{\mathrm{F}}}l}\mathbb{1}_{2\times 2}. \tag{A.38}$$

Let our junction be described by the scattering matrix S. We now attach on both sides superconducting leads with different gaps and of different lengths. Then, the total scattering matrix S^{tot} of the junction plus the leads can be written as

$$S^{\mathrm{tot}} = \begin{pmatrix} T_{\mathrm{L}}(l_{\mathrm{L}}) & 0 \\ 0 & T_{\mathrm{R}}(l_{\mathrm{R}}) \end{pmatrix} S \begin{pmatrix} T_{\mathrm{L}}(l_{\mathrm{L}}) & 0 \\ 0 & T_{\mathrm{R}}(l_{\mathrm{R}}) \end{pmatrix}, \tag{A.39}$$

giving for the density of states

$$\rho(E) = \rho_{\mathrm{con}}(E) + \rho^{\mathrm{L}}_{\mathrm{lead}}(l_{\mathrm{L}}) + \rho^{\mathrm{R}}_{\mathrm{lead}}(l_{\mathrm{R}}), \tag{A.40}$$

where we defined the density of states contribution due to the lead as

$$\rho^{\beta}_{\mathrm{lead}}(l) = \frac{2l}{\pi\hbar v_{\mathrm{F}}}\frac{E}{\sqrt{E^2-\Delta_\beta^2}}. \tag{A.41}$$

Note that we have four quasiparticle states (electrons and holes, left-moving and right-moving), giving a factor of 4 with respect to the single mode result. Further note that we could have chosen the wave functions normalized via the square root of the volume (the length in 1D), such that the length does not appear in the density of states. For the intermediate regime, the term corresponding to the lead with smaller gap will be absent and for the bound state regime both additional terms will be absent. For a normal metal lead the contribution reads $\rho_{\mathrm{N}} = \frac{nl}{2\pi\hbar v_{\mathrm{F}}}$, where n is the number of modes. Consequently,

the density of states contribution of the leads in above equation is just the BCS density of states of the (bulk) superconductors.

For the $\mathrm{s}/\mathrm{p_x}$ junction, we can write the explicit continuum expression of the density of states (see Eq. (A.10)) in the following form

$$\rho_{\mathrm{con}} = A\frac{1}{\Delta_{\mathrm{R}}} + B\frac{1}{\Delta_{\mathrm{L}}}, \tag{A.42}$$

where the coefficients A and B are unitless. The superconducting coherence length of lead β is given by $\xi_\beta = \frac{\hbar v_{\mathrm{F}}}{\Delta_\beta}$. In the short junction limit, the central part of length l that is described by the scattering matrix S is short compared to the coherence lengths, i.e., $l \ll \xi_\beta \, \forall \beta$. The assumption of long leads, i.e., $l_\beta \gg \frac{\hbar v_{\mathrm{F}}}{\Delta_\beta} = \xi_\beta \, \forall \beta$, can be recast to

$$\frac{l_\beta}{\hbar v_{\mathrm{F}}} \gg \frac{1}{\Delta_\beta}, \tag{A.43}$$

giving

$$\rho^\beta_{\mathrm{lead}} \gg \rho_{\mathrm{con}}. \tag{A.44}$$

This relation ensures that the density of states is positive. Even though the modification of the density of states due to the junction ρ_{con} can be negative, $\rho^\beta_{\mathrm{lead}}$ is always positive. $\rho^\beta_{\mathrm{lead}}$ does not depend on the phase difference ϕ and therefore does not contribute to the current. Further, the density of states of the leads does not contribute to the spontaneous magnetization.

B Josephson current expression

The aim of this appendix is to derive Eq. (4.21) on page 60. We want to obtain an expression for the current through the $\mathrm{s/p_x}$ Josephson junction at finite temperature. We want to express the current using the scattering matrices that can be obtained in a scattering approach. We follow an approach developed for conventional junctions in Ref. [213] and apply it to our $\mathrm{s/p_x}$ junction. We use the free energy expression in Eq. (4.19). Using the abstract expressions for the density of states given in Eqs. (A.7), (A.13), and (A.32), we can express the free energy using a continuous energy variable. After a partial integration and introducing a complex energy variable, the current can be written as

$$I = -\frac{2e}{\hbar}\frac{1}{i\pi\beta}\sum_{\sigma}\frac{d}{d\phi}\oint_{\mathcal{C}} dz \ln\det(1 - s_{\mathrm{A}}^{\sigma}(z)s_{\mathrm{N}}^{\sigma}(z))\tanh z. \tag{B.1}$$

Here, we have chosen the integration contour $\mathcal{C}$ in the following way: We integrate over a line parallel to the real axis and offset by 0^+. We close the contour at infinity for positive imaginary parts. The integration contour has to be offset by a positive imaginary part, in order to obtain the correct expression for α in the continuum, defined in Eq. (4.4). In the language of Green's functions, the sign choice is imposed by causality. We could close the integration contour, since $\lim_{|z|\to\infty}\alpha(z) = 0$. Further, in order to establish Eq. (B.1), we used the following relation for the Andreev scattering matrix

$$\Sigma_x s_{\mathrm{A}}(t + i0^+)\Sigma_x = -s_{\mathrm{A}}^*(-t + i0^+), \tag{B.2}$$

where

$$\Sigma_x = \begin{pmatrix} 0 & \mathbb{1}_{N\times N} \\ \mathbb{1}_{N\times N} & 0 \end{pmatrix} \tag{B.3}$$

for N conduction channels. With help of Eq. (B.2), we could relate the complex conjugate of the determinant to the determinant at negative energy arguments. This enables us to rewrite the imaginary part of the determinant (in the density of states expression) that is initially integrated over positive energies, as an integral over the entire real axis. For the evaluation of the boundary term in the partial integration step, we made use of

$$\ln\det(1 - s_{\mathrm{A}}s_{\mathrm{N}}) = \sum_{k=1}^{\infty} -\frac{1}{2k}\mathrm{Tr}(s_{\mathrm{A}}s_{\mathrm{N}})^{2k} \tag{B.4}$$

in order to determine the following scaling behavior

$$\ln\det(1 - s_{\mathrm{A}}(z)s_{\mathrm{N}}(z)) \sim \alpha^2(z) + \mathcal{O}(\alpha^4(z)), \tag{B.5}$$

that shows that the boundary term obtained in the partial integration step vanishes. Using the residue theorem the current in Eq. (B.1) reads

$$I = -\frac{4e}{\hbar\beta}\Re\frac{d}{d\phi}\sum_{\sigma\in\{\pm\}}\sum_{n=0}^{\infty}\ln\det(1 - s_{\mathrm{A}}^{\sigma}(i\omega_n)s_{\mathrm{N}}^{\sigma}(i\omega_n)), \tag{B.6}$$

where the sum is evaluated at the fermionic Matsubara frequencies given by

$$\omega_n = (2n+1)\pi\beta^{-1}. \tag{B.7}$$

Eq. (B.6) and Eq. (B.7) are Eq. (4.21) and Eq. (4.22) of the main text.

C Wave functions of the s/p_x junction

The work presented in this appendix has been published as an appendix to Ref. [198]. In this appendix, we derive the eigenstates of the Bogoliubov – de Gennes Hamiltonian, Eq. (4.2). In order to obtain the eigenstates of the Hamiltonian in Eq. (4.2), we determine the general form of the wave functions in the leads in Sec. C.1. The wave functions are given in the basis $\eta \otimes \tau$, where η denotes the R/L space and τ the particle-hole space. Then we use the boundary condition at the junction to establish the wave functions for the bound states in Sec. C.2, and for the continuum states in Sec. C.3. We provide simple expressions both in the cases of a transparent and an opaque junction. As the wave functions are 2π-periodic, we restrict our considerations to the interval $\phi \in [0, 2\pi[$.

C.1 Wave functions in the leads

In the left (s-wave) lead, $x < 0$, the Hamiltonian in (4.2) reduces to

$$\mathcal{H}_s = \hbar v_F p \eta_z \tau_z - \Delta \tau_x. \tag{C.1}$$

It has a block-diagonal structure in the R/L space. In each block, characterized by $\eta_z = \pm 1$, we thus need to solve an auxiliary 2×2 eigenvalue problem given by

$$(\pm \hbar v_F p \tau_z - \Delta \tau_x) \begin{pmatrix} u \\ v \end{pmatrix} = E \begin{pmatrix} u \\ v \end{pmatrix}. \tag{C.2}$$

Using the solutions for this problem, we find that the most general form of the wave functions associated with the Hamiltonian in Eq. (C.1) at energies above the gap, $|E| > \Delta$, is the superposition of four independent spinors,

$$\psi(x) = \frac{1}{\sqrt{1+\alpha^2}} \left[A_{\mathrm{e}}^{\mathrm{in}} \begin{pmatrix} 1 \\ -\alpha \\ 0 \\ 0 \end{pmatrix} e^{ikx} + A_{\mathrm{h}}^{\mathrm{out}} \begin{pmatrix} -\alpha \\ 1 \\ 0 \\ 0 \end{pmatrix} e^{-ikx} \right. \\ \left. + A_{\mathrm{e}}^{\mathrm{out}} \begin{pmatrix} 0 \\ 0 \\ 1 \\ -\alpha \end{pmatrix} e^{-ikx} + A_{\mathrm{h}}^{\mathrm{in}} \begin{pmatrix} 0 \\ 0 \\ -\alpha \\ 1 \end{pmatrix} e^{ikx} \right]. \tag{C.3}$$

Here, $\alpha = (E - \mathrm{sgn}(E)\sqrt{E^2 - \Delta^2})/\Delta$ and $k = \mathrm{sgn}(E)\sqrt{E^2 - \Delta^2}/(\hbar v_{\mathrm{F}})$. The prefactor in Eq. (C.3) ensures that each 4-spinor is normalized to unity. Furthermore,

$$\frac{1}{\sqrt{1+\alpha^2}} = \sqrt{\frac{1}{2}\left(1 + \frac{\sqrt{E^2-\Delta^2}}{|E|}\right)}, \tag{C.4}$$

$$\frac{\alpha}{\sqrt{1+\alpha^2}} = \mathrm{sgn}(E)\sqrt{\frac{1}{2}\left(1 - \frac{\sqrt{E^2-\Delta^2}}{|E|}\right)} \tag{C.5}$$

are the BCS coherence factors. Thus, the spinors with the coefficients $A_{\mathrm{e}}^{\mathrm{in}}$, $A_{\mathrm{h}}^{\mathrm{out}}$, $A_{\mathrm{e}}^{\mathrm{out}}$, and $A_{\mathrm{h}}^{\mathrm{in}}$ in Eq. (C.3) describe right-moving electron-like, left-moving hole-like, left-moving electron-like, and right moving hole-like quasiparticles, respectively.

Below the gap, $|E| < \Delta$, there are only two evanescent solutions, such that the most general form of the wave functions associated with the Hamiltonian in Eq. (C.1) reads

$$\psi(x) = \left[B_{\mathrm{h}} \begin{pmatrix} -\alpha \\ 1 \\ 0 \\ 0 \end{pmatrix} + B_{\mathrm{e}} \begin{pmatrix} 0 \\ 0 \\ 1 \\ -\alpha \end{pmatrix} \right] e^{\kappa x}. \tag{C.6}$$

Here $\alpha = (E - i\sqrt{\Delta^2 - E^2})/\Delta$, which may be written as $\alpha = e^{-i\chi}$, where $\chi \in \mathbb{R}$ is the energy-dependent phase shift acquired in an Andreev reflection process, and $\kappa = \sqrt{\Delta^2 - E^2}/(\hbar v_{\mathrm{F}})$ gives the decay length in the lead.

In the right (p_x-wave) lead, $x > L$, the Hamiltonian Eq. (4.2) reduces to

$$\mathcal{H}_{\mathrm{p}} = \hbar v_{\mathrm{F}} p \eta_z \tau_z - \Delta \eta_z \tau_x e^{-i\tau_z \phi}. \tag{C.7}$$

We notice that

$$\mathcal{H}_{\mathrm{p}} = U^{\dagger} \mathcal{H}_{\mathrm{s}} U, \tag{C.8}$$

where

$$U = \exp\left[i\tau_z \left(\frac{\phi}{2} + \frac{\pi}{4}(1+\eta_z) \right) \right]. \tag{C.9}$$

This allows us to write the general form of the wave functions both in the continuum,

$$\begin{aligned} \psi(x) = & \frac{1}{\sqrt{1+\alpha^2}} \left[C_{\mathrm{e}}^{\mathrm{out}} \begin{pmatrix} 1 \\ \alpha e^{-i\phi} \\ 0 \\ 0 \end{pmatrix} e^{ikx} + C_{\mathrm{h}}^{\mathrm{in}} \begin{pmatrix} \alpha e^{i\phi} \\ 1 \\ 0 \\ 0 \end{pmatrix} e^{-ikx} \right. \\ & \left. + C_{\mathrm{e}}^{\mathrm{in}} \begin{pmatrix} 0 \\ 0 \\ 1 \\ -\alpha e^{-i\phi} \end{pmatrix} e^{-ikx} + C_{\mathrm{h}}^{\mathrm{out}} \begin{pmatrix} 0 \\ 0 \\ -\alpha e^{i\phi} \\ 1 \end{pmatrix} e^{ikx} \right], \end{aligned} \tag{C.10}$$

and below the gap,

$$\psi(x) = \left[D_{\mathrm{e}} \begin{pmatrix} 1 \\ \alpha e^{-i\phi} \\ 0 \\ 0 \end{pmatrix} + D_{\mathrm{h}} \begin{pmatrix} 0 \\ 0 \\ -\alpha e^{i\phi} \\ 1 \end{pmatrix} \right] e^{-\kappa x}. \tag{C.11}$$

To determine the coefficients in the wave functions introduced above, we need to match them at the junction. For this, we derive the transfer matrix M associated with the scalar potential $U(x) = U_0 \theta[x(L-x)]$ in the normal part of the junction. When U_0 is

large, the wave functions with energy E in the normal part of the junction, $0 < x < L$, are readily obtained as

$$\psi(x) = E_{\mathrm{e}}^{<} \begin{pmatrix} 1 \\ 0 \\ -i \\ 0 \end{pmatrix} e^{-\lambda x} + E_{\mathrm{e}}^{>} \begin{pmatrix} 1 \\ 0 \\ i \\ 0 \end{pmatrix} e^{\lambda x} + E_{\mathrm{h}}^{<} \begin{pmatrix} 0 \\ i \\ 0 \\ 1 \end{pmatrix} e^{-\lambda x} + E_{\mathrm{h}}^{>} \begin{pmatrix} 0 \\ -i \\ 0 \\ 1 \end{pmatrix} e^{\lambda x}, \tag{C.12}$$

where $\lambda = U_0/(\hbar v_{\mathrm{F}})$. Using the continuity conditions for the wave functions at $x = 0$ and $x = L$, we can get rid of the coefficients $E_{\mathrm{e}}^{<}, E_{\mathrm{e}}^{>}, E_{\mathrm{h}}^{<}, E_{\mathrm{h}}^{>}$, and establish the relation

$$\psi(L) = M\psi(0), \tag{C.13}$$

where $M = \cosh(\lambda L) + \sinh(\lambda L)\eta_y$. The coefficients in the transfer matrix can be related to the junction transparency, $T = \cosh^{-2}(\lambda L)$. (For definiteness, we will assume $\lambda > 0$ below.) At $T = 0$, the two superconductors are decoupled. In that case, the boundary condition Eq. (C.13) reduces to

$$(1 + \eta_y)\psi(0) = 0, \tag{C.14}$$

$$(1 - \eta_y)\psi(L) = 0. \tag{C.15}$$

Below we use the matching condition Eq. (C.13) to obtain the bound state and continuum wave functions. Furthermore, we consider the short junction limit, $L \to 0$, while keeping the product $U_0 L$, that determines the transparency, constant.

C.2 Bound state wave functions

In the transparent case, $T = 1$, the matching equation provides two solutions in the R and L sectors, respectively. The energy of the solution in the R sector is given by

$$E_{\mathrm{R}} = \Delta \sin \frac{\phi}{2} \mathrm{sgn}(\sin \phi). \tag{C.16}$$

Its wave function is obtained with $D_\mathrm{h} = B_\mathrm{e} = 0$ and $D_\mathrm{e} = ie^{i\phi/2}\mathrm{sgn}(\sin\phi)B_\mathrm{h}$. Using the normalization condition for the wave function, we can fix $B_\mathrm{h} = \sqrt{\Delta|\cos(\phi/2)|/(2\hbar v_\mathrm{F})} = \sqrt{\kappa_\mathrm{R}/2}$. The energy of the solution in the L sector is given by

$$E_\mathrm{L} = \Delta\cos\frac{\phi}{2}. \tag{C.17}$$

Its wave function is obtained with $D_\mathrm{e} = B_\mathrm{h} = 0$ and $D_\mathrm{h} = -e^{-i\phi/2}B_\mathrm{e}$, where $B_\mathrm{e} = \sqrt{\Delta|\sin(\phi/2)|/(2\hbar v_\mathrm{F})} = \sqrt{\kappa_\mathrm{L}/2}$.

The two states cross at $\phi = \pi/2$ and $\phi = 3\pi/2$. The connection to the energy E_+ (E_-) given in Eq. (4.9) is made by taking for each interval the state with the higher (lower) absolute value of the energy, i.e.,

$$E_+(\phi) = \mathrm{sgn}(\sin\phi)\max\{|E_\mathrm{R}(\phi)|, |E_\mathrm{L}(\phi)|\}, \tag{C.18}$$

$$E_-(\phi) = \mathrm{sgn}(\sin\phi)\min\{|E_\mathrm{R}(\phi)|, |E_\mathrm{L}(\phi)|\}. \tag{C.19}$$

At finite backscattering, these solutions hybridize and an avoided crossing appears near the phases $\phi = \frac{\pi}{2}$ and $\phi = \frac{3\pi}{2}$. In the opaque case, $T = 0$, the state with higher energy merges with the continuum while the matching equation provides a unique bound state solution with energy $E_- = 0$ that resides on the right side of the junction only. The coefficients are given as $B_\mathrm{h} = B_\mathrm{e} = 0$ and $D_\mathrm{h} = e^{-i\phi}D_\mathrm{e}$ with $D_\mathrm{e} = \sqrt{\Delta/(2\hbar v_\mathrm{F})} = \sqrt{\kappa_-/2}$.

At arbitrary transmission, we find two eigenstates with energies given by Eq. (4.9). Using the matching condition, Eq. (C.13), and the normalization condition, $\int dx\,|\Psi(x)|^2 = 1$, we obtain the coefficients for the bound state with energy E_ν:

$$B_\mathrm{e}^\nu = \sqrt{T}\cos\left(\chi_\nu + \frac{\phi}{2}\right)C^\nu, \tag{C.20}$$

$$B_\mathrm{h}^\nu = -i\sqrt{T(1-T)}\cos\frac{\phi}{2}C^\nu, \tag{C.21}$$

$$D_\mathrm{e}^\nu = \sqrt{1-T}e^{i\frac{\phi}{2}}\sin\chi_\nu C^\nu, \tag{C.22}$$

$$D_\mathrm{h}^\nu = \left[(1-T)\cos\frac{\phi}{2} - e^{-i\chi_\nu}\cos\left(\chi_\nu + \frac{\phi}{2}\right)\right]C^\nu, \tag{C.23}$$

where

$$C^\nu = \sqrt{\frac{\kappa_\nu}{2\cos 2\chi_\nu(T\cos^2\frac{\phi}{2} - \sin^2\chi_\nu)}}. \tag{C.24}$$

Note that the expressions previously given for the special cases $T = 0$ and $T = 1$ differ by an irrelevant global phase factor.

C.3 Continuum wave functions

For a fixed energy in the continuum, $|E| > \Delta$, the relation between the four incoming and four outgoing wave functions encoded in Eqs. (C.3) and (C.10) can be expressed through a scattering matrix $S(E)$ such that

$$\begin{pmatrix} A_{\mathrm{e}}^{\mathrm{in}} \\ C_{\mathrm{e}}^{\mathrm{in}} \\ A_{\mathrm{h}}^{\mathrm{in}} \\ C_{\mathrm{h}}^{\mathrm{in}} \end{pmatrix} = S^{-1}(E) \begin{pmatrix} A_{\mathrm{e}}^{\mathrm{out}} \\ C_{\mathrm{e}}^{\mathrm{out}} \\ A_{\mathrm{h}}^{\mathrm{out}} \\ C_{\mathrm{h}}^{\mathrm{out}} \end{pmatrix}. \tag{C.25}$$

The scattering matrix is unitary, i.e., $S^{-1} = S^{\dagger}$. At energies $|E| \gg \Delta$, the scattering matrix simplifies to $S = -i\sqrt{1-T}\tau_z + \sqrt{T}\eta_x$, in agreement with the transfer matrix introduced in Eq. (C.13).

For a transparent junction, $T = 1$, the scattering matrix is block diagonal as the R and L sectors decouple. It reads

$$S = \begin{pmatrix} 0 & \frac{1-\alpha^2}{1-\alpha^2 e^{i\phi}} & \frac{\alpha(1-e^{i\phi})}{1-\alpha^2 e^{i\phi}} & 0 \\ \frac{1-\alpha^2}{1+\alpha^2 e^{-i\phi}} & 0 & 0 & -\frac{\alpha(1+e^{i\phi})}{1+\alpha^2 e^{-i\phi}} \\ \frac{\alpha(1+e^{-i\phi})}{1+\alpha^2 e^{-i\phi}} & 0 & 0 & \frac{1-\alpha^2}{1+\alpha^2 e^{-i\phi}} \\ 0 & \frac{\alpha(e^{-i\phi}-1)}{1-\alpha^2 e^{i\phi}} & \frac{1-\alpha^2}{1-\alpha^2 e^{i\phi}} & 0 \end{pmatrix}. \tag{C.26}$$

For the opaque junction, $T = 0$, scattering states are confined within each lead and the scattering matrix reads

$$S = \begin{pmatrix} -i & 0 & 0 & 0 \\ 0 & i\frac{\alpha^2-1}{1+\alpha^2} & 0 & -\frac{2\alpha}{1+\alpha^2}e^{i\phi} \\ 0 & 0 & i & 0 \\ 0 & \frac{2\alpha}{1+\alpha^2}e^{-i\phi} & 0 & -i\frac{\alpha^2-1}{1+\alpha^2} \end{pmatrix} = \begin{pmatrix} -i & 0 & 0 & 0 \\ 0 & i\sqrt{1-\frac{\Delta^2}{E^2}} & 0 & -\frac{\Delta}{E}e^{i\phi} \\ 0 & 0 & i & 0 \\ 0 & \frac{\Delta}{E}e^{-i\phi} & 0 & -i\sqrt{1-\frac{\Delta^2}{E^2}} \end{pmatrix}, \tag{C.27}$$

where we used Eqs. (C.4) and (C.5) in the last step.

In the general case, using the matching condition in Eq. (C.13) and the continuum wave functions in Eqs. (C.3) and (C.10), the inverse scattering matrix can be written as $S^{-1} = B^{-1}A$ with

$$A = \begin{pmatrix} 0 & -1 & -\alpha\sqrt{T} & -i\sqrt{1-T}\alpha e^{i\phi} \\ 0 & -\alpha e^{-i\phi} & \sqrt{T} & i\sqrt{1-T} \\ \sqrt{T} & -i\sqrt{1-T} & 0 & \alpha e^{i\phi} \\ -\alpha\sqrt{T} & -i\sqrt{1-T}\alpha e^{-i\phi} & 0 & -1 \end{pmatrix}, \tag{C.28}$$

$$B = \begin{pmatrix} -\sqrt{T} & -i\sqrt{1-T} & 0 & \alpha e^{i\phi} \\ \alpha\sqrt{T} & i\alpha\sqrt{1-T}e^{-i\phi} & 0 & 1 \\ 0 & 1 & \alpha\sqrt{T} & i\sqrt{1-T}\alpha e^{i\phi} \\ 0 & -\alpha e^{-i\phi} & -\sqrt{T} & i\sqrt{1-T} \end{pmatrix}. \tag{C.29}$$

In the following we will use the outgoing continuum states. Their wave function is obtained by setting one of the outgoing coefficients $A_{\mathrm{e}}^{\mathrm{out}}, C_{\mathrm{e}}^{\mathrm{out}}, A_{\mathrm{h}}^{\mathrm{out}}, C_{\mathrm{h}}^{\mathrm{out}}$ to unity and computing the incoming coefficients via the scattering matrix, Eq. (C.25).

D Transition rates

The work presented in this appendix has been published as an appendix to Ref. [198]. In this section we calculate the ionization and refill rates induced by a weak ac Zeeman field using second order perturbation theory. For this, we first derive the Hamiltonian due to the Zeeman field, Eq. (5.2), in the unperturbed basis of the wave functions introduced in Appendix C. Introducing the Bogoliubov transformation,

$$\Psi(x) = \sum_{\lambda} \psi_{\lambda}(x)\gamma_{\lambda}, \tag{D.1}$$

inserting it into Eq. (5.1), and symmetrizing the resulting expression, we obtain

$$H_{\mathrm{Z}} = \frac{\mu_{\mathrm{B}} B}{2} \sum_{\lambda\lambda'} V_{\lambda,\lambda'}\gamma_{\lambda}\gamma_{\lambda'} + \mathrm{h.}c., \tag{D.2}$$

where $V_{\lambda,\lambda'}$ is given below Eq. (5.2) on page 68. Note that $V_{\lambda,\lambda'} = -V_{\lambda',\lambda}$. This allows writing Eq. (D.2) as

$$H_{\mathrm{Z}} = \mu_{\mathrm{B}} B e^{-i\Omega t} \left(V_{+,-}\gamma_{+}\gamma_{-} + \sum_{E;\mu,\nu} V_{\nu,E\mu}\gamma_{\nu}\gamma_{E\mu} + \frac{1}{2} \sum_{E,E';\mu,\mu'} V_{E\mu,E'\mu'}\gamma_{E\mu}\gamma_{E'\mu'} \right) + \mathrm{h.c.}, \tag{D.3}$$

which is Eq. (5.2). Using the definition of the ionization and refill rates (shown in Fig. 5.1 on page 69), we can calculate them by applying Fermi's golden rule to the Hamiltonian in Eq. (D.3). We obtain

$$\Gamma_{\nu}^{\mathrm{I/R}}(\Omega) = 2\pi\hbar^{-1}(\mu_{\mathrm{B}} B)^2 \sum_{E,\mu} |V_{\nu,E\mu}|^2 \, \delta(\hbar\Omega + E_{\nu} + E) \, \theta(\mp E E_{\nu}). \tag{D.4}$$

Here, the upper sign is for an ionization process, whereas the lower sign is for a refill process. The Heaviside function θ appears due to the Fermi-Dirac distributions at zero temperature, ensuring that in a refill process the bound state and the continuum state are empty, and in an ionization process the bound state is occupied whereas the continuum state is empty. Using $\mathrm{sgn}(E_{\nu}) = \mathrm{sgn}(\sin\phi)$, we obtain

$$\Gamma_{\nu}^{\mathrm{I/R}}(\Omega) = 2\pi\hbar^{-1}(\mu_{\mathrm{B}} B)^2 \sum_{E'>0,\mu} \left| V_{\nu;\mp E'\mathrm{sgn}(\sin\phi),\mu} \right|^2 \delta[\hbar\Omega + (|E_{\nu}| \mp E')\mathrm{sgn}(\sin\phi)]. \tag{D.5}$$

Using the density of states in the leads $\rho(E)$, we can replace the sum by an integral and obtain Eq. (5.16).

To obtain the matrix elements $V_{\nu,E\mu}$, we use the general expressions for the bound state wave functions and the continuum wave functions, defined in Eqs. (C.6), (C.11) and (C.3), (C.10), respectively. After integration over the real space coordinate and reorganization, we obtain

$$V_{\nu,E\mu} = \frac{1}{\sqrt{1+\alpha^2}} \left(\frac{F_1^\nu}{\kappa_\nu + ik} + \frac{F_2^\nu}{\kappa_\nu - ik} \right), \tag{D.6}$$

where

$$F_1^\nu = (B_\mathrm{e} A_\mathrm{e}^\mathrm{in} - B_\mathrm{h} A_\mathrm{h}^\mathrm{in})(\alpha - e^{-i\chi_\nu}) + (D_\mathrm{h} C_\mathrm{h}^\mathrm{in} e^{i\phi} + D_\mathrm{e} C_\mathrm{e}^\mathrm{in} e^{-i\phi})(\alpha + e^{-i\chi_\nu}), \tag{D.7}$$

$$F_2^\nu = (B_\mathrm{e} A_\mathrm{h}^\mathrm{out} - B_\mathrm{h} A_\mathrm{e}^\mathrm{out})(\alpha e^{-i\chi_\nu} - 1) + (D_\mathrm{h} C_\mathrm{e}^\mathrm{out} - D_\mathrm{e} C_\mathrm{h}^\mathrm{out})(1 + \alpha e^{-i\chi_\nu}). \tag{D.8}$$

Using the outgoing wave functions, Eq. (D.6) can be evaluated numerically to obtain the rates for arbitrary transmission, for an example see Fig. 5.3. In the following, we consider the two special cases of a transparent and a tunnel junction, for which we give analytical expressions.

D.1 Transparent junction

Here, we want to calculate the rates given by Eq. (5.16) for $T = 1$. We have seen, that there are two bound states, labeled by R and L, with energies given in Eqs. (C.16) and (C.17). For each of them, we need to evaluate (D.6). Since the calculation is very similar in both cases, we will only show the explicit calculation for $\nu = \mathrm{L}$. Using the coefficients for $T = 1$, given below Eq. (C.17), and $\chi_\mathrm{L} = \phi/2$, we find

$$\begin{aligned} V_{\mathrm{L},E\mu} = \sqrt{\frac{\kappa_\mathrm{L}}{2(1+\alpha^2)}} \Bigg[& \frac{A_\mathrm{e}^\mathrm{in} \left(\alpha - e^{-i\frac{\phi}{2}}\right) - C_\mathrm{h}^\mathrm{in} \left(\alpha e^{i\frac{\phi}{2}} + 1\right)}{\kappa_\mathrm{L} + ik} \\ & + \frac{A_\mathrm{h}^\mathrm{out} \left(\alpha e^{-i\frac{\phi}{2}} - 1\right) - e^{-i\frac{\phi}{2}} C_\mathrm{e}^\mathrm{out} \left(1 + \alpha e^{-i\frac{\phi}{2}}\right)}{\kappa_\mathrm{L} - ik} \Bigg]. \end{aligned} \tag{D.9}$$

For the transparent junction, there are only two outgoing states, $C_{\mathrm{e}}^{\mathrm{out}} = 1$ or $A_{\mathrm{h}}^{\mathrm{out}} = 1$. Then,

$$\begin{aligned}\sum_{\mu} |V_{\mathrm{L},E\mu}|^2 = \frac{\kappa_{\mathrm{L}}}{2(1+\alpha^2)} \Bigg\{ & \frac{2(1+\alpha^2)}{\kappa_{\mathrm{L}}^2+k^2} + \frac{\alpha^2 - 2\alpha\epsilon_{\mathrm{L}} + 1}{\kappa_{\mathrm{L}}^2+k^2} \left(|S_{21}|^2 + |S_{31}|^2\right) \\ & + \frac{\alpha^2 + 2\alpha\epsilon_{\mathrm{L}} + 1}{\kappa_{\mathrm{L}}^2+k^2} \left(|S_{24}|^2 + |S_{34}|^2\right) \\ & - \frac{2}{\kappa_{\mathrm{L}}^2+k^2} \Re\left[(\alpha - e^{-i\frac{\phi}{2}})(1+\alpha e^{-i\frac{\phi}{2}})(S_{21}^* S_{24} + S_{31}^* S_{34})\right] \\ & + 2\Re\left[\frac{1}{(\kappa_{\mathrm{L}}+ik)^2} H_1\right] + 2\Re\left[\frac{1}{(\kappa_{\mathrm{L}}-ik)^2} H_2\right] \Bigg\},\end{aligned} \tag{D.10}$$

where

$$H_1 = (\alpha - e^{-i\frac{\phi}{2}})(-S_{21}^*(\alpha e^{-i\phi} + e^{i\frac{\phi}{2}}) + S_{31}^*(-1 + \alpha e^{i\frac{\phi}{2}})), \tag{D.11}$$

$$H_2 = -(1+\alpha e^{-i\frac{\phi}{2}})(-S_{24}(\alpha e^{-i\phi} + e^{-i\frac{\phi}{2}}) + S_{34}(-1 + \alpha e^{-i\frac{\phi}{2}})). \tag{D.12}$$

Using the unitarity of the scattering matrix, $\sum_k S_{ik} S_{jk}^* = \delta_{ij}$, we find

$$\sum_{\mu} |V_{\mathrm{L},E\mu}|^2 = \frac{2\kappa_{\mathrm{L}}}{\kappa_{\mathrm{L}}^2+k^2} + \frac{\kappa_{\mathrm{L}}}{1+\alpha^2} \left(\frac{\kappa_{\mathrm{L}}^2 - k^2}{(\kappa_{\mathrm{L}}^2+k^2)^2} \Re[H_1 + H_2] + \frac{2\kappa_{\mathrm{L}} k}{(\kappa_{\mathrm{L}}^2+k^2)^2} \Im[H_1 - H_2] \right), \tag{D.13}$$

which after lengthy, but straightforward, algebraic manipulation yields

$$\begin{aligned}\sum_{\mu} |V_{\mathrm{L},E\mu}|^2 &= \frac{2\kappa_{\mathrm{L}}}{\kappa_{\mathrm{L}}^2+k^2} \left[1 + \frac{\kappa_{\mathrm{L}}^2 - k^2}{\kappa_{\mathrm{L}}^2+k^2} \frac{1 - 4\alpha^2 + \alpha^4 - 2\alpha^2\cos\phi}{1 + \alpha^4 + 2\alpha^2\cos\phi} \right. \\ &\quad \left. + \frac{\kappa_{\mathrm{L}} k}{\kappa_{\mathrm{L}}^2+k^2} \frac{8\alpha^2(\alpha^2-1)\sin\phi}{(1+\alpha^2)(1+\alpha^4+2\alpha^2\cos\phi)} \right]. \\ &= \frac{\hbar v_{\mathrm{F}}}{\Delta} \frac{4\left|\sin\frac{\phi}{2}\right|(\epsilon^2-1)}{(\epsilon^2 - \cos^2\frac{\phi}{2})^2(\epsilon^2 - \sin^2\frac{\phi}{2})} \left[1 - \frac{\sin\phi \left|\sin\frac{\phi}{2}\right|}{\epsilon} \right],\end{aligned} \tag{D.14}$$

where $\epsilon = E/\Delta$. Repeating the calculation for $\nu = \mathrm{R}$ and using the expressions for the bound state energies, Eqs. (C.16) and (C.17), we finally obtain

$$\sum_{\eta} |V_{\nu,\eta}|^2 = \frac{\hbar v_{\mathrm{F}}}{\Delta} \frac{4|\epsilon_{\bar{\nu}}|(\epsilon^2-1)}{(\epsilon^2 - \epsilon_\nu^2)^2(\epsilon^2 - \epsilon_{\bar{\nu}}^2)} \left[1 - \frac{\sin\phi\,|\epsilon_{\bar{\nu}}|}{\epsilon} \right], \tag{D.15}$$

where $\epsilon_\nu = E_\nu/\Delta$ and $\bar{R} = L$ and $\bar{L} = R$. Substituting (D.15) into (D.5) and using the energy conservation condition, $|\epsilon| = |\tilde{\Omega}| + |\epsilon_\nu|$ for an ionization process and $|\epsilon| = |\tilde{\Omega}| - |\epsilon_\nu|$ for a refill process, we find the rates given in Eq. (5.17).

D.2 Opaque junction

We evaluate (D.6) for the opaque junction, $T = 0$, where only the bound state $\nu = -$ exists. Using the coefficients derived in Sec. C.2, we obtain

$$V_{-,E\mu} = e^{-i\phi}\sqrt{\frac{\kappa_-}{2(1+\alpha^2)}}\left[-i\frac{C_\mathrm{h}^\mathrm{in}e^{i\phi}+C_\mathrm{e}^\mathrm{in}}{\kappa_- + ik}(1+i\alpha) + \frac{C_\mathrm{e}^\mathrm{out} - C_\mathrm{h}^\mathrm{out}e^{i\phi}}{\kappa_- - ik}(1-i\alpha)\right]. \tag{D.16}$$

As in the transparent case, there are only two outgoing states, either $C_\mathrm{e}^\mathrm{out} = 1$ or $C_\mathrm{h}^\mathrm{out} = 1$. After some algebra and using the unitarity of the scattering matrix, we find

$$\sum_\mu |V_{-,E\mu}|^2 = \frac{\kappa_-}{1+\alpha^2}\left\{2\frac{1+\alpha^2}{\kappa_-^2+k^2} - \Im\left[\frac{(1-i\alpha)^2}{(\kappa_- - ik)^2}(S_{22} - S_{24} + e^{-i\phi}S_{44} - e^{i\phi}S_{42})\right]\right\}. \tag{D.17}$$

Using the scattering matrix in Eq. (C.27), we finally obtain

$$\sum_\mu |V_{-,E\mu}|^2 = \frac{\hbar v_\mathrm{F}}{\Delta}\frac{16(\epsilon^2-1)}{\epsilon^6}. \tag{D.18}$$

The corresponding rate is given in Eq. (5.19).

E Expressions for the traces for the current through the half-metal/superconductor interface

The procedure for the current calculation is explained in Sec. 7.5. Here, we only present the results for the expressions obtained after a considerable amount of algebra and after taking the trace over spin and Nambu space. These expressions enter Eq. (7.84). The expression obtained for the regime of pure Andreev reflection S_1 is particularly important for the low frequency behavior of the junction. In the tunnel limit the expressions agree with the results obtained from Fermi's golden rule.

We use the previously defined dimensionless parameters $\epsilon = E/\Delta$, $\omega = \frac{\hbar\Omega}{\Delta}$, $U = \frac{eV}{\Delta}$ and $\alpha = \pi^2 \nu_S \nu_\uparrow t^2$. Additionally, we define

$$\tilde{\alpha}_\sigma = \alpha \frac{\epsilon_\sigma}{\sqrt{1-\epsilon_\sigma^2}}, \tag{E.1}$$

$$\bar{\alpha}_\sigma = \alpha \frac{|\epsilon_\sigma|}{\sqrt{\epsilon_\sigma^2-1}}, \tag{E.2}$$

$$\epsilon_\sigma = \epsilon + \sigma \frac{\omega}{2}. \tag{E.3}$$

Recall the following two definitions given in Eqs. (7.15) and (7.19):

$$(F_{\mathrm{S}})_\sigma = \tanh \frac{E + \frac{\hbar\Omega}{2}\sigma}{2kT}, \tag{E.4}$$

$$(F_{\mathrm{F}})_{\tau\sigma} = \cos^2\frac{\theta}{2} \tanh \frac{E + \frac{\hbar\Omega}{2}\sigma + eV\tau}{2kT} + \sin^2\frac{\theta}{2} \tanh \frac{E - \frac{\hbar\Omega}{2}\sigma + eV\tau}{2kT}. \tag{E.5}$$

Here, we use the distribution function obtained from the model considering relaxation in an adjacent normal metal. The expression in the pure Andreev reflection regime reads

$$S_1 = \frac{\sin^2\theta(\epsilon_\uparrow^{-1}\tilde{\alpha}_\uparrow - \epsilon_\downarrow^{-1}\tilde{\alpha}_\downarrow)^2(F_{\uparrow\uparrow} - F_{\downarrow\downarrow})}{D_1}, \tag{E.6}$$

where the denominator is given by

$$\begin{aligned} D_1 = \Bigg[1 - \left(\tilde{\alpha}_\uparrow \cos^2\frac{\theta}{2} + \tilde{\alpha}_\downarrow \sin^2\frac{\theta}{2}\right)\left(\tilde{\alpha}_\uparrow \sin^2\frac{\theta}{2} + \tilde{\alpha}_\downarrow \cos^2\frac{\theta}{2}\right) \\ + \cos^2\frac{\theta}{2}\sin^2\frac{\theta}{2}\left(\epsilon_\uparrow^{-1}\tilde{\alpha}_\uparrow - \epsilon_\downarrow^{-1}\tilde{\alpha}_\downarrow\right)^2\Bigg]^2 + (\tilde{\alpha}_\uparrow + \tilde{\alpha}_\downarrow)^2. \end{aligned} \tag{E.7}$$

This expression is used to obtain the current in the limit of small frequencies, as presented in Sec. 7.5. The other expressions can be written as

$$
\begin{aligned}
S_2 = \frac{-2}{D_2}\Big\{ & \cos\theta\cos^2\frac{\theta}{2}\sin^2\frac{\theta}{2}\epsilon_\uparrow^{-1}\bar{\alpha}_\uparrow(\bar{\alpha}_\uparrow^2\epsilon_\uparrow^{-1}+\tilde{\alpha}_\downarrow^2\epsilon_\downarrow^{-1})[(G_\uparrow - F_{\downarrow\downarrow})+(G_\uparrow - F_{\uparrow\uparrow})] \\
& + \epsilon_\downarrow^{-1}\bar{\alpha}_\downarrow^2\cos^2\frac{\theta}{2}\sin^2\frac{\theta}{2}[2\epsilon_\downarrow^{-1}+\epsilon_\downarrow^{-1}\bar{\alpha}_\uparrow+\epsilon_\uparrow^{-1}\bar{\alpha}_\uparrow](F_{\downarrow\downarrow}-F_{\uparrow\uparrow}) \\
& + \bar{\alpha}_\uparrow\cos^2\frac{\theta}{2}[(1+\bar{\alpha}_\uparrow\sin^2\frac{\theta}{2})^2+\tilde{\alpha}_\downarrow^2\cos^4\frac{\theta}{2}-\cos^2\frac{\theta}{2}\sin^2\frac{\theta}{2}(\epsilon_\uparrow^{-2}\bar{\alpha}_\uparrow^2+\epsilon_\downarrow^{-2}\tilde{\alpha}_\downarrow^2)](G_\uparrow-F_{\uparrow\uparrow}) \\
& - \bar{\alpha}_\uparrow\sin^2\frac{\theta}{2}[(1+\bar{\alpha}_\uparrow\cos^2\frac{\theta}{2})^2+\tilde{\alpha}_\downarrow^2\sin^4\frac{\theta}{2}-\cos^2\frac{\theta}{2}\sin^2\frac{\theta}{2}(\epsilon_\uparrow^{-2}\bar{\alpha}_\uparrow^2+\epsilon_\downarrow^{-2}\tilde{\alpha}_\downarrow^2)](G_\uparrow-F_{\downarrow\downarrow})\Big\},
\end{aligned}
\tag{E.8}
$$

$$
\begin{aligned}
D_2 = & \left\{1+\bar{\alpha}_\uparrow+\cos^2\frac{\theta}{2}\sin^2\frac{\theta}{2}[\bar{\alpha}_\uparrow^2(1-\epsilon_\uparrow^{-2})-\tilde{\alpha}_\downarrow^2(1-\epsilon_\downarrow^{-2})]\right\}^2 \\
& + [\tilde{\alpha}_\downarrow+\bar{\alpha}_\uparrow\tilde{\alpha}_\downarrow+2\cos^2\frac{\theta}{2}\sin^2\frac{\theta}{2}\bar{\alpha}_\uparrow\tilde{\alpha}_\downarrow(\epsilon_\uparrow^{-1}\epsilon_\downarrow^{-1}-1)]^2,
\end{aligned}
\tag{E.9}
$$

$$
\begin{aligned}
S_3 = \frac{-2}{D_3}\Big\{ & -\cos\theta\cos^2\frac{\theta}{2}\sin^2\frac{\theta}{2}\epsilon_\downarrow^{-1}\bar{\alpha}_\downarrow(\tilde{\alpha}_\uparrow^2\epsilon_\uparrow^{-1}+\bar{\alpha}_\downarrow^2\epsilon_\downarrow^{-1})[(G_\downarrow - F_{\downarrow\downarrow})+(G_\downarrow - F_{\uparrow\uparrow})] \\
& + \epsilon_\uparrow^{-1}\tilde{\alpha}_\uparrow^2\cos^2\frac{\theta}{2}\sin^2\frac{\theta}{2}[2\epsilon_\uparrow^{-1}+\epsilon_\uparrow^{-1}\bar{\alpha}_\downarrow+\epsilon_\downarrow^{-1}\bar{\alpha}_\downarrow](F_{\downarrow\downarrow}-F_{\uparrow\uparrow}) \\
& + \bar{\alpha}_\downarrow\sin^2\frac{\theta}{2}[(1+\bar{\alpha}_\downarrow\cos^2\frac{\theta}{2})^2+\tilde{\alpha}_\uparrow^2\sin^4\frac{\theta}{2}-\cos^2\frac{\theta}{2}\sin^2\frac{\theta}{2}(\epsilon_\uparrow^{-2}\tilde{\alpha}_\uparrow^2+\epsilon_\downarrow^{-2}\bar{\alpha}_\downarrow^2)](G_\downarrow-F_{\uparrow\uparrow}) \\
& - \bar{\alpha}_\downarrow\cos^2\frac{\theta}{2}[(1+\bar{\alpha}_\downarrow\sin^2\frac{\theta}{2})^2+\tilde{\alpha}_\uparrow^2\cos^4\frac{\theta}{2}-\cos^2\frac{\theta}{2}\sin^2\frac{\theta}{2}(\epsilon_\uparrow^{-2}\tilde{\alpha}_\uparrow^2+\epsilon_\downarrow^{-2}\bar{\alpha}_\downarrow^2)](G_\downarrow-F_{\downarrow\downarrow})\Big\},
\end{aligned}
\tag{E.10}
$$

$$
\begin{aligned}
D_3 = & \left\{1+\bar{\alpha}_\downarrow+\cos^2\frac{\theta}{2}\sin^2\frac{\theta}{2}[\bar{\alpha}_\downarrow^2(1-\epsilon_\downarrow^{-2})-\tilde{\alpha}_\uparrow^2(1-\epsilon_\uparrow^{-2})]\right\}^2 \\
& + [\tilde{\alpha}_\uparrow+\tilde{\alpha}_\uparrow\bar{\alpha}_\downarrow+2\cos^2\frac{\theta}{2}\sin^2\frac{\theta}{2}\tilde{\alpha}_\uparrow\bar{\alpha}_\downarrow(\epsilon_\uparrow^{-1}\epsilon_\downarrow^{-1}-1)]^2,
\end{aligned}
\tag{E.11}
$$

$$
\begin{aligned}
S_4 =& 8\left[\left(1+\bar{\alpha}_\uparrow\cos^2\frac{\theta}{2}+\bar{\alpha}_\downarrow\sin^2\frac{\theta}{2}\right)\left(1+\bar{\alpha}_\uparrow\sin^2\frac{\theta}{2}+\bar{\alpha}_\downarrow\cos^2\frac{\theta}{2}\right)\right.\\
&\left.-\sin^2\frac{\theta}{2}\cos^2\frac{\theta}{2}\left(\epsilon_\uparrow^{-1}\bar{\alpha}_\uparrow-\epsilon_\downarrow^{-1}\bar{\alpha}_\downarrow\right)^2\right]^{-2}\\
&\cdot\left[D_{\uparrow\downarrow}\bar{\alpha}_\uparrow\sin^2\frac{\theta}{2}\left(\left(1+\bar{\alpha}_\uparrow\cos^2\frac{\theta}{2}+\bar{\alpha}_\downarrow\sin^2\frac{\theta}{2}\right)^2\right.\right.\\
&\left.-\left(\epsilon_\uparrow^{-1}\bar{\alpha}_\uparrow-\epsilon_\downarrow^{-1}\bar{\alpha}_\downarrow\right)\cos^2\frac{\theta}{2}\left(\sin^2\frac{\theta}{2}+\epsilon_\uparrow^{-1}(\bar{\alpha}_\uparrow-\bar{\alpha}_\downarrow)\cos\theta\right)\right)\\
&+D_{\downarrow\downarrow}\bar{\alpha}_\downarrow\cos^2\frac{\theta}{2}\left(\left(1+\bar{\alpha}_\uparrow\cos^2\frac{\theta}{2}+\bar{\alpha}_\downarrow\sin^2\frac{\theta}{2}\right)^2\right.\\
&\left.\left.-\left(\epsilon_\uparrow^{-1}\bar{\alpha}_\uparrow-\epsilon_\downarrow^{-1}\bar{\alpha}_\downarrow\right)\sin^2\frac{\theta}{2}\left(\cos^2\frac{\theta}{2}-\epsilon_\downarrow^{-1}(\bar{\alpha}_\uparrow-\bar{\alpha}_\downarrow)\cos\theta\right)\right)\right].
\end{aligned}
\tag{E.12}
$$

Here, we introduced the distribution function combination $D_{\alpha\beta} = (F_\mathrm{S})_\alpha - (F_\mathrm{F})_{\beta\beta}$, reading

$$
\begin{aligned}
D_{\alpha\beta} =& \cos^2\frac{\theta}{2}\left[f(E+\beta\frac{\hbar\Omega}{2}+\beta eV)-f(E+\alpha\frac{\hbar\Omega}{2})\right]\\
&+\sin^2\frac{\theta}{2}\left[f(E-\beta\frac{\hbar\Omega}{2}+\beta eV)-f(E+\alpha\frac{\hbar\Omega}{2})\right].
\end{aligned}
\tag{E.13}
$$

The expressions given in this appendix are used to obtain Figs. 7.4 and 7.5. Further, the calculation of the current for high frequencies, presented in Appendix F, uses these expressions.

F Current through the half-metal/superconductor interface at high frequencies

In this appendix we determine the current through the half-metal/superconductor interface at zero temperature, zero voltage ($V = 0$) and in the limit of infinite frequency ($\omega \to \infty$). We assume relaxation in an adjacent normal metal layer corresponding to the distribution function in Eq. (7.19). The current at infinite frequency corresponds to the plateau value that the current may reach, see also Fig. 7.4 on page 128. As defined by Eqs. (7.84) and (7.85) and Tab. 7.1 on page 124, the current is given as the sum of four contributions. In the following we evaluate the total current in the limit of infinite frequency, using the explicit expressions for the traces given in Appendix E.

For the first contribution the occupation factor gives directly $I_1 = 0$, since $\omega > 2$.

Note the following useful relation, valid for both distribution functions and also at finite temperature and voltage bias: $I_2 = I_3$ since $S_2(-E) = S_3(E)$ (as evident from Eqs. (E.8) and (E.10)). Using $\omega \to \infty$ and shifting the integration variable, we can show

$$I_2 = \frac{\alpha^2}{2}\frac{e\Delta}{h}\sin^2\theta\cos\theta\int_{-1}^{0} d\epsilon \frac{z_0 + z_2\epsilon^2}{n_0 - n_2\epsilon^2}, \tag{F.1}$$

where we made the following definitions

$$z_0 = 2(2+\alpha), \tag{F.2}$$

$$z_2 = -2(1+\alpha), \tag{F.3}$$

$$n_0 = (1 + \alpha + 2\alpha^2\cos^2\frac{\theta}{2}\sin^2\frac{\theta}{2})^2, \tag{F.4}$$

$$n_2 = n_0 - \alpha^2(1 + \alpha - 2\alpha\cos^2\frac{\theta}{2}\sin^2\frac{\theta}{2})^2. \tag{F.5}$$

The integral is easily solved giving

$$I_2 + I_3 = \alpha^2\frac{e\Delta}{h}\sin^2\theta\cos\theta\left[-\frac{z_2}{n_2} + \left(\frac{z_0}{n_0} + \frac{z_2}{n_2}\right)\frac{\operatorname{arctanh}\sqrt{\frac{n_2}{n_0}}}{\sqrt{\frac{n_2}{n_0}}}\right]. \tag{F.6}$$

The contribution I_4 can be evaluated numerically. We will now discuss the scaling of the current in two limiting cases.

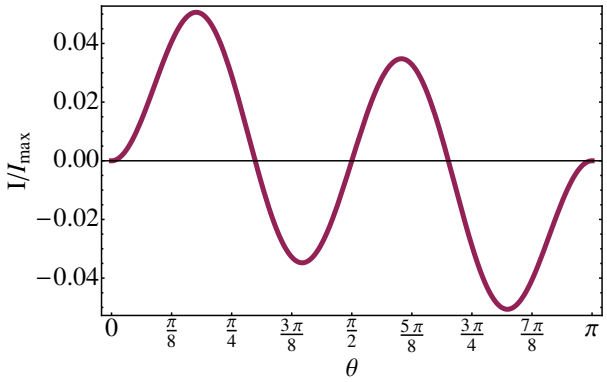

Fig. F.1: Deviation of the angular dependence of the current for a transparent interface (given in Eq. (F.8)) from the tunnel junction angular dependence $\cos\theta \sin^2\theta$. As evident from this plot, the deviations from the angular dependence in the tunnel case are small.

First, consider the tunnel limit $\alpha \ll 1$. In lowest order in α, we can use $\frac{n_2}{n_0} \approx 1 - \alpha^2$ and $\operatorname{arctanh}\sqrt{1-\alpha^2} \approx \ln\frac{2}{\alpha}$ to obtain using Eq. (F.6)

$$I_2 + I_3 \approx 2\alpha^2 \frac{e\Delta}{h} \sin^2\theta \cos\theta \ln\frac{2}{\alpha} + \mathcal{O}\left(\alpha^2\right). \tag{F.7}$$

Numerically, we can prove that $I_4 \sim \alpha^2 \ln\alpha$ for $\alpha \ll 1$. The angle dependence in the tunnel limit is thus $\sin^2\theta\cos\theta$.

Now consider the limit of a transparent interface, i.e., $\alpha = 1$. Eq. (F.6) simplifies to

$$I_2 + I_3 = \frac{e\Delta}{h} \sin^2\theta \cos\theta \left[\frac{1}{\sin^2\theta} + \frac{3\sin^2\theta - 2(1+\frac{\sin^2\theta}{4})^2}{2\sin^3\theta(1+\frac{\sin^2\theta}{4})} \operatorname{arctanh}\left(\frac{\sin\theta}{1+\frac{\sin^2\theta}{4}}\right)\right]. \tag{F.8}$$

Numerically, we obtain $I_2 + I_3(\alpha = 1) \gg I_4(\alpha = 1)$. Further note that we find $I_4 \sim \alpha^2$ for $\alpha \gg 1$, giving $I \approx I_2 + I_3$ in this parameter regime.

For the transparent interface, the angle dependence is obviously more complicated than in the tunnel case. The angle for the maximum current $\theta_{\max} \approx 0.922$ (as obtained numerically from above expression), is slightly shifted with respect to the tunnel case ($\arctan\sqrt{2} \approx 0.955$). However, the term in the brackets $[...]$ is nearly constant. Therefore, the angle dependence is not significantly changed with respect to the tunnel case. Fig. F.1 shows the difference between the angular dependence as given by Eq. (F.8) with respect to the dependence in the tunnel limit $\sin^2\theta\cos\theta$.

G Integral in the Andreev current

During the calculation of the Andreev current in Chapter 8 integrals of the following form appear

$$A = \int_1^\infty d\epsilon \frac{1}{\sqrt{\epsilon^2 - 1}} \frac{1}{\epsilon - a}, \tag{G.1}$$

where $a \in \mathbb{R}$. We use three consecutive substitutions to solve the integral. With the first substitution $\epsilon = \frac{1}{\cos x}$, we get rid of the square root, yielding

$$A = \int_0^{\frac{\pi}{2}} dx \frac{\cos^{-1} x}{\cos^{-1} x - a}. \tag{G.2}$$

The aim of the second substitution is to replace the trigonometric functions. We use $s = \tan \frac{x}{2}$ and obtain

$$A = 2 \int_0^1 \frac{ds}{1 + s^2 - a(1 - s^2)}. \tag{G.3}$$

With the third substitution $u = s\sqrt{\frac{1+a}{1-a}}$ we obtain (supposing $a < 1$)

$$A = \frac{2}{\sqrt{1 - a^2}} \int_0^{\sqrt{\frac{1+a}{1-a}}} \frac{du}{1 + u^2}. \tag{G.4}$$

This is a standard integral giving the solution

$$A = \frac{2}{\sqrt{1 - a^2}} \arctan \sqrt{\frac{1 + a}{1 - a}}. \tag{G.5}$$

H Disorder average of the non-local density of states

We want to calculate the disorder average of the non-local density of states. The calculation presented in this appendix can be found in Ref. [268]. Consider a Gaussian disorder model, where only the second cumulant of the disorder potential $V(\boldsymbol{r})$ is nonzero, i.e.,

$$\langle V(\boldsymbol{r})\rangle = 0, \tag{H.1}$$

$$\langle V(\boldsymbol{r})V(\boldsymbol{r'})\rangle = B(\boldsymbol{r}-\boldsymbol{r'}). \tag{H.2}$$

If the electron wavelength is much bigger than the characteristic decay length of the correlations, the potential can be approximated as being local:

$$\langle V(\boldsymbol{r})V(\boldsymbol{r'})\rangle = B\delta(\boldsymbol{r}-\boldsymbol{r'}) \tag{H.3}$$

Consecutive scattering events are thus uncorrelated. The non-local density of states is defined by

$$\begin{aligned} K_\epsilon(\boldsymbol{r},\boldsymbol{r'}) &= \sum_n \phi_n^*(\boldsymbol{r})\phi_n(\boldsymbol{r'})\delta(\epsilon-\epsilon_n) \\ &= -\frac{1}{\pi}\left\langle \boldsymbol{r'}\middle|\Im G^{\mathrm{R}}\middle|\boldsymbol{r}\right\rangle \\ &= \frac{i}{2\pi}\left(G^{\mathrm{R}}(\boldsymbol{r},\boldsymbol{r'},\epsilon)-G^{\mathrm{A}}(\boldsymbol{r},\boldsymbol{r'},\epsilon)\right), \end{aligned} \tag{H.4}$$

where $\phi_n(\boldsymbol{r})$ is the eigenfunction for the energie ϵ_n. Further $\Im$ denotes the imaginary part and G^{R} (G^{A}) is the retarded (advanced) Green's function. A perturbation expansion of the full Green's function G, treating V as a perturbation, can be written as a Dyson series

$$\begin{aligned} G(\boldsymbol{r},\boldsymbol{r'}) = G_0(\boldsymbol{r},\boldsymbol{r'}) &+ \int d\boldsymbol{r_1} G_0(\boldsymbol{r},\boldsymbol{r_1})V(\boldsymbol{r_1})G_0(\boldsymbol{r_1},\boldsymbol{r'}) \\ &+ \int d\boldsymbol{r_1}\int d\boldsymbol{r_2} G_0(\boldsymbol{r},\boldsymbol{r_1})V(\boldsymbol{r_1})G_0(\boldsymbol{r_1},\boldsymbol{r_2})V(\boldsymbol{r_2})G_0(\boldsymbol{r_2},\boldsymbol{r'}) + \mathcal{O}\left(V^3\right), \end{aligned} \tag{H.5}$$

where G_0 is the unperturbed Green's function. We take the disorder average, denoted by $\langle \cdots \rangle$ and obtain

$$\langle G(\boldsymbol{r}, \boldsymbol{r'}) \rangle = G_0(\boldsymbol{r}, \boldsymbol{r'}) + \int d\boldsymbol{r_1} \int d\boldsymbol{r_2} G_0(\boldsymbol{r}, \boldsymbol{r_1}) B(\boldsymbol{r_1} - \boldsymbol{r_2}) G_0(\boldsymbol{r_1}, \boldsymbol{r_2}) G_0(\boldsymbol{r_2}, \boldsymbol{r'}) + \mathcal{O}\left(B^2\right). \tag{H.6}$$

After a Fourier transform we obtain

$$G(\boldsymbol{k}) = G_0(\boldsymbol{k}) + G_0(\boldsymbol{k}) \left[\int d\boldsymbol{q} B(\boldsymbol{q}) G_0(\boldsymbol{k} - \boldsymbol{q}) G_0(\boldsymbol{k}) + \mathcal{O}\left(B^2\right) \right], \tag{H.7}$$

from which we can extract the first order term of the self-energy

$$\Sigma_1(\boldsymbol{k}) = \int d\boldsymbol{q} B(\boldsymbol{q}) G_0(\boldsymbol{k} - \boldsymbol{q}). \tag{H.8}$$

We use the retarded self-energy in order to define the elastic mean collision time τ_e via

$$\frac{1}{2\tau_\mathrm{e}} = -\Im \Sigma_1^\mathrm{R}(\boldsymbol{k}, \epsilon). \tag{H.9}$$

Neglecting the real part of the self-energy (that shifts the energy levels), we have

$$\left\langle G^{\mathrm{R/A}}(\boldsymbol{k}, \epsilon) \right\rangle = \frac{1}{\epsilon - \epsilon(\boldsymbol{k}) \pm \frac{i}{2\tau_\mathrm{e}}}. \tag{H.10}$$

We consider the dispersion $\epsilon(\boldsymbol{k}) = \frac{k^2}{2m}$ and define $k_\mathrm{e}^2 = k^2 \pm \frac{i}{2\tau_\mathrm{e}}$. Let us further consider the limit of weak disorder, i.e., $k l_\mathrm{e} \gg 1$, where $l_\mathrm{e} = \frac{k\tau_\mathrm{e}}{m}$ is the mean free path. We obtain

$$k_\mathrm{e} \approx k \pm \frac{i}{2l_\mathrm{e}}. \tag{H.11}$$

Using a three dimensional Fourier transform to real space, we obtain

$$\left\langle G^{\mathrm{R/A}}(\boldsymbol{r_i}, \boldsymbol{r}, \epsilon) \right\rangle = \frac{m}{2\pi R} e^{\pm ikR} e^{-\frac{R}{2l_\mathrm{e}}} = -\pi \rho_0 \frac{e^{\pm ikR}}{kR} e^{-\frac{R}{2l_\mathrm{e}}}, \tag{H.12}$$

where $R = |\boldsymbol{r} - \boldsymbol{r_i}|$. Using this expression, the disorder averaged non-local density of states (using Eq. (H.4)) reads

$$\langle K_\epsilon(R) \rangle = \rho_0 \frac{\sin kR}{kR} e^{-\frac{R}{2l_\mathrm{e}}}. \tag{H.13}$$

We can obtain the result for leads without disorder, developping this expression for $R \ll l_\mathrm{e}$.

I Integrals over Green's functions for the extended ballistic interface

We want to solve the integrals in Eq. (8.38) that read

$$X = \int d\boldsymbol{r_1} \int d\boldsymbol{r_2} \int d\boldsymbol{r_3}\, \tilde{g}_0(\boldsymbol{r_1})\tilde{g}_0(-\boldsymbol{r_2})\tilde{g}_0(\boldsymbol{r_2}+\boldsymbol{r_3})\tilde{g}_0(\boldsymbol{r_1}+\boldsymbol{r_3}) \tag{I.1}$$

First, we rewrite Eq. (I.1) introducing the Fourier transform of $\tilde{g}(\boldsymbol{r})$, given by

$$f(\boldsymbol{k}) = \frac{1}{2\pi} \int d^2\boldsymbol{r} e^{i\boldsymbol{kr}} \tilde{g}(\boldsymbol{r}), \tag{I.2}$$

giving a deconvoluted expression

$$\begin{aligned} X = \frac{1}{(2\pi)^4} \int d\boldsymbol{r_1} \int d\boldsymbol{r_2} \int d\boldsymbol{r_3} \int d\boldsymbol{k_1} \int d\boldsymbol{k_2} \int d\boldsymbol{k_3} \int d\boldsymbol{k_4} \\ \cdot e^{i\boldsymbol{k_1 r_1}} e^{i\boldsymbol{k_2}(-\boldsymbol{r_2})} e^{i\boldsymbol{k_3}(\boldsymbol{r_2}+\boldsymbol{r_3})} e^{i\boldsymbol{k_4}(\boldsymbol{r_1}+\boldsymbol{r_3})} f(\boldsymbol{k_1}) f(\boldsymbol{k_2}) f(\boldsymbol{k_3}) f(\boldsymbol{k_4}). \end{aligned} \tag{I.3}$$

We use the definition of the Dirac-δ distribution

$$\int d\boldsymbol{r} e^{ir(\boldsymbol{k})} = (2\pi)^2 \delta(\boldsymbol{k}) \tag{I.4}$$

to obtain after integation

$$X = (2\pi)^2 \int d\boldsymbol{k} f^3(\boldsymbol{k}) f(-\boldsymbol{k}). \tag{I.5}$$

We now have to compute the Fourier transform in Eq. (I.2) with the radial symmetric function $\tilde{g}(\boldsymbol{r})$. In order to obtain dimensionless variables, we introduce $\boldsymbol{x} = k_\mathrm{F}\boldsymbol{r}$ and $\boldsymbol{q} = k_\mathrm{F}^{-1}\boldsymbol{k}$. We define $\tilde{g}(\boldsymbol{r}) = k_\mathrm{F}^2 h(\boldsymbol{x})$ with

$$h(\boldsymbol{x}) = \frac{x\cos x - \sin x}{x^3}. \tag{I.6}$$

Using the integral representation of the Bessel function of first kind of nth order

$$J_n(x) = \frac{1}{2\pi} \int_{-\pi}^{\pi} e^{i(n\tau - x\sin\tau)} d\tau, \tag{I.7}$$

we can write Eq. (I.2) as

$$f(\boldsymbol{q}) = H_0(q) = \int_0^\infty dx\, x J_0(qx) h(x). \tag{I.8}$$

Here, we used the definition of the Hankel transform of order ν of a function $h(x)$ given by

$$H_\nu(q) = \int_0^\infty h(x) J_\nu(qx) x dx. \tag{I.9}$$

Let us use that the result depends only on the absolute value of $\boldsymbol{q}$, giving for the integral to be solved

$$X = (2\pi)^3 k_{\mathrm{F}}^2 \int_0^\infty dq\, q [H_0(q)]^4. \tag{I.10}$$

Let us now evaluate $H_0(q)$. Using $xh(x) = \frac{d}{dx}\frac{\sin x}{x}$, we obtain after a partial integration for Eq. (I.8)

$$H_0(q) = -1 + q \int_0^\infty dx\, J_1(qx) \frac{\sin x}{x}, \tag{I.11}$$

where we used $\frac{d}{dx} J_0(x) = -J_1(x)$. Using the relation [287]

$$\int_0^\infty J_\nu(\alpha x) \frac{\sin(\beta x)}{x} dx = \begin{cases} \frac{1}{\nu} \sin(\nu \arcsin \frac{\beta}{\alpha}) & \text{for} \quad \beta \leq \alpha, \\ \frac{\alpha^\nu \sin \frac{\nu\pi}{2}}{\nu(\beta + \sqrt{\beta^2 - \alpha^2})} & \text{for} \quad \beta \geq \alpha, \end{cases} \tag{I.12}$$

that is valid for $\Re\nu > -1$, we obtain

$$H_0(q) = -\sqrt{1 - q^2}\Theta(1 - q), \tag{I.13}$$

giving for the integral to be solved (Eq. (I.10))

$$X = \frac{(2\pi)^3}{6} k_{\mathrm{F}}^2. \tag{I.14}$$

J Fourier transform of the solution of the 3D diffusion equation

We want to calculate the Fourier transform of the function $f(\omega) = e^{-(1-i)a\sqrt{\omega}}$, given by

$$f(t) = \int_{-\infty}^{\infty} \frac{d\omega}{\sqrt{2\pi}} e^{-i\omega t} f(\omega). \tag{J.1}$$

The idea is to transform this integral into a Gaussian integral, since the exponent contains an ω and a $\sqrt{\omega}$ term. We use the complex substitution $i\omega = z^2$. Consider the complex frequencies plane. The original integral is taken over the real frequency axis ω. After the substitution, the integral is over an axis that is rotated by $\frac{\pi}{4}$ with respect to the real axis. Let us define a contour in the complex plane that is given by the real axis, the rotated axis, and two parts of a circle that connect the two axes (at infinity). Since the function $f(\omega)$ decays exponentially for the frequency going to infinity, the parts at infinity do not contribute to the integral. Further, the exponential function is holomorphic everywhere and therefore no singularity is enclosed by the contour. Using the residue theoreme, the total integral over the contour is zero, giving that the two contributions (over the real and the rotated axis) are identical. The resulting integral reads

$$f(t) = -\frac{2i}{\sqrt{2\pi}} e^{-\frac{a^2}{2t}} \int_{-\infty}^{\infty} dz z e^{-t(z-i\frac{a}{\sqrt{2t}})^2}. \tag{J.2}$$

Now, we have to use a complex linear substitution $x = z - i\frac{a}{\sqrt{2t}}$. The new integration axis is parallel to the old one, offset by $\frac{a}{\sqrt{2t}}$. Let us define an integration contour that is a parallelogram, containing both integration axes and being closed at infinity. Then, the two parts at infinity do not contribute to the integral. Again, since the exponential function is holomorphic, we obtain using the residue theorem

$$f(t) = -\frac{2i}{\sqrt{2\pi}} e^{-\frac{a^2}{2t}} \int_{-\infty}^{\infty} dx (x + i\frac{a}{\sqrt{2t}}) e^{-tx^2}. \tag{J.3}$$

The integral $\int_{-\infty}^{\infty} dx x e^{-tx^2}$ is trivially integrated and gives zero. The other integral gives the well-known result $\int_{-\infty}^{\infty} dx e^{-tx^2} = \sqrt{\frac{\pi}{t}}$, where we suppose $t > 0$. We finally obtain the Fourier transform

$$f(t) = a e^{-\frac{a^2}{2t}} t^{-\frac{3}{2}}. \tag{J.4}$$

Acknowledgments

This PhD thesis would not exist in its present form without the help of others.

First of all, I want to thank Julia Meyer and Manuel Houzet for the possibility to work as a PhD student in their group. Even though, I formally had two supervisiors, it didn't feel for me like this, since they harmonized very well with each other. I gratefully acknowledge their support throughout the entire three years. They did not only give me the possibility to gain a deeper understanding in mesoscopic superconductivity, but made me also aware of the importance to present science in simple words and short equations. I am also very happy about the possibility to attend summer schools in Les Houches, Göteborg and in Canada.

Further, I am thankful to the post-docs Tatiana Krishtop, Konstantin Nesterov, Erik Eriksson and especially my former bureau collegue Roman Riwar for interesting discussions and helpful comments. I also thank Christoph Groth for his linux support and fixing - at least twice - my USB key. I like to thank Joseph Weston, with whom I have started at the same time, for discussions about Josephson junctions and mathematical and organisatorical problems. Further, I thank my bureau collegue Mathieu Istas, as well as Pacôme Armagnat and Vladimir Maryasin for interesting discussions. I also want to thank the aforementioned people for nice spare time activities, including biking, hiking and skiing in the mountains around Grenoble.

Finally, I acknowledge the entire theory group (former and current members) for providing a good working atmosphere. I also thank the "pipotage" group, including Salha Jebari, Andrea Corna, Alexandre Artaud, Florian Blanchet, Alexander Grimm for interesting seminars.

Last but not least, I want to thank everybody else who supported me during the three years.

References

[1] H. K. Onnes. “The resistance of pure mercury at helium temperatures”. In: *Commun. Phys. Lab. Univ. Leiden* 12 (1911), p. 120 (cit. on pp. 1, 11).

[2] W. Meissner and R. Ochsenfeld. “Ein neuer Effekt bei Eintritt der Supraleitfähigkeit”. German. In: *Naturwissenschaften* 21.44 (1933), pp. 787–788. DOI: 10.1007/BF01504252 (cit. on p. 1).

[3] F. London and H. London. “The Electromagnetic Equations of the Supraconductor”. In: *Proceedings of the Royal Society of London. Series A - Mathematical and Physical Sciences* 149.866 (1935), pp. 71–88. DOI: 10.1098/rspa.1935.0048 (cit. on p. 1).

[4] Emanuel Maxwell. “Isotope Effect in the Superconductivity of Mercury”. In: *Physical Review* 78.4 (May 1950), 477–477. DOI: 10.1103/physrev.78.477 (cit. on p. 1).

[5] C. A. Reynolds, B. Serin, W. H. Wright, and L. B. Nesbitt. “Superconductivity of Isotopes of Mercury”. In: *Physical Review* 78.4 (May 1950), 487–487. DOI: 10.1103/physrev.78.487 (cit. on p. 1).

[6] V. L. Ginzburg and L. D. Landau. “To the Theory of Superconductivity”. In: *Zh. Eksp. Teor. Fiz.* 20 (1950), p. 1064 (cit. on p. 1).

[7] J. Bardeen, L. N. Cooper, and J. R. Schrieffer. “Theory of Superconductivity”. In: *Phys. Rev.* 108 (Dec. 1957), pp. 1175–1204. DOI: 10.1103/PhysRev.108.1175 (cit. on pp. 1, 11, 12).

[8] J. Bardeen, L. N. Cooper, and J. R. Schrieffer. “Microscopic Theory of Superconductivity”. In: *Physical Review* 106.1 (Apr. 1957), 162–164. DOI: 10.1103/physrev.106.162 (cit. on pp. 1, 11).

[9] Leon N. Cooper. “Bound Electron Pairs in a Degenerate Fermi Gas”. In: *Phys. Rev.* 104 (Nov. 1956), pp. 1189–1190. DOI: 10.1103/PhysRev.104.1189 (cit. on pp. 1, 12).

[10] Ivar Giaever. “Energy Gap in Superconductors Measured by Electron Tunneling”. In: *Physical Review Letters* 5.4 (Aug. 1960), 147–148. DOI: 10.1103/physrevlett.5.147 (cit. on p. 1).

[11] Ivar Giaever. “Electron Tunneling Between Two Superconductors”. In: *Physical Review Letters* 5.10 (Nov. 1960), 464–466. DOI: 10.1103/physrevlett.5.464 (cit. on p. 1).

[12] J. G. Bednorz and K. A. Müller. "Possible high T_c superconductivity in the Ba-La-Cu-O system". In: *Zeitschrift fur Physik B Condensed Matter* 64 (June 1986), pp. 189–193. DOI: 10.1007/BF01303701 (cit. on pp. 1, 15).

[13] M. K. Wu, J. R. Ashburn, C. J. Torng, et al. "Superconductivity at 93 K in a new mixed-phase Y-Ba-Cu-O compound system at ambient pressure". In: *Physical Review Letters* 58.9 (Mar. 1987), 908–910. DOI: 10.1103/physrevlett.58.908 (cit. on p. 1).

[14] D. A. Wollman, D. J. Van Harlingen, W. C. Lee, D. M. Ginsberg, and A. J. Leggett. "Experimental determination of the superconducting pairing state in YBCO from the phase coherence of YBCO-Pb dc SQUIDs". In: *Physical Review Letters* 71.13 (Sept. 1993), 2134–2137. DOI: 10.1103/physrevlett.71.2134 (cit. on pp. 1, 2).

[15] C. C. Tsuei and J. R. Kirtley. "Pairing symmetry in cuprate superconductors". In: *Rev. Mod. Phys.* 72.4 (Oct. 2000), 969–1016. DOI: 10.1103/revmodphys.72.969 (cit. on pp. 1, 17).

[16] F. Steglich, J. Aarts, C. D. Bredl, et al. "Superconductivity in the Presence of Strong Pauli Paramagnetism: $CeCu_2Si_2$". In: *Physical Review Letters* 43.25 (Dec. 1979), 1892–1896. DOI: 10.1103/physrevlett.43.1892 (cit. on pp. 2, 15).

[17] D. Jérome, A. Mazaud, M. Ribault, and K. Bechgaard. "Superconductivity in a synthetic organic conductor $(TMTSF)_2PF_6$". In: *J. Physique Lett.* 41.4 (1980), 95–98. DOI: 10.1051/jphyslet:0198000410409500 (cit. on pp. 2, 15, 52).

[18] Manfred Sigrist and Kazuo Ueda. "Phenomenological theory of unconventional superconductivity". In: *Rev. Mod. Phys.* 63 (Apr. 1991), pp. 239–311. DOI: 10.1103/RevModPhys.63.239 (cit. on p. 2).

[19] Andrew Peter Mackenzie and Yoshiteru Maeno. "The superconductivity of Sr_2RuO_4 and the physics of spin-triplet pairing". In: *Rev. Mod. Phys.* 75 (May 2003), pp. 657–712. DOI: 10.1103/RevModPhys.75.657 (cit. on pp. 2, 17).

[20] B. D. Josephson. "Possible new effects in superconductive tunnelling". In: *Physics Letters* 1.7 (1962), pp. 251 –253. DOI: 10.1016/0031-9163(62)91369-0 (cit. on pp. 2, 22, 23).

[21] J. M. Rowell, P. W. Anderson, and D. E. Thomas. "Image of the Phonon Spectrum in the Tunneling Characteristic Between Superconductors". In: *Physical Review Letters* 10.8 (Apr. 1963), 334–336. DOI: 10.1103/physrevlett.10.334 (cit. on p. 2).

[22] A. F. Andreev. "The thermal conductivity of the intermediate state in superconductors". In: *Soviet Physics JETP-USSR* 19.5 (1964), pp. 1228–1231 (cit. on pp. 2, 19).

[23] Xiao-Liang Qi and Shou-Cheng Zhang. "Topological insulators and superconductors". In: *Rev. Mod. Phys.* 83 (Oct. 2011), pp. 1057–1110. DOI: 10.1103/RevModPhys.83.1057 (cit. on pp. 2, 15).

[24] A. Yu. Kitaev. "Unpaired Majorana fermions in quantum wires". In: *Physics-Uspekhi* 44.10S (2001), p. 131. DOI: 10.1070/1063-7869/44/10S/S29 (cit. on pp. 2, 17, 57).

[25] Liang Fu and C. L. Kane. “Josephson current and noise at a superconductor/quantum-spin-Hall-insulator/superconductor junction”. In: *Phys. Rev. B* 79 (Apr. 2009), p. 161408. DOI: 10.1103/PhysRevB.79.161408 (cit. on p. 2).

[26] C. W. J. Beenakker. “Search for Majorana Fermions in Superconductors”. In: *Annual Review of Condensed Matter Physics* 4.1 (Apr. 2013), 113–136. DOI: 10.1146/annurev-conmatphys-030212-184337 (cit. on p. 2).

[27] J. Wiedenmann, E. Bocquillon, R. S. Deacon, et al. “4π-periodic Josephson supercurrent in HgTe-based topological Josephson junctions”. In: *Nat Comms* 7 (Jan. 2016), p. 10303. DOI: 10.1038/ncomms10303 (cit. on pp. 2, 18).

[28] H.-J. Kwon, K. Sengupta, and V.M. Yakovenko. “Fractional ac Josephson effect in p- and d-wave superconductors”. In: *The European Physical Journal B - Condensed Matter and Complex Systems* 37.3 (2004), pp. 349–361. DOI: 10.1140/epjb/e2004-00066-4 (cit. on pp. 2, 3, 36, 51, 56, 62).

[29] Sungkit Yip. “Weak link between conventional and unconventional superconductors”. In: *Journal of Low Temperature Physics* 91.3-4 (May 1993), pp. 203–218. DOI: 10.1007/BF00120849 (cit. on pp. 2, 3, 51).

[30] Sungkit Yip. “Josephson current-phase relationships with unconventional superconductors”. In: *Physical Review B* 52.5 (Aug. 1995), 3087–3090. DOI: 10.1103/physrevb.52.3087 (cit. on p. 2).

[31] Yasuhiro Asano. “Direct-current Josephson effect in SNS junctions of anisotropic superconductors”. In: *Physical Review B* 64.22 (Nov. 2001). DOI: 10.1103/PhysRevB.64.224515 (cit. on pp. 2, 32, 51).

[32] T. Löfwander, V. S. Shumeiko, and G. Wendin. “Andreev bound states in high-T_c superconducting junctions”. In: *Supercond. Sci. Technol.* 14.5 (Apr. 2001), R53–R77. DOI: 10.1088/0953-2048/14/5/201 (cit. on p. 2).

[33] Yukio Tanaka. “Josephson effect between s wave and $d_{x^2-y^2}$ wave superconductors”. In: *Physical Review Letters* 72.24 (June 1994), 3871–3874. DOI: 10.1103/physrevlett.72.3871 (cit. on p. 2).

[34] Alexandre M. Zagoskin. “The half-periodic Josephson effect in an s-wave superconductor - normal-metal - d-wave superconductor junction”. In: *J. Phys.: Condens. Matter* 9.31 (Aug. 1997), L419–L426. DOI: 10.1088/0953-8984/9/31/001 (cit. on p. 2).

[35] Nobukatsu Yoshida, Yukio Tanaka, Satoshi Kashiwaya, and Junichiro Inoue. “Theory of the AC Josephson effect in triplet superconducting junction”. In: *Journal of Low Temperature Physics* 117.3-4 (1999), pp. 563–567. DOI: 10.1023/A:1022587615448 (cit. on pp. 2, 3, 51).

[36] Yasuhiro Asano, Yukio Tanaka, Manfred Sigrist, and Satoshi Kashiwaya. “Josephson current in s -wave-superconductor/ Sr_2RuO_4 junctions”. In: *Phys. Rev. B* 67.18 (May 2003). DOI: 10.1103/physrevb.67.184505 (cit. on pp. 2, 3, 51).

[37] V. B. Geshkenbein and A. I. Larkin. “The Josephson effect in superconductors with heavy fermions”. In: *JETP Letters* 43.6 (Mar. 1986), 395–399 (cit. on p. 2).

[38] M. Sigrist. “Time-Reversal Symmetry Breaking States in High-Temperature Superconductors”. In: *Progress of Theoretical Physics* 99.6 (June 1998), 899–929. DOI: 10.1143/ptp.99.899 (cit. on p. 2).

[39] Satoshi Kashiwaya and Yukio Tanaka. “Tunnelling effects on surface bound states in unconventional superconductors”. In: *Reports on Progress in Physics* 63.10 (2000), p. 1641. DOI: 10.1088/0034-4885/63/10/202 (cit. on p. 2).

[40] E. Il’ichev, M. Grajcar, R. Hlubina, et al. “Degenerate Ground State in a Mesoscopic $YBa_2Cu_3O_{7-x}$ Grain Boundary Josephson Junction”. In: *Physical Review Letters* 86.23 (June 2001), 5369–5372. DOI: 10.1103/physrevlett.86.5369 (cit. on p. 2).

[41] Satoshi Kashiwaya, Hiromi Kashiwaya, Hiroshi Kambara, et al. “Edge States of Sr_2RuO_4 Detected by In-Plane Tunneling Spectroscopy”. In: *Phys. Rev. Lett.* 107 (Aug. 2011), p. 077003. DOI: 10.1103/PhysRevLett.107.077003 (cit. on p. 2).

[42] Lars Elster, Christian Platt, Ronny Thomale, Werner Hanke, and Ewelina M. Hankiewicz. “Accessing topological superconductivity via a combined STM and renormalization group analysis”. In: *Nat Comms* 6 (Sept. 2015), p. 8232. DOI: 10.1038/ncomms9232 (cit. on p. 2).

[43] P. J. Turner, R. Harris, S. Kamal, et al. “Observation of Weak-Limit Quasiparticle Scattering via Broadband Microwave Spectroscopy of a d-Wave Superconductor”. In: *Physical Review Letters* 90.23 (June 2003). DOI: 10.1103/physrevlett.90.237005 (cit. on p. 2).

[44] K. Sengupta and Victor M. Yakovenko. “Spontaneous Spin Accumulation in Singlet-Triplet Josephson Junctions”. In: *Phys. Rev. Lett.* 101 (Oct. 2008), p. 187003. DOI: 10.1103/PhysRevLett.101.187003 (cit. on pp. 3, 51, 52, 58, 63, 65, 66).

[45] Alfonso Romano, Paola Gentile, Canio Noce, Ilya Vekhter, and Mario Cuoco. “Control of magnetism in singlet-triplet superconducting heterostructures”. In: *Physical Review B* 93.1 (Jan. 2016). DOI: 10.1103/physrevb.93.014510 (cit. on p. 3).

[46] P. Zeeman. “The Effect of Magnetisation on the Nature of Light Emitted by a Substance”. In: *Nature* 55.1424 (Feb. 1897), 347–347. DOI: 10.1038/055347a0 (cit. on p. 3).

[47] G. E. Uhlenbeck and S. Goudsmit. “Spinning Electrons and the Structure of Spectra”. In: *Nature* 117.2938 (Feb. 1926), 264–265. DOI: 10.1038/117264a0 (cit. on p. 3).

[48] F. S. Bergeret, P. Virtanen, T. T. Heikkilä, and J. C. Cuevas. “Theory of Microwave-Assisted Supercurrent in Quantum Point Contacts”. In: *Physical Review Letters* 105.11 (Sept. 2010). DOI: 10.1103/physrevlett.105.117001 (cit. on p. 3).

[49] F. S. Bergeret, P. Virtanen, A. Ozaeta, T. T. Heikkilä, and J. C. Cuevas. “Supercurrent and Andreev bound state dynamics in superconducting quantum point contacts under microwave irradiation”. In: *Physical Review B* 84.5 (Aug. 2011). DOI: 10.1103/physrevb.84.054504 (cit. on p. 3).

[50] L. Bretheau, C. Ö. Girit, H. Pothier, D. Esteve, and C. Urbina. “Exciting Andreev pairs in a superconducting atomic contact”. In: *Nature* 499.7458 (July 2013), pp. 312–315. DOI: 10.1038/nature12315 (cit. on pp. 3, 24).

[51] L. Bretheau, Ç. Ö. Girit, C. Urbina, D. Esteve, and H. Pothier. “Supercurrent Spectroscopy of Andreev States”. In: *Phys. Rev. X* 3 (Dec. 2013), p. 041034. DOI: 10.1103/PhysRevX.3.041034 (cit. on p. 3).

[52] L. Bretheau, Ç. Ö. Girit, M. Houzet, et al. “Theory of microwave spectroscopy of Andreev bound states with a Josephson junction”. In: *Physical Review B* 90.13 (Oct. 2014). DOI: 10.1103/physrevb.90.134506 (cit. on pp. 3, 24).

[53] C. Janvier, L. Tosi, L. Bretheau, et al. “Coherent manipulation of Andreev states in superconducting atomic contacts”. In: *Science* 349.6253 (2015), pp. 1199–1202. DOI: 10.1126/science.aab2179 (cit. on pp. 4, 24).

[54] J. Michelsen, V. S. Shumeiko, and G. Wendin. “Manipulation with Andreev states in spin active mesoscopic Josephson junctions”. In: *Phys. Rev. B* 77 (May 2008), p. 184506. DOI: 10.1103/PhysRevB.77.184506 (cit. on p. 4).

[55] S. Teber, C. Holmqvist, and M. Fogelström. “Transport and magnetization dynamics in a superconductor/single-molecule magnet/superconductor junction”. In: *Phys. Rev. B* 81 (May 2010), p. 174503. DOI: 10.1103/PhysRevB.81.174503 (cit. on pp. 4, 6).

[56] W. Heisenberg. “Mehrkörperproblem und Resonanz in der Quantenmechanik”. German. In: *Z. Physik* 38.6-7 (June 1926), 411–426. DOI: 10.1007/bf01397160 (cit. on p. 4).

[57] P. A. M. Dirac. “On the Theory of Quantum Mechanics”. In: *Proceedings of the Royal Society A: Mathematical, Physical and Engineering Sciences* 112.762 (Oct. 1926), 661–677. DOI: 10.1098/rspa.1926.0133 (cit. on p. 4).

[58] J. M. D. Coey and M. Venkatesan. “Half-metallic ferromagnetism: Example of CrO_2 (invited)”. In: *Journal of Applied Physics* 91.10 (2002), p. 8345. DOI: 10.1063/1.1447879 (cit. on p. 4).

[59] M. N. Baibich, J. M. Broto, A. Fert, et al. “Giant Magnetoresistance of (001)Fe/(001)Cr Magnetic Superlattices”. In: *Physical Review Letters* 61.21 (Nov. 1988), 2472–2475. DOI: 10.1103/physrevlett.61.2472 (cit. on p. 5).

[60] G. Binasch, P. Grünberg, F. Saurenbach, and W. Zinn. “Enhanced magnetoresistance in layered magnetic structures with antiferromagnetic interlayer exchange”. In: *Physical Review B* 39.7 (Mar. 1989), 4828–4830. DOI: 10.1103/physrevb.39.4828 (cit. on p. 5).

[61] M. Julliere. “Tunneling between ferromagnetic films”. In: *Physics Letters A* 54.3 (Sept. 1975), 225–226. DOI: 10.1016/0375-9601(75)90174-7 (cit. on p. 5).

[62] S. V. Vonsovskii (Eds.) *Ferromagnetic Resonance. The Phenomenon of Resonant Absorption of a High-Frequency Magnetic Field in Ferromagnetic Substances*. Elsevier, 1966 (cit. on pp. 5, 24).

[63] J. H. E. Griffiths. “Anomalous High-frequency Resistance of Ferromagnetic Metals”. In: *Nature* 158.4019 (Nov. 1946), 670–671. DOI: 10.1038/158670a0 (cit. on pp. 5, 24).

[64] E. K. Zavoiskii. In: *J. Phys. USSR* 10 (1946), p. 197 (cit. on pp. 5, 24).

[65] I. I. Rabi. “Space Quantization in a Gyrating Magnetic Field”. In: *Physical Review* 51.8 (Apr. 1937), 652–654. DOI: 10.1103/physrev.51.652 (cit. on p. 5).

[66] I. I. Rabi, J. R. Zacharias, S. Millman, and P. Kusch. “A New Method of Measuring Nuclear Magnetic Moment”. In: *Physical Review* 53.4 (Feb. 1938), 318–318. DOI: 10.1103/physrev.53.318 (cit. on p. 5).

[67] S. Al’tshuler, E. Zavoisky, and B. Kozyrev. In: *Zh. Eksp. Teor. Fiz.* 14 (1944), p. 407 (cit. on p. 5).

[68] F. Bloch, W. W. Hansen, and Martin Packard. “Nuclear Induction”. In: *Physical Review* 69.3-4 (Feb. 1946), 127–127. DOI: 10.1103/physrev.69.127 (cit. on p. 5).

[69] F. Bloch, W. W. Hansen, and M. Packard. “The Nuclear Induction Experiment”. In: *Physical Review* 70.7-8 (Oct. 1946), 474–485. DOI: 10.1103/physrev.70.474 (cit. on p. 5).

[70] E. M. Purcell, H. C. Torrey, and R. V. Pound. “Resonance Absorption by Nuclear Magnetic Moments in a Solid”. In: *Physical Review* 69.1-2 (Jan. 1946), 37–38. DOI: 10.1103/physrev.69.37 (cit. on p. 5).

[71] Charles Kittel. “On the Theory of Ferromagnetic Resonance Absorption”. In: *Physical Review* 73.2 (Jan. 1948), 155–161. DOI: 10.1103/physrev.73.155 (cit. on pp. 5, 25).

[72] Yaroslav Tserkovnyak, Arne Brataas, and Gerrit E. W. Bauer. “Enhanced Gilbert Damping in Thin Ferromagnetic Films”. In: *Physical Review Letters* 88.11 (Feb. 2002). DOI: 10.1103/physrevlett.88.117601 (cit. on pp. 5, 27, 91, 120).

[73] Yaroslav Tserkovnyak, Arne Brataas, and Gerrit E. W. Bauer. “Spin pumping and magnetization dynamics in metallic multilayers”. In: *Physical Review B* 66.22 (Dec. 2002). DOI: 10.1103/physrevb.66.224403 (cit. on pp. 5, 28).

[74] M. V. Costache, M. Sladkov, S. M. Watts, C. H. van der Wal, and B. J. van Wees. “Electrical Detection of Spin Pumping due to the Precessing Magnetization of a Single Ferromagnet”. In: *Physical Review Letters* 97.21 (Nov. 2006). DOI: 10.1103/physrevlett.97.216603 (cit. on pp. 5, 29, 92).

[75] Y. Pu, P. M. Odenthal, R. Adur, et al. “Ferromagnetic Resonance Spin Pumping and Electrical Spin Injection in Silicon-Based Metal-Oxide-Semiconductor Heterostructures”. In: *Physical Review Letters* 115.24 (Dec. 2015). DOI: 10.1103/physrevlett.115.246602 (cit. on p. 5).

[76] J. C. Slonczewski. “Current-driven excitation of magnetic multilayers”. In: *Journal of Magnetism and Magnetic Materials* 159.1-2 (June 1996), L1–L7. DOI: 10.1016/0304-8853(96)00062-5 (cit. on pp. 5, 27, 28).

[77] L. Berger. “Emission of spin waves by a magnetic multilayer traversed by a current”. In: *Physical Review B* 54.13 (Oct. 1996), 9353–9358. DOI: 10.1103/physrevb.54.9353 (cit. on pp. 5, 27).

[78] E. B. Myers. “Current-Induced Switching of Domains in Magnetic Multilayer Devices”. In: *Science* 285.5429 (Aug. 1999), 867–870. DOI: 10.1126/science.285.5429.867 (cit. on pp. 5, 27).

[79] D. C. Ralph and M. D. Stiles. “Spin transfer torques”. In: *Journal of Magnetism and Magnetic Materials* 320.7 (Apr. 2008), 1190–1216. DOI: 10.1016/j.jmmm.2007.12.019 (cit. on pp. 5, 27).

[80] S. A. Wolf. “Spintronics: A Spin-Based Electronics Vision for the Future”. In: *Science* 294.5546 (Nov. 2001), 1488–1495. DOI: 10.1126/science.1065389 (cit. on p. 5).

[81] Igor Žutić, Jaroslav Fabian, and S. Das Sarma. “Spintronics: Fundamentals and applications”. In: *Rev. Mod. Phys.* 76.2 (Apr. 2004), 323–410. DOI: 10.1103/revmodphys.76.323 (cit. on p. 5).

[82] Dai Aoki, Frédéric Hardy, Atsushi Miyake, et al. “Properties of ferromagnetic superconductors”. In: *Comptes Rendus Physique* 12.5-6 (June 2011), 573–583. DOI: 10.1016/j.crhy.2011.04.007 (cit. on pp. 5, 17).

[83] Dai Aoki, Andrew Huxley, Eric Ressouche, et al. “Coexistence of superconductivity and ferromagnetism in URhGe”. In: *Nature* 413.6856 (Oct. 2001), 613–616. DOI: 10.1038/35098048 (cit. on p. 5).

[84] F. Levy. “Magnetic Field-Induced Superconductivity in the Ferromagnet URhGe”. In: *Science* 309.5739 (Aug. 2005), 1343–1346. DOI: 10.1126/science.1115498 (cit. on p. 5).

[85] S. S. Saxena, P. Agarwal, K. Ahilan, et al. “Superconductivity on the border of itinerant-electron ferromagnetism in UGe_2”. In: *Nature* 406.6796 (Aug. 2000), 587–592. DOI: 10.1038/35020500 (cit. on p. 5).

[86] P. M. Tedrow and R. Meservey. “Spin-Dependent Tunneling into Ferromagnetic Nickel”. In: *Physical Review Letters* 26.4 (Jan. 1971), 192–195. DOI: 10.1103/physrevlett.26.192 (cit. on p. 6).

[87] R. Meservey and P. M. Tedrow. “Spin-polarized electron tunneling”. In: *Physics Reports* 238.4 (Mar. 1994), 173–243. DOI: 10.1016/0370-1573(94)90105-8 (cit. on p. 6).

[88] R. J. Soulen Jr. “Measuring the Spin Polarization of a Metal with a Superconducting Point Contact”. In: *Science* 282.5386 (Oct. 1998), 85–88. DOI: 10.1126/science.282.5386.85 (cit. on p. 6).

[89] M. J. M. de Jong and C. W. J. Beenakker. “Andreev Reflection in Ferromagnet-Superconductor Junctions”. In: *Physical Review Letters* 74.9 (Feb. 1995), 1657–1660. DOI: 10.1103/physrevlett.74.1657 (cit. on pp. 6, 91, 122).

[90] M. Giroud, H. Courtois, K. Hasselbach, D. Mailly, and B. Pannetier. “Superconducting proximity effect in a mesoscopic ferromagnetic wire”. In: *Physical Review B* 58.18 (Nov. 1998), R11872–R11875. DOI: 10.1103/physrevb.58.r11872 (cit. on p. 6).

[91] V. T. Petrashov, I. A. Sosnin, I. Cox, A. Parsons, and C. Troadec. “Giant Mutual Proximity Effects in Ferromagnetic/Superconducting Nanostructures”. In: *Physical Review Letters* 83.16 (Oct. 1999), 3281–3284. DOI: 10.1103/physrevlett.83.3281 (cit. on p. 6).

[92] F. S. Bergeret, A. F. Volkov, and K. B. Efetov. “Long-Range Proximity Effects in Superconductor-Ferromagnet Structures”. In: *Physical Review Letters* 86.18 (Apr. 2001), 4096–4099. DOI: 10.1103/physrevlett.86.4096 (cit. on pp. 6, 91).

[93] F. S. Bergeret, A. F. Volkov, and K. B. Efetov. “Josephson current in superconductor-ferromagnet structures with a nonhomogeneous magnetization”. In: *Physical Review B* 64.13 (Sept. 2001). DOI: 10.1103/physrevb.64.134506 (cit. on pp. 6, 91).

[94] M. Houzet and A. I. Buzdin. “Long range triplet Josephson effect through a ferromagnetic trilayer”. In: *Physical Review B* 76.6 (Aug. 2007). DOI: 10.1103/physrevb.76.060504 (cit. on pp. 6, 91).

[95] V. Braude and Yu. V. Nazarov. “Fully Developed Triplet Proximity Effect”. In: *Physical Review Letters* 98.7 (Feb. 2007). DOI: 10.1103/physrevlett.98.077003 (cit. on pp. 6, 91).

[96] B. Crouzy, S. Tollis, and D. A. Ivanov. “Josephson current in a superconductor-ferromagnet junction with two noncollinear magnetic domains”. In: *Physical Review B* 75.5 (Feb. 2007). DOI: 10.1103/physrevb.75.054503 (cit. on pp. 6, 91).

[97] A. F. Volkov and K. B. Efetov. “Odd spin-triplet superconductivity in a multilayered superconductor-ferromagnet Josephson junction”. In: *Physical Review B* 81.14 (Apr. 2010). DOI: 10.1103/physrevb.81.144522 (cit. on pp. 6, 91).

[98] N. Banerjee, J.W.A. Robinson, and M. G. Blamire. “Reversible control of spin-polarized supercurrents in ferromagnetic Josephson junctions”. In: *Nat Comms* 5 (Aug. 2014), p. 4771. DOI: 10.1038/ncomms5771 (cit. on p. 6).

[99] Klaus Halterman, Oriol T. Valls, and Chien-Te Wu. “Charge and spin currents in ferromagnetic Josephson junctions”. In: *Physical Review B* 92.17 (Nov. 2015). DOI: 10.1103/physrevb.92.174516 (cit. on pp. 6, 91).

[100] R. S. Keizer, S. T. B. Goennenwein, T. M. Klapwijk, et al. “A spin triplet supercurrent through the half-metallic ferromagnet CrO_2”. In: *Nature* 439.7078 (Feb. 2006), 825–827. DOI: 10.1038/nature04499 (cit. on pp. 6, 91).

[101] J. W. A. Robinson, J. D. S. Witt, and M. G. Blamire. “Controlled Injection of Spin-Triplet Supercurrents into a Strong Ferromagnet”. In: *Science* 329.5987 (June 2010), 59–61. DOI: 10.1126/science.1189246 (cit. on p. 6).

[102] Trupti S. Khaire, Mazin A. Khasawneh, W. P. Pratt, and Norman O. Birge. “Observation of Spin-Triplet Superconductivity in Co-Based Josephson Junctions”. In: *Physical Review Letters* 104.13 (Mar. 2010). DOI: 10.1103/physrevlett.104.137002 (cit. on pp. 6, 91).

[103] Mazin A. Khasawneh, Trupti S. Khaire, Carolin Klose, William P. Pratt Jr., and Norman O. Birge. “Spin-triplet supercurrent in Co-based Josephson junctions”. In: *Supercond. Sci. Technol.* 24.2 (Jan. 2011), p. 024005. DOI: 10.1088/0953-2048/24/2/024005 (cit. on pp. 6, 91).

[104] A. Singh, S. Voltan, K. Lahabi, and J. Aarts. “Colossal Proximity Effect in a Superconducting Triplet Spin Valve Based on the Half-Metallic Ferromagnet CrO_2”. In: *Physical Review X* 5.2 (May 2015). DOI: 10.1103/physrevx.5.021019 (cit. on p. 6).

[105] J. Linder and Jason W. A. Robinson. “Superconducting spintronics”. In: *Nature Physics* 11.4 (Apr. 2015), 307–315. DOI: 10.1038/nphys3242 (cit. on pp. 6, 93).

[106] Matthias Eschrig. “Spin-polarized supercurrents for spintronics: a review of current progress”. In: *Reports on Progress in Physics* 78.10 (Sept. 2015), p. 104501. DOI: 10.1088/0034-4885/78/10/104501 (cit. on p. 6).

[107] C. Holmqvist, S. Teber, and M. Fogelström. “Nonequilibrium effects in a Josephson junction coupled to a precessing spin”. In: *Phys. Rev. B* 83.10 (Mar. 2011). DOI: 10.1103/physrevb.83.104521 (cit. on p. 6).

[108] F. Konschelle and A. Buzdin. “Magnetic Moment Manipulation by a Josephson Current”. In: *Physical Review Letters* 102.1 (Jan. 2009). DOI: 10.1103/physrevlett.102.017001 (cit. on p. 6).

[109] N. G. Pugach and A. I. Buzdin. “Magnetic moment manipulation by triplet Josephson current”. In: *Applied Physics Letters* 101.24 (2012), p. 242602. DOI: 10.1063/1.4769900 (cit. on pp. 6, 91).

[110] Jacob Linder and Takehito Yokoyama. “Supercurrent-induced magnetization dynamics in a Josephson junction with two misaligned ferromagnetic layers”. In: *Physical Review B* 83.1 (Jan. 2011). DOI: 10.1103/physrevb.83.012501 (cit. on p. 6).

[111] S. Hikino, M. Mori, S. Takahashi, and S. Maekawa. “Microwave-induced supercurrent in a ferromagnetic Josephson junction”. In: *Supercond. Sci. Technol.* 24.2 (Jan. 2011), p. 024008. DOI: 10.1088/0953-2048/24/2/024008 (cit. on p. 6).

[112] Mircea Trif and Yaroslav Tserkovnyak. “Dynamic Magnetoelectric Effect in Ferromagnet/Superconductor Tunnel Junctions”. In: *Physical Review Letters* 111.8 (Aug. 2013). DOI: 10.1103/physrevlett.111.087602 (cit. on pp. 6, 7, 98, 130, 134).

[113] T. Moriyama, R. Cao, X. Fan, et al. “Tunnel Barrier Enhanced Voltage Signal Generated by Magnetization Precession of a Single Ferromagnetic Layer”. In: *Physical Review Letters* 100.6 (Feb. 2008). DOI: 10.1103/physrevlett.100.067602 (cit. on pp. 6, 29, 92).

[114] Jiang Xiao, Gerrit E. W. Bauer, and Arne Brataas. “Charge pumping in magnetic tunnel junctions: Scattering theory”. In: *Physical Review B* 77.18 (May 2008). DOI: 10.1103/physrevb.77.180407 (cit. on p. 6).

[115] Y. Tserkovnyak, T. Moriyama, and J. Q. Xiao. “Tunnel-barrier-enhanced dc voltage signals induced by magnetization dynamics in magnetic tunnel junctions”. In: *Physical Review B* 78.2 (July 2008). DOI: 10.1103/physrevb.78.020401 (cit. on pp. 6, 29, 98, 120, 121).

[116] F. W. J. Hekking and Yu. V. Nazarov. “Interference of two electrons entering a superconductor”. In: *Physical Review Letters* 71.10 (Sept. 1993), 1625–1628. DOI: 10.1103/physrevlett.71.1625 (cit. on p. 7).

[117] F. W. J. Hekking and Yu. V. Nazarov. “Subgap conductivity of a superconductor–normal-metal tunnel interface”. In: *Physical Review B* 49.10 (Mar. 1994), 6847–6852. DOI: 10.1103/physrevb.49.6847 (cit. on pp. 7, 131, 144, 153, 154).

[118] Pierre-Gilles de Gennes. *Superconductivity of metals and alloys*. Frontiers in physics ; 24. New York: Benjamin, 1966. DOI: 10.1016/0375-9474(67)90080-2 (cit. on pp. 12, 20, 31, 32).

[119] M. Tinkham. *Introduction to Superconductivity: Second Edition*. Dover Books on Physics. Dover Publications, 2004 (cit. on p. 12).

[120] N. N. Bogoliubov. "On a new method in the theory of superconductivity". In: *Il Nuovo Cimento (1955-1965)* 7.6 (1958), pp. 794–805. DOI: 10.1007/BF02745585 (cit. on pp. 13, 19, 20, 31, 36).

[121] Vladimir P. Mineev and K. V. Samokhin. *Introduction to unconventional superconductivity*. Originally published in Russian as 'Vvedenie v teoriiu neobychnoĭ sverkhprovodimosti' : Moscow : MFTI, 1998. Amsterdam, The Netherlands: Gordon and Breach Science Publishers, 1999 (cit. on pp. 14, 15, 32, 54).

[122] Liang Fu, C. L. Kane, and E. J. Mele. "Topological Insulators in Three Dimensions". In: *Phys. Rev. Lett.* 98 (Mar. 2007), p. 106803. DOI: 10.1103/PhysRevLett.98.106803 (cit. on p. 15).

[123] Markus König, Steffen Wiedmann, Christoph Brüne, et al. "Quantum Spin Hall Insulator State in HgTe Quantum Wells". In: *Science* 318.5851 (2007), pp. 766–770. DOI: 10.1126/science.1148047 (cit. on p. 15).

[124] M. Z. Hasan and C. L. Kane. "*Colloquium* : Topological insulators". In: *Rev. Mod. Phys.* 82 (Nov. 2010), pp. 3045–3067. DOI: 10.1103/RevModPhys.82.3045 (cit. on p. 15).

[125] Shinsei Ryu, Andreas P. Schnyder, Akira Furusaki, and Andreas W. W. Ludwig. "Topological insulators and superconductors: tenfold way and dimensional hierarchy". In: *New Journal of Physics* 12 (June 2010). DOI: 10.1088/1367-2630/12/6/065010 (cit. on p. 15).

[126] Ching-Kai Chiu, Jeffrey C. Y. Teo, Andreas P. Schnyder, and Shinsei Ryu. "Classification of topological quantum matter with symmetries". In: (May 2015). arXiv: 1505.03535 (cit. on p. 15).

[127] Ettore Majorana. "Teoria simmetrica dell'elettrone e del positrone". Italian. In: *Il Nuovo Cimento* 14.4 (1937), pp. 171–184. DOI: 10.1007/BF02961314 (cit. on pp. 15, 17).

[128] G. R. Stewart. "Superconductivity in iron compounds". In: *Rev. Mod. Phys.* 83.4 (Dec. 2011), 1589–1652. DOI: 10.1103/revmodphys.83.1589 (cit. on p. 17).

[129] Yuval Oreg, Gil Refael, and Felix von Oppen. "Helical Liquids and Majorana Bound States in Quantum Wires". In: *Phys. Rev. Lett.* 105 (Oct. 2010), p. 177002. DOI: 10.1103/PhysRevLett.105.177002 (cit. on p. 17).

[130] Roman M. Lutchyn, Jay D. Sau, and S. Das Sarma. "Majorana Fermions and a Topological Phase Transition in Semiconductor-Superconductor Heterostructures". In: *Phys. Rev. Lett.* 105 (Aug. 2010), p. 077001. DOI: 10.1103/PhysRevLett.105.077001 (cit. on p. 17).

[131] V. Mourik, K. Zuo, S. M. Frolov, et al. “Signatures of Majorana Fermions in Hybrid Superconductor-Semiconductor Nanowire Devices”. In: *Science* 336.6084 (2012), pp. 1003–1007. DOI: 10.1126/science.1222360 (cit. on p. 18).

[132] Alexandre M. Zagoskin. *Quantum Theory of Many-Body Systems*. Springer New York, 1998. DOI: 10.1007/978-1-4612-0595-1 (cit. on pp. 19, 20).

[133] C. W. J. Beenakker. “Universal limit of critical-current fluctuations in mesoscopic Josephson junctions”. In: *Phys. Rev. Lett.* 67 (Dec. 1991), pp. 3836–3839. DOI: 10.1103/PhysRevLett.67.3836 (cit. on pp. 20, 22, 39, 61, 171, 175).

[134] C. W. J. Beenakker. “Three ‘universal’ mesoscopic Josephson effects”. In: *Transport Phenomena in Mesoscopic Systems. Proceedings of the 14th Taniguchi Symposium*. Ed. by H. Fukuyama and T. Ando. Transport Phenomena in Mesoscopic Systems. 14th Taniguchi Symposium, 10-14 Nov. 1991, Shima, Japan. Berlin, Germany: Springer-Verlag, 1992, 235–53. DOI: 10.1007/978-3-642-84818-6_22 (cit. on pp. 20, 39, 54, 172).

[135] C. W. J. Beenakker. “Random-matrix theory of quantum transport”. In: *Reviews of Modern Physics* 69.3 (July 1997), pp. 731–808. DOI: 10.1103/RevModPhys.69.731 (cit. on pp. 20, 39, 171, 176).

[136] Yuli V. Nazarov and Yaroslav M. Blanter. *Quantum transport: introduction to nanoscience*. Cambridge: Cambridge Univ. Press, 2009. DOI: 10.1080/00107510903282549 (cit. on pp. 20, 36, 39).

[137] I. O. Kulik. “Macroscopic quantization and proximity effect in S-N-S junctions”. In: *Soviet Physics JETP-USSR* 30.5 (1970), p. 944 (cit. on p. 22).

[138] I. O. Kulik and A. G. Omelyanchuk. “Properties of Superconducting Microbridges in the Pure Limit”. In: *Sov. J. Low Temp. Phys.* 3 (1978), pp. 459–461 (cit. on p. 22).

[139] P. W. Anderson and J. M. Rowell. “Probable Observation of the Josephson Superconducting Tunneling Effect”. In: *Physical Review Letters* 10.6 (Mar. 1963), 230–232. DOI: 10.1103/physrevlett.10.230 (cit. on p. 23).

[140] T. A. Fulton and R. C. Dynes. “Current-Phase Relations in Superconducting Bridges”. In: *Physical Review Letters* 25.12 (Sept. 1970), 794–797. DOI: 10.1103/physrevlett.25.794 (cit. on p. 24).

[141] L. D. Jackel, R. A. Buhrman, and W. W. Webb. “Direct measurement of current-phase relations in superconducting weak links”. In: *Physical Review B* 10.7 (Oct. 1974), 2782–2785. DOI: 10.1103/physrevb.10.2782 (cit. on p. 24).

[142] Robert Rifkin and Bascom S. Deaver. “Current-phase relation and phase-dependent conductance of superconducting point contacts from rf impedance measurements”. In: *Phys. Rev. B* 13 (May 1976), pp. 3894–3901. DOI: 10.1103/PhysRevB.13.3894 (cit. on p. 24).

[143] M. L. Della Rocca, M. Chauvin, B. Huard, et al. “Measurement of the Current-Phase Relation of Superconducting Atomic Contacts”. In: *Physical Review Letters* 99.12 (Sept. 2007). DOI: 10.1103/physrevlett.99.127005 (cit. on p. 24).

[144] Charles Kittel. “Interpretation of Anomalous Larmor Frequencies in Ferromagnetic Resonance Experiment”. In: *Physical Review* 71.4 (Feb. 1947), 270–271. DOI: 10.1103/physrev.71.270.2 (cit. on p. 25).

[145] C. Kittel. *Introduction to Solid State Physics*. Wiley, 2004 (cit. on p. 25).

[146] T. L. Gilbert. “A Lagrangian Formulation of the Gyromagnetic Equation of the Magnetization Field”. In: *Phys. Rev.* 100 (1955), p. 1243 (cit. on p. 26).

[147] L. D. Landau and E. Lifshitz. “On the theory of the dispersion of magnetic permeability in ferromagnetic bodies”. In: *Phys. Z. Sowjet.* 8 (1935), p. 153 (cit. on p. 26).

[148] Takao Iwata. “A thermodynamical approach to the irreversible magnetization in single-domain particles”. In: *Journal of Magnetism and Magnetic Materials* 31-34 (Feb. 1983), 1013–1014. DOI: 10.1016/0304-8853(83)90774-6 (cit. on p. 26).

[149] D. D. Stancil and A. Prabhakar. *Spin Waves: Theory and Applications*. Springer US, 2009. DOI: 10.1007/978-0-387-77865-5 (cit. on p. 26).

[150] O. Mosendz, J. E. Pearson, F. Y. Fradin, et al. “Quantifying Spin Hall Angles from Spin Pumping: Experiments and Theory”. In: *Physical Review Letters* 104.4 (Jan. 2010). DOI: 10.1103/physrevlett.104.046601 (cit. on pp. 27, 30).

[151] Y. Guan, W. E. Bailey, E. Vescovo, C.-C. Kao, and D. A. Arena. “Phase and amplitude of element-specific moment precession in $Ni_{81}Fe_{19}$”. In: *Journal of Magnetism and Magnetic Materials* 312.2 (May 2007), 374–378. DOI: 10.1016/j.jmmm.2006.10.1111 (cit. on p. 27).

[152] A. G. Aronov and G. E. Pikus. “Spin Injection into semiconductors”. In: *Soviet Physics Semiconductors-USSR* 10.6 (1976), 698–700 (cit. on p. 27).

[153] M. Johnson and R. H. Silsbee. “Interfacial charge-spin coupling: Injection and detection of spin magnetization in metals”. In: *Physical Review Letters* 55.17 (Oct. 1985), 1790–1793. DOI: 10.1103/physrevlett.55.1790 (cit. on p. 27).

[154] M. Johnson and R. H. Silsbee. “Spin-injection experiment”. In: *Physical Review B* 37.10 (Apr. 1988), 5326–5335. DOI: 10.1103/physrevb.37.5326 (cit. on p. 27).

[155] Arne Brataas, Yu. V. Nazarov, and Gerrit E. W. Bauer. “Finite-Element Theory of Transport in Ferromagnet–Normal Metal Systems”. In: *Physical Review Letters* 84.11 (Mar. 2000), 2481–2484. DOI: 10.1103/physrevlett.84.2481 (cit. on pp. 28, 119).

[156] K. Xia, P. J. Kelly, G. E. W. Bauer, A. Brataas, and I. Turek. “Spin torques in ferromagnetic/normal-metal structures”. In: *Physical Review B* 65.22 (May 2002). DOI: 10.1103/physrevb.65.220401 (cit. on p. 28).

[157] Arne Brataas, Yaroslav Tserkovnyak, Gerrit E. W. Bauer, and Bertrand I. Halperin. “Spin battery operated by ferromagnetic resonance”. In: *Physical Review B* 66.6 (Aug. 2002). DOI: 10.1103/physrevb.66.060404 (cit. on pp. 28, 92, 120).

[158] Xuhui Wang, Gerrit E. W. Bauer, Bart J. van Wees, Arne Brataas, and Yaroslav Tserkovnyak. “Voltage Generation by Ferromagnetic Resonance at a Nonmagnet to Ferromagnet Contact”. In: *Physical Review Letters* 97.21 (Nov. 2006). DOI: 10.1103/physrevlett.97.216602 (cit. on pp. 29, 161).

[159] J. Zhu, J. A. Katine, G. E. Rowlands, et al. “Voltage-Induced Ferromagnetic Resonance in Magnetic Tunnel Junctions”. In: *Physical Review Letters* 108.19 (May 2012). DOI: 10.1103/physrevlett.108.197203 (cit. on p. 29).

[160] M.I. Dyakonov and V.I. Perel. “Current-induced spin orientation of electrons in semiconductors”. In: *Physics Letters A* 35.6 (July 1971), 459–460. DOI: 10.1016/0375-9601(71)90196-4 (cit. on p. 29).

[161] M. I. D’yakonov and V. I. Perel’. “Possibility of Orienting Electron Spins with Current”. In: *Soviet Journal of Experimental and Theoretical Physics Letters* 13 (June 1971), p. 467 (cit. on p. 29).

[162] J. E. Hirsch. “Spin Hall Effect”. In: *Physical Review Letters* 83.9 (Aug. 1999), 1834–1837. DOI: 10.1103/physrevlett.83.1834 (cit. on p. 29).

[163] Y. K. Kato. “Observation of the Spin Hall Effect in Semiconductors”. In: *Science* 306.5703 (Dec. 2004), 1910–1913. DOI: 10.1126/science.1105514 (cit. on p. 29).

[164] E. Saitoh, M. Ueda, H. Miyajima, and G. Tatara. “Conversion of spin current into charge current at room temperature: Inverse spin-Hall effect”. In: *Applied Physics Letters* 88.18 (2006), p. 182509. DOI: 10.1063/1.2199473 (cit. on p. 30).

[165] Hui Zhao, Eric J. Loren, H. M. van Driel, and Arthur L. Smirl. “Coherence Control of Hall Charge and Spin Currents”. In: *Physical Review Letters* 96.24 (June 2006). DOI: 10.1103/physrevlett.96.246601 (cit. on p. 30).

[166] S. O. Valenzuela and M. Tinkham. “Direct electronic measurement of the spin Hall effect”. In: *Nature* 442.7099 (July 2006), 176–179. DOI: 10.1038/nature04937 (cit. on p. 30).

[167] K. Ando, Y. Kajiwara, S. Takahashi, et al. “Angular dependence of inverse spin–Hall effect induced by spin pumping investigated in a $Ni_{81}Fe_{19}$/Pt thin film”. In: *Physical Review B* 78.1 (July 2008). DOI: 10.1103/physrevb.78.014413 (cit. on p. 30).

[168] F. D. Czeschka, L. Dreher, M. S. Brandt, et al. “Scaling Behavior of the Spin Pumping Effect in Ferromagnet-Platinum Bilayers”. In: *Physical Review Letters* 107.4 (July 2011). DOI: 10.1103/physrevlett.107.046601 (cit. on p. 30).

[169] J. G. Valatin. “Comments on the theory of superconductivity”. In: *Il Nuovo Cimento (1955-1965)* 7.6 (1958), pp. 843–857. DOI: 10.1007/BF02745589 (cit. on p. 31).

[170] C. Bruder. “Andreev scattering in anisotropic superconductors”. In: *Phys. Rev. B* 41 (Mar. 1990), pp. 4017–4032. DOI: 10.1103/PhysRevB.41.4017 (cit. on pp. 32, 34, 35).

[171] Nikolai M. Chtchelkatchev and Yu. V. Nazarov. “Andreev Quantum Dots for Spin Manipulation”. In: *Physical Review Letters* 90.22 (June 2003). DOI: 10.1103/physrevlett.90.226806 (cit. on p. 36).

[172] Anthony J. Leggett. “A theoretical description of the new phases of liquid ^{3}He”. In: *Rev. Mod. Phys.* 47.2 (Apr. 1975), 331–414. DOI: 10.1103/revmodphys.47.331 (cit. on p. 36).

[173] M. V. Moskalets. *Scattering Matrix Approach to Non-Stationary Quantum Transport*. World Scientific Publishing Co, Sept. 2012. DOI: 10.1142/9781848168350_0001 (cit. on p. 36).

[174] R. Landauer. "Spatial Variation of Currents and Fields Due to Localized Scatterers in Metallic Conduction". In: *IBM Journal of Research and Development* 1.3 (July 1957), pp. 223–231. DOI: 10.1147/rd.13.0223 (cit. on pp. 36, 38, 112).

[175] Rolf Landauer. "Electrical resistance of disordered one-dimensional lattices". In: *Philosophical Magazine* 21.172 (Apr. 1970), 863–867. DOI: 10.1080/14786437008238472 (cit. on p. 36).

[176] M. Büttiker. "Four-Terminal Phase-Coherent Conductance". In: *Physical Review Letters* 57.14 (Oct. 1986), 1761–1764. DOI: 10.1103/physrevlett.57.1761 (cit. on p. 36).

[177] M. Büttiker. "Scattering theory of thermal and excess noise in open conductors". In: *Physical Review Letters* 65.23 (Dec. 1990), 2901–2904. DOI: 10.1103/physrevlett.65.2901 (cit. on p. 36).

[178] M. Büttiker. "Scattering theory of current and intensity noise correlations in conductors and wave guides". In: *Physical Review B* 46.19 (Nov. 1992), 12485–12507. DOI: 10.1103/physrevb.46.12485 (cit. on pp. 36, 38).

[179] Pier A. Mello and Narendra Kumar. *Quantum Transport in Mesoscopic Systems*. Oxford University Press (OUP), May 2004. DOI: 10.1093/acprof:oso/9780198525820.001.0001 (cit. on p. 38).

[180] L. P. Kadanoff and G. Baym. *Quantum statistical mechanics: Green's function methods in equilibrium and nonequilibrium problems*. Frontiers in physics. W. A. Benjamin, 1962. DOI: 10.1126/science.139.3553.399-b (cit. on p. 39).

[181] L. V. Keldysh. "Diagram technique for nonequilibrium processes". In: *Soviet Physics JETP-USSR* 20.4 (1965), p. 1018 (cit. on pp. 39, 42).

[182] J. Rammer and H. Smith. "Quantum field-theoretical methods in transport theory of metals". In: *Rev. Mod. Phys.* 58.2 (Apr. 1986), 323–359. DOI: 10.1103/revmodphys.58.323 (cit. on pp. 40, 41).

[183] Jørgen Rammer. *Quantum Field Theory of Non-Equilibrium States*. Cambridge: Cambridge Univ., 2007. DOI: 10.1017/CBO9780511618956 (cit. on p. 40).

[184] Julian Schwinger. "Brownian Motion of a Quantum Oscillator". In: *Journal of Mathematical Physics* 2.3 (1961), p. 407. DOI: 10.1063/1.1703727 (cit. on p. 40).

[185] S. Fujita. "Thermodynamic Evolution Equation for a Quantum Statistical Gas". In: *Journal of Mathematical Physics* 6.12 (1965), p. 1877. DOI: 10.1063/1.1704736 (cit. on p. 42).

[186] Shigeji Fujita. "Resolution of the Hierarchy of Green's Functions for Fermions". In: *Physical Review A* 4.3 (Sept. 1971), 1114–1122. DOI: 10.1103/physreva.4.1114 (cit. on p. 42).

[187] A. G. Hall. “Non-equilibrium Green functions: generalized Wick’s theorem and diagrammatic perturbation with initial correlations”. In: *Journal of Physics A: Mathematical and General* 8 (1975), p. 214. DOI: 10.1088/0305-4470/8/2/012 (cit. on p. 42).

[188] Y. A. Kukharenko and S. G. Tikhodeev. “Diagram technique in the theory of relaxation processes”. In: *Zhurnal Eksperimentalnoi i Teoreticheskoi Fiziki* 83 (1982), 1444–1456 (cit. on p. 42).

[189] A. I. Larkin and Y. N. Ovchinnikov. “Nonlinear conductivity of superconductors in mixed state”. Russian. In: *Zhurnal Eksperimentalnoi i Teoreticheskoi Fiziki* 68.5 (1975), 1915–1927 (cit. on p. 42).

[190] Karl Blum. “Density Matrix Theory and Applications”. In: *Springer Series on Atomic, Optical, and Plasma Physics* (2012). DOI: 10.1007/978-3-642-20561-3 (cit. on pp. 44, 46).

[191] U. Fano. “Description of States in Quantum Mechanics by Density Matrix and Operator Techniques”. In: *Rev. Mod. Phys.* 29.1 (Jan. 1957), 74–93. DOI: 10.1103/revmodphys.29.74 (cit. on p. 47).

[192] W. H. Louisell. *Quantum statistical properties of radiation*. Wiley Series in Pure and Applied Optics Series. John Wiley & Sons Canada, Limited, 1973 (cit. on p. 47).

[193] Yasuhiro Asano and Satoshi Yamano. “Josephson effect in noncentrosymmetric superconductor junctions”. In: *Physical Review B* 84.6 (Aug. 2011). DOI: 10.1103/PhysRevB.84.064526 (cit. on p. 51).

[194] Pablo Burset, Felix Keidel, Yukio Tanaka, Naoto Nagaosa, and Björn Trauzettel. “Transport signatures of superconducting hybrids with mixed singlet and chiral triplet states”. In: *Phys. Rev. B* 90.8 (Aug. 2014). DOI: 10.1103/physrevb.90.085438 (cit. on p. 51).

[195] Chi-Ken Lu and Sungkit Yip. “Spin current and spin accumulation near a Josephson junction between a singlet and triplet superconductor”. In: *Phys. Rev. B* 80.2 (July 2009). DOI: 10.1103/physrevb.80.024504 (cit. on p. 51).

[196] Suk Bum Chung, Joshua Horowitz, and Xiao-Liang Qi. “Time-reversal anomaly and Josephson effect in time-reversal-invariant topological superconductors”. In: *Physical Review B* 88.21 (Dec. 2013). DOI: 10.1103/physrevb.88.214514 (cit. on pp. 51, 62).

[197] Z. H. Yang, J. Wang, and K. S. Chan. “Spin accumulation in triplet Josephson junction”. In: *Journal of Physics: Condensed Matter* 23.8 (Mar. 2011), p. 085701. DOI: 10.1088/0953-8984/23/8/085701 (cit. on p. 51).

[198] Lars Elster, Manuel Houzet, and Julia S. Meyer. “Magnetic resonance in a singlet-triplet Josephson junction”. In: *Physical Review B* 93.10 (Mar. 2016). DOI: 10.1103/physrevb.93.104519 (cit. on pp. 52, 67, 69, 76, 82, 84, 85, 183, 190).

[199] I. J. Lee, M. J. Naughton, G. M. Danner, and P. M. Chaikin. “Anisotropy of the Upper Critical Field in $(TMTSF)_2PF_6$”. In: *Physical Review Letters* 78.18 (May 1997), 3555–3558. DOI: 10.1103/physrevlett.78.3555 (cit. on p. 52).

[200] I. J. Lee, P. M. Chaikin, and M. J. Naughton. “Exceeding the Pauli paramagnetic limit in the critical field of $(TMTSF)_2PF_6$”. In: *Phys. Rev. B* 62 (Dec. 2000), R14669–R14672. DOI: 10.1103/PhysRevB.62.R14669 (cit. on p. 52).

[201] M. Greenblatt, W. H. McCarroll, R. Neifeld, M. Croft, and J. V. Waszczak. “Quasi two-dimensional electronic properties of the lithium molybdenum bronze, $Li_{0.9}Mo_6O_{17}$”. In: *Solid State Communications* 51.9 (Sept. 1984), 671–674. DOI: 10.1016/0038-1098(84)90944-x (cit. on p. 52).

[202] A. G. Lebed and O. Sepper. “Possible triplet superconductivity in the quasi-one-dimensional conductor $Li_{0.9}Mo_6O_{17}$”. In: *Physical Review B* 87.10 (Mar. 2013). DOI: 10.1103/physrevb.87.100511 (cit. on p. 52).

[203] Jin-Ke Bao, Ji-Yong Liu, Cong-Wei Ma, et al. “Superconductivity in Quasi-One-Dimensional $K_2Cr_3As_3$ with Significant Electron Correlations”. In: *Physical Review X* 5.1 (Feb. 2015). DOI: 10.1103/physrevx.5.011013 (cit. on p. 52).

[204] Zhang-Tu Tang, Jin-Ke Bao, Yi Liu, et al. “Unconventional superconductivity in quasi-one-dimensional $Rb_2Cr_3As_3$”. In: *Physical Review B* 91.2 (Jan. 2015). DOI: 10.1103/physrevb.91.020506 (cit. on pp. 52, 53).

[205] J.-F. Mercure, A. F. Bangura, Xiaofeng Xu, et al. “Upper Critical Magnetic Field far above the Paramagnetic Pair-Breaking Limit of Superconducting One-Dimensional $Li_{0.9}Mo_6O_{17}$ Single Crystals”. In: *Physical Review Letters* 108.18 (May 2012). DOI: 10.1103/physrevlett.108.187003 (cit. on p. 52).

[206] E. A. Demler, G. B. Arnold, and M. R. Beasley. “Superconducting proximity effects in magnetic metals”. In: *Physical Review B* 55.22 (June 1997), 15174–15182. DOI: 10.1103/physrevb.55.15174 (cit. on p. 53).

[207] A. I. Buzdin. “Proximity effects in superconductor-ferromagnet heterostructures”. In: *Rev. Mod. Phys.* 77.3 (Sept. 2005), 935–976. DOI: 10.1103/revmodphys.77.935 (cit. on p. 53).

[208] Matthias Eschrig. “Spin-polarized supercurrents for spintronics”. In: *Physics Today* 64.1 (2011), p. 43. DOI: 10.1063/1.3541944 (cit. on p. 53).

[209] K. K. Likharev. “Superconducting weak links”. In: *Rev. Mod. Phys.* 51.1 (Jan. 1979), 101–159. DOI: 10.1103/revmodphys.51.101 (cit. on p. 54).

[210] J. Alicea. “New directions in the pursuit of Majorana fermions in solid state systems”. In: *Reports on Progress in Physics* 75.7 (July 2012), p. 076501. DOI: 10.1088/0034-4885/75/7/076501 (cit. on p. 57).

[211] Li-Fu Chang and Philip Bagwell. “Ballistic Josephson-current flow through an asymmetric superconductor–normal-metal–superconductor junction”. In: *Physical Review B* 49.22 (June 1994), pp. 15853–15863. DOI: 10.1103/PhysRevB.49.15853 (cit. on pp. 58, 63).

[212] P. W. Anderson. “Special Effects in Superconductivity”. In: *Lectures on the Many-Body Problem*. Ed. by E. R. Caianiello. 1964, p. 113 (cit. on p. 60).

[213] P. W. Brouwer and C. W. J. Beenakker. “Anomalous temperature dependence of the supercurrent through a chaotic Josephson junction”. In: *Chaos, Solitons & Fractals* 8.7-8 (July 1997), pp. 1249–1260. DOI: 10.1016/S0960-0779(97)00018-0 (cit. on pp. 60, 181).

[214] W. Haberkorn, H. Knauer, and J. Richter. “A theoretical study of the current-phase relation in Josephson contacts”. In: *Phys. Stat. Sol. (a)* 47.2 (June 1978), K161–K164. DOI: 10.1002/pssa.2210470266 (cit. on p. 61).

[215] D. G. Olivares, A. Levy Yeyati, L. Bretheau, et al. “Dynamics of quasiparticle trapping in Andreev levels”. In: *Phys. Rev. B* 89 (Mar. 2014), p. 104504. DOI: 10.1103/PhysRevB.89.104504 (cit. on pp. 72, 82, 159).

[216] R.-P. Riwar, M. Houzet, J. S. Meyer, and Y. V. Nazarov. “Shooting quasiparticles from Andreev bound states in a superconducting constriction”. In: *Journal of Experimental and Theoretical Physics* 119.6 (2014), pp. 1028–1033 (cit. on p. 72).

[217] M. Eschrig, J. Kopu, J. C. Cuevas, and G. Schön. “Theory of Half-Metal/Superconductor Heterostructures”. In: *Physical Review Letters* 90.13 (Apr. 2003). DOI: 10.1103/physrevlett.90.137003 (cit. on p. 91).

[218] J. Kopu, M. Eschrig, J. C. Cuevas, and M. Fogelström. “Transfer-matrix description of heterostructures involving superconductors and ferromagnets”. In: *Physical Review B* 69.9 (Mar. 2004). DOI: 10.1103/physrevb.69.094501 (cit. on p. 91).

[219] Yasuhiro Asano, Yukio Tanaka, Alexander A. Golubov, and Satoshi Kashiwaya. “Conductance Spectroscopy of Spin-Triplet Superconductors”. In: *Physical Review Letters* 99.6 (Aug. 2007). DOI: 10.1103/physrevlett.99.067005 (cit. on p. 91).

[220] Matthias Eschrig and Tomas Löfwander. “Triplet supercurrents in clean and disordered half-metallic ferromagnets”. In: *Nature Physics* 4.2 (Jan. 2008), 138–143. DOI: 10.1038/nphys831 (cit. on p. 91).

[221] Artem V. Galaktionov, Mikhail S. Kalenkov, and Andrei D. Zaikin. “Josephson current and Andreev states in superconductor–half metal–superconductor heterostructures”. In: *Physical Review B* 77.9 (Mar. 2008). DOI: 10.1103/physrevb.77.094520 (cit. on p. 91).

[222] Jacob Linder, Takehito Yokoyama, and Asle Sudbø. “Theory of superconducting and magnetic proximity effect in S/F structures with inhomogeneous magnetization textures and spin-active interfaces”. In: *Physical Review B* 79.5 (Feb. 2009). DOI: 10.1103/physrevb.79.054523 (cit. on p. 91).

[223] Kuei Sun, Nayana Shah, and Smitha Vishveshwara. “Transport in multiterminal superconductor/ferromagnet junctions having spin-dependent interfaces”. In: *Physical Review B* 87.5 (Feb. 2013). DOI: 10.1103/physrevb.87.054509 (cit. on p. 91).

[224] A. Kadigrobov, R. I. Shekhter, and M. Jonson. “Quantum spin fluctuations as a source of long-range proximity effects in diffusive ferromagnet-super conductor structures”. In: *Europhys. Lett.* 54.3 (May 2001), 394–400. DOI: 10.1209/epl/i2001-00107-2 (cit. on p. 91).

[225] F. S. Bergeret, A. F. Volkov, and K. B. Efetov. “Odd triplet superconductivity and related phenomena in superconductor-ferromagnet structures”. In: *Rev. Mod. Phys.* 77.4 (Nov. 2005), 1321–1373. DOI: 10.1103/revmodphys.77.1321 (cit. on p. 91).

[226] Z. Pajović, M. Božović, Z. Radović, J. Cayssol, and A. Buzdin. “Josephson coupling through ferromagnetic heterojunctions with noncollinear magnetizations”. In: *Physical Review B* 74.18 (Nov. 2006). DOI: 10.1103/physrevb.74.184509 (cit. on p. 91).

[227] Joern N. Kupferschmidt and Piet W. Brouwer. “Andreev reflection at half-metal/superconductor interfaces with nonuniform magnetization”. In: *Physical Review B* 83.1 (Jan. 2011). DOI: 10.1103/physrevb.83.014512 (cit. on p. 91).

[228] Manuel Houzet. “Ferromagnetic Josephson Junction with Precessing Magnetization”. In: *Physical Review Letters* 101.5 (Aug. 2008). DOI: 10.1103/physrevlett.101.057009 (cit. on pp. 91, 97).

[229] S. E. Barnes, M. Aprili, I. Petković, and S. Maekawa. “Ferromagnetic resonance with a magnetic Josephson junction”. In: *Supercond. Sci. Technol.* 24.2 (Jan. 2011), p. 024020. DOI: 10.1088/0953-2048/24/2/024020 (cit. on p. 91).

[230] I. Petković, M. Aprili, S. E. Barnes, F. Beuneu, and S. Maekawa. “Direct dynamical coupling of spin modes and singlet Josephson supercurrent in ferromagnetic Josephson junctions”. In: *Physical Review B* 80.22 (Dec. 2009). DOI: 10.1103/physrevb.80.220502 (cit. on p. 91).

[231] S. Takahashi, S. Hikino, M. Mori, J. Martinek, and S. Maekawa. “Supercurrent Pumping in Josephson Junctions with a Half-Metallic Ferromagnet”. In: *Physical Review Letters* 99.5 (Aug. 2007). DOI: 10.1103/physrevlett.99.057003 (cit. on pp. 91, 161).

[232] J.-X. Zhu, Z. Nussinov, A. Shnirman, and A. V. Balatsky. “Novel Spin Dynamics in a Josephson Junction”. In: *Physical Review Letters* 92.10 (Mar. 2004). DOI: 10.1103/physrevlett.92.107001 (cit. on p. 91).

[233] J.-X. Zhu and A. V. Balatsky. “Josephson current in the presence of a precessing spin”. In: *Physical Review B* 67.17 (May 2003). DOI: 10.1103/physrevb.67.174505 (cit. on p. 91).

[234] Grygoriy Tkachov, Edward McCann, and Vladimir I. Fal’ko. “Subgap transport in ferromagnet-superconductor junctions due to magnon-assisted Andreev reflection”. In: *Physical Review B* 65.2 (Dec. 2001). DOI: 10.1103/physrevb.65.024519 (cit. on p. 91).

[235] E. McCann and V. I. Fal’ko. “Magnon-assisted Andreev reflection in a ferromagnet-superconductor junction”. In: *Europhys. Lett.* 56.4 (Nov. 2001), 583–589. DOI: 10.1209/epl/i2001-00560-3 (cit. on p. 91).

[236] M. S. Anwar, F. Czeschka, M. Hesselberth, M. Porcu, and J. Aarts. “Long-range supercurrents through half-metallic ferromagnetic CrO_2”. In: *Physical Review B* 82.10 (Sept. 2010). DOI: 10.1103/physrevb.82.100501 (cit. on p. 91).

[237] V. N. Krivoruchko, V. Yu. Tarenkov, A. I. D'yachenko, and V. N. Varyukhin. "Subgap magnetotransport in Pb/LaCaMnO point contacts". In: *Europhys. Lett.* 75.2 (July 2006), 294–300. DOI: 10.1209/epl/i2006-10115-8 (cit. on p. 91).

[238] V. N. Krivoruchko and V. Yu. Tarenkov. "Local triplet superconductivity of $La_{0.65}Ca_{0.35}MnO_3$ - X point contacts (X = Pb, MgB_2)". In: *Physical Review B* 75.21 (June 2007). DOI: 10.1103/physrevb.75.214508 (cit. on p. 91).

[239] I. Sosnin, H. Cho, V. T. Petrashov, and A. F. Volkov. "Superconducting Phase Coherent Electron Transport in Proximity Conical Ferromagnets". In: *Physical Review Letters* 96.15 (Apr. 2006). DOI: 10.1103/physrevlett.96.157002 (cit. on p. 91).

[240] Jérôme Cayssol and Gilles Montambaux. "Incomplete Andreev reflection in a clean superconductor-ferromagnet-superconductor junction". In: *Physical Review B* 71.1 (Jan. 2005). DOI: 10.1103/physrevb.71.012507 (cit. on p. 91).

[241] Arne Brataas and Yaroslav Tserkovnyak. "Spin and Charge Pumping by Ferromagnetic-Superconductor Order Parameters". In: *Physical Review Letters* 93.8 (Aug. 2004). DOI: 10.1103/physrevlett.93.087201 (cit. on p. 92).

[242] A. Singh, C. Jansen, K. Lahabi, and J. Aarts. *Growth of half-metallic CrO_2 nanostructures for superconducting spintronic applications*. Mar. 2016. arXiv: 1603.02675 (cit. on p. 92).

[243] C. Bell, S. Milikisyants, M. Huber, and J. Aarts. "Spin Dynamics in a Superconductor-Ferromagnet Proximity System". In: *Physical Review Letters* 100.4 (Feb. 2008). DOI: 10.1103/physrevlett.100.047002 (cit. on p. 92).

[244] N. Poli, J. P. Morten, M. Urech, et al. "Spin Injection and Relaxation in a Mesoscopic Superconductor". In: *Physical Review Letters* 100.13 (Apr. 2008). DOI: 10.1103/physrevlett.100.136601 (cit. on p. 92).

[245] T. Wakamura, N. Hasegawa, K. Ohnishi, Y. Niimi, and Y. Otani. "Spin Injection into a Superconductor with Strong Spin-Orbit Coupling". In: *Physical Review Letters* 112.3 (Jan. 2014). DOI: 10.1103/physrevlett.112.036602 (cit. on p. 92).

[246] C. H. L. Quay, D. Chevallier, C. Bena, and M. Aprili. "Spin imbalance and spin-charge separation in a mesoscopic superconductor". In: *Nature Physics* 9.2 (Jan. 2013), 84–88. DOI: 10.1038/nphys2518 (cit. on p. 92).

[247] Caroline Richard, Manuel Houzet, and Julia S. Meyer. "Andreev Current Induced by Ferromagnetic Resonance". In: *Physical Review Letters* 109.5 (July 2012). DOI: 10.1103/physrevlett.109.057002 (cit. on pp. 97, 127).

[248] Caroline Richard. "Interplay of ferromagnetism and superconductivity". PhD thesis. Université de Grenoble, Nov. 2013 (cit. on p. 97).

[249] Yaroslav Tserkovnyak, Arne Brataas, Gerrit E. W. Bauer, and Bertrand I. Halperin. "Nonlocal magnetization dynamics in ferromagnetic heterostructures". In: *Rev. Mod. Phys.* 77.4 (Dec. 2005), 1375–1421. DOI: 10.1103/revmodphys.77.1375 (cit. on p. 99).

[250] C. Caroli, R. Combescot, P. Nozieres, and D. Saint-James. “Direct calculation of the tunneling current”. In: *Journal of Physics C: Solid State Physics* 4.8 (June 1971), 916–929. DOI: 10.1088/0022-3719/4/8/018 (cit. on pp. 102, 106, 108).

[251] C. Caroli, R. Combescot, D. Lederer, P. Nozieres, and D. Saint-James. “A direct calculation of the tunnelling current. II. Free electron description”. In: *Journal of Physics C: Solid State Physics* 4.16 (1971), p. 2598. DOI: 10.1088/0022-3719/4/16/025 (cit. on pp. 102, 106).

[252] J. C. Cuevas, A. Martín-Rodero, and A. Levy Yeyati. “Hamiltonian approach to the transport properties of superconducting quantum point contacts”. In: *Physical Review B* 54.10 (Sept. 1996), 7366–7379. DOI: 10.1103/physrevb.54.7366 (cit. on pp. 107, 108, 111).

[253] Juan Carlos Cuevas and Elke Scheer. *Molecular Electronics: An Introduction to Theory and Experiment (Nanotechnology and Nanoscience) (World Scientific Series in Nanoscience and Nanotechnology)*. World Scientific Publishing Company, 2010. DOI: 10.1142/7434 (cit. on pp. 107, 108).

[254] A. Martín-Rodero, F. J. García-Vidal, and A. Levy Yeyati. “Microscopic theory of Josephson mesoscopic constrictions”. In: *Physical Review Letters* 72.4 (Jan. 1994), 554–557. DOI: 10.1103/physrevlett.72.554 (cit. on pp. 107, 108).

[255] A. Levy Yeyati, A. Martín-Rodero, and F. J. García-Vidal. “Self-consistent theory of superconducting mesoscopic weak links”. In: *Physical Review B* 51.6 (Feb. 1995), 3743–3753. DOI: 10.1103/physrevb.51.3743 (cit. on p. 107).

[256] Wolfgang Belzig, Frank K. Wilhelm, Christoph Bruder, Gerd Schön, and Andrei D. Zaikin. “Quasiclassical Green’s function approach to mesoscopic superconductivity”. In: *Superlattices and Microstructures* 25.5-6 (May 1999), 1251–1288. DOI: 10.1006/spmi.1999.0710 (cit. on pp. 110, 111).

[257] Albert Schmid and Gerd Schön. “Linearized kinetic equations and relaxation processes of a superconductor near T_c”. In: *Journal of Low Temperature Physics* 20.1 (1975), pp. 207–227. DOI: 10.1007/BF00115264 (cit. on p. 111).

[258] Yu. A. Genenko and Yu. M. Ivanchenko. “Exact calculation of the current in the tunnel Hamiltonian method”. In: *Theoretical and Mathematical Physics* 69.1 (1985), pp. 1056–1061. DOI: 10.1007/BF01037682 (cit. on p. 111).

[259] J. Ferrer, A. Martín-Rodero, and F. Flores. “Contact resistance in the scanning tunneling microscope at very small distances”. In: *Physical Review B* 38.14 (Nov. 1988), 10113–10115. DOI: 10.1103/physrevb.38.10113 (cit. on p. 111).

[260] G. E. Blonder, M. Tinkham, and T. M. Klapwijk. “Transition from metallic to tunneling regimes in superconducting microconstrictions: Excess current, charge imbalance, and supercurrent conversion”. In: *Phys. Rev. B* 25 (Apr. 1982), pp. 4515–4532. DOI: 10.1103/PhysRevB.25.4515 (cit. on pp. 111, 114–116).

[261] F. Pistolesi, G. Bignon, and F. W. J. Hekking. “Subgap noise of a superconductor–normal-metal tunnel interface”. In: *Physical Review B* 69.21 (June 2004). DOI: 10.1103/physrevb.69.214518 (cit. on p. 131).

[262] Guillaume Bignon. “Corrélations de courant dans les structures mésoscopiques supraconducteur - métal normal”. French. PhD thesis. Université Joseph Fourier - Grenoble I, 2005 (cit. on p. 131).

[263] G. Falci, D. Feinberg, and F. W. J. Hekking. “Correlated tunneling into a superconductor in a multiprobe hybrid structure”. In: *Europhys. Lett.* 54.2 (Apr. 2001), 255–261. DOI: 10.1209/epl/i2001-00303-0 (cit. on p. 131).

[264] Nikolai M. Chtchelkatchev and Igor S. Burmistrov. “Andreev conductance of a domain wall”. In: *Physical Review B* 68.14 (Oct. 2003). DOI: 10.1103/physrevb.68.140501 (cit. on p. 131).

[265] Richard P. Feynman and A. R. Hibbs. *Quantum Mechanics and Path Integrals*. First Edition. 1965 (cit. on p. 134).

[266] E. Prada and F. Sols. “Entangled electron current through finite size normal-superconductor tunneling structures”. In: *Eur. Phys. J. B* 40.4 (Aug. 2004), 379–396. DOI: 10.1140/epjb/e2004-00284-8 (cit. on p. 142).

[267] Y. V. Sharvin. “A possible method for studying Fermi surfaces”. In: *Soviet Physics JETP-USSR* 21.3 (1965), p. 655 (cit. on p. 143).

[268] Eric Akkermans and Gilles Montambaux. *Mesoscopic Physics of Electrons and Photons*. Cambridge Books Online. Cambridge University Press, 2007. DOI: 10.1017/CBO9780511618833 (cit. on pp. 144, 145, 147, 148, 156, 200).

[269] Sidney Shapiro. “Josephson Currents in Superconducting Tunneling: The Effect of Microwaves and Other Observations”. In: *Physical Review Letters* 11.2 (July 1963), 80–82. DOI: 10.1103/physrevlett.11.80 (cit. on p. 160).

[270] A. Balatsky, I. Vekhter, and Jian-Xin Zhu. “Impurity-induced states in conventional and unconventional superconductors”. In: *Rev. Mod. Phys.* 78.2 (May 2006), 373–433. DOI: 10.1103/revmodphys.78.373 (cit. on p. 160).

[271] P. W. Anderson. “Knight Shift in Superconductors”. In: *Physical Review Letters* 3.7 (Oct. 1959), 325–326. DOI: 10.1103/physrevlett.3.325 (cit. on p. 160).

[272] D. Fang, H. Kurebayashi, J. Wunderlich, et al. “Spin–orbit-driven ferromagnetic resonance”. In: *Nature Nanotechnology* 6.7 (May 2011), 413–417. DOI: 10.1038/nnano.2011.68 (cit. on p. 161).

[273] Ioan Mihai Miron, Gilles Gaudin, Stéphane Auffret, et al. “Current-driven spin torque induced by the Rashba effect in a ferromagnetic metal layer”. In: *Nat Mater* (Jan. 2010). DOI: 10.1038/nmat2613 (cit. on p. 161).

[274] A. Manchon and S. Zhang. “Theory of nonequilibrium intrinsic spin torque in a single nanomagnet”. In: *Physical Review B* 78.21 (Dec. 2008). DOI: 10.1103/physrevb.78.212405 (cit. on p. 161).

[275] A. Manchon and S. Zhang. “Theory of spin torque due to spin-orbit coupling”. In: *Physical Review B* 79.9 (Mar. 2009). DOI: 10.1103/physrevb.79.094422 (cit. on p. 161).

[276] Mathias Duckheim and Piet W. Brouwer. “Andreev reflection from noncentrosymmetric superconductors and Majorana bound-state generation in half-metallic ferromagnets”. In: *Physical Review B* 83.5 (Feb. 2011). DOI: 10.1103/physrevb.83.054513 (cit. on p. 161).

[277] Kai Chen and Shufeng Zhang. “Spin Pumping in the Presence of Spin-Orbit Coupling”. In: *Physical Review Letters* 114.12 (Mar. 2015). DOI: 10.1103/physrevlett.114.126602 (cit. on p. 161).

[278] Petra Högl, Alex Matos-Abiague, Igor Žutić, and Jaroslav Fabian. “Magnetoanisotropic Andreev Reflection in Ferromagnet-Superconductor Junctions”. In: *Physical Review Letters* 115.11 (Sept. 2015). DOI: 10.1103/physrevlett.115.116601 (cit. on p. 161).

[279] Cecilia Holmqvist, Wolfgang Belzig, and Mikael Fogelström. *Non-equilibrium charge and spin transport in SFS point contacts*. Mar. 2016. arXiv: 1603.01299 (cit. on p. 161).

[280] M. Garst and T. Kopp. “Random-Matrix Theory: Distribution of Mesoscopic Supercurrents through a Chaotic Cavity”. In: *J. Low Temp. Phys.* 126, (2002), p. 1305. DOI: 10.1023/A:1013844019470 (cit. on p. 171).

[281] Eyal Doron and Uzy Smilansky. “Chaotic spectroscopy”. In: *Physical Review Letters* 68.9 (Mar. 1992), pp. 1255–1258. DOI: 10.1103/PhysRevLett.68.1255 (cit. on p. 171).

[282] M. L. Goldberger and K. M. Watson. *Collision Theory*. 3ed. Wiley, 1967. DOI: 10.1126/science.148.3668.354-a (cit. on p. 171).

[283] Eugene P. Wigner. “Lower Limit for the Energy Derivative of the Scattering Phase Shift”. In: *Physical Review* 98.1 (Apr. 1955), 145–147. DOI: 10.1103/physrev.98.145 (cit. on p. 171).

[284] Eugene P. Wigner. “On a Class of Analytic Functions from the Quantum Theory of Collisions”. In: *The Annals of Mathematics* 53.1 (Jan. 1951), p. 36. DOI: 10.2307/1969342 (cit. on p. 171).

[285] Doron Cohen. *Lecture Notes in Quantum Mechanics*. 2013. arXiv: quant-ph/0605180 (cit. on p. 171).

[286] C. W. J. Beenakker. “Quantum transport in semiconductor-superconductor microjunctions”. In: *Physical Review B* 46.19 (Nov. 1992), pp. 12841–12844. DOI: 10.1103/PhysRevB.46.12841 (cit. on p. 176).

[287] I. S. Gradshteyn and I. M. Ryzhik. *Table of integrals, series, and products*. 7th ed. Academic Press, 2007 (cit. on p. 203).